Strathclyde Institute of Pharmacy and Biomedical Sciences

Thesis presented in fulfilment of the requirement for the degree of Doctor of Philosophy

COMPARATIVE METABOLOMIC ANALYSIS OF PHYLOGENETICALLY DIVERSE ACTINOMYCETES

MARLA ITZEL MACIAS CONTRERAS

Primary Supervisor: Dr. Katherine Duncan
Second Supervisor: Dr. Paul Herron

Glasgow, Scotland-October 2025

DECLARATION

This thesis is the result of the author's original research. It has been composed by the author and has not been previously submitted for examination which has led to the award of a degree. The copyright of this thesis belongs to the author under the terms of the United Kingdom Copyright Acts as qualified by University of Strathclyde Regulation 3.50. Due acknowledgement must always be made of the use of any material contained in, or derived from, this thesis. The figures used in this thesis are a result of work carried out by the author.

Signed:

Date: 27/10/2025

It is not knowledge, but the act of learning, not possession but the act of getting there, which grants the greatest enjoyment!!!
Carl Friedrich Gauss

ACKNOWLEDGEMENTS

A mis padres (**Olivia** y **Noe**), por su apoyo económico y emocional incondicional en cada etapa de mi formación académica. Gracias por soportar la distancia y por darme la libertad de seguir mis sueños, incluso cuando eso significó estar lejos de casa. Hoy, por fin, puedo decir que estudié hasta el final.

A mis hermanos, **Sococo** y **Noe**, por su compañía constante a través de memes y chistes, que hicieron la distancia mucho más llevadera.

A **Mario**, alias *el roomie*, por tu inconmensurable paciencia, por prestarme tus oídos durante mis quejas, por tu apoyo incondicional y por ser quien más me impulsó a cumplir esta meta. Tu sabes todo lo que significas.

A **Alemao**, por tu amistad incondicional incluso antes de conocernos en persona. Gracias por abrirme las puertas de tu casa; gracias a ti no dormí en el parque durante mis primeros días.

A **Thalia**, **Carola**, **David y Abril**, gracias por regalarme su tiempo, su amistad y por acompañarme en tantas bonitas aventuras.

A **Dulce**, por regalarme tu amistad durante tantos años y por recomendarme a mi directora de tesis; gracias a ti pude estudiar lo que realmente me apasiona.

A **CONACYT/SECIHTI**, por el apoyo económico otorgado a través de la beca, que hizo posible que pudiera dedicarme plenamente a mis estudios y a la realización de esta tesis.

A mis gatos (**Max, Diva y Siete**), por su peluda compañía y su amor silencioso.

Y finalmente, gracias a **mí**. Citando a Snoop Dogg: *"I want to thank me for believing in me, for doing all this hard work. I want to thank me for having no days off. I want to thank me for never quitting. I want to thank me for always being generous and trying to give more than I receive. I want to thank me for trying to do more right than wrong. I want to thank me for being me at all times and under any circumstances."*

First and foremost, I would like to thank my supervisor, **Katherine Duncan**, for welcoming me into her research group, for helping me secure additional financial support, and for believing in me—often more than I believed in myself. Your patience, kindness, and unwavering encouragement, together with the emotional support you offered whenever it was needed, were fundamental to the completion of this work.

I am also deeply grateful to my examiners, **Rainer Ebel** and **Daniel Walker**, for their patience and kindness during my defence, which greatly helped to put me at ease. I would additionally like to thank **RuAngelie Edrada-Ebel** for her guidance and for providing thoughtful and constructive feedback throughout the process.

My sincere thanks also go to **Grace Tedman**, who has always been incredibly supportive with any administrative matters I needed help with, from the very beginning.

I would like to thank **Cathel Robertson** for choosing me as his housemate and, over time, for becoming a dear friend. My house will always be your house bro.

To **Artem**, thank you for making every day in the lab enjoyable. I genuinely would not have coped as well with the stress and anxiety of the PhD without your humour and companionship. I also apologise for not always being as sociable as I could have been. My thanks also go to your wonderful fiancée, **Shara**, for her constant warmth and lovely company.

To **George**, **Veronika**, **Vasilisa**, **Chris**, **Panos (Tanos)**, **Timoleon (Timos)**, and **Aidan**, thank you for your friendship, your time, and the many interesting conversations shared over lunch.

Finally, I would like to thank to **Shaun Hughes** who greeted me so warmly each day at the entrance to the Medical School at Newcastle University. Those small daily interactions helped my days begin and end with a smile, something that means more than words can express during a PhD journey.

Table of Contents

LIST OF FIGURES

LIST OF TABLES

ABSTRACT:

In the ongoing search for new antibiotics, ‘rare’ actinomycetes are increasingly recognised as an untapped source of biomedically relevant chemistry. Genera such as *Salinispora*, *Pseudonocardia* and *Micromonospora* have recently yielded both biosynthetic and chemical novelty. Clinically important antibiotics including erythromycin, vancomycin, teicoplanin and fidaxomicin trace their origins to these rare taxa, underscoring their pharmaceutical significance. In this study, we investigated the influence of abiotic factors—temperature and salinity—on secondary metabolite production by *Rhodococcus* and *Micromonospora* strains, respectively. Seven *Rhodococcus* spp. and ten *Micromonospora* spp., isolated from diverse marine environments including a Mexican lagoon, the sub-Arctic, and Antarctica, were cultured under varying conditions. *Rhodococcus* strains were grown at 20 °C, 25 °C, and 30 °C using strain-specific growth curves to normalise extraction stage, while *Micromonospora* strains were cultured on solid A1 medium across salinities of 0 ‰, 15 ‰, 25 ‰, 35 ‰, and 40 ‰. These treatments generated 94 *Rhodococcus* and 63 *Micromonospora* cultures, all analysed by LC-HRMS/MS. Our results revealed that *Rhodococcus* KRD197 exhibited an increased production of polyketides and carbohydrates under reduced temperature conditions. Meanwhile, *Micromonospora* KRD324 displayed antimicrobial activity against *Enterococcus faecalis* and *Bacillus subtilis*, potentially linked to a cluster of macrolides with high similarity to the juvenimicin-family of antibiotics.

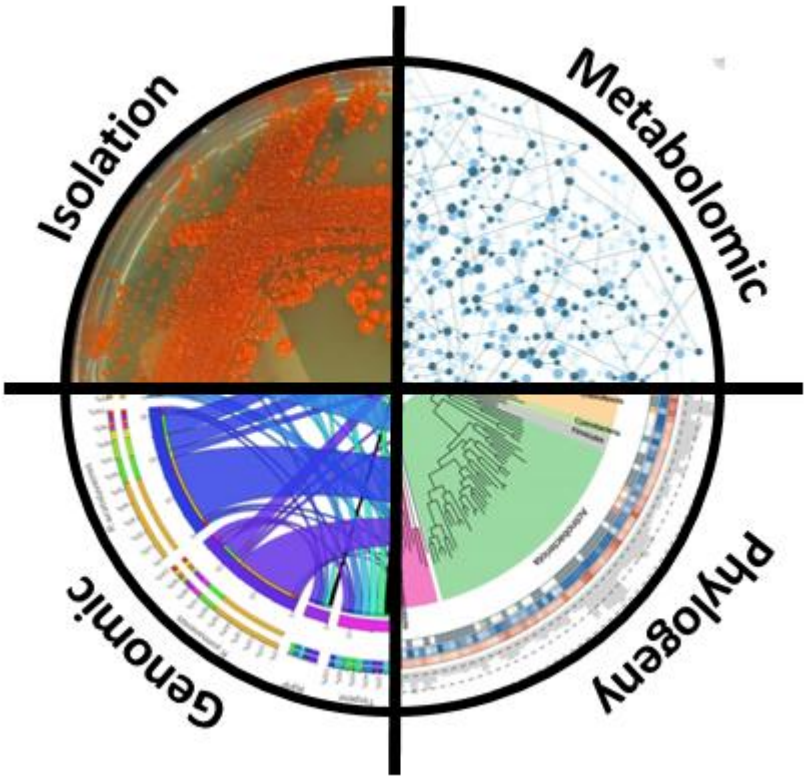

1 CHAPTER 1: INTRODUCTION

1.1 Antibiotics and antimicrobial resistance (AMR)

1.1.1 Antibiotics

The term *antibiotic* was originally introduced by Selman Waksman in 1942, who defined it as a substance produced by microorganisms that inhibits the growth of, or kills, other microorganisms (Clardy *et al.,* 2009). Over time, the definition has broadened to include not only natural products but also semisynthetic and fully synthetic compounds that act at low concentrations against bacteria without causing significant harm to the host (Walsh, 2003; Leisner, 2020). While the broader term *antimicrobial* refers to agents active against viruses, fungi, and parasites, antibiotics are specifically restricted to antibacterial compounds (Salam *et al.,* 2023). In clinical and microbiological practice, antibiotics are typically classified by their mechanism of action, which includes: (i) inhibition of bacterial cell wall biosynthesis, as observed with β-lactams (penicillins: Fleming, 1929; cephalosporins: Abraham and Chain; 1940; carbapenems: Kahan *et al.,* 1979) that block penicillin-binding proteins required for peptidoglycan cross-linking (Elshamy & Aboshanab, 2020), and glycopeptides (vancomycin: McCormick *et al.,* 1956) that bind to peptidoglycan precursors (Kim *et al.,* 2008); (ii) disruption of cell membrane integrity, for example polymyxins (colistin: Koyama *et al.,* 1950) that interact with lipopolysaccharides of Gram-negative bacterial membranes, or lipopeptides (daptomycin: Debono *et al.,*1987) that insert into Gram-positive bacterial membranes and cause depolarization; (iii) inhibition of nucleic acid and/or protein synthesis, such as aminoglycosides (gentamicin: Weinstein *et al.,* 1963; streptomycin: Schatz *et al.,*1944) that causes misreading of mRNA, tetracyclines (doxycycline: Stephens *et al.,* 1958) that block the A-site of the ribosome, macrolides (erythromycin: McGuire *et al.,* 1952; azithromycin: Banić Tomišić, 2011) that prevent peptide chain elongation, oxazolidinones (linezolid: Zurenko *et al.,* 1996) that inhibit ribosome assembly, fluoroquinolones (ciprofloxacin: Sanders, 1988) that interfere with DNA gyrase/topoisomerase (Collins and Osheroff, 2024), and rifamycins (rifampicin: Sensi *et al.,* 1959) that inhibit RNA polymerase (Derek *et al.,* 2018); and (iv) interference with key metabolic processes, such as sulfonamides (Domagk, 1935) and trimethoprim (Roth *et al.,* 1962), which act as competitive inhibitors in the folate pathway, blocking nucleotide biosynthesis (Ghilchik *et al.,* 1970).

They can also be classified according to origin—whether natural (penicillin: Chain *et al.,* 1940; streptomycin: Schatz *et al.,* 1944), semisynthetic (penicillin derivatives: methicillin: Jevons, 1961; oxacillin: Gourevitch *et al.,* 1961; and nafcillin: Schwichtenberg, 1965), or synthetic (fluoroquinolones: ciprofloxacin: Wise *et al.,* 1983; levofloxacin: Hayakawa *et al.,* 1986; and moxifloxacin: Petersen *et al.,* 1991)—or by their spectrum of activity, as broad-spectrum or narrow-spectrum agents. Broad-spectrum refers to agents that are active against a wide taxonomic range of bacteria; e.g. some tetracyclines and extended-spectrum cephalosporins (Ernstmeyer & Christman, 2023), whereas narrow-spectrum agents target a limited set of pathogens (for example vancomycin (McCormick *et al.,* 1956) for Gram-positive strains or isoniazid for *Mycobacterium tuberculosis*) (Melander *et al.,* 2018). While indispensable in clinical practice, the widespread and often indiscriminate use of antibiotics has accelerated the emergence of resistance, which is now recognised as one of the greatest threats to global health (Sirwan *et al.,* 2024).

1.1.2 Antimicrobial resistance (AMR)

Resistance to antibiotics is not a new phenomenon: as early as 1940, only five years after the introduction of penicillin, a strain of *Escherichia coli* was found to inactivate the drug through the production of penicillinase (Abraham & Chain, 1940). The golden age of antibiotics began with the discovery of penicillin in 1928 and continued with streptomycin in the 1940s, leading to the detection of most major antibiotic classes during the following two decades (Schatz *et al.,* 1944; Sharma *et al.,* 2018). However, this prolific period rapidly declined by the early 1960s, largely because the most readily accessible natural products from well-studied bacterial taxa had already been discovered, leading to increasing rates of rediscovery of known compounds (Stach & Bull, 2005; Jagannathan *et al.,* 2021). Alongside this decline, the widespread and often excessive use of antibiotics became a major driver of resistance. In the United States alone, nearly 20% of all emergency department visits are antibiotic-related events (Lode, 2010; Ventola, 2015). Globally, antibiotic consumption in 67 countries (e.g. United State, Brazil) increased by 16.3 %, rising from 29.5 to 34.3 billion defined daily doses (DDDs) between 2016 and 2023, which corresponds to an increase in the consumption rate from 13.7 to 15.2 DDDs per 1,000 inhabitants per day (Klein *et al.,* 2024). Resistance has expanded rapidly: historically, more than 70% of pathogenic bacteria have been reported resistant to at least one antibiotic (Sharma *et al.,* 2018)

and estimates up to 2019 suggest that resistant infections caused over 35,000 deaths annually in the EU/EEA (ECDC, 2024).

The scale of the problem is now global. In 2019, antimicrobial resistance (AMR) was directly responsible for 1.27 million deaths and associated with 4.95 million deaths worldwide (Murray *et al.,* 2022; WHO, 2024). Projections are alarming: if no substantial interventions are made, AMR could directly cause 3.9 million deaths annually by 2050, contribute to over 8 million deaths in total each year, and result in more than 39 million deaths globally between 2025 and 2050 (Murray *et al.,* 2022). This global expansion is driven not only by overuse of antibiotics in clinical and agricultural settings but also by the horizontal transfer of mobile genetic elements carrying resistance genes such as *mcr-3* (colistin) and *CTX-M-15* (third-generation cephalosporins), which spread rapidly through farming practices, environmental contamination, and international food trade (Liu *et al.,* 2016; Holmes *et al.,* 2016).

Given the accelerating spread of resistance, in 2017, the World Health Organization (WHO) published a priority list of pathogens urgently requiring new antibiotics, highlighting the so-called ESKAPE pathogens (*Enterococcus faecium, Staphylococcus aureus, Klebsiella pneumoniae, Acinetobacter baumannii, Pseudomonas aeruginosa,* and *Enterobacter* spp.), many of which are resistant to multiple last-line therapies (Tacconelli *et al.,* 2018). This list is regularly updated to reflect the evolving threat. In the most recent update (WHO, 2024), the critical priority group includes *Acinetobacter baumannii* (carbapenem-resistant), *Enterobacterales* such as *Escherichia coli* and *Klebsiella pneumoniae* (carbapenem-resistant), *Enterobacterales* resistant to third-generation cephalosporins, *Mycobacterium tuberculosis* (TB) (carbapenem-and rifampicin-resistant strains). The emergence of new drug-resistant lineages such as extensively drug-resistant (XDR) strains limits treatment options even further, with TB in particular causing great concern (Seung *et al.,* 2015). Pathogens classified as high priority include *Salmonella typhi* (fluoroquinolone-resistant), *Shigella* spp. (fluoroquinolone-resistant), *Enterococcus faecium* (vancomycin-resistant), *Pseudomonas aeruginosa* (carbapenem-resistant), *Neisseria gonorrhoeae* (third-generation cephalosporin- and/or fluoroquinolone-resistant), and *Staphylococcus aureus* (methicillin-resistant, MRSA). Notably, the development of newer agents such as ceftazidime-avibactam (Torres-del-Pliego *et al.,* 2017) and cefiderocol (Wu *et al.,* 2020) has provided options against resistant

Gram-negative infections, although resistance to these novel drugs has already been reported in some regions (Wang *et al.,* 2025; Chevotar *et al.,* 2025).

Given the increasing threat of antimicrobial resistance, there is a pressing need to identify novel bioactive compounds. Bacteria provide a particularly rich source of such molecules (Wali *et al.,* 2024): while their primary metabolism sustains essential cellular functions, their secondary metabolism gives rise to diverse natural products, including many clinically important antibiotics. Understanding the distinction between these two metabolic realms is therefore fundamental to exploring microbial biosynthetic potential (Ahmad *et al.,* 2025).

1.2 Metabolism in bacteria

1.2.1 Primary metabolism

Primary metabolism comprises the essential biochemical processes that sustain growth, development, and reproduction in microorganisms (Sanchez & Demain, 2008). These pathways involve central carbon metabolism, nitrogen assimilation, respiration, and the biosynthesis of building blocks such as amino acids, nucleotides, fatty acids, and vitamins (Sanchez & Demain, 2008). Due to their indispensable role, primary metabolic functions are highly conserved across species, remaining under strong evolutionary constraints that ensure genetic stability (Mukherjee *et al.,* 2015). While crucial for viability, primary metabolites tend to be structurally simple and therefore of limited direct interest for drug discovery, as they lack the chemical diversity and specialised bioactivities typically associated with secondary metabolites.

1.2.2 Secondary metabolism

In contrast, secondary metabolism (often referred to as “specialised metabolism,” in recent literature) (Chevrette & Handelsman, 2021) is responsible for the production of compounds that are not strictly required for survival, but which provide adaptive advantages in natural environments. These metabolites mediate ecological functions such as competition as in the case of *P. aeruginosa* that up-regulates siderophore production in competition with *Staphylococcus aureus* (Leinweber *et al.,* 2018); signaling as in rhizobia bacteria which use flavonoids to facilitate nutrient exchange (Liu & Murray, 2016), and symbiosis like *Pseudomonas* that has been shown to

produce antimicrobial 2,4-diacetylphloroglucinol (DAPG) to protect its plant host (Sánchez Carrillo & Guerra Ramírez, 2022).

At the genomic level in bacteria, secondary metabolites are typically biosynthesised by enzymes encoded by biosynthetic gene clusters (BGCs). These are defined as physically grouped sets of two or more genes within a genome that collectively encode the enzymatic machinery to produce a particular metabolite and its structural variants (Medema *et al.,* 2015). Unlike the conserved core regions that house primary metabolism and other fundamental functions, these BGC-containing regions are more variable in their genetic composition, which is reflected in greater sequence diversity and a faster rate of evolution. Indeed, they often serve as hotspots for horizontal gene transfer (HGT) (Hall *et al.,* 2020), thus enabling rapid diversification and a wide range of biosynthetic capabilities. This high degree of genomic plasticity emphasises that secondary metabolism is not only ecologically adaptive but also an evolutionary driver of microbial diversity. This was seen, for example, when studying the marine genus *Salinispora*, where HGT, gene duplication, and mutation enabled the acquisition and diversification of BGCs, resulting in the biosynthesis of new natural products, increasing the overall metabolic repertoire of the population and contributing to species delineation which is believed to contribute to niche specialisation and diversification within microbial populations (Ziemert *et al.,* 2014).

1.2.3 Secondary metabolites classes

Secondary metabolites can be grouped into major classes based on their chemical scaffolds and biosynthetic logic, these are polyketides, non-ribosomal peptides, terpenoids, alkaloids, ribosomally-synthesised and post-translationally modified peptides (RiPPs) and others, which are BGCs that do not meet a specific abundance threshold and that cannot be confidently assigned to any of the known, well-defined classes.

Nonribosomal peptides (NRPs)

Nonribosomal peptides (NRPs) represent one of the best-characterised classes of microbial secondary metabolites, produced by large nonribosomal peptide synthetases (NRPSs) (Duban *et al.,* 2022). These enzymes are modular, with each module responsible for the incorporation of one amino acid into the growing peptide

chain. A typical module consists of three core domains: (i) an adenylation (A) domain, which selects and activates the specific amino acid substrate as an aminoacyl-adenylate; (ii) a thiolation (T) or peptidyl carrier protein (PCP) domain**,** which transfers the activated amino acid to a phosphopantetheinyl arm; and (iii) a condensation (C) domain, which catalyses peptide bond formation between adjacent substrates. Additional tailoring domains—such as epimerization (E), methylation (M), oxidation (Ox), or cyclization (Cy) domains—introduce structural diversity, giving rise to bioactive molecules with antibacterial (e.g., vancomycin), antifungal (e.g., echinocandins), or immunosuppressive activity (e.g., cyclosporin Fig. 1.1[**1**]) (Duban *et al.,* 2022). The modular logic of NRP assembly allows prediction of peptide structures from genomic data, although in many cases auxiliary enzymes contribute additional modifications not encoded within the NRPS cluster, making complete pathway elucidation challenging.

Polyketides (PKs)

Polyketides are another major family of secondary metabolites, biosynthesised by polyketide synthases (PKSs), which share mechanistic similarities with fatty acid synthases but display greater structural flexibility (Lin *et al.,* 2024). Three major PKS types have been described:

- Type I PKSs are large, multifunctional enzymes organised in modules, each containing domains for ketosynthase (KS), acyltransferase (AT), and acyl carrier protein (ACP), with optional domains, like ketoreductase (KR), dehydratase (DH) and enoyl reductase (ER), controlling the reduction state of the growing chain. This modular assembly-line mechanism produces highly complex macrolides such as erythromycin (McGuire *et al.,* 1952) (Dutta *et al.,* 2014)**.**
- Type II PKSs are composed of separate enzymes that act iteratively to biosynthesise aromatic polyketides, such as tetracyclines and doxorubicin (Fig. 1.1[**2**]), through repeated condensation of malonyl-CoA units. A crucial component is the acyl carrier protein (ACP), which serves as a central hub by transporting malonyl-derived building blocks to the catalytic enzymes. The process is iterative: the main catalytic enzymes, together with the ACP, repeatedly condense malonyl-CoA units to form the polyketide backbone, which then undergoes cyclisation and further modifications (Wang *et al.,*

2020). The biosynthesis of aromatic polyketides involves four main stages: (1) loading of the α-carboxylated precursor: acetate is attached to the ACP, forming acyl-ACP. (2) iterative chain elongation and ketone reduction: acyl-ACP is transferred to the KS subunit and repeatedly extended with malonyl-CoA units to produce the poly-β-keto chain, (3) cyclisation and/or aromatisation: the poly-β-keto chain is processed by aromatases (ARO) and oxygenases to form the aromatic polyketide core abd(4) post-modification: oxygenases, methyltransferases and glycosyltransferases modify this aromatic core to produce the final polyketide (Hertweck *et al.,* 2007; Zhang *et al.,* 2017)

- Type III PKSs are homodimeric enzymes that catalyze the condensation of simple CoA-linked substrates without ACP intermediates, producing small aromatic polyketides such as chalcones**.** They employ iterative decarboxylative Claisen condensation reactions to build a polyketide chain from starter and extender units (Katsuyama & Ohnishi, 2012).

As with NRPS pathways, PKS products undergo extensive post-PKS tailoring, including glycosylation, hydroxylation, or halogenation, which often determine their final bioactivity. Importantly, hybrid NRPS–PKS systems further expand structural diversity by integrating modules from both pathways (Little and Hertweck, 2022). Well-known examples of hybrid systems include rapamycin (Fig. 1.1[**3**]) (Schwecke *et al.,* 1995; Ganesh & Subathra, 2023) and the clinically important glycopeptide bleomycin (Chen *et al.,* 2020).

Terpenes

Terpenes are structurally diverse metabolites derived from the universal precursors isopentenyl pyrophosphate (IPP) and dimethylallyl pyrophosphate (DMAPP), which are synthesised via the methylerythritol phosphate (MEP) pathway —predominant in most bacteria and plant plastids—or the mevalonate (MVA) pathway, which is mainly found in eukaryotes (such as plants and fungi) and in some archaea. The key enzymes are prenyltransferases, which assemble linear polyisoprenoid chains (e.g., geranyl pyrophosphate, farnesyl pyrophosphate), and terpene synthases (TPSs), which catalyse cyclization and rearrangement to generate diverse skeletons (Christianson, 2017). Subsequent tailoring by oxidases, glycosyltransferases, or methyltransferases produces functionalized terpenoids (Tian *et al.,* 2022). In

actinomycetes, terpenes include geosmin (Fig. 1.1[**4**]) (Gerber & Lechevalier, 1965) (responsible for the “earthy” smell of soil), and albaflavenone (Gürtler *et al.,* 1994) (an antibacterial sesquiterpene). Despite their ubiquity, the ecological functions of many actinomycete terpenes remain poorly understood, and only a fraction of the predicted terpene synthase gene clusters have been experimentally characterised (Chhalodia *et al.,* 2023).

Alkaloids

Alkaloids are nitrogen-containing secondary metabolites derived primarily from amino acid precursors such as tryptophan, tyrosine, lysine, or ornithine. Their biosynthesis generally begins with amino-acid decarboxylation, retaining the nitrogen that defines this metabolite class. In some specialised pathways, transamination generates an α-keto intermediate that subsequently regains a nitrogen source. These steps are then followed by cyclization and modification steps catalysed by oxidases, methyltransferases, or reductases (Lichman, 2021). Actinomycetes produce diverse alkaloids, including indolocarbazoles (e.g., staurosporine (Fig. 1.1[**5**]) (Omura *et al.,* 1977), a potent protein kinase inhibitor), quinoline derivatives, and pyrrolobenzodiazepines (antitumor antibiotics). While many alkaloids biosynthetic routes remain incompletely resolved, genome mining has uncovered numerous candidate clusters, especially in rare genera (Schorn *et al.,* 2016). These findings suggest that alkaloid diversity in actinomycetes is far greater than currently recognised.

Ribosomally-synthesized and post-translationally modified peptides (RiPPs)

RiPPs originate from short ribosomally synthesised precursor peptides, linking them directly to primary metabolism and the protein biosynthesis machinery. Unlike non-ribosomal peptides (NRPs), which are assembled by large multimodular synthetases, RiPPs begin as simple peptides encoded in the genome and translated by the ribosome. These precursors are then extensively modified by dedicated enzymes to yield mature bioactive structures. Modifications include cyclization, dehydration, heterocycle formation, methylation, and glycosylation, generating highly stable and potent molecules (Arnison *et al.,* 2013; Han & Won, 2024). Examples of actinomycete produced RiPPs include lantipeptides (e.g., actagardine: Kettenring *et al.,* 1990), lasso peptides (e.g., siamycin: Tsunakawa *et al.,* 1995), thiopeptides (e.g., thiostrepton: Fig. 1.1[**6**]; Donovick *et al.,* 1955), and glycocins (Poorinmohammad *et*

al., 2019). RiPPs are notable for their structural complexity and potency; thiostrepton (Donovick *et al.,* 1955), for instance, is a thiopeptide antibiotic that inhibits bacterial ribosomes (Walter *et al.,* 2012). Advances in genomics have revealed an unexpectedly large diversity of RiPP biosynthetic gene clusters in actinomycetes, yet many remain cryptic, and their natural products are still unknown (Zdouc *et al.,* 2023).

Further classes of secondary metabolites

Beyond these canonical chemical classes (PK, NRP, terpenes, RiPPs, or alkaloids), actinomycetes also encode additional and more specialised secondary metabolite families. Many of these can be viewed as functional subgroups or hybrid pathways derived from the major classes, but they nonetheless contribute important chemical and ecological diversity.

Thiopeptides, for instance, are highly modified RiPPs characterised by extensive cyclodehydrations and azole formations. They have been identified from multiple non-*Streptomyces* genera: *Nocardiopsis* sp. produces TP-1161, a thiopeptide antibiotic with potent activity against methicillin-resistant *Staphylococcus aureus* (MRSA) (Engelhardt *et al.,* 2010). Similarly, siderophores represent another broadly conserved class, typically originating from NRPS, PKS, NRPS–PKS hybrid pathways or NRPS-independent siderophore (NIS). They mediated iron acquisition under limiting conditions. A well-studied case is the loihichelins A–F suite from *Halomonas* sp. LOB-5, which reflects adaptation to the manganese- and iron-rich environment of the Loihi Seamount (Homann *et al.,* 2009).

Some actinomycetes also produce compatible solutes, such as ectoine (Fig. 1.1[**7**]) (Galinski *et al.,* 1985), an osmo-protectant, providing resilience against salinity and desiccation stress (Kumar *et al.,* 2025). Although not a classical antibiotic, ectoine illustrates how secondary metabolism contributes to physiological resilience. Moreover, certain actinomycetal genera encode unusual β-lactones and γ-butyrolactones with regulatory or cytotoxic functions. A prominent example is salinosporamide A (marizomib) from *Salinispora tropica*, a β-lactone–γ-lactam hybrid that functions as a proteasome inhibitor and has progressed to clinical use in oncology (Feling *et al.,* 2003; Jensen, 2022). Taken together, these examples illustrate that actinomycetes produce specialised and sometimes hybrid metabolite classes that complement the major biosynthetic pathways. While not ecologically “more relevant” than canonical classes, they highlight how secondary metabolism supports functions

ranging from nutrient acquisition and osmoprotection to microbial competition. This ecological perspective will be further explored in the following section.

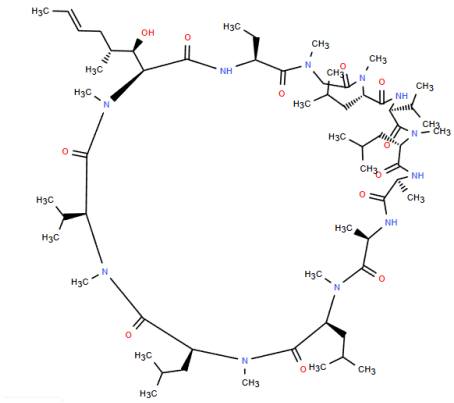

Nonribosomal peptide
Cyclosporin
(1)

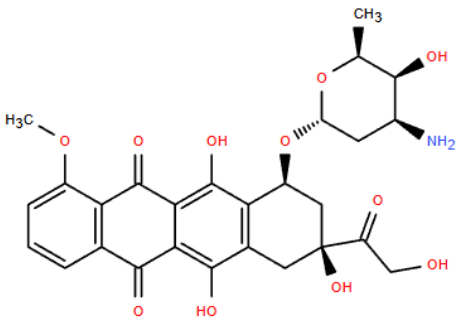

Polyketide
doxorubicin
(2)

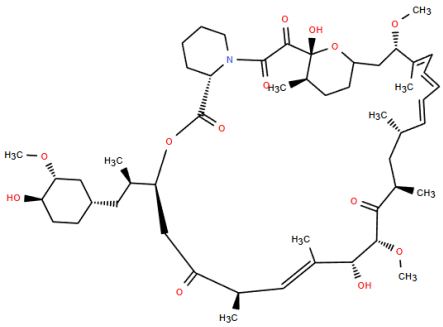

Hybrid NRPS–PKS
Rapamycin
(3)

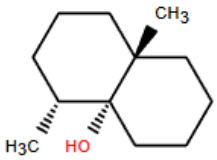

Terpene
geosmin
(4)

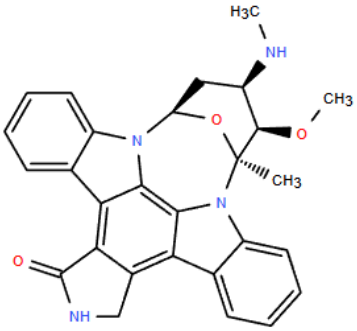

Alkaloid
staurosporine
(5)

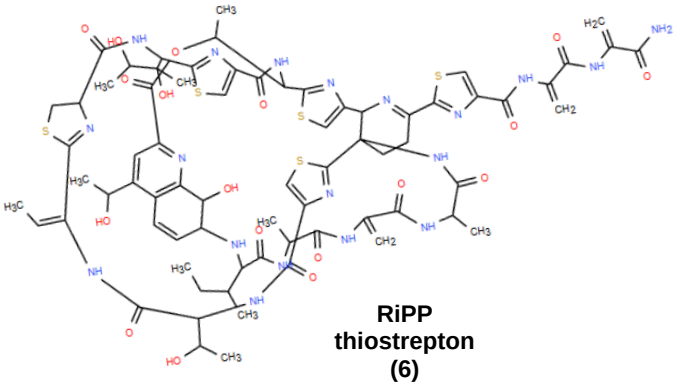

RiPP
thiostrepton
(6)

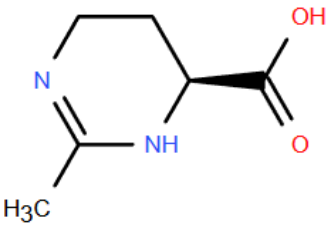

Further class
ectoine
(7)

Figure 1.1. Representative chemical structures illustrating major classes of secondary metabolites commonly produced by microorganisms. Including nonribosomal peptides (1), polyketides (2), hybrid NRPS–PKS compounds (3), terpenes (4), alkaloids (5), RiPPs (6) and a further class example (7).

1.2.4 Secondary metabolism and ecological function

The production of secondary metabolites also plays a central ecological role. These compounds are not mere by-products of metabolism but function as adaptive tools that enable microorganisms to persist, compete, and communicate in dynamic environments (Hibbing *et al.,* 2010). The corresponding BGCs have undergone extensive modification—through mutation, gene duplication, recombination and horizontal gene transfer—to optimise the production of compounds that confer a selective advantage in specific niches (Chevrette *et al*., 2020).

Antibiotics and antifungals exemplify defensive molecules that can provide protection against competing microorganisms, shaping niche structure and influencing microbial community composition (Deveau *et al.,* 2018). For example, *Streptomyces* species have been shown to produce streptomycin and tetracycline that inhibit diverse soil bacteria (Procópio *et al.,* 2012), while *Bacillus subtilis* secretes fengycin and surfactin to suppress fungal competitors (Cawoy *et al.,* 2014). Resource acquisition is another key function, particularly under nutrient limitation: siderophores, for instance, enable survival under iron scarcity by efficiently mobilising this essential element. They can also function as competitive weapons by sequestering iron away from neighbouring microorganisms, effectively starving competitors and reshaping community structure (Kramer *et al.,* 2020). Classic examples include enterobactin production by *Escherichia coli* (Gehring *et al.,* 1997) and pyoverdine production by *Pseudomonas aeruginosa* (Schalk & Guillon, 2013), both of which have been shown to confer a strong competitive advantage in iron-limited niches. Other noteworthy siderophores —often derived from NRPS or NRPS–PKS hybrid pathways—include desferrioxamine production by *Streptomyces* spp. and rhodochelin production by *Rhodococcus* spp., which expand the ecological strategies available to Actinomycetota (Traxler *et al.,* 2013; De Carvalho, 2012).

Beyond defense and resource capture, secondary metabolites are also deeply embedded in microbial communication. Quorum sensing molecules have been shown to coordinate multicellular behaviours such as sporulation, biofilm development, and metabolite production, linking environmental sensing to collective microbial strategies (Zeng *et al.,* 2023). A well-studied case is acyl-homoserine lactones (AHLs) production by Gram-negative bacteria such as *Vibrio fischeri*, which regulated bioluminescence in symbiosis with squid hosts. In Actinomycetota, γ-butyrolactones

have been shown to function as signalling molecules that regulate morphological differentiation and secondary metabolism (Fuqua *et al.,* 1994). Similarly, pigments and other protective molecules can act as shields against abiotic stressors—including oxidative stress, UV radiation, or desiccation (Orlandi *et al.,* 2022; Agarwal *et al.,* 2023)—while in some contexts also serving as info-chemicals that may mediate interspecies interactions (Gonçalves & Vasconcelos, 2021). For example, carotenoid produciton by extremophilic bacteria has been shown to provide UV protection in desert environments (Núñez *et al.,* 2025), while melanin produced by *Streptomyces* spp. was shown to aid intolerance to oxidative and radiation stress (Santos *et al.,* 2006) and violacein, another well-studied pigment, with exhibits antioxidant and antimicrobial properties has been linked stress protection to competition (Choi *et al.,* 2015).

Additional functional roles include biosurfactants, which have been shown to facilitate nutrient access, swarming, and biofilm structuring, as well as ecological modulators that may influence interactions with plants or other hosts by affecting colonisation and immune responses (Ron & Rosenberg, 2001). Classic examples include rhamnolipids of *Pseudomonas aeruginosa*, which promotes surface motility and biofilm formation (Glick *et al.,* 2010), and surfactin from *Bacillus subtilis*, which acts both as a biosurfactant and as an antimicrobial compound (Zhen *et al.,* 2023). Lichenysin from *Bacillus licheniformis*, is similarly notable for its activity under extreme conditions (Ongena & Jacques, 2008). In plant–microbe interactions, lipopeptides such as iturins from *Bacillus* species, can suppress phytopathogens and enhance root colonisation, highlighting their dual role in ecological competition and symbiosis (Balleux *et al.,* 2024). Collectively, these examples show that many secondary metabolites act as competitive, defensive, or signalling molecules. However, others—such as osmolytes and photoprotective pigments—primarily support stress tolerance rather than microbial competition. Osmolytes (e.g., ectoine) mitigate osmotic stress, while pigments and mycosporine-like amino acids (MAAs) protect against radiation; these metabolites enhance survival in extreme environments but do not directly inhibit competitors.

These functional categories, together with representative examples, are summarised in Table 1. The ecological importance of secondary metabolites is increasingly being explored, and many pathways show to be closely linked to environmental cues. For instance, siderophore biosynthesis by *Pseudomonas aeruginosa* was found to be

regulated by iron availability via the ferric uptake regulator (*Fur)* system, directly linking environmental nutrient levels to metabolite production (Reinhart & Oglesby-Sherrouse, 2016). Extreme or fluctuating conditions, such as high salinity, thermal stress, nutrient limitation, or intense radiation, shape microbial metabolism by favouring metabolites that enhance survival rather than competition. For example, halophilic Actinomycetota from saline lakes have been shown to up-regulate osmolyte and pigment production under salt stress (Oren, 2010), while thermophilic *Streptomyces* strains adjust their secondary metabolism to produce heat-stable antibiotics (Sayed *et al.,* 2020) and marine cyanobacteria under UV radiation accumulate MAAs, which are believed to function as natural sunscreens (Wada *et al.,* 2013). Thus, secondary metabolic diversity reflects not only microbial competition but also the need to withstand physicochemical stress, a theme further explored in the following section.

Table 1.1 Representative examples of bacterial secondary metabolites and their ecological functions. The table summarises major functional categories—including defence, resource acquisition, signalling, stress protection, and host interactions—with illustrative metabolites and their producing taxa and suggested ecological roles**.** Collectively, these examples highlight the diversity of chemical strategies used by microorganisms to persist, compete, and adapt to environmental challenges.

Functional Category	Ecological Role	Examples	Reference
Antibiotics / Antimicrobials	Defence, niche protection, interference competition.	Rifamycin (*Amycolatopsis* spp.), Juvenimicins (*Micromonospora* spp.)	Baltz, 2008; Kishi *et al.,* 1976
Siderophores	Resource acquisition under iron limitation, survival advantage.	Desferrioxamine (*Streptomyces* spp.), Rhodochelin (*Rhodococcus* spp.)	Traxler *et al.* 2013; Bosello, 2012
Antifungals	Defence against fungal competitors, control of microbial community composition.	Candicidin (*Streptomyces* spp.), Salinisporamycin (*Salinispora* spp.)	Gil and Campelo-Diez, 2003; Matsuda *et al.,* 2009
Quorum Sensing Signals	Coordination of multicellular behaviours: biofilm formation, sporulation, secondary metabolism.	N-acyl homoserine lactones (Gram-negative bacteria), γ-butyrolactones (Actinomycetes)	Parsek & Greenberg, 2000; Kudo *et al.,* 2025
Pigments / Protective Molecules	Protection from environmental stressors, potential signalling or deterrence.	Melanin (*Streptomyces* spp.), Carotenoids (*Micromonospora* spp.)	Santos *et al*. 2006; Carro *et al.,* 2024
Surface-Active Agents (Biosurfactants)	Biofilm structuring, swarming, defence, facilitating access to nutrients.	Surfactin (*Bacillus subtilis*), Lichenysin (*Bacillus licheniformis*)	Ongena and Jacques, 2008; Yeak *et al.,* 2022

Ecological Modulators / Plant Interaction Compounds	Root colonisation, mutualism, modulation of plant immune responses.	Indole-3-acetic acid (IAA) (Rhizobacteria), Rhizobactin (*Pseudomonas* spp.)	Duca *et al*., 2014; Kügler *et al*., 2020

1.2.5 Extreme environments

The ecological functions of secondary metabolites become particularly evident under conditions of environmental stress, where survival can often depend on rapid and versatile chemical responses. Such roles have been widely documented, with evidence that extreme or fluctuating habitats select for unique biosynthetic repertoires that primarily support adaptation to harsh abiotic conditions, and in some cases also influence microbial interactions (Demain & Fang, 2000; Keller, 2019)**.** Extreme environments—including hyper-arid deserts, deep-sea sediments, hydrothermal vents, permafrost soils, and hypersaline ecosystems—combine abiotic stressors such as anoxia, aridity, extreme temperatures, salinity, nutrient scarcity, and radiation. The potential of extremophiles as reservoirs of novel chemistry has been widely demonstrated.

Rather than just being isolated chemical curiosities, these compounds illustrate how microorganisms living in extreme environments have evolved distinct metabolic strategies to persist and withstand resource-limited and physicochemically harsh niches. Thermophilic and deep-sea isolates, for instance, have yielded structurally diverse anticancer compounds, including 2-amino-6-hydroxy-[1,4]-benzoquinone from *Geobacillus* sp. E263 (Xu *et al.,* 2017), akazamycin/actinofuranone from *Nonomuraea* sp. AKA32 (Yang *et al.,* 2019), and trienomycins J–H from *Ochrobactrum* sp. OUCMDZ 2164 (Fan *et al.,* 2018). These examples highlight how thermophiles use chemically sophisticated molecules to mediate stress tolerance and, in some contexts, microbial interactions, in deep-sea habitats. In cold marine ecosystems, *Paenibacillus* sp. SVB7, isolated from Arctic sediments, produced the rare lipodipeptides svalbamides A and B (Du *et al.,* 2021). Beyond their chemopreventive activity, these lipodipeptides likely contribute to stress tolerance and survival under low-temperature, oligotrophic conditions, and have been suggested to influence microbial interactions, although their precise ecological role remains unclear. Likewise, *Pseudoalteromonas* sp. WY3, associated with Antarctic krill, harbours BGCs predicted to biosynthesise 4-HBA with antimicrobial and anticancer

activity (Wang *et al.,* 2024), although these pharmacological properties are unlikely to reflect its natural ecological function.

Additionally, hydrothermal-vent *Streptomyces* sp. SCSIO ZS0520 has been shown to biosynthesise actinopyrones, elaiophilins, and minipyrones with potent antimicrobial properties (Zhang *et al.,* 2022). Similarly, *Halomonas* sp. from hypersaline lakes has been shown to produce diketopiperazines and macrolactins that exhibit broad-spectrum antimicrobial activity (Perumal *et al.,* 2024), which illustrates the potential ecological roles of chemical communication and defense molecules in stabilising microbial communities in extreme, high-salinity environments. While quantitative comparisons of BGC abundance across extremophiles and mesophiles remain limited, current examples suggest that extreme environments may select for distinctive biosynthetic capacities, shaping microbial survival and ecological interactions.

Extreme environments are considered promising sources of novel chemistry, although current genome-mining evidence does not necessarily indicate that extremophiles possess intrinsically larger biosynthetic repertoires than mesophilic organisms. Rather, their apparent novelty is partly a consequence of being understudied, especially given that a substantial fraction of actinomycete BGCs—estimated at 70–90%—remains silent or cryptic under standard laboratory conditions (Rutledge & Challis, 2015; van Bergeijk *et al*., 2020). Together, these observations suggest that extreme environments hold considerable potential for uncovering unexplored metabolic diversity with ecological and applied relevance.

1.3 Actinomycetes biology

Actinomycetes (from the Greek “aktis” = ray and “mykes” = fungus) are Gram-positive filamentous bacteria, mostly aerobic, with a high genomic G+C content (Barka, *et al.* 2016; Segaran *et al.,* 2017). Their cell wall exhibits distinct bacterial characteristics, consisting of a thin phospholipid bilayer (derived from muramic acid) with embedded proteins and peptides, unlike fungi which contain sterols in their membrane (Bonifaz-Trujillo, 2015). The phylum Actinomycetota (formerly Actinobacteria) is among the largest in the bacterial domain, comprising six assigned classes (*Acidimicrobiia, Actinomycetales* [commonly referred to as ‘actinomycetes’]*, Coriobacteriia,*

Nitriliruptoria, Rubrobacteria, and *Thermoleophilia*) and approximately 35 recognised orders according to the latest taxonomic revisions (Freese *et al.,* 2025).

Strains are widely distributed in the environment, and they are found in both terrestrial and marine ecosystems, as well as extreme environments (Jensen, *et al.* 2005; Takahashi & Nakashima, 2018). Their abundance in soil has been estimated to range from 10^4 to 10^8 cells per gram, with members of the genus *Streptomyces* typically dominating these communities (Barka, *et al.* 2016; Takahashi & Nakashima *et al.,* 2018; Alam *et al.,* 2022). In research practice, actinomycetes are commonly divided into *Streptomyces*—the most extensively studied due to their ease of cultivation and prolific production of secondary metabolites—and so-called rare actinomycetes (*Micromonospora, Salinispora, Nocardiopsis*, among others), which are less frequently isolated and studied (which is where the term 'rare' comes from) but have been increasingly recognised as important sources of chemically novel metabolites (Ngamcharungchit *et al.,* 2023; Ezeobiora *et al.,* 2022). This distinction has become central in natural product discovery and underpins later sections of this thesis.

They display a broad spectrum of morphologies—from coccoid forms to fragmenting hyphae— (Subramani & Sipkema, 2019; Ezeobiora *et al.,* 2022); and can be distinguished by the presence or absence of aerial or substrate mycelium, spore structure (single cells, chains or sporangia), pigmentation (ranging from brown, red, yellow and orange to blue, green and purple) and colony morphology (Barka *et al.,* 2016; Ngamcharungchit *et al.,* 2023). Colonies may appear elevated or flat, with textures from soft and pasty to firm and compact. Surfaces can be smooth, wrinkled, granular or scaly, and are often structured into concentric radial zones depending on the strain, culture medium and age of the colony (Barka *et al.,* 2016; Devanshi *et al.* 2021). At the genomic level, members of this phylum possess a typical prokaryotic organisation with a single chromosome, which may be circular or, in the case of *Streptomyces*, linear. Genome sizes vary from approximately one (e.g., *Tropheryma whipplei* 0.92 Mb: Raoult *et al.,* 2003) to 13 Mb (e.g. *Nonomuraea* sp. ATCC 55076 13.1 Mb: Nazari *et al.,* 2017), reflecting their physiological and metabolic diversity (Gao and Gupta, 2012; Lewin *et al.,* 2016).

1.3.1 Growth and reproduction

Actinomycetes typically display fungal-like growth through the formation of hyphae and often reproduce by sporulation, a strategy that helps them survive in extreme environments (Barka *et al.,* 2016; van der Meij *et al.,* 2017). On solid media, they form colonies that may appear bacteriform or filamentous, whereas in liquid media they typically grow as mycelial aggregates or granules (Bonifaz-Trujillo, 2015). The general life cycle of actinomycetes grown on solid medium (Fig. 1.2) begins with the germination of free spores. When conditions are favourable, spores produce a germ tube that develops into a substrate mycelium (hyphae embedded within the medium), marking the vegetative growth phase. Expansion at this stage occurs through a combination of tip extension and branching (Chater & Losick, 1997; Barka *et al.,* 2016). Under nutrient limitation, abiotic stress, or microbial competition, cells can switch to aerial growth with secondary mycelium rising above the surface, often adopting a spiral morphology. Septa then partition these aerial hyphae, producing chains of spores, each harbouring a single chromosome copy (Chater & Losick, 1997). Concurrently, the substrate mycelium undergoes autolysis, releasing amino acids, sugars, nucleotides, and lipids (Fernández & Sánchez, 2002). At this stage, actinomycetes can also initiate secondary metabolite production (Bibb, 2005; van Wezel & McDowall, 2011). It has been proposed that antibiotic biosynthesis serves as a protective mechanism, preventing competitors from exploiting the nutrients released during mycelial degradation (Barka *et al.,* 2016). Once mature, spores are released into the environment to complete the cycle (Jakimowicz and van Wezel, 2012). These generated spores can be of different types and lengths. For example, strains of the genus *Frankia* form vesicles or sporangia, which are essentially spore sacs, while members of the genera *Streptomyces, Nocardioides, Kitasatospora, Streptoverticillium*, and some *Nocardia* spp. produce very long chains of up to 100 spores. Several actinomycetes (e.g. *Rhodococcus*, *Corynebacterium*, *Gordonia*) do not reproduce by sporulation, but instead, they proliferate through binary fission, displaying growth patterns more like non-filamentous bacteria (Conville and Witebsky, 2015).

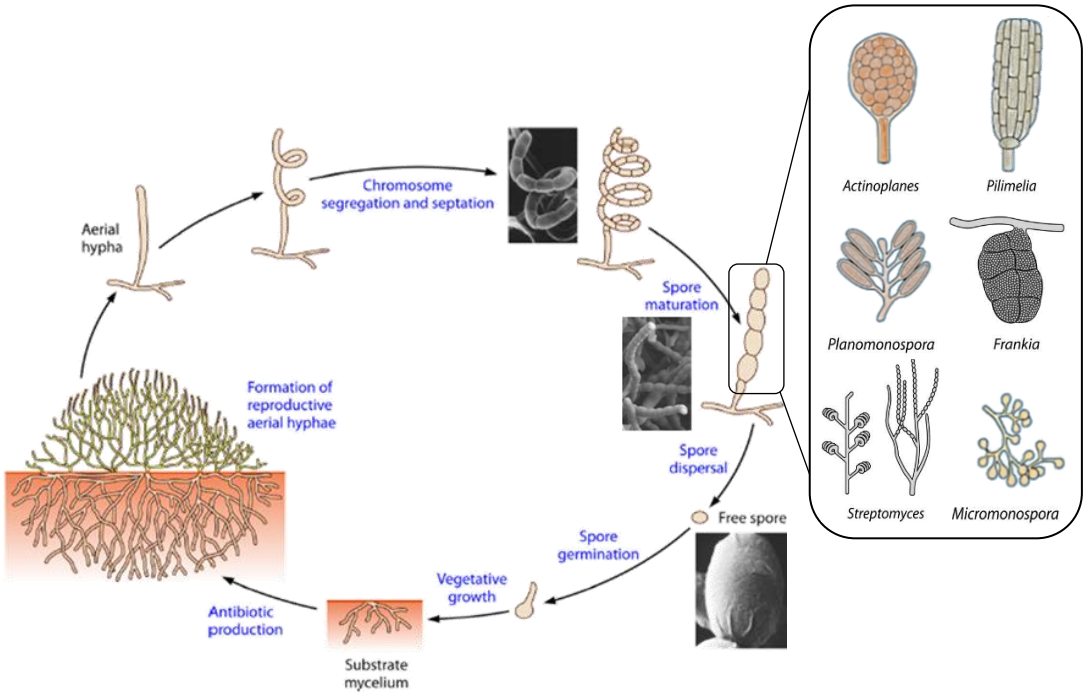

Figure. 1.2 Life cycle of sporulating Actinomycetota. Taken and modified from Barka *et al.,* 2016.

1.3.2 Actinomycete isolation methods

The isolation and cultivation of actinomycetes is often challenging due to their slow growth and the presence of faster-growing competing organisms (Ezeobiora *et al.,* 2022). Many genera form spores that are highly resistant to desiccation, heat, and chemicals (Subramani & Sipkema, 2019). This characteristic can be exploited to suppress non-target microbes during the isolation process (Ezeobiora *et al.,* 2022). In addition, genera such as *Rhodococcuss* have cell walls rich in mycolic acids, which confer resistance to desiccation and chemical stress (de Carvalho, 2010). In such cases, selective isolation relies less on spore survival and more on metabolic enrichment strategies. These enrichment-based strategies have been successfully applied in practice. For example, *Rhodococcus daqingensis* was isolated from petroleum-contaminated soil on humic acid-vitamin agar supplemented with cycloheximide and nalidixic acid (antibiotics), which suppressed faster-growing fungi and bacteria, enriching for the target organism (Wang *et al.,* 2019). Another example

includes *Rhodococcus phenolicus*, isolated using phenol (a xenobiotic) as the sole carbon source, showing that these actinomycetes can be enriched under harsh chemical conditions (Rehfuss, 2006).

Sample pre-treatment methods that take advantage of spores include air-drying under laminar flow (Fang *et al.,* 2017), heat shock (Rashad *et al.,* 2015), calcium carbonate treatment (Ezeobiora *et al.,* 2022), exposure to phenol, microwave irradiation (Ezeobiora *et al.,* 2022; Wang *et al.,* 2013), centrifugation (Kumar & Jadeja, 2016), and sonication (Ezeobiora *et al.,* 2022) to separate propagules from pellets. Selective media are often supplemented with antibiotics and antifungals tailored to suppress specific groups of competitors: for example, cycloheximide and nystatin inhibit fungal growth, while nalidixic acid, rifampin, and penicillin reduce the growth of fast-growing Gram-negative bacteria (Ezeobiora *et al.,* 2022; Subramani & Aalbersberg, 2013). Practical applications if these approaches include phenol and SDS treatment of mangrove sediments, which facilitated the recovery of rare genera such as *Actinomadura, Nocardia, Micromonospora, Rhodococcus, and Verrucosispora* (Hong *et al.,* 2009), while similar strategies (UV, microwave, and heat shock) applied to Norwegian marine sediments enabled the isolation of *Nocardiopsis, Pseudonocardia,* and *Streptosporangium* (Bredholdt *et al.,* 2007). Across studies, these pre-treatments consistently enrich for rare actinomycetes, highlighting that combining physical and chemical stress with selective media increases isolation efficiency (Maldonado *et al.,* 2009; Pathom-aree *et al.,* 2006). For example, phenol treatment (1.5%) of Indian forest soils enabled, 40% recovery of rare actinomycete strains such as *Micromonospora, Actinoplanes, Actinomadur*a and *Microbispora* (Bundale *et al.,* 2018).

Apart from physical and chemical pre-treatments, selective isolation can also rely on sample dilution, a standard and essential procedure in microbial isolation workflows. This is generally done in sterile seawater, saline, or Ringer's solution before inoculation into the culture medium. The latter typically contains complex macromolecules such as casein, chitin, starch, or humic acid as carbon and nitrogen sources. This strategy has yielded good results: for example, 68 actinomycete strains were isolated from marine sediments of Valparaíso Bay, Chile using seawater-diluted samples on selective media (Claverías *et al.,* 2015); 73 strains of diverse genera were recovered from Arctic Ocean sediments by applying saline dilutions combined with low-nutrient media (Yuan *et al.,* 2014); and nearly 300 isolates were obtained from

marine sediments when variety of media and this selective isolation techniques (dry, dilution, heat, freeze) were used (Jensen *et al.,* 2005). Collectively, these results demonstrate that coupling dilution methods with nutrient-limited selective media significantly enhances the recovery of rare actinomycetes from diverse marine ecosystems.

1.3.3 The genera *Streptomyces*: an overview

Since the discovery of *Streptomyces griseus* in the mid-20th century, the family Streptomycetaceae within the Actinomycetota phylum has been extensively studied (Schatz & Waksman, 1945). Today, *Streptomyces* is recognised as the largest genus of the family, both in terms of taxonomic diversity and ecological distribution, with over 1,100 described species spanning terrestrial, marine, and extreme environments (Schlimpert & Elliot, 2023). Historically, this genus provided the first examples of actinomycete-derived antibiotics, including actinomycin from *S. antibioticus* (Waksman & Woodruff, 1940), streptothricin from *S. lavendulae* (Waksman & Woodruff, 1942), and streptomycin from *S. griseus* (Schatz & Waksman, 1944). Later studies revealed that *Streptomyces* accounts for the majority of bioactive natural products, with more recent estimates suggesting that they produce 70–80% of all natural compounds with pharmacological or agrochemical applications (Harir *et al.,* 2018; Abdel-Razek *et al.,* 2020; Alam *et al.,* 2022). It should be noted, however, that this percentage reflects the disproportionate research attention given to *Streptomyces*, rather than an unbiased measure of global metabolic diversity. These compounds include many clinically important antibiotics, such as tetracyclines, macrolides (e.g., erythromycin: McGuire *et al.,* 1952), glycopeptides (e.g., vancomycin: McCormick *et al.,* 1956), lipopeptides (e.g., daptomycin: Debono *et al.,* 1987), and β-lactamase inhibitors (e.g., clavulanic acid: Howart *et al.,* 1976). Beyond this historical phase, *Streptomyces* has remained a prolific source of novel metabolites (Quinn & Dyson, 2024). Contemporary examples include daptomycin from *S. roseosporus*, a lipopeptide antibiotic widely used against multidrug-resistant Gram-positive pathogens (FDA approval 2003) (Steenbergen *et al.,* 2005), and fidaxomicin from *S. fidaxomicini*, approved in 2011 for the treatment of *Clostridioides difficile* infections (Daniels & So, 2011). More recently, genome-guided approaches have uncovered metabolites such as malacidins, calcium-dependent antibiotics active against multidrug-resistant pathogens (Hover *et al.,* 2018), and tiancimycins, potent

antitumor compounds from *Streptomyces* sp. CB03234 (Yan *et al.,* 2016), highlighting the continuing biomedical relevance of the genus.

1.3.4 Rare actinomycetes

“Rare actinomycetes” is a term used for genera that are infrequently recovered under standard isolation procedures, despite being taxonomically diverse and widespread across multiple environments (Parra *et al.,* 2023) — This designation does not necessarily imply ecological scarcity, but rather reflects their limited recovery under conventional isolation conditions. Indeed, rare actinomycetes have been reported from a remarkable diversity of habitats, ranging from soils (e.g. *Micromonospora*, *Actinoplanes*, *Lentzea, Microbispora*) (Seong *et al.,* 2001), to caves *(Actinoplanes, Nocardioides, Micromonospora, Agromyces, Oerskovia, Rhodococcus)* (Long *et al.,* 2019), insect symbionts such as *Pseudonocardia* associated with leafcutter ants (Goldstein & Klassen, 2020), and aquatic or marine systems, including freshwater lakes and deep-sea sediments (*Actinomadura, Nocardia, Salinibacterium, Streptomyces, Rhodococcus, Kocuria*) (Pathom-aree *et al.,* 2006; Benhadj *et al.,* 2019; Yuan *et al.,* 2014). Their ability to colonise extreme environments — such as hypersaline lagoons, hydrothermal vents, or high-temperature springs — further illustrates their ecological adaptability (Jose & Jebakumar, 2013; Saito *et al.,* 2020; Zamora-Quintero *et al.,* 2022). This ecological breadth, combined with their historical under-sampling and understudied nature and novelty, means that rare actinomycetes often carry biosynthetic gene clusters (BGCs) that show low similarity to known pathways, making them promising sources of new metabolites, since fewer studies mean more novelties to be discovered. Recent large-scale surveys of extreme environments reinforce this idea. For instance, from the Karakum Desert in Turkmenistan, 56 Actinomycetota strains were isolated, of which nearly half represented rare actinomycete genera such as *Jiangella*, *Microbacterium*, *Nocardioides*, and *Kribbella*. Genome sequencing and antiSMASH analyses of representative strains revealed an abundance of unique BGCs with the potential to encode novel secondary metabolites, many of which showed <10% similarity to any known cluster, reflecting how little these lineages have been sampled and studied historically. Within this collection, *Jiangella aurantiaca* strain 8K307^T was particularly striking, as it contained BGCs distantly related to tetarimycin A (~5% gene identity)

and other yet-uncharacterised scaffolds, demonstrating that rare actinomycetes from underexplored habitats can provide a reservoir of poorly characterised biosynthetic pathways with potential to yield new chemical scaffolds (Saygin *et al.,* 2025).

Remarkably, rare actinomycetes collectively span more than 220 genera, yet many remain understudied (Hug *et al.,* 2018; Ezeobiora *et al.,* 2022). Between 2007 and mid-2013 alone, around 80 new metabolites were isolated only from 38 marine rare actinomycete strains across 15 genera, notably *Salinispora*, *Verrucosispora*, *Nocardiopsis*, *Actinoalloteichus*, and *Micromonospora* (Subramani and Sipkema, 2019). This discovery rate surged from mid-2013 to 2017, with 167 additional new compounds reported from 58 strains covering 24 genera—including over 40 from *Nocardiopsis*, 37 from *Micromonospora*, and 21 from *Salinispora* (Subramani and Sipkema, 2019). More recently, between 2018 and 2022, over 200 additional compounds were reported across more than 30 genera, with *Nocardiopsis*, *Micromonospora*, *Nonomuraea*, and *Actinokineospora* among the most prolific metabolite-producing lineages, reflecting a steady, but not unprecedented, rate of discovery (Parra *et al.,* 2023).

These examples highlight the growing importance of exploring “rare” lineages as complementary sources of chemical diversity, especially at a time when the rediscovery of known metabolites produced by *Streptomyces* remains a persistent challenge. For instance, clinically relevant metabolites such as salinosporamide A (Feling *et al.,* 2003) from *Salinispora tropica* (an FDA-approved proteasome inhibitor) (Jensen, 2022) and nocardithiocin from *Nocardia pseudobrasiliensis* (a potent thiopeptide antibiotic) with strong activity against rifampicin-resistant *Mycobacterium tuberculosis* (Mukai *et al.,* 2009) illustrate the therapeutic promise and the chemical novelty that rare actinomycetes contribute. Additional examples include lomaiviticin A and B from *Micromonospora* spp., highly cytotoxic glycosides with antitumor potential (He *et al.,* 2001), and kanglemycins from *Amycolatopsis rifamycinica* which aresemisynthetic rifamycin analogues active against rifampicin-resistant *Mycobacterium tuberculosis* (Peek *et al.,* 2018). Similarly, *Actinoplanes* spp. have yielded teicoplanin (Taurino *et al.,* 2011), a clinically important glycopeptide antibiotic widely used as a vancomycin alternative. Together, these cases underscore that rare actinomycetes are not only prolific metabolite producers but also valuable contributors to the clinical pipeline, with multiple examples already in therapeutic use.

However, despite their biosynthetic capacity, rare actinomycetes are underrepresented at the genomic level compared to *Streptomyces*. Of the 45,956 Actinomycetota genomes available at NCBI, only 630 correspond to rare actinomycete strains with reference status (versus tens of thousands of *Streptomyces*). Furthermore, in the MIBiG database, 74% of the known BGCs of the phylum are assigned to *Streptomyces*, leaving only a quarter for all other genera combined (Parra *et al.,* 2023). This inequality suggests that rare genera may harbor much greater chemical potential than previously perceived, and that intensified study of them could eventually surpass the discovery potential offered by *Streptomyces* which highlights the importance of genomics as a methodological bridge to systematically explore the potential of rare actinomycetes.

1.4 Microbial genomics

1.4.1 Genome sequencing and delimitation of new species

The term Bacterium marked one of the earliest attempts to name and classify rod-shaped cells (Murray & Holt, 2005). In fact, all early classification was largely based on morphology, biochemical characteristics, and pathogenicity, alongside the source of isolation (Janda & Abbott, 2002; Baron, 1996). In 1964, Sokal and Sneath proposed using biochemical tests to improve species characterisation, including the calculation of similarity coefficients between strains — a quantitative measure (ranging from 0 to 1) that reflected the proportion of shared phenotypic traits. For example, if two strains share 90 out of 100 biochemical traits, their similarity coefficient is 0.90, indicating a high phenetic affinity. Sokal and Sneath further refined these associations by introducing formulas to account for ambiguous (“NC”) character states, calculating the coefficient even when data was incomplete — a method that involved averaging the similarity across possible character-state combinations (Sokal & Sneath, 1963). By the 1980s, with the advent of nucleic acid extraction techniques, DNA–DNA hybridization (DDH) was employed to refine species delimitation. This method measured genomic similarity by evaluating how well single-stranded DNA from two strains can reconnect — strains exhibiting ≥ 70 % hybridization (and similar melting profiles) were typically considered conspecific, offering a numerical and reproducible species boundary (Richter and Rosselló-Móra, 2009). Later, the development of the

polymerase chain reaction (PCR) allowed for the widespread use of the 16S rRNA gene as a phylogenetic marker. Its utility lies in its moderate length (~1,500 base pairs (bp)), universal presence in bacteria and archaea, and the combination of conserved (which facilitate universal primer design) and hypervariable (which enable taxonomic discrimination) regions (Yang *et al.,* 2016; dos Santos *et al.,* 2019; Church *et al.,* 2020). Based on this, a similarity threshold of 98.7–99% was proposed for species delimitation, depending on the genus (Stackebrandt and Ebers, 2006), establishing the 16S rRNA gene as a widely accepted reference in bacterial taxonomy. Nevertheless, its discriminatory power is inherently limited due to the slow evolution of the gene, which results in insufficient sequence variability to distinguish closely related taxa. This means that distinct species can share nearly identical 16S rRNA gene sequences, while some strains within the same species may display unexpectedly low similarity due to intragenomic heterogeneity or sequencing of different operon copies (Větrovský & Baldrian, 2013; Hassler *et al.,* 2022). For example, *Bordetella hinzii* strain H720 shows 99% sequence similarity with other *Bordetella* species such as *B. pseudohinzii* and *B. parapertussis*, reflecting recent divergence and conservation of the 16S rRNA gene, despite ecological and phenotypic differences. Conversely, two *Flavobacterium psychrophilum* strains may share only 93% similarity in this region — likely due to the presence of divergent 16S rRNA gene copies within their genomes — while it is equally possible that sequences of *Flavobacterium* species can exceed 98% identity, demonstrating that the 16S rRNA gene alone cannot reliably resolve all taxonomic relationships (Ivanov *et al.,* 2016; Ramsrud *et al.,* 2007; Strepparava *et al.,* 2014).

For this reason, whole-genome sequencing (WGS) has become a central tool in bacterial systematics, enabling precise species delimitation and robust phylogenomic analyses. Its adoption accelerated with the introduction of high-throughput platforms such as Illumina NovaSeq, PacBio HiFi, and Oxford Nanopore, which dramatically reduced sequencing costs to the low hundreds of USD per bacterial genome (Bogaerts *et al.,* 2024; Abdi *et al.,* 2024). WGS is defined as the process of determining the complete nucleotide sequence of an organism's DNA (Bagger *et al.,* 2024). Its origins can be traced back to the chain-termination method developed by Frederick Sanger in 1977, which enabled the sequencing of small viral genomes such as bacteriophage λ (~48.5 kb) (Sanger *et al.,* 1977). Over the following three decades, Sanger sequencing dominated the field, particularly for small genomes, until its landmark application in 1995 resulting in the first complete bacterial genome,

Haemophilus influenzae (Fleischmann *et al.,* 1995). The next major advance was the introduction of next-generation sequencing (NGS), characterised by massively parallel sequencing reactions. The first commercial platform, Roche/454, was introduced in 2005 (Margulies *et al.,* 2005), followed by Illumina sequencing-by-synthesis technology, which remains the dominant short-read system today due to its high accuracy and throughput. These approaches are termed “short-read technologies”, producing reads between 50 and 300 bp (Kremer *et al.,* 2017), in contrast to the ~800–1000 bp typical of Sanger sequencing.

Subsequently, third-generation sequencing (TGS) introduced the ability to generate long reads in real time without prior amplification. These technologies fall under the category of single-molecule real-time sequencing (SMRT). They include the SMRT technology from Pacific Biosciences (PacBio), capable of producing reads longer than 10 kilobase (kb) (Heather & Chain, 2016), and Oxford Nanopore Technologies, which can produce reads ranging from 10 kb up to 880 kb (Delahaye & Nicolas, 2021). Despite their higher error rates (~13% for PacBio; 6–10% for Nanopore) (Koren *et al.,* 2013), these platforms are particularly valuable for resolving repetitive or complex genomic regions. Once sequencing reads are generated, hybrid assemblies can be performed, integrating the accuracy of Illumina short reads with the continuity of PacBio or Nanopore long reads. This approach has become standard practice because it yields more accurate and complete genomes. For example, the hybrid assembly of *Corynespora cassiicola* strain XJ genome reduced the scaffold count from 244 to 23 and improved the N50 from 2.51 Mb to 4.63 Mb, reaching 99.5% completeness (parameters defined below) (Xu *et al.,* 2021). This improvement illustrates how hybrid strategies markedly enhance assembly continuity and overall quality.

Genome assembly is the process of reconstructing the genome from raw sequencing data by computationally aligning and merging overlapping reads into longer contiguous sequences. The fundamental unit of assembly is the contig (from “contiguous sequence”), which represents a stretch of DNA assembled without gaps from overlapping reads (Pop, 2009). Contigs are then linked into larger structures called scaffolds, which integrate additional information — such as mate-pair reads, optical maps, or chromosomal contact data — to order and orient contigs, often leaving unresolved gaps between them (Nagarajan & Pop, 2013; Salzberg *et al.,* 2012). For example, the hybrid assembly of *Escherichia coli* K-12 using Illumina short

reads and Oxford Nanopore long reads produced a single scaffold corresponding to the complete circular chromosome, while assemblies relying only on short reads typically yield dozens to hundreds of fragmented contigs (Koren *et al.,* 2012).

To evaluate the quality of an assembly, several parameters are commonly reported. The number of contigs provides a first indication of completeness, with fewer contigs generally reflecting a contiguous genome (Chun *et al.,* 2018). The N50 statistic, defined as the minimum contig length for which 50% of the genome is covered by contigs of that size or longer, is widely used to measure assembly continuity (Salzberg *et al.,* 2012), indicating how well the genome has been assembled into larger, continuous pieces. A higher N50 generally suggests a better assembly with fewer, larger contigs. For instance, the draft assembly of the Human Genome Project in 2001 had an N50 of only ~57 kb (International Human Genome Sequencing Consortium, 2001). In contrast, the recent telomere-to-telomere assembly of the human genome (T2T-CHM13) achieved a contig N50 of ~25 Mb (Nurk *et al.,* 2022), reflecting the dramatic improvement that was enabled by long-read technologies. The coverage is also an indicator of quality and is defined as the average number of times each base is sequenced, and therefore it reflects how well the genome is represented; bacterial assemblies are typically considered reliable above 30× coverage (Donkor, 2013; Schatz *et al.,* 2010). Finally, genome size and completeness are assessed by comparing the assembly length to the expected size and by searching for sets of universal single-copy genes, as implemented in tools such as BUSCO (Benchmarking Universal Single-Copy Orthologs) (Simão *et al.,* 2015) which assesses genome completeness by searching for the presence of universal single-copy orthologs, providing a measure of how well essential genes are represented in the assembly (Simão *et al.,* 2015). A wide range of bioinformatic tools are available for genome assembly and quality assessment. Among the most widely used are Flye**,** which is specifically designed for assembling long-read data from technologies such as Oxford Nanopore and PacBio and is particularly effective for microbial genomes (Kolmogorov *et al.,* 2019), and QUAST (Quality Assessment Tool for Genome Assemblies), a reference-based tool that reports key metrics such as contig number, N50, and genome size, allowing straightforward evaluation of assembly quality (Gurevich *et al.,* 2013). Together, these tools provide a reliable framework to generate accurate, contiguous, and biologically meaningful genome assemblies, which form the basis for downstream phylogenomic and genome-mining analyses.

As a result of all this advance, public repositories like National Center for Biotechnology Information (NCBI) now offer hundreds of thousands of bacterial genomes, with notable representation of major phyla such as Pseudomonadota (previously known as Proteobacteria) with 1,560,459 genomes; Bacillota (formerly Firmicutes) with 635,062 genomes, and Actinomycetota with 99,811 genomes (Sayers *et al.,* 2024). In 2020, the International Journal of Systematic and Evolutionary Microbiology and the International Committee on Systematics of Prokaryotes recommended that valid publication of new prokaryotic species should include WGS data and genome-based metrics such as Average Nucleotide Identity (ANI) and digital DNA-DNA hybridisation (dDDH) (Zong, 2020). As such, they are becoming the genomic standard for species delimitation effectively replacing labour-intensive laboratory DDH experiments (Auch *et al.,* 2010; Nouioui and Sangal; *et al*., 2022). ANI is an index that represents the mean percentage of identical nucleotides across all orthologous genomic regions shared by two genomes, typically computed using sliding-window comparisons; where values of ≥ 95–96 % indicate the same species (Goris *et al.,* 2007; Richter & Rosselló-Móra, 2009). dDDH simulates the traditional hybridization experiment *in silico* by aligning genome sequences, estimating the proportion of shared DNA, applying statistical corrections (Meier-Kolthoff *et al.,* 2013) and providing a value that mimics the experimental DDH, keeping a threshold of 70 % as the accepted species boundary (Chun *et al.,* 2018).

Online platforms such as the Genome-to-Genome Distance Calculator (GGDC) and JspeciesWS automate these analyses: for example, by uploading draft genome assemblies, users can instantly obtain ANI or dDDH scores alongside confidence intervals, allowing direct comparison against taxonomic cut-offs. The GGDC computes dDDH values using three distinct formulas. Of these, formula 2 is generally recommended, as it is independent of genome size and yields robust estimates, even when working with incomplete draft genomes (Auch *et al.,* 2010). Specifically, formula 2 (GBDP formula d4) is defined as the sum of all identities found in high-scoring segment pairs (HSPs) divided by the overall HSP length. These genome-based metrics have driven numerous reclassifications, such as the transfer of *Clostridium difficile* to *Clostridioides difficile* (Lawson *et al.,* 2016) and the reassignment of *Lelliottia aquatilis* as *Lelliottia jeotgali* (Wu & Zong, 2019). In marine actinomycetes, comparative ANI/dDDH analyses helped delimit cryptic *Salinispora* species, revealing genomic divergence that was not apparent from 16S rRNA gene comparisons alone (Millan-Aguinaga *et al.,* 2017; Roman-Ponce *et al.,* 2020).

These methodological advances, together with online platforms, have become essential tools for delineating bacterial species in the genomic era. Beyond taxonomy, they are also critical for obtaining complete and biologically informative assemblies, since fragmented genomes can bias downstream analyses such as metabolic pathway reconstruction or phylogenomic inference (Chen *et al.,* 2020; Mirete *et al.,* 2025). In particular, accurate and well-annotated genomes provide the foundation for genome-mining approaches, which are increasingly used to explore the secondary metabolite potential of microorganisms.

1.4.2 Genome mining

With advances in sequencing technologies, the number of available bacterial genomes for exploration increased dramatically, from only a few dozen complete genomes in the early 2000s to more than 2,787,189 bacterial genomes deposited in NCBI by 2025. However, the vast volume of available data made manual annotation of BGCs a slow and error-prone process, which in turn drove the emergence of the first *in silico* tools for this task. This expansion gave rise to the concept of genome mining, defined as the application of bioinformatic algorithms to detect gene clusters with biosynthetic potential, particularly those responsible for producing natural products such as antibiotics and other bioactive compounds or BGCs. Although BGCs are strongly associated with secondary metabolism, automated genome-mining tools can occasionally annotate primary metabolic pathways—such as fatty acid synthases or certain terpene synthases—as putative BGCs due to shared domain architectures or gene organisation patterns (Medema *et al.,* 2011; Rutledge & Challis, 2015). ClustScan was the first of these, designed for the rapid and semi-automated annotation of DNA sequences encoding modular biosynthetic enzymes, including polyketide synthases (PKS), non-ribosomal peptide synthetases (NRPS), and hybrid PKS/NRPS enzymes (Starcevic *et al.,* 2008). This was followed by NP.searcher (Li *et al.,* 2009) and SBSPKS (Anand *et al.,* 2010), although these tools were generally limited to the analysis of core genes involved in type I polyketide and non-ribosomal peptide synthesis. These early platforms marked the beginning of the transition towards more comprehensive systems, which eventually culminated in the development of antiSMASH as the current gold standard for BGC annotation.

antiSMASH (Antibiotics and Secondary Metabolite Analysis Shell) is the most widely used bioinformatic platform for the identification and annotation of BGCs in microbial genomes (Blin *et al.,* 2025). It is widely adopted because it allows rapid, standardised, and large-scale screening of genomes, serving as a first-pass filter to identify candidate BGCs before experimental validation, and providing a comparative framework across studies (Medema, *et al*, 2011). This tool can identify all major classes of secondary metabolite biosynthetic pathways while providing detailed functional annotations and even predicting chemical structures (Medema *et al.,* 2011). It also integrates multiple prediction algorithms to scan genomic sequences for genes encoding key biosynthetic domains, such as PKS, NRPS, terpenes, and ribosomally synthesised and post-translationally modified peptides (RiPPs). The tool then compares the identified clusters against a database to assess their similarity to known reference clusters (Kautsar *et al.,* 2019). The similarity percentage reported by antiSMASH reflects the proportion of genes or biosynthetic domains within the predicted cluster that share similarity with those in a reference BGC. A high percentage indicates that the cluster is closely related to a characterised pathway, whereas lower percentages may suggest a divergent or potentially new biosynthetic pathway. However, these values should be interpreted cautiously, as they are not strict measures of chemical identity but rather gene similarity at the cluster level (Blin *et al.,* 2021).

Despite its widespread adoption, antiSMASH presents several limitations. First, its predictions are limited to gene clusters with detectable homology to known biosynthetic genes, which means that highly novel or cryptic pathways may remain undetected (Weber *et al.,* 2015). For instance, in one systematic analysis of bacterial genomes from food-fermentation environments, antiSMASH failed to recover BGCs of novel types, because the reference library lacked analogous clusters (Du *et al.,* 2023). Second, the tool often overpredicts biosynthetic potential, reporting partial or fragmented clusters that may not correspond to functional metabolites. In draft genomes of *Salinispora* spp., Ziemert, *et al*. (2014) reported multiple fragmented PKS/NRPS predictions by antiSMASH that lacked synteny with functional clusters, demonstrating the risk of false positives in incomplete assemblies. Third, antiSMASH cannot reliably predict the regulation, expression, or ecological relevance of the detected BGCs, so the presence of a cluster does not guarantee metabolite production. Additionally, while antiSMASH can propose putative chemical structures for certain compound classes, these predictions are often incomplete or imprecise,

especially for hybrid or atypical clusters (Medema *et al.,* 2015). Ultimately, while antiSMASH is an invaluable tool for guiding genome mining and prioritising candidate clusters, the gold standard for natural product discovery remains the isolation, chemical characterisation, and biological testing of the corresponding metabolites.

antiSMASH compares and annotates BGCs using its own library of predicted clusters together with the Minimum Information about a Biosynthetic Gene Cluster (MIBiG) repository, a community-standardised database of experimentally validated BGCs. The latest release, MIBiG 4.0, contains more than 2,700 curated clusters (Zdouc *et al.,* 2025), which can facilitate cross-comparison of predicted BGCs with well-characterised references to assess novelty and function, thereby guiding the discovery of new natural products (Kautsar *et al.,* 2021; Bachmann *et al.,* 2014). Moreover, genome mining has expanded far beyond individual strains, now encompassing large-scale analyses of entire genera and even complex microbiomes. To support this shift, new computational frameworks such as BiG-SCAPE (Biosynthetic Gene Similarity Clustering and Prospecting Engine) and CORASON (Core Analysis of Syntenic Orthologs to Prioritize Natural Product Gene Clusters) were developed (Navarro-Muñoz *et al.,* 2020). While antiSMASH detects and annotates individual clusters, BiG-SCAPE groups them into Gene Cluster Families (GCFs) based on sequence similarity, producing network visualisations where nodes represent clusters and edges denote relationships. The similarity scores generated by BiG-SCAPE are based on domain architecture comparisons, sequence identity, and synteny of BGCs. Clusters that exceed a defined similarity threshold are grouped into the same GCF. This categorisation not only aids in comparative genomics but also allows integration with experimental metabolomic data, thus enabling correlation between BGC families and compound families (the so-called “metabologenomics” approach). CORASON then complements this by reconstructing phylogenetic relationships within these GCFs (Navarro-Muñoz *et al.,* 2020). Together, these methods allow researchers to not only classify BGCs but also identify evolutionary lineages and prioritise unexplored clusters with the highest potential to encode new chemistry, helping to reveal the vast biosynthetic capacity of actinomycetes, including those lineages considered “rare”. For example, in the case of *Micromonospora* sp. ATCC 39149, the applications of these platforms revealed cryptic BGCs encoding new aminoglycoside-like scaffolds. Subsequent genome mining–guided co-culture experiments with a *Rhodococcus* sp. enabled the activation and characterisation of the corresponding biosynthetic pathway, ultimately leading to the discovery of keyicin,

a unique glycosidic antibiotic with antimicrobial activity (Adnani *et al.,* 2017). Similarly, comparative genomics of *Actinoalloteichus hymeniacidonis*, a sponge-associated rare actinomycete, uncovered hybrid NRPS-PKS clusters absent in close relatives, suggesting adaptation to the marine host environment and a source of structurally unprecedented compounds (Schaffert *et al.,* 2016). At a broader taxonomic scale, large-scale comparative genome mining of *Rhodococcus* species revealed a wealth of cryptic BGCs, many of which showed no close similarity to entries in MIBiG, highlighting the utility of network-based approaches for prioritising unexplored biosynthetic diversity (Undabarrena *et al.,* 2021).

Despite these successes, it is important to recognise that network-based genome mining tools such as BiG-SCAPE also present methodological limitations. First, the clustering results are highly sensitive to the input dataset and parameter selection (e.g. similarity thresholds), which may affect the reproducibility of analyses. For example, *Amycolatopsis* isolates showed that modifying the similarity threshold could merge functionally distinct BGCs into the same GCF, obscuring their chemical diversity (Adamek *et al.,* 2018). Second, the tool is designed to work primarily with antiSMASH-annotated clusters, meaning that its accuracy depends on the quality of the initial annotation. For instance, in one study of Actinomycetota, BiG-SCAPE failed to group siderophore-associated BGCs into the same family despite chemical similarity when sequence identity was low (Serna-Cardona *et al.,* 2024). Third, while BiG-SCAPE can identify relationships between clusters, it does not provide direct information on the chemical structures or biological activities of the corresponding metabolites. Consequently, computational predictions must be complemented by experimental workflows that include cultivation under appropriate conditions, fermentation optimisation, compound isolation, structural elucidation, and biological activity testing (Navarro-Muñoz *et al.,* 2020). In this context, metabolomic data should not be viewed as an independent validation strategy, but rather as an integrative component within a broader natural product discovery pipeline. Only through the combination of genome mining, metabolomics, and classical natural product chemistry can predicted biosynthetic potential be translated into chemically and biologically meaningful outcomes.

1.5 Metabolomics

1.5.1 Mass Spectrometry (MS): historical foundations

Mass spectrometry (MS) is one of the most influential analytical technologies in natural products research, with its origins in the early 20th century: for example, J. J. Thomson described positive-ray instruments capable of separating ions by their mass-to-charge ratio (*m/z*) (Thomson, 1913). Francis W. Aston soon refined these ideas: in 1919 he reported isotopic separations (e.g., neon) using a mass-spectrograph, and over the following years developed the technique further (Aston, 1920). These milestones established MS as a tool not only for qualitative detection, but also for precise mass determination and isotopic analysis.

For several decades, MS was primarily applied to gases and volatile compounds because of limitations in ionisation and sample introduction technologies, until the mid-20th century, when gas chromatography (GC) was developed (James & Martin, 1952) and then coupled to mass spectrometry (GC-MS) in the late 1950s (e.g., Gohlke, 1959). GC provides chromatographic separation primarily based on volatility and boiling point, and by coupling separation and detection, GC-MS transformed analytical chemistry, enabling the structural elucidation of complex mixtures. The subsequent development of liquid chromatography–mass spectrometry (LC-MS) extended the technique to non-volatile and thermally labile metabolites and has become widely adopted in natural-products research because of its high sensitivity and broad chemical scope (Pitt, 2009). LC-MS enables compounds to be chromatographically separated according to polarity and other physicochemical properties, eluting at distinct retention times before entering the mass spectrometer, where they are ionised and detected as ions by their mas to charge (*m/z*) ratio (Mukherjee, 2019).

Among available ionisation techniques, electrospray ionisation (ESI) emerged as the method of choice in microbial metabolomics. ESI operates by dispersing a liquid sample into a fine spray of charged droplets that gradually release ions into the gas phase. Because it imparts relatively little energy to analytes, ESI is considered a “soft” ionisation technique: it generates abundant molecular ions with minimal fragmentation, simplifying spectral interpretation and annotation (Pitt, 2009). In contrast, “hard” ionisation sources such as the electron impact method in GC-MS produce extensive fragmentation, which can complicate identification (Pitt, 2009).

Importantly, ESI can be operated in positive, negative, or polarity-switching modes, broadening its applicability across chemical classes: positive mode enhances the detection of protonated molecules ($[M+H]^+$) and common adducts such as sodium adducts ($[M+Na]^+$), while negative mode often yields superior sensitivity for acidic metabolites through deprotonated species ([M−H]−), as demonstrated by Liigand, *et al*. (2017), who observed improved detection for nearly half of the compounds tested in negative polarity.

Detection is commonly achieved using quadrupole analysers, which filter ions within a defined *m/z* window. Modern instruments often combine multiple quadrupoles in tandem (LC-MS/MS), providing not only high sensitivity but also structural resolution via fragmentation analysis (Grebe & Singh, 2011). This has enabled the confirmation of metabolites directly from microbial extracts; for example, LC-MS/MS validated rifamycin analogues predicted from genomic data of *Salinispora* strains (Kim *et al.,* 2006; Bose *et al.,* 2015). Also, several studies illustrate the utility of LC-MS/MS in detecting new metabolites from rare actinomycetes. For example, marine *Micromonospora* strains yielded a new family of pyrrole-derived alkaloids, phallusialides A–E, detected using high-resolution MS/MS and structurally-confirmed by NMR (Zhang *et al.,* 2019). In another case, the marine-derived *Micromonospora* strain WMMD956 produced several new everninomicin analogues, identified using metabolomics-guided approaches and LC-MS/MS, followed by full structural elucidation by NMR (Lee *et al.,* 2025). Similarly, *Micromonospora* sp. C-3509 was found to produce mintaimycins, a group of four novel peptide metabolites initially characterised by HR-MS/MS and subsequently elucidated by NMR analyses (Hu *et al.,* 2022). More broadly, large-scale exploratory metabolomic profiling of diverse rare Actinomycetota revealed over 1,000 putative metabolites across 60 strains, including several unusual molecules such as 4-methoxychalcone (Cheema *et al.,* 2021; Gamaleldin *et al.,* 2022).

In parallel, advances in MS have led to the development of *in situ* analytical methods, enabling the direct detection of metabolites from microbial colonies or environmental samples without the need for exhaustive extraction and separation steps. Techniques such as Matrix-Assisted Laser Desorption Ionisation (MALDI-TOF) allow rapid identification of microbial strains by comparing peptide mass fingerprints against reference libraries (Claydon *et al.,* 1996; Singhal *et al.,* 2015). Similarly, desorption electrospray ionisation (DESI) has been applied to analyse metabolites directly on

surfaces under ambient conditions, facilitating spatial metabolomics and ecological studies. More recently, *in situ* detection platforms such as SMIRC (Small Molecule *In Situ* Resin Capture) and I-SMEL (*In Situ* Marine moleculE Logger) have extended metabolomic analysis into natural ecosystems, enabling the capture of metabolites directly from sediments and seawater (Bogdanov *et al.,* 2023; Mauduit *et al.,* 2023). These tools highlight how MS-based metabolomics has moved beyond laboratory cultures, providing a direct window into the ecological roles of metabolites in their native environments.

1.5.2 Comparative metabolomics and dereplication

Once mass spectra are generated, the challenge shifts from simple detection to the interpretation of chemical diversity, a process that gave rise to metabolomics as a discipline. Metabolomics is broadly defined as the comprehensive characterisation of the small molecules produced by an organism under specific physiological conditions, providing a functional readout of metabolic activity — the metabolome (Alarcón-Barrera *et al.,* 2022). Unlike genomics, which can only predict biosynthetic potential, metabolomics provides a real-time snapshot of metabolic events, thus directly linking environmental inputs to phenotypic outputs (Clish, 2015; Wishart, 2016). However, inaccurate extraction methods, suboptimal solvents, or inadequate culture conditions may lead to incomplete or biased metabolite profiles, emphasising the need for careful optimisation of experimental workflows (Dettmer *et al.,* 2011; Ivanisevic *et al.,* 2013).

Beyond these technical challenges, natural product discovery faces a persistent bottleneck: the repeated rediscovery of known metabolites. This limitation has driven the development of dereplication strategies, which aim to identify and exclude previously characterised metabolites early in the workflow, thereby directing resources towards unexplored chemical space (Reynolds, 2017; Lianza *et al.,* 2021). Dereplication relies on access to curated libraries of natural product structures and spectral signatures, such as SuperNatural (Dunkel *et al.,* 2006) and AntiBase. However, these databases remained fragmented and unintegrated until the development of the Global Natural Products Social (GNPS) platform (Wang *et al.,* 2016). GNPS remains the largest open-access repository of MS/MS data for natural products, though it still covers only a fraction (~2.5%) of known metabolites (van der Hooft *et al.,* 2020). The major innovation of GNPS lies in its molecular networking framework, which represents chemical space as networks of nodes (metabolites)

connected by edges reflecting similarity in their MS/MS fragmentation patterns (Yang *et al.,* 2013). This approach clusters structurally related metabolites into molecular families, enabling the recognition of known scaffolds and prioritisation of new analogues. Alongside GNPS, complementary computational tools such as Dereplicator+ extend dereplication by directly matching experimental MS/MS spectra to natural product databases, including not only canonical metabolites but also modified derivatives (Mohimani *et al.,* 2018). This ability is particularly relevant for polyketides and nonribosomal peptides, which often occur as glycosylated or methylated analogues. Such workflows have enabled the rapid annotation of dozens of metabolites in complex extracts, streamlining prioritisation for further validation. For example, through the combination of HPLC-MS, molecular networking and Dereplicator+, a total of 51 compounds — including xanthohumol, kushenol A, and trifolirhizin — were annotated and dereplicated from *Sophora flavescens* samples (Wang & Ding, 2025). Although this study focused on a plant source, it illustrates the capacity of Dereplicator+ to efficiently annotate complex mixtures and exclude known metabolites from prioritisation.

Beyond these database-driven approaches, *in silico* fragmentation tools such as MS-FINDER (Tsugawa *et al.,* 2016), CFM-ID (Allen *et al.,* 2014), MetFrag (Ruttkies *et al.,* 2019), ChemDistiller (Laponogov *et al.,* 2018), and CSI:FingerID (Hoffmann *et al.,* 2022) were developed to predict fragmentation patterns and assign candidate structures from databases. While useful, these methods still rely on the existence of reference compounds. By contrast, SIRIUS integrates fragmentation tree analysis with molecular formula prediction, making it uniquely capable of proposing plausible structures even for compounds absent from any database (Dührkop *et al.,* 2019). This is particularly powerful when investigating rare actinomycetes with poorly characterised metabolomes. A striking example is the soil-derived *Amycolatopsis sp.*, where SIRIUS predicted the molecular formula of the antibiotic ECO-0501; this information was used to prioritise the compound for further study, and the full structure was subsequently elucidated through classical fermentation, isolation, and NMR analysis, demonstrating how SIRIUS can guide prioritisation of novel metabolites (Hamed *et al.,* 2023). SIRIUS calculates molecular formulas by comparing observed and theoretical mass values, reporting the median mass error in parts per million (ppm). Errors <1 ppm are considered excellent, 1–3 ppm reliable, 3–5 ppm acceptable in simple mixtures, and >5 ppm questionable, often reflecting calibration drift, adduct misassignment, or the increasing number of possible candidate molecular formulas at

higher molecular weights, which can limit confident formula prediction (Olsen *et al.,* 2005; Waters, 2023; Böcker *et al.,* 2009). Throughout this work, mass accuracy is therefore discussed in terms of absolute ppm error (± ppm), as the sign of the deviation simply indicates whether the observed mass is slightly higher or lower than the theoretical value and is not meaningful in isolation (Dührkop *et al.,* 2019). Beyond formula prediction, SIRIUS integrates CSI:FingerID, which provides probabilistic substructure annotation and chemical class prediction, further refining the interpretation of uncharacterised features. Together, these tools underscore the dual role of comparative metabolomics: accelerating dereplication to avoid redundancy while also prioritising unique metabolite families for structural elucidation. Ultimately, integration with genomics remains essential to connect metabolite families to their BGCs, thereby unlocking the ecological and evolutionary context of chemical diversity in rare actinomycetes.

1.6 Bridging the genomic–metabolomic gap: activation of secondary metabolism

Comparative genomics has shown that although thousands of BGCs can be computationally predicted, only a small fraction (<10%) have been experimentally linked to characterised metabolites (Cimermancic *et al.,* 2014; van der Hooft *et al.,* 2020), with the number of BGCs far exceeding the number of secondary metabolites detected under standard laboratory conditions (Doroghazi *et al.,* 2014; van Bergeijk *et al.,* 2020). For instance, *Streptomyces* genomes typically contain 20–40 BGCs, yet fewer than 10 metabolites are commonly observed from culture extracts (Rutledge & Challis, 2015), while in *Salinispora* species more than 75% of BGCs identified remain unassigned to known products, underlining the extent of hidden chemical diversity (Ziemert *et al.,* 2014). This disparity highlights a fundamental bottleneck: while the genetic potential for novel chemistry exists, its expression remains largely inaccessible.

A major contributor to this mismatch is the prevalence of *silent* or *cryptic* BGCs. Strictly speaking, the terms describe different situations: *silent* BGCs are those known but transcriptionally inactive under typical laboratory conditions; in contrast, *cryptic* BGCs refer to cases where a metabolite can or cannot be observed (*cryptic* natural product) but its genetic origin is not immediately evident from sequence data alone (Hoskisson

& Seipke, 2020; Covington *et al.,* 2021). In practice, however, the two terms are often used interchangeably in the natural products literature. Their activation or assignment is believed to require specific ecological cues such as nutrient limitation, stress, or microbial interactions. For example, in *Streptomyces lividans* TK23, a cryptic polyketide was only traced back to its biosynthetic genes when activated through co-culture with *Tsukamurella pulmonis* TP-B0596, leading to the discovery of novel antibiotics (Onaka *et al.,* 2011).

Paradoxically, the development of new genomic and cultivation technologies has made the mismatch even more evident. For example, diffusion-based isolation devices such as the iChip (which enables *in situ* cultivation of previously uncultured bacteria) have expanded access to rare taxa, leading to landmark discoveries like teixobactin and clovibactin from *Eleftheria terrae* (Ling *et al.,* 2015; Shukla *et al.,* 2023). Yet, despite such breakthroughs, many microorganisms remain uncultured and not amenable to traditional isolation methods. Culture-independent approaches have provided complementary solutions. Environmental DNA (eDNA) mining and metagenomics have revealed tens of thousands of novel BGCs, though only a fraction have been experimentally linked to new compounds—typically through heterologous expression, targeted gene knockouts, or correlation of metabolomic and genomic data (Paoli *et al.,* 2022; Padhi *et al.,* 2024). Examples include protease-inhibiting RiPPs such as graspetides and spliceotides recovered from lake microbial mats (Padhi *et al.,* 2024), novel PKS-derived metamycins from the human microbiome (Sugimoto *et al.,* 2019), and structurally diverse peptides such as malacidins, cadasides, and lapcin from soil metagenomes (Hover *et al.,* 2018; Wu *et al.,* 2019; Wang *et al.,* 2022).

Beyond genomics, environmental metabolomics approaches are beginning to bridge the gap between genetic potential and chemical reality. By capturing metabolites directly from sediments and seawater, *in situ* detection platforms have revealed compounds that are often missed in standard laboratory cultures, highlighting the chemical diversity present in natural environments (Tuttle *et al.,* 2019; Mauduit *et al.,* 2023). These strategies not only validate ecological roles—for example, the detection of the antibiotic attinimicin in ant nests (Fukuda *et al.,* 2021)—but also illuminate the transcriptional silence of many biosynthetic gene clusters (BGCs) and the limited experimental access to microbial and chemical diversity.

Because many biosynthetic gene clusters remain silent or cryptic under standard laboratory conditions, and *in situ* detection platforms are still limited, culture-based activation strategies remain a practical and tractable route to acces hidden metabolic potential. These methods include the widely explored One Strain–Many Compounds (OSMAC) approach (Mao *et al.,* 2018), co-cultivation, the use of epigenetic modifiers, ribosome and genetic engineering and high-throughput elicitor screening. Importantly, strategies that enable reproducible metabolite production at the sub-milligram to milligram scale are particularly valuable, as meaningful biological evaluation and full structural characterisation by NMR require the isolation of pure compounds in sufficient quantities.

The OSMAC strategy, developed by Zeeck and colleagues in 2002, is a simple yet powerful method to activate silent or cryptic gene clusters by cultivating microorganisms under different conditions designed to mimic environmental variation. This approach involves modifying parameters such as nutrient composition, trace metals, salinity, and temperature (Romano *et al.,* 2018). Such abiotic shifts have been shown to modulate gene expression, with transcriptomic studies demonstrating the differential activation of biosynthetic gene clusters under altered culture conditions. For example, in *Rhodococcus*, a global transcriptome study revealed that in the *R. jostii* RHA1 strain, 438 genes were upregulated and 114 downregulated after a heat shock (30 °C → 35 °C), with gene expression increasing as a function of stress duration (Ekpanyaskun, 2006). Likewise, RNA-seq analysis of *Rhodococcus* sp. JG3 showed 359 transcripts induced at –5 °C compared with +25 °C, with positively regulated genes linked to translation, amino acid metabolism, siderophore synthesis, iron uptake, and oxidative stress responses (Raymond-Bouchard *et al.,* 2018). In addition to transcriptomic changes, culturing the fungi *Talaromyces pinophilus* CCM-UEA-F0414 and *Penicillium paxilli* CCM-UEA-F0591, in five different culture media to modulate the production of secondary metabolites showed that ethyl acetate extracts exhibited significant antimicrobial activity against Gram-positive and Gram-negative bacteria, as well as pathogenic yeasts. Chemical analyses revealed the presence of phenolic compounds, particularly caffeic and chlorogenic acids, demonstrating that variations in culture media substantially affect both the metabolite profiles and the antimicrobial efficacy of the extracts (de Andrade *et al*., 2025).

As mentioned, within the OSMAC framework, environmental factors themselves can act as powerful triggers of secondary metabolism. A growing body of evidence shows

that abiotic parameters—such as nutrient availability, metal ion concentrations, temperature, salinity, and light—can significantly reshape microbial biosynthetic output. Nutrient shifts provide a clear example: in *Streptomyces globisporus* SCSIO LCY30, culturing in seven different fermentation media yielded distinct chemical profiles dominated by angucyclines (mayamycin A–B, rabelomycin), streptophenazines, and the macrolide dinactin; notably, mayamycin A and rabelomycin displayed potent cytotoxic and antibacterial activities (Li *et al.,* 2023). Similarly, varying glycerol and ammonium sulphate concentrations in *Pseudomonas aeruginosa* altered rhamnolipid production through oxidative stress responses (Santamaria *et al.,* 2022).

Metal ions are another potent environmental cue. Exposure to nickel induced the biosynthesis of the new antibiotics estremycins A and B in *Streptomyces pratensis* NA-ZhouS1 (Akhter, 2018), while the discovery of loihichelins A–F siderophores in *Halomonas* sp. LOB-5 at the Loihi Seamount reflected adaptation to elevated manganese and iron levels, with metal chelation activity closely matching environmental geochemical pressures (Homann *et al.,* 2009). These findings support a recurring pattern: metal stress frequently enhances siderophore biosynthesis, reinforcing its ecological role in nutrient acquisition and microbial competition.

Salinity and temperature are among the most extensively studied abiotic stressors, reflecting their fundamental impact on microbial physiology and their ecological relevance in marine and extremophilic environments. In *Vibrio* spp., elevated salinity enhanced the production of prodigiosin, a bioactive pigment with antimicrobial and anticancer properties (Gallardo *et al.,* 2016), while halophilic actinomycetes were shown to upregulate osmoprotectants and polyketides under salt stress (Rateb *et al.,* 2011; Ma *et al.,* 2010). Temperature gradients can similarly reshape metabolic output; for instance, in the psychrotolerant micromycete *Penicillium vulpinum* KPB F-290, cultivation at different temperatures shifted production toward β-lactam antibiotics and peptide antimicrobials (Kuvarina *et al.,* 2022).

Light quality and intensity also represent regulatory axes for secondary metabolism, particularly in phototrophic microbes. In *Synechocystis* PCC 6803, changes from white/polychromatic to monochromatic light (blue, red, or orange) triggered differential expression of photosystem and pigment biosynthesis genes, activating additional metabolic pathways (Luimstra *et al.,* 2020). Similarly, in bloom-forming cyanobacteria

(*Hapalosiphon* and *Planktothricoides*), variations in light intensity and temperature altered secondary metabolite output—including terpenoids and quinones—with light accounting for ~19% of the observed variance (Mohanty *et al.,* 2022).

Within this broader conceptual framework, one of the most widely applied experimental strategies is co-cultivation, in which two or more microbial species are grown together under the same conditions (Goers *et al.,* 2014). Interactions in this context—whether competition for nutrients or cooperative exchanges—can stimulate the production of new metabolites or enhance the yield of known ones. For example, the bacterium *Streptomyces coelicolor* increases antibiotic production when in co-culture with *Myxococcus xanthus*, using nutrient competition as a biochemical trigger to activate antibiotic biosynthesis pathways (Lee *et al*., 2020). Similarly, *Dunaliella salina* have showed that in co-culture with epibiotic bacteria not only increases β-carotene production but also induces the synthesis of new bioactive compounds, including fatty acids with antimicrobial properties (Punitha & Sampathkumar, 2022). These cases illustrate that microbial interactions can unlock otherwise silent metabolic pathways, although metabolite production is not always reproducible, and the resulting mixtures can complicate compound isolation and complete characterisation.

Beyond pairwise co-cultures, symbiotic associations also provide powerful ecological cues for metabolite induction. Marine invertebrates such as sponges and tunicates host dense microbial consortia, within which these bacterial and other symbionts produce bioactive metabolites that contribute to host defence and intermicrobial signalling (Pita *et al.,* 2018). A classic example is the sponge *Theonella swinhoei*, which harbours the symbiotic bacterium *Entotheonella* responsible for producing polyketide-derived compounds such as onnamides and theopederins—potent cytotoxins with antifungal and anticancer properties (Wilson *et al.,* 2014). Another case is the coral-associated bacterium *Endozoicomonas* spp., linked to the production of antimicrobial peptides that support coral health and resistance against opportunistic pathogens (Neave *et al.,* 2016). Actinomycetes have also been identified as symbionts. A classic example is *Pseudonocardia*, which is found in specialized glands in the cuticle (outer body surface) of ants. This bacterium produces antifungal and antibacterial metabolites, such as dentigerumcin, nystatin-like polyenes, and selvamicin, which inhibit the growth of specialized fungal parasites (Escovopsis) and other pathogens that could harm the ants or their fungal garden (Goldstein & Klassen, 2020).

In a broader sense, microbial communication systems exemplify how interspecies interactions regulate and induce secondary metabolism. Quorum sensing, in particular, coordinates biofilm formation and metabolite production in response to cell density and ecological signals (Fuqua *et al.,* 1994). For instance, marine *Pseudomonas aeruginosa* strains modulate biosurfactant production and biofilm architecture through LasR–LasI quorum sensing circuits in the presence of Actinomycetota competitors (Traxler *et al.,* 2012). Similarly, *Vibrio fischeri* employs acyl-homoserine lactone quorum sensing to regulate bioluminescence in symbiosis with squid hosts, a system that also influences secondary metabolite expression and highlights how communication links ecological context with chemical output (Visick & Ruby, 2006).

Although interaction-based strategies highlight the ecological triggers of secondary metabolism, they are not always feasible or reproducible under laboratory conditions. Chemical elicitors therefore provide a more controlled alternative, with compounds such as *N*-acetylglucosamine and γ-butyrolactone widely used to stimulate silent biosynthetic pathways. A well-characterised case is the γ-butyrolactone A-factor, which activates the transcriptional regulator AdpA in *Streptomyces*, thereby promoting morphological differentiation and secondary metabolism (Horinouchi & Beppu, 2007). More recently, sublethal concentrations of antibiotics (e.g., trimethoprim, rifampicin, and ceftazidime) were used in the growth medium of *Burkholderia ambifaria* AMMD and *Burkholderia gladioli*, leading to the induction or suppression of specific compounds (toxoflavin, bongkrekic acid, gladiolin, and caryoynencin) that were not produced under standard conditions (Webster *et al.,* 2020). While sensitive, elicitors depend heavily on precise concentration, requiring carefully optimized protocols, since inappropriate levels can trigger localised cell death, ultimately reducing or abolishing the production of the desired metabolite.

Together, the strategies outlined above provide a conceptual framework for exploring how cultivation conditions and ecological interactions shape secondary metabolism. This framework is applied in the following section to marine actinomycetes, a group well known for its biosynthetic richness and environmental adaptability.

1.7 Project scope

This thesis focuses on the comparative genomic and metabolomic analysis of rare actinomycetes isolated from underexplored marine environments, with particular emphasis on members of the genera *Rhodococcus* and *Micromonospora*. The work investigates how selected environmental parameters, specifically temperature and salinity, influence biosynthetic gene content and secondary metabolite production. To address this scope, the thesis is organised as follows. Chapter 2 describes the general materials, cultivation conditions, and analytical methodologies employed throughout the thesis, including genomic, phylogenetic, and metabolomic approaches. Chapter 3 examines the phylogenetic relationships and biosynthetic potential of Antarctic *Rhodococcus* strains through genomic sequencing and BGC comparison. Chapter 4 builds upon this by assessing how temperature influences the metabolomic profiles of *Rhodococcus*, while Chapter 5 shifts the focus to *Micromonospora* strains from contrasting marine environments, combining genomic and metabolomic approaches to evaluate the effect of salinity on metabolite production and to identify juvenimycin-like macrolides. Finally, a summary of all experimental findings is provided in Chapter 6, which also offers critical reflections on the implications for natural product discovery and outlines future perspectives for exploiting environmental factors to unlock novel bioactive metabolites.

1.8 General aims

1. **To explore the genomic features and BGC diversity of *Rhodococcus* strains isolated from Antarctica.**

Specific Objectives:

a) To generate and analyse whole-genome sequences of selected *Rhodococcus* strains to support taxonomic and comparative genomic analyses.
b) To examine phylogenetic relationships among the isolated strains using 16S rRNA gene sequences and genome-based approaches.
c) To explore the diversity and distribution of biosynthetic gene clusters within these genomes and assess their potential specialised metabolic capacity.

2. **To assess the effect of temperature on the metabolic profile of polar *Rhodococcus* strains using comparative metabolomics approaches.**

Specific Objectives:

a) To examine the phylogenetic diversity and antimicrobial activity of *Rhodococcus* strains isolated from polar and temperate marine sediments.
b) To assess the effect of different cultivation temperatures on the metabolomic profiles of selected strains using LC-MS/MS-based molecular networking.
c) To compare metabolomic profiles across temperature conditions in order to evaluate temperature-associated changes in secondary metabolite production.

3. **To explore the secondary metabolite production of *Micromonospora* strains under varying salinity conditions using an integrated genomic and metabolomics approach.**

Specific Objectives:

a) To assess the phylogenetic diversity and antimicrobial activity of selected *Micromonospora* strains from contrasting environments.
b) To evaluate the effect of salinity on metabolite production using LC-MS/MS-based metabolomic approaches.
c) To analyse genome sequences of selected strains to explore biosynthetic gene clusters in relation to observed metabolomic profiles.
d) To explore and identify metabolites of potential bioactive interest under the tested culture conditions.

2 CHAPTER 2. MATERIAL AND METHODS

2.1 Sediment collection

Sediment samples were collected from three study areas: Scotland (Fionnphort Beach, 56.3559 N, -6.3599 W), Mexico (Ojo de Libre lagoon, 27°45′0″ N, 114°15′0″ W), and Polar regions: Antarctica and the Arctic (Millán-Aguiñaga *et al.,* 2019). Four Mexican sediments (Fig. 2.1A) were collected in June 2018 by free diving to a maximum depth of 13 m, these were stored on ice in sterile Whirl-Pak bags until processed in the laboratory as previously reported (Zamora-Quintero *et al.,* 2022). The Scottish sample (Fig.2.1B) was collected aseptically by hand in the shallow coastal zone, using a sterile 50 mL falcon tube, preserved on ice and stored at -20 °C until further analysis. Sediment samples from the Antarctic and Arctic regions were obtained during research expeditions aboard the PS Polarstern (2002) and RRS James Clark Ross (2005) cruise, as previously reported (Millán-Aguiñaga *et al.,* 2019) (Fig.2.1, C1 and C2).

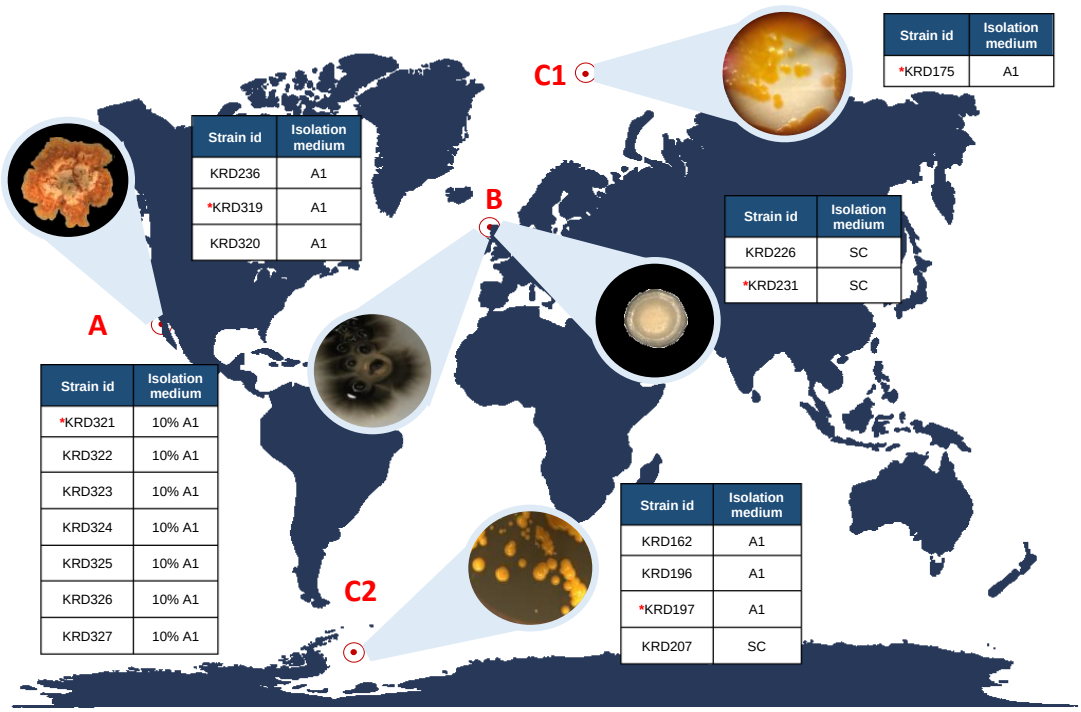

Figure 2.1. Marine sediment sampling locations and photographs of representative isolated bacteria. (A) *Micromonospora* strains KRD321–327 from Ojo de Liebre lagoon, Mexico. (B) Strains KRD226, KRD231, KRD236, KRD319, and KRD320 from Scotland and (C1, C2) strain KRD162, KRD196, KRD197, KRD207

from Antarctica and strain KRD175 from the Arctic. The red asterisk indicates the strain depicted on the map. The base map was adapted from a free vector template available at Vecteezy (https://es.vecteezy.com/).

2.1.1 Bacterial isolation

Polar sediments were processed following the protocol detailed by Millán-Aguiñaga *et al.* (2019). Briefly, 1 g of sediment was aseptically placed into a sterile Petri dish, dried over 48 h in a laminar flow hood, pressed into a sterile foam (20 mm in diameter), and inoculated onto three different agar media by stamping six or seven times in a circular fashion, giving a serial dilution effect. The three media were A1, SW and SC, all containing Instant Ocean (18 g l−1), cycloheximide (25 µg ml−1) and nystatin (25 µg ml−1). Scottish sediments were pre-treated and bacterial isolation was performed using the dry/stamp (DS) method as described by Jensen *et al.* (2005). Briefly, 1 g of sediment was placed in a sterile Petri dish and dried in a laminar flow hood overnight. Subsequently, the sediment was stamped with a sterile sponge (20 mm diameter) and inoculated on Starch Casein Nitrate agar (SC) pH 7.8 - 8.30 (Küster Williams, 1964). Mexican sediment was pre-treated by heat shock at 45°C for 30 min and stamped with a sterile sponge (20 mm diameter) and inoculated on Humic Acid - Vitamin Agar (HA) (Hayakawa & Nomura, 1987); Soya Flour Mannitol (SFM) (Kieser, T. *et al.,* 2000; Hobbs *et al.,* 1989); Colloidal Chitin agar (CC) (Hsu & Lockwood, 1975); Gause's No. 1 (G1) (Zhou *et al.,* 2017); ISP3 (Shirling and Gottlieb, 1966); SW (agar, 14 g/l) and 10% A1 (Gontang *et al.,* 2007; Ahmed *et al.,* 2013; Zamora-Quintero, *et al.* 2022) (Table 2.1). To inhibit the growth of fungi and Gram-negative bacteria, the isolation media was supplemented with 25 µg/mL cycloheximide (fungicide), 25 µg/mL nystatin (fungicide) and 10 µg/mL nalidixic acid (antibiotic). The bacterial isolation plates were incubated at room temperature for 3-4 weeks and colonies displaying morphological characteristics of actinomycetes (tough, leathery colonies) were sub-cultured onto fresh SC agar (Scottish strains) or A1 agar (Mexican strains) until pure colonies were obtained. All strains were cryopreserved in 25% glycerol (v/v), and stored at -80 °C.

All *Rhodococcus* strains from the Duncan lab culture collection selected for analysis were inoculated on to ISP2 agar (Shirling & Gottlieb, 1966), supplemented with 18 g/L Instant Ocean® Sea Salt (IO) (Instant Ocean, USA) and incubated for seven days at 30 °C. In contrast, all *Micromonospora* strains from the Duncan Lab culture

collection were inoculated on to A1 agar (Gontang *et al*. 2007) supplemented with 18 g/L Instant Ocean® Sea Salt (IO) (Instant Ocean, USA) and incubated for three weeks at room temperature (25 °C).

Table 2.1. Bacterial media composition used for bacterial analysis.

Growth medium	Components (g/L)	Reference
Starch Casein Nitrate agar (SC)	Soluble starch (10); Sodium caseinate (1); KNO_3 (2); KH_2PO_4 (0.5); $MgSO_4$ (0.5), Instant Ocean® Sea Salt (18); Agar (18).	Küster and Williams, 1964.
Humic Acid-Vitamin Agar (HA)	Humic acid (1); KCl (1.7); $NaHPO_4$ (0.5); $MgSO_4 \cdot 7H_2O$ (0.05); $CaCO_3$ (0.02); $FeSO_4 \cdot 7H_2O$ (0.01); Thiamine (0.5mg); Riboflavin (0.5mg); Inositol (0.5mg); Biotin (0.25mg); Agar (15).	Hayakawa and Nomura, 1987
Soya Flour Mannitol (SFM)	Mannitol (20); Soya Flour (20); Agar (20).	Kieser, T. *et al.,* 2000; Hobbs *et al.,* 1989
Colloidal chitin agar (CC)	Chitin (4); K_2HPO_4 (0.7); KH_2PO (0.3); $FeSO_4 \cdot 7H_2O$ (0.01); $MgSO_4 \cdot 5H_2O$ (0.5); $ZnSO_4$ (0.001); $MnCl_2$ (0.001); Agar (20).	Hsu and Lockwood, 1975
Gause's No. 1 (G1)	Soluble Starch (20); KNO_3 (1); K_2HPO_4 (0.5); NaCl (0.5); $MgSO_4$ (0.50); $FeSO_4$ (0.01); Agar (10).	Zhou *et al.,* 2017
Oats/ISP3	Commercial oats (14); Agar (14).	Shirling and Gottlieb, 1966
SW	Agar (14); Instant Ocean® Sea Salt (18).	Ahmed, *et al*. 2013
A1	Starch (10); Yeast (4); Peptone (2); Agar (14); Instant Ocean® Sea Salt (18).	Gontang, *et al.* 2007
10% A1	Starch (1); Yeast (0.4); Peptone (0.2); Agar (14); Instant Ocean® Sea Salt (18).	Gontang, *et al*. 2007; Zamora-Quintero, *et al.* 2022
Streptomyces Project 2 (ISP2)	Yeast extract (4); Malt extract (10); Glucose (4); Instant Ocean® Sea Salt (18); Agar (20).	Shirling and Gottlieb, 1966
Streptomyces Project 4 (ISP4)	Soluble Starch (10); $MgSO_4$ x $7H_2O$ (1); NaCl (1); $(NH_4)_2SO_4$ (2); $CaCO_3$ (2); Agar (20); Trace salts solution (1 mL): [0.1 g $FeSO_4$ x $7H_2O$; 0.1 g $MnCl_2$ x $4H_2O$; 0.1 g $ZnSO_4$ x $7H_2O$; 100 mL dH_2O]	Shirling and Gottlieb, 1966
Streptomyces Project 5 (ISP5)	L-asparagine (anhydrous) (1); Glycerol (10); K_2HPO_4 (1); Trace salts solution (1 mL): [0.1 g $FeSO_4$ x $7H_2O$; 0.1 g $MnCl_2$ x $4H_2O$;0.1 g $ZnSO_4$ x $7H_2O$; 100 mL dH_2O]; Agar (20).	Shirling and Gottlieb, 1966

LB media	Yeast Extract (5); NaCl (10); Tryptone (10); Agar (20).	Bertani, 1951
Nutrient Agar	Difco Nutrient Broth Powder (4); Agar (10).	Harrigan *et al.,* 1966

2.2 Antibacterial assays using agar plug diffusion method

Antibacterial assays were performed following previously published method (Balouiri *et al.,* 2016). A panel of ESKAPE pathogens (*Enterococcus faecalis* ATCC51299*), Staphylococcus aureus* ATCC43300*, Klebsiella pneumonia* ATCC700603*, Acinetobacter baumannii* ATCC19606*, Pseudomonas aeruginosa* ATCC27853), and additionally *Escherichia coli* ATCC25922 and *Bacillus subtilis* ATCC23857 were cultured overnight using LB medium (5 mL, 30 °C, 82.1 × g) (Bertani, 1951). These were used to inoculate Nutrient Agar (NA, 25 mL per plate) (Harrigan *et al.,* 1966), with the pathogen adjusted to an optical density (OD) of 0.01 before plating. Previously, all *Rhodococcus* were grown on ISP2 agar for 7 days (Shirling and Gottlieb, 1966). An agar plug (7 mm) of the actinomycete lawn was then transferred to the NA pathogen culture and incubated (overnight, 30 °C) before measuring the zone of inhibition around the actinomycete plug (mm) (Osama *et al.,* 2022). An ISP2 agar (Shirling and Gottlieb, 1966) plug was used as a negative control and a sterile paper disk with 10 µg/µL gentamicin was used as a positive control.

2.3 DNA isolation, amplification and sequencing of the 16S rRNA gene

Strains were grown for seven days at 28 °C with constant agitation in liquid ISP2 medium (Shirling and Gottlieb, 1966) (*Rhodococcus*) and on solid agar A1 for 21 days at 25 °C (*Micromonospora*). *Rhodococcus* cells were concentrated by centrifugation (9,633 × g x 15 min). For *Micromonospora* a single colony was suspended in medium A1 and subjected to two freeze–thaw cycles (–80 °C for 5 min followed by 95 °C for 5 min). In both cases, genomic DNA was extracted using the salting out method from Kieser *et al.* (2000) and Feeney *et al*. (2022). DNA was quantified using a Nanodrop spectrophotometer and assessed for quality (high molecular weight) by electrophoresis on a 1% agarose gel with a 1000 bp reference ladder (BioLabs). Samples were then stored at −20 °C. Amplification of the 16S rRNA gene was carried out by Polymerase Chain Reaction (PCR) using two sets of primers. The universal primers FC27 (5′-AGAGTTTGGATCMTGGCTCAG-3′) and

RC1492 (5′-CGGTTACCTTGTTACGACTT-3′) were used to amplify a ~1500 bp fragment for *Rhodococcus* strains (Gontang, 2007). Additionally, the primers M558F (5′-CGGCTTGTCGCGTCGACT-3′) and C1028R (5′-ATGCACCACCTGTGACCGC-3′) where used to amplify an approximately 470 bp fragment of the 16S rRNA gene specific to *Micromonospora* (Qiu *et al.,* 2008). PCR conditions were as follows: denaturation at 95 °C for 15 min followed by 32 cycles at 95 °C for 1 min, 61 °C for 1 min and 72 °C for 1 min, ending with a final extension at 72 °C for 7 min (Becerril-Espinosa *et al*. 2013). Amplicons were verified by agarose gel electrophoresis (1% agarose) with a 1000 bp reference ladder (BioLabs), using distilled water as a negative control, while pure genomic DNA from a *Rhodococcus* and *Micromonospora* strain served as a positive control. Amplicons were purified using a QIAquick PCR cleanup kit (QIAGEN Inc., Manchester, UK) according to the manufacturer's protocol and sent to Eurofins Genomics (Germany) for sequencing. The obtained 16S rRNA gene sequences were manually inspected and trimmed with bioedit sequence alignment editor (Hall, 1999) and multiple alignment was achieved using the BLAST tool in the NCBI platform (NCBI, 2023).

2.4 Phylogenetic analysis

Phylogenies were inferred using the GGDC web server (Meier-Kolthoff *et al.,* 2021) and the DSMZ phylogenomics pipeline (Meier-Kolthoff *et al.,* 2014) adapted to single genes. A multiple sequence alignment was created with MUSCLE (Edgar, 2004). Maximum likelihood (ML) and maximum parsimony (MP) trees were inferred from the alignment using RAxML (Stamatakis, 2014) and TNT (Goloboff, *et al.* 2008), respectively, using the GTR+GAMMA substitution model. For ML, rapid bootstrapping in conjunction with the autoMRE bootstopping criterion (Pattengale, *et al*. 2010) and subsequent search for the best tree was used; for MP, 1000 bootstrapping replicates were used in conjunction with tree-bisection-and-reconnection branch swapping and ten random sequence addition replicates. The sequences were checked for a compositional bias using the X^2 test as implemented in PAUP* (Swofford, 2002). For visualisation and post modification of the phylogenetic tree FigTree v1.4.3 was used (Rambaut, 2009).

2.5 Whole genome sequencing

2.5.1 DNA extraction

A single bacterial colony of strains KRD162 and KRD197 (*Rhodococcus* sp.) was grown in ISP2 liquid medium (5 mL) supplemented with 18 g/L Instant Ocean (3 days at 28 °C). In the case of strain KRD324 (*Micromonospora* sp.), it was grown in A1 medium (50 mL) similarly supplemented with Instant Ocean (14 days at 25 °C). Subsequently, high molecular weight genomic DNA was extracted using the Wizard® HMW DNA Extraction Kit | High-Molecular-Weight DNA | Long-Read Sequencing (Promega) following the specified protocol. The isolated DNA was re-suspended in 50 µL nuclease-free water. The quality of the extracted DNA was evaluated using a NanoDrop 1000 spectrophotometer (Lab-tech), ensuring a concentration of 50 ng/µL.

2.5.2 Genome sequencing

Genomic DNA of strains KRD162, KRD197, and KRD324 was first sequenced by Novogene (Cambridge, UK) using Illumina short-read whole genome sequencing. Briefly, genomic DNA was randomly fragmented to an average size of ~350 bp, followed by end-repair, A-tailing, and ligation of Illumina sequencing adapters. Adapter-ligated fragments were then PCR-amplified, size-selected, and purified to generate the final sequencing library. Additionally, long-read sequencing was performed by Plasmidsaurus (London, UK) using Oxford Nanopore Technologies (ONT) with the most recent V14 chemistry on R10.4.1 flow cells. Genomic DNA was prepared for sequencing using an amplification-free, primerless library preparation protocol optimised for high molecular weight DNA, thereby minimising sequence-dependent fragmentation and preserving native base modifications. Sequencing on R10.4.1 flow cells enable improved resolution of homopolymeric regions and structural variants due to the pores enhanced basecalling accuracy. Raw signal data were basecalled using ONT's high-accuracy model to generate FASTQ reads. According to the provider's specifications, consensus assemblies were derived from multiple passes of the same molecule, increasing per-base accuracy, and were accompanied by genome annotation using Bakta, which identifies coding sequences, rRNAs, tRNAs, and other genomic features. Full methodological details are available from the service provider (https://www.plasmidsaurus.com/).

2.5.3 De novo genome assembly

The genome assembly of KRD162, KRD197 and KRD324 were performed through a hybrid approach, including ONT long and Illumina short reads. Long read sequences were assembled with Flye (V.2.9.5) (Lin, *et al*. 2016), a tool optimised for long-read assemblies that efficiently resolves repetitive regions. Short reads were then mapped onto the assembly using Bowtie2 (V. 2.5.3) (Langmead & Salzberg, 2012), a fast and accurate aligner for short-read sequences, and the alignments were processed with Samtools sort (V.1.20) (Danecek *et al.,* 2021), to generate ordered BAM files. The assemblies were polished with Pilon tool (V. 1.20) (Walker *et al.,* 2014), which improves consensus accuracy by correcting base errors, small indels, and filling gaps. Assembly quality was assessed with the Quast tool (V. 5.2.0) (Mikheenko *et al.,* 2018) which provides standard assembly metrics such as N50, number of contigs, and GC content, while completeness was evaluated with BUSCO (V. 5.7.1) (Simao *et al.,* 2015) based on benchmarking against single copy orthologs. The genome sequences of *Rhodococcus* species were submitted to the NCBI database (CP190354=KRD162 and CP190355=KRD197).

2.6 Whole-genome phylogenomic and biosynthetic analysis

2.6.1 Genomic distance: dDDH and FastANI

To investigate species-level relatedness, digital DNA–DNA hybridisation (dDDH) values were calculated using the Genome-to-Genome Distance Calculator (GGDC v4.0; Auch *et al.,* 2010), applying formula 2 (GBDP formula d4) and the recommended threshold of 70% for species delineation (Chun *et al.,* 2018). In parallel, Average Nucleotide Identity (ANI) values based on BLAST (ANIb) analysis were obtained via the JSpeciesWS server (https://jspecies.ribohost.com/jspeciesws/). A genome-scale phylogenetic tree was generated using autoMLST (https://automlst.ziemertlab.com) (Mohammad *et al.,* 2019) under the *de novo* workflow, which by default selects ~100 conserved single-copy housekeeping genes shared among the query and reference genomes. This employs multilocus sequence alignment followed by phylogenetic reconstruction using IQ-TREE with 1000 ultrafast bootstrap replicates. To complement this analysis, a whole-genome-based phylogenetic tree was inferred using the Type (Strain) Genome Server (TYGS; https://tygs.dsmz.de). Unlike autoMLST, TYGS does not rely on a subset of conserved genes; instead, it identifies related type strains via: (1) whole-genome MASH comparisons, and (2) 16S rRNA

BLAST searches of sequences extracted using RNAmmer. Pairwise genomic distances were calculated using the Genome BLAST Distance Phylogeny (GBDP) method with the *trimming* algorithm and distance formula d5. These distances were then used to infer a balanced minimum evolution tree using FASTME 2.1.6.1, with 100 pseudo-bootstrap replicates. The resulting tree was midpoint-rooted and visualised using PhyD3, with branch lengths scaled according to GBDP distances and node support values were shown for bootstrap values ≥60%.

2.6.2 Biosynthetic Gene Cluster annotation and comparison.

Biosynthetic Gene Clusters (BGCs) were annotated using antiSMASH v7.0 (Blin *et al.,* 2023). From the resulting GenBank (.gbk) output files, a sequence similarity network was constructed using BiG-SCAPE v1.1.8 (Navarro-Muñoz *et al.,* 2019), executed via the Galaxy Europe platform (The Galaxy Community, 2024). BiG-SCAPE groups BGCs into Gene Cluster Families (GCFs) based on comparisons of protein domain architecture, domain arrangement, copy number, and sequence identity. The MIBiG database v2.1 was included to facilitate reference-based matching. The resulting network was visualised using Cytoscape v3.7.2. (Shannon *et al.,* 2003).

2.7 Cultivation of *Rhodococcus* under variable temperatures: growth kinetics analysis

2.7.1 The effect of temperature: *Rhodococcus* cultured at 20 °C, 25 °C and 30 °C.

Rhodococcus strains were pre-cultured (ISP2 broth (Shirling & Gottlieb, 1966), 10 mL, 30 °C, 250 rpm, 7 days) and used to inoculate (2.5 mL) cultures in triplicate (50 mL, ISP2 broth). ISP2 medium was chosen as it supported the cultivation of all strains in this study, enabling direct comparison of metabolite production across temperatures. For each strain, the inoculated flasks were incubated at three temperatures (20 °C, 25 °C, and 30 °C), with a total of nine flasks per strain, resulting in 54 flasks for all six strains. A media control (no bacteria culture added) was included in triplicate at each temperature (9 flasks total). Four hours after inoculation, 1 mL was taken from each flask and transferred to a disposable spectrophotometer cuvette to measure the absorbance at 600 nm or optical density (OD) (Jenway 6300,

UV/Vis Spectrophotometers). Aliquots were collected every 12 h after inoculation for 168 h (7 days) (Kaufmann, 1981).

Growth curves were generated by plotting the average OD of each triplicate sample against time (h), with standard deviations represented as vertical error bars (Kaufmann, 1981). The onset of the stationary phase was determined using GraphPad Prism (v8.0.1) (GraphPad, 2018). The specific growth rate (μ) was calculated using formula (1), applied to the log-transformed OD values corresponding to the exponential growth phase, as shown in Fig. S4.1. Statistical differences in growth rates between temperature conditions were assessed using pairwise t-tests in GraphPad Prism (v8.0.1) (GraphPad, 2018). To account for multiple comparisons, a false discovery rate correction was applied following the Benjamini, Krieger, and Yekutieli method (Q = 1%).

(1) $\mu = [\ln(N_t) - \ln(N_0)] / (t - t_0) * 100$

μ is the specific growth rate (%)
N_0 is the biomass at the beginning of the exponential growth phase (g)
N_t is the biomass at the end of the exponential growth phase (g)
$t\text{-}t_0$ is the duration of the exponential phase (days)

In this study, OD600 values were used as a proxy for biomass (N).

2.7.2 The effect of salinity: *Micromonospora* cultured at 0, 15, 25, 35 and 40% w/v using Instant Ocean® Sea Salt.

Micromonospora strains were pre-cultured on A1 agar (Gontang, *et al*. 2007) at 25 °C for 21 days. A1 agar (solid) was selected as it supported the growth of all six strains and enabled a direct comparison of metabolite production under varying salinity. Each strain was cultured in triplicate Petri dishes on A1 agar (solid) with 0‰, 15‰, 25‰, 35‰, and 40‰ w/v sea salt, and incubated (25 °C, three weeks). As a media control, un-inoculated A1 agar Petri dishes were included in triplicate for each salinity condition.

2.8 Scale - up culturing of *Micromonospora* KRD324.

A pre-culture of KRD324 was inoculated using a single colony (200 mL of A1 medium in a 1 L Erlenmeyer flask), was then incubated (25 °C, 21 days, 250 rpm) and 10 mL of this pre-culture was used to inoculate 13 individual 1 L flasks, each containing 200 mL of fresh A1 medium. These production cultures were incubated under identical conditions (25 °C, 250 rpm, 21 days).

2.9 Physiology and chemotaxonomic description of *Rhodococcus* KRD162 and *Rhodococcus* KRD197

2.9.1 Morphological assessment

The colony morphology of strains KRD162 and KRD197, along with the reference strain *R. fascians* DSM 20669, was examined when cultured on ISP2, ISP3, ISP4 and ISP5 agar (Shirling & Gottlieb, 1966). The salinity and pH tolerance of the strains was measured using ISP2 medium (28°C, 5 days) at pH 5.0 – 8.0 (at intervals of 1.0 pH units) and with 0, 15, 25 and 35% (w/v) NaCl.

2.9.2 Chemotaxonomic evaluation: fatty acids

Fatty acid analysis was carried out by the identification service at the Leibniz Institute DSMZ – German Collection of Microorganisms and Cell Cultures GmbH (Braunschweig, Germany). Biomass was obtained from strains grown on ISP2 agar at 28 °C for 7 days. Cellular fatty acids were converted to Fatty Acid Methyl Esters (FAMEs) by saponification, methylation, and extraction, following the protocol of Sasser (1990). FAME mixtures were separated by gas chromatography and detected with a flame ionization detector. Final identification of fatty acids was performed by gas chromatography – mass spectrometry (GC–MS) on an Agilent 7000D system, with peak identities assigned based on retention times and mass spectra compared against reference libraries used by DSMZ.

2.9.3 Electron microscopy

Coverslips (13 mm) were cleaned with detergent, rinsed with distilled water, coated with 0.025% poly-L-lysine, and air-dried overnight. Cultures were grown under standard conditions (*Rhodococcus* KRD162 and KRD197 in ISP2 broth, 3 days at 28

°C; *Micromonospora* KRD324 in A1 broth, 7 days at 25 °C). Cells were harvested (1 mL), washed, and fixed using 2% glutaraldehyde in Sorenson's phosphate buffer for 24 h at 4 °C. After centrifugation, cells were immobilized on poly-L-lysine–coated coverslips by incubation in glutaraldehyde buffer with 20 µL of sample for 10 min. Samples were dehydrated in an ethanol series (25%, 50%, 75%, 100%; 10 min each), mounted on Aluminum stubs with Silver Dag Agar, and dried overnight. Specimens were sputter-coated with 5–10 nm gold (Polaron SEM coater) and imaged with a Tescan Vega LMU scanning electron microscope (EM Research Services, Newcastle University). Energy-dispersive X-ray spectroscopy (EDX) was performed using a Bruker Flash 6130 detector with Esprit v2.1 software (EMRS, 2024).

2.10 HR LC-MS/MS

2.10.1 Metabolite extraction of bacterial cultures

Metabolite extraction of *Rhodococcus* cultures was performed 24 h after each culture reached stationary phase. To increase metabolite adsorption, HP-20 resin (2.5 g) was added to each flask two hours prior to extraction, following protocols routinely used in our lab (Millán-Aguiñaga, *et al.* 2019; Soldatou *et al.,* 2021). After 2 h, the culture and resin were centrifuged (15 min, 4 °C and 4140 × g), the supernatant discarded, and the cell/resin pellet frozen at −80 °C overnight. The cell/resin pellet was then lyophilised (Christ Alpha 1-2) until completely dry, transferred to an Erlenmeyer flask and extracted twice with ethyl acetate (20 mL, VWR HPLC grade) for 2 h at 250 rpm. The three replicate metabolite extracts were combined, dried under Nitrogen, weighed and stored at 4 °C. Solvent blank and a medium control (no bacteria) were also included.

Metabolite extraction of *Micromonospora* strains was done directly from agar plates. The entire agar (A1) plate (including bacterial biomass) was cut into pieces, transferred into 50 mL Falcon tubes, and lyophilised (until completely dry). The dried agar material was transferred to Erlenmeyer flasks and extracted under the same conditions as above (2 × 20 mL ethyl acetate, 2 h, 250 rpm). Extracts were evaporated under nitrogen, weighed, and stored at 4 °C. For the scaled-up liquid cultures (200 mL per flask) of *Micromonospora* KRD324, 2.5 g of HP-20 resin was added to each flask two hours prior to extraction. After incubation, cultures were centrifuged (15 min, 4 °C and 4140 × g), the supernatant discarded, and the cell/resin

pellet frozen at −80 °C overnight. After lyophilisation, the dried pellet was extracted twice with ethyl acetate (20 mL, VWR HPLC grade, 2 h, 250 rpm), pooled, evaporated, and stored at 4 °C (Soldatou *et al.,* 2021). Solvent blank and a medium control (no bacteria) were also included.

2.10.2 LC-MS/MS analysis of crude metabolites extracts

The extracts were re-suspended in acetonitrile (HPLC grade, MERCK, UK) to a concentration of 1 mg/mL and analysed by Liquid Chromatography – High-Resolution Mass Spectrometry (LC-MS), a service provided by the University of Edinburgh. Analyses were performed using a Dionex UltiMate™ 3000 coupled to Q-Exactive™ (Thermo-Scientific, Germany) mass spectrometer with an electrospray ionization (ESI) source and a mass range of *m/z* 100 – 1050 in positive ionization mode with a spray voltage of 1.5 kV and capillary temperature of 250 °C. Thermo Fisher Scientific Accucore™ C18 company (100 × 2.1 mm) column was used for chromatographic separation at 45 °C. Mobile phase A consisted of H_2O with 0.1% formic acid (Fluka® Analytical, Switzerland) and mobile phase B consisted of acetonitrile Optima™ LC/MS (Fisher Scientific, UK) with 0.1% formic acid. A gradient was used starting from 1% B and increasing to 50% at 2 min. Then to 99% at 10.5 min, and it was held constant for 0.5 min. Finally, B was brought back to initial conditions and held for 5 min for a total run time of 15 min. A flow rate of 300 µL/min and an injection volume of 5 µL was used. Tandem MS (MS/MS) was performed in data-dependent acquisition (DDA) mode at a resolution of 17,500 (at *m/z* 200) (standard settings for Q Exactive Orbitrap), using an isolation window of 1 *m/z* with no offset. Stepped collision energies were applied at 20, 30, and 40 eV.

2.10.3 Data pre-processing and peak detection

The raw mass spectrometry data were first converted to mzML file format using Proteowizard MSConvert (Chambers *et al.,* 2012), ensuring compatibility for processing in MZmine3 (Shmid *et al.,* 2023). Using MZmine, the following specifications were followed: mass peaks were detected in positive mode using a centroid mass detector to identify and extract the signal peaks from raw data based on their mass-to-charge ratio (*m/z*). The noise level was set to 1.0×10^6 for MS1 data (precursor ions) and 1.0×10^3 for MS2 data (fragment ions) to exclude low-

intensity signals likely to represent background noise. Chromatograms were constructed using the ADAP module (Myers *et al.,* 2017), which links detected peaks over time to form chromatographic features. Parameters included a minimum maximum intensity of 5.0×10^4 and an *m/z* tolerance of 0.002. To separate overlapping peaks into distinct features, the chromatograms were deconvoluted using the minimum local baseline search algorithm with a minimum retention time range of 0.05 min, a minimum relative height of 0%, and a minimum absolute height of 5.0×10^4. Finally, a peak alignment list was created using the Join Aligner module, with *m/z* tolerance of 0.0015, a retention time tolerance of 0.1 min, and weights for a retention time of 1 and for a *m/z* of 3.

2.10.4 Statistical analysis and visualisation of filtered peaks

The final list of molecular features generated in MZmine 3 was exported as a .csv file and used for downstream statistical analyses (e.g., comparative profiling across treatments and visualization of abundance patterns). In addition, the corresponding fragmentation spectra (MS2) were exported as a .mgf file. These spectral data enable metabolite annotation and classification into chemical classes by ensuring compatibility with external bioinformatics tools (e.g., GNPS, DEREPLICATOR+). Together, these exported datasets provided the basis for both quantitative (feature intensity comparisons) and qualitative (structural and chemical class assignment) analyses. The statistical analysis included both univariate and multivariate approaches. The Cyclic Loess algorithm was implemented in NormalyzerDE (http://quantitativeproteomics.org/normalyzerde); to ensure that the replicate groups were normalised independently, reducing technical variation and enabling meaningful comparisons across experimental groups (Willforss *et al.,* 2019). Univariate statistical analysis was achieved through volcano plots using Metaboanalyst 6.0 (Ewald *et al.,* 2024) to identify features with statistically significant differences between groups. This approach combined fold-change analysis and statistical significance (e.g., p-value) to highlight key metabolites of interest. Multivariate statistical analysis and visualisation was achieved using hierarchical grouping and heatmap visualisation with Metaboanalyst 6.0. Before creating heatmaps, the data were filtered to exclude features with a relative standard deviation (RSD) greater than 25%, ensuring reliability. The data were then

transformed to a log 2 scale, which stabilised variance and enhanced the interpretability of patterns in the dataset.

2.10.5 Molecular networking

A molecular network was created with the Feature-Based Molecular Networking (FBMN) workflow (Nothias *et al.,* 2020) on GNPS (http://gnps.ucsd.edu) (Wang *et al.,* 2016) using .mzML files. The mass spectrometry data were first processed with MZmine3 (Shmid *et al.,* 2023) for peaks and noise filtering and the results were exported to GNPS for FBMN analysis. The data were filtered by removing all MS/MS fragment ions within +/- 17 Da of the precursor *m/z*. MS/MS spectra were window-filtered by choosing only the top 6 fragment ions in the +/- 50 Da window throughout the spectrum. The minimum fragment ion intensity in the MS/MS spectra was set to 1000. The precursor ion mass tolerance was set to 0.02 Da and the MS/MS fragment ion tolerance to 0.02 Da. A molecular network was then created where edges were filtered to have a cosine score above 0.7 and more than 6 matched peaks. Furthermore, edges between two nodes were kept in the network if and only if each of the nodes appeared in each other respective top 10 most similar nodes. Finally, the maximum size of a molecular family was set to 100, and the lowest-scoring edges were removed from molecular families until the molecular family size was below this threshold. The spectra in the network were then searched against GNPS spectral libraries (Wang *et al.,* 2016; Horai *et al.,* 2010). The library spectra were filtered in the same manner as the input data. All matches kept between network spectra and library spectra were required to have a score above 0.7 and at least 6 matched peaks. The DEREPLICATOR was used to annotate MS/MS spectra (Mohimani *et al.,* 2018), higher scores (typically above 0.7 or >10 in DEREPLICATOR+) indicate stronger spectral alignment, though all annotations remain putative unless supported by additional evidence. The molecular networks were visualised using Cytoscape software (Shannon *et al.,* 2003).

2.10.6 Metabolite prediction

The *in-silico* structure prediction was performed using SIRIUS software (v.5.8.6) (Duhrkop *et al.,* 2019), integrating CSI:FingerID (Hoffmann *et al.,* 2022) for structure

prediction and CANOPUS (Duhrkop, *et al*. 2021) for chemical class assignment based on NPClassifier ontology (Kim *et al.,* 2021). Only metabolites with a molecular weight <850 Da were included to reduce computational time. Prediction was based on fragmentation spectra, isotope patterns, and exact mass. CSI:FingerID predictions were retained if the structure match score exceeded 90%, as this threshold has been shown to minimize false positives while retaining confident candidate structures (Dührkop *et al.,* 2015; Dührkop *et al.,* 2021). Likewise, CANOPUS chemical class assignments were considered reliable when class probability scores exceeded 0.7, following the recommendations of the developers, who demonstrated that this cut-off balances sensitivity and specificity across diverse metabolite classes (Dührkop *et al.,* 2019) No custom settings were applied beyond the default mass accuracy parameters provided by SIRIUS. In both Feature-Based Molecular Networking (FBMN) and SIRIUS workflows, biological replicates were treated as independent samples.

2.11 Metabolite fractionation of *Micromonospora* KRD324 crude extract

One of the crude extracts obtained from the scale up fermentation (200 mL) of *Micromonospora* KRD324 was fractionated using a pre-packed reversed-phase C18 cartridge (HyperSep™ C18, 200 mg, Thermo Scientific). The column was pre-conditioned with 1 mL of acetonitrile (MeCN) containing 0.1% formic acid (LC/MS Grade, Thermo Scientific), followed by 1 mL of H_2O with 0.1% formic acid (Merck, HPLC grade) to equilibrate. The crude extract was dissolved in 5% MeCN/H_2O (0.1% formic acid) to a final concentration of 2 mg/mL and loaded onto the column in 200 µL aliquots. Stepwise elution was performed using 400 µL of eluting solvent from 100% H_2O to 100% MeCN, with an additional final wash using methanol (MeOH). Elution was facilitated using a low-pressure vacuum pump (Fisherbrand™ Two-stage rotatory). Eight fractions were collected as follows:

- Fraction 1= H_2O:MeCN (100:0)
- Fraction 2= H_2O:MeCN (80:20)
- Fraction 3= H_2O:MeCN (60:40)
- Fraction 4= H_2O:MeCN (50:50)
- Fraction 5= H_2O:MeCN (40:60)
- Fraction 6= H_2O:MeCN (20:80)
- Fraction 7= H_2O:MeCN (0:100)
- Fraction 8= MeOH (100%)

Each fraction was dried under nitrogen and stored at 4 °C for subsequent analysis. The column was regenerated between sample runs by washing sequentially with 2 mL each of MeOH, MeCN, and H_2O per 200 µL of loaded extract. Fractions were analysed as described in section 2.10.2 and targeted metabolites were monitored and localised by mzMine using the raw files.

3 CHAPTER 3. Characterisation of *Rhodococcus cryophilus* sp. nov. (KRD162) and *Rhodococcus polaris* sp. nov. (KRD197), two novel actinomycetes isolated from Antartica environments

3.1 INTRODUCTION

The genus *Rhodococcus*, along with *Nocardia*, belongs to the family *Nocardiaceae* within the suborder *Corynebacterineae*. Members of this genus are obligate aerobes, Gram-positive, catalase-positive, non-motile, non-sporulating bacteria that are partially acid-fast. A key taxonomic feature of *Rhodococcus* is the presence of mycolic acids in their cell wall and their nocardioform morphology, characterised by mycelial growth that fragments into coccoid or rod-shaped cells (Van der Geize & Dijkhuizen, 2004; Lechevalier, 1989). Colonies can appear smooth or rough, with pigmentation ranging from cream, red, orange, and yellow to brown (Sánchez *et al.,* 2004). The name '*Rhodococcus*' was first introduced by Zopf in 1891, but the genus was redefined by Goodfellow and Alderson in 1977 to encompass strains formerly classified under *Nocardia*, *Corynebacterium*, and *Mycobacterium* (Goodfellow & Alderson, 1977).

The genus *Rhodococcus* includes several pathogenic species with relevance to both plant and animal health. *R. fascians*, for example, is a well-characterised phytopathogen known to induce gall formation by manipulating plant hormone levels—specifically cytokinin and auxin—and can infect a wide range of herbaceous and some woody plants (Goethals *et al.,* 2001; Putnam and Miller, 2007; Depuydt *et al.,* 2009). In the animal context, *R. equi* is a zoonotic pathogen primarily associated with granulomatous pneumonia and lung abscesses in foals (Muscatello *et al.,* 2007). Importantly, *R. equi* is also an opportunistic human pathogen, particularly in immunocompromised individuals. Its incidence has increased notably among HIV-infected patients, where it causes pulmonary infections with clinical manifestations

like those observed in equines (Díaz-Corrales & Serrano, 2003; Camponovo & García, 2006; Nasser & Bizri, 2001).

Beyond its occurrence in animals, plants, and humans, *Rhodococcus* species are frequently isolated from a broad range of environmental niches. Soil remains one of the most common sources, with examples including the isolation of ninety strains from soil samples in Tennessee (Ward *et al.,* 2018), *Rhodococcus kunmingensis* from rhizosphere soil in China (Wang *et al.,* 2008), and *Rhodococcus* sp. Y22 from the soil of a tobacco plantation (Gong *et al.,* 2009). However, representatives of the genus have also been recovered from more extreme or unconventional habitats such as rocks, insects, water bodies, and marine sediments. For instance, *R. qingshengii* S10 was isolated from a weathered rock core in Russia (Khilyas *et al.,* 2021), and *R. rhodnii* was found in the intestinal tract and feces of the insect *Rhodnius ecuadoriensis* (Rodriguez *et al.,* 2011). Marine-derived species such as *R. nanhaiensis* sp. nov. were obtained from sediments of the South China Sea (Li *et al.,* 2012), while Heald *et al*. (2001) reported a diverse collection of *Rhodococcus* isolates from deep-sea sediments spanning coastal, abyssal, and hadal trench environments in the Northwest Pacific Ocean. This ecological breadth is mirrored by the remarkable metabolic versatility of the genus, which has attracted significant attention for biotechnological and industrial applications. *Rhodococcus* species can degrade a wide array of organic compounds and producing value-added molecules such as surfactants, flocculants, amides, and polymers (Cappelletti *et al.,* 2020). Additionally, more recent studies have revealed their ability to produce bioactive secondary metabolites. For example, *R. erythropolis* was shown to biosynthesise biosurfactants when grown on glycerol (Ciapina *et al.,* 2006), while *R. jostii* K01-B0171 was found to produce lariantin A and B, which exhibited inhibitory activity against *Mycobacterium smegmatis* and *Mycobacterium tuberculosis* (Iwatsuki *et al.,* 2006; Iwatsuki *et al.,* 2007).

Despite its proven ecological adaptability and metabolic versatility, the genus *Rhodococcus* remains relatively underexplored in terms of secondary metabolite production. Recent studies have started to uncover its latent biosynthetic potential. For instance, Hu, *et al*. (2024) employed a combined elicitor-based and untargeted metabolomic strategy to analyse a marine-derived *Rhodococcus* strain, leading to the discovery of previously uncharacterised auraquinone-like compounds. Similarly, Undabarrena, *et al*. (2021) highlighted its untapped chemical repertoire, suggesting that traditional culturing approaches may underestimate its full biosynthetic capacity.

This is supported by recent genomic data. As of March 2025, a total of 934 *Rhodococcus* genomes have been deposited in the NCBI database, 143 of them are complete or at the chromosomal level. The antiSMASH database (Blin *et al.,* 2025) reports 4,503 Biosynthetic Gene Clusters (BGCs) within the genomes of strains from this genus, with the most frequent classes representing non-ribosomal peptide synthetases (NRPS; 43%), ribosomally synthesized and post-translationally modified peptides (RiPPs; 16%), polyketide synthases (PKS; 14%), and terpenes (12%). In addition, a focused analysis of 30 complete genomes in this study revealed an average of 17 BGCs per strain, further underscoring the genus remarkable biosynthetic richness. For comparison, *Streptomyces* species, the classical model of natural product discovery, often harbor between 25 and 45 BGCs per genome (Caicedo-Montoya *et al.,* 2021), while other rare actinomycetes such as *Micromonospora* can encode 7–28 BGCs (Hifnawy *et al.,* 2020). Thus, *Rhodococcus* occupies an intermediate position. *Rhodococcus* genomes range from 3 to 11 Megabases (Mb) in size and may carry circular or linear chromosomes, often accompanied by plasmids (Hu *et al.,* 2024; Larkin, 2010). Although *Rhodococcus* harbors fewer biosynthetic gene clusters than classical producers like *Streptomyces*, the substantial number of biosynthetic gene clusters it harbors highlights its untapped potential as a source of novel natural products.

Despite this taxonomic and ecological diversity, the genus *Rhodococcus* remains comparatively understudied in terms of its secondary metabolites, especially when contrasted with other actinomycetal genera such as *Streptomyces* or *Micromonospora*. While various environmental isolates have demonstrated promising bioactivities, including antimicrobial and anticancer properties, the underlying BGCs and metabolites produced are only beginning to be explored. This gap is particularly evident with strains from extreme or under-sampled environments, such as Antarctica, where selective pressures may drive the evolution of unique biosynthetic capabilities. For these reasons and considering the yet unexplored biosynthetic potential of the genus *Rhodococcus*, this study investigates the genomes of two Antarctic *Rhodococcus* strains. A hybrid sequencing strategy combining short-read (Illumina) and long-read (Oxford Nanopore) technologies was employed to generate high-quality genome assemblies. Subsequently, bioinformatic tools such as antiSMASH (Blin *et al.,* 2025) were used for the identification and annotation of BGCs, while BiG-SCAPE (Navarro-Munoz *et al.,* 2020) was applied to classify these BGCs into families and analyse their evolutionary relationships. This approach enabled a more precise

exploration of the biosynthetic potential of the strains studied, contributing to the broader understanding of specialised metabolites by *Rhodococcus* as well as the formal description of two new species.

3.2 RESULTS

3.2.1 Genome sequencing and assembly of *Rhodococcus cryophilus* sp. nov. (KRD162) and *Rhodococcus polaris* sp. nov. (KRD197)

Long-read Nanopore sequencing of *Rhodococcus* strains KRD162 and KRD197 was performed, resulting in a *de novo* nanopore-only assembly generated by the sequencing provider, in which Fitlong v0.2.1 (default parameters) (Wick, 2017) was used to filter low-quality reads (i.e., removing very short sequences) and the assemblers Miniasm (Li, 2016) and Flye (Kolmogorov *et al.,* 2019) were used to join the contigs. The genome scaffolds of KRD162 and KRD197 (Table 3.1) were 6.2 Mb and 5.4 Mb in size, with a coverage of 40x and 91x, comprising five and two contigs respectively, with an estimated completeness of 99% for both assemblies. While the assemblies exhibit high structural completeness, the relatively low read depth compromises base accuracy, a limitation already established for assemblies performed solely with Nanopore sequences.

To improve base-level accuracy and resolve structural gaps, previously generated short-read Illumina sequencing data were incorporated into the Nanopore-based assemblies. These reads were mapped onto the Nanopore-based assemblies using Bowtie2 (Langmead & Salzberg, 2012) and Samtools (Danecek, *et al*. 2021) to perform base-level error correction, resolve potential assembly artefacts. Remaining gaps were closed with Pilon (Walker *et al.,* 2014), to correct the draft assemblies. The quality of the hybrid (Nanopore-Illumina) assemblies was assessed using multiple metrics. The N50 value was 5.148 Kilobases (kb) for KRD162 (5 contigs) and 5.275 kb for KRD197 (2 contigs) (Table 3.1). The N50 statistic indicates the length at which 50% of the assembly is contained in contigs of that length or greater and is commonly used as an indicator of assembly contiguity. The increase in N50 values reflects the improvement in assembly contiguity following hybrid error correction and gap resolution, compared to the initial Nanopore-only assemblies, which were considerably more fragmented (N50 = 9495 and 16600 bp, for KRD162 and KRD197).

3.2.2 Genome architecture: chromosome map + plasmid detection.

Genome completeness was assessed using BUSCO (Simão, *et al.* 2015) and both assemblies showed completeness of 100%, suggesting that essential single copy orthologs were effectively captured. These results confirm that the integration of Illumina sequencing into the Nanopore-based assemblies helped to resolve repetitive regions, errors and structural gaps that could not be addressed with Nanopore long-read data alone. Finally, the overall genome coverage increased from 91× and 40× to 271.8× and 296.6× for KRD162 and KRD197, respectively, following integration of Illumina short reads. This increase in depth of coverage not only enhanced base-level confidence but also reduced potential sequencing artefacts, as reflected by the complete removal of mismatches per 100 kbp in the hybrid assemblies (Table 3.1). Furthermore, the percentage of complete single-copy orthologues identified using BUSCO rose from 99.84% to 100% in KRD162 and from 99.47% to 100% in KRD197, confirming improved genome completeness. These improvements provide a more robust foundation for downstream applications such as accurate BGC prediction, variant detection (Blin *et al.,* 2025), which rely on high-contiguity and low-error assemblies for accurate annotation.

The complete chromosomes of strains KRD162 and KRD197 were annotated using the Proksee (Bakta) platform, which combines structural gene prediction with curated functional annotations. It was selected for its rapid execution and alignment-free gene calling strategy, which is particularly suitable for high-GC Gram-positive bacteria such as *Rhodococcus*. While less exhaustive than tools like RAST or PGAP, Bakta provides concise annotations and compatibility with downstream analyses (e.g., BGC identification), making it appropriate for this exploratory genomic analysis. A summary of annotated features is presented in supplementary Table S3.1, which includes the number of predicted protein-coding sequences (CDS), tRNAs, rRNAs, and non-coding RNAs. For strain KRD162, the genome includes 2,237 protein-coding genes**,** 14 non-coding RNAs**,** 46 tRNAs, and 12 rRNA operons. These figures are within the expected range for *Rhodococcus* species, though the relatively high number of rRNA operons may indicate robust transcriptional capacity or has been associated with an enhanced ability to rapidly adjust gene expression in response to changing environmental conditions, as reported for metabolically versatile, free-living Actinomycetota. Similarly, the KRD197 genome contained 4,860 protein-coding

genes**,** 13 non-coding RNAs**,** 47 tRNAs**,** 12 rRNA operons, and 17 BGCs. This strain displays a considerably smaller genome compared to KRD162 (5.39 Mb vs. 6.06 Mb), which is consistent with previous reports of *Rhodococcus* strains, where the genome size of this genus can range from 3 to 11 Mb (Undabarrena *et al*., 2021). The larger genomes often include extensive accessory gene content associated with xenobiotic degradation, secondary metabolite biosynthesis, and environmental adaptation.

Table 3.1 Genome assembly metrics for *Rhodococcus* strains KRD162 and KRD197. Long-read Nanopore-only assemblies and hybrid Nanopore and Illumina reads assemblies are compared. Metrics include the number of contigs, total assembly length, largest contig size, average coverage, N50, and genome completeness based on BUSCO analysis. "N/A" indicates values not calculated. Plasmid counts represent extrachromosomal contigs annotated using MOB-suite.

Genome assembly metric	Fitlong + Miniasm and Flye (Nanopore)		Flye + Pilon tool (Nanopore + illumna)	
Parameter	**KRD162**	**KRD197**	**KRD162**	**KRD197**
Number of contigs	5	2	5	2
Total length	6.2 Mb	5.4 Mb	6.06 Mb	5.4 Mb
Largest contig (bp)	5170196	5275272	5148399	5275250
Average coverage	91x	40x	271.7x	296.6x
GC%	N/A	N/A	64.34	64.13
N50 (bp)	9495	16600	5148399	5275250
Mismatches per 100 Kbp	N/A	N/A	0	0
Busco (complete single-copy genes)	99.84	99.47	100	100
Plasmid number	4	1	3	1

To determine whether any of the contigs corresponded to putative plasmid sequences two complementary bioinformatic tools were used PlasFlow (Krawczyk *et al.,* 2018) and MOB-recon (Robertson and Nash, 2018). These tools rely on different principles to distinguish plasmid DNA from chromosomal DNA, allowing cross-validation of predictions. PlasFlow, uses a deep neural network trained on k-mer frequencies from plasmid and chromosomal sequences to assign a probability score to each contig, classifying it as plasmid-derived or chromosomal. In simple terms, this approach assesses whether the overall sequence composition of a contig more closely resembles known plasmids or chromosomes, without relying on explicit gene annotations. MOB-recon, in contrast, identifies plasmid contigs by aligning them against a curated database of known plasmid-associated genes, including replication genes (replicons) and relaxes genes, which encode enzymes required for plasmid mobilisation during conjugation. The tool also attempts to reconstruct full plasmid

structures when multiple related contigs are present. Each prediction is assigned a confidence level based on the presence and consistency of these hallmark plasmid genes, with higher confidence scores indicating stronger support for a plasmid origin.

Both tools were used to increase reliability of plasmid detection: PlasFlow provided composition-based evidence, while MOB-recon added functional and database-driven annotation. Full classification and circularity results from both tools are summarised in Table 3.2, which reports the predicted origin of each contig (chromosomal or plasmid) and whether the sequence is likely circular, a typical structural feature of bacterial plasmids. The identification of plasmid-derived contigs was supported by cross-validation between PlasFlow and MOB-recon, in combination with contig size. In the case of strain KRD197, for example, one of the tools (PlasFlow) classified the smaller contig as plasmid-derived (Plasmid.Actinobacteria), while the larger contig remained unclassified. In contrast, MOB-recon annotated both as chromosomal. Given the typical size expectations for plasmids (usually a few kb to <500 kb) versus chromosomes (commonly 3–10 Mb), and the sequence-based classification from PlasFlow, the smaller contig (117.99 kbp) was prioritised as the most likely plasmid candidate, while the biggest one (5.28 Mbp) was considered the chromosomal.

In the case of strain KRD162, three contigs were classified as putative plasmids using both PlasFlow and MOB-recon, and were designated pRKRD162-A, pRKRD162-B, and pRKRD162-C. Among these, pRKRD162-A showed evidence of being a complete extrachromosomal element, as it was predicted to be circular by MOB-recon and taxonomically classified as Plasmid.Actinobacteria by PlasFlow. This plasmid harbours *parA*, a key partitioning gene, along with genetic elements associated with antimicrobial resistance (e.g., *qacA*_1, *qacA*_2), mobile elements (*IS110*, *IS21*, *Tn3*), recombination (*xerC*), and toxin-antitoxin systems (*higA2*, higB2) (Table S3.2). These features collectively suggest a role in horizontal gene transfer and possibly in environmental fitness or resistance phenotypes. The remaining plasmids (pRKRD162-B/C) were either incomplete or lacked sufficient annotation evidence and were therefore not analysed.

Table 3.2. Results from MOB-Recon and PlasFlow analyses for *Rhodococcus* strains KRD162 and KRD197. a) PlasFlow was employed to estimate the probability of plasmid origin for individual contigs, while b) MOB-Recon was used to detect and classify plasmid contigs based on replicon typing and mobility predictions.

a)

PlasFlow: Prediction of plasmid sequences from contigs			
Strain	Contig number	Contig length	Prediction
KRD162			
	1	17019	Unclassiffied.Actinobacteria
	2	205177	Plasmid.Actinobacteria
	3	598199	Plasmid.Actinobacteria
	4	5148399	Chromosome.Actinobacteria
	5	91214	Plasmid.Actinobacteria
KRD197			
	1	5275250	Unclassiffied.Actinobacteria
	2	117999	Plasmid.Actinobacteria

b)

MOB-suite: Plasmid clustering, reconstruction, and typing from draft assemblies				
Strain	Contig number	Contig length	Type	Circularity status
KRD162				
	1	17019	Chromosome	Incomplete
	2	205177	Chromosome	Circular
	3	598199	Chromosome	Incomplete
	4	5148399	Chromosome	Incomplete
	5	91214	Chromosome	Incomplete
KRD197				
	1	5275250	Chromosome	Incomplete
	2	117999	Chromosome	Incomplete

In contrast, for strain KRD197, a single contig aside from the chromosome was detected. While MOB-recon predicted this to be chromosomal, PlasFlow assigned it to Plasmid.Actinobacteria. Due to its small size (117999 bp), the incongruent annotations, and the lack of replication genes typically associated with chromosomal sequences, this contig was designated as pRKRD197-A, a candidate for an incomplete plasmid or a plasmid integrated into the chromosome. These two scenarios suggest distinct genomic architectures: the former (incomplete plasmid) would imply potential fragmentation or misassembly during sequencing, while the

latter (integration) could represent a genuine recombination event or functional plasmid domestication. To discriminate between these possibilities and verify the physical existence of extrachromosomal plasmids, further experimental validation is required. Pulsed-field gel electrophoresis (PFGE) would separate large circular DNA, such as chromosomes and plasmids to provide confirmation of extrachromosomal elements through distinct band migration. Finally, the circular chromosome maps of *Rhodococcus* KRD162 and KRD197, along with their corresponding plasmids, are shown in Figure 3.1. These maps not only illustrate the overall genome architecture but also highlight differences between strains: KRD162 harbors a smaller chromosome (5.15 Mbp) but contains a complete, well-structured plasmid (pRKRD162-A), whereas KRD197 possesses a larger chromosome (5.3 Mbp) and only a candidate plasmid contig (pRKRD197-A) of uncertain status. This contrast underscores the variability of plasmid content within the genus, suggesting that while chromosomal backbones remain conserved, plasmid acquisition, loss, or integration may contribute significantly to strain-specific adaptation and biosynthetic potential.

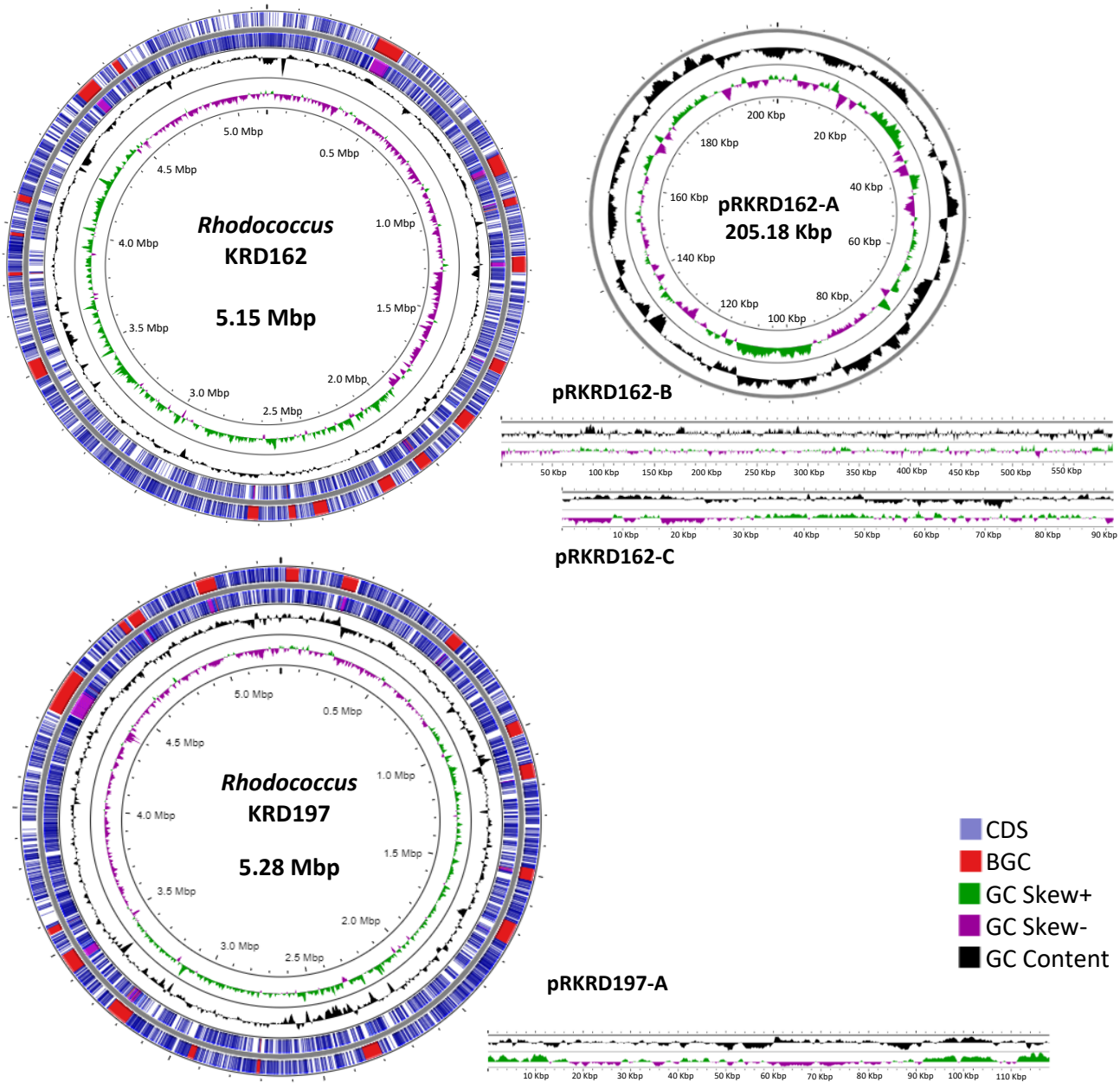

Figure 3.1. Circular representation of the chromosomes of *Rhodococcus* KRD162 (top) and *Rhodococcus* KRD197 (bottom) and their corresponding plasmids. The concentric rings represent (from the outside): protein coding sequences (CDS, purple); biosynthetic gene clusters (BGC, red); guanine and cytosine content (GC, black); higher abundance of guanine compared to cytosine (GC Skew+, green) and vice versa (GC Skew-, pink) and scale line in Mbps.

3.2.3 BGC mining of *Rhodococcus* KRD162 and KRD197 strains

Taking advantage of the high-quality genome assemblies for *Rhodococcus* KRD162 and KRD197, BGCs were predicted by antiSMASH (v.7.0) (Blin *et al.,* 2025). This tool uses domain-based homology and rules-based prediction to identify known and putative natural product BGCs. While antiSMASH is a powerful first-pass predictor, it relies on accurately assembled genomes. In high-GC genomes with complex architecture, assembly challenges can result in fragmented contigs, which in turn may cause biosynthetic gene clusters to appear artificially split or over-predicted. Consequently, antiSMASH outputs were interpreted cautiously and used as indicative rather than definitive annotations. KRD162 contained a total of 17 BGCs, dominated by NRPS-like clusters (n = 9), alongside smaller numbers of terpene (n = 2), PKS (n = 2), ectoine (n = 1), lassopeptide (n = 1), butyrolactone (n = 1), and one putative cofactor-associated BGC (Fig. S3.1a). In contrast, KRD197 also encoded 17 BGCs but exhibited a distinct distribution, with fewer NRPS-like clusters (n = 7), a higher number of PKS clusters (n = 4), and the presence of hybrid RiPP/NRPS-like BGCs (n = 2), in addition to terpene (n = 2), ectoine (n = 1), and RiPP-like clusters (n = 1) (Fig. S3.1b). KRD197 have 3 more PKS BGCs, with notable differences in hybrid clusters and specialised RiPP-related regions, which highlights the biosynthetic diversity, even between closely related Antarctic strains. It is important to note that, within the antiSMASH framework, similarity values are based on the proportion of biosynthetic and accessory genes in a predicted cluster that match those in experimentally validated BGCs deposited in the MIBiG database. These values do not represent direct nucleotide or protein sequence identity. Accordingly, low or moderate matches (<70%) should not be interpreted as confirmation of novelty per se, but rather as partial overlap, gene content divergence, or limitations in the current reference database. In this study, approximately 80% of the BGCs present in the genome of strains KRD162 and KRD197 showed only partial matches to known clusters; therefore, definitive conclusions about novelty will require additional comparative genomic and functional validation. Despite having the same total number of BGCs (17), KRD197 showed a distinct cluster composition, including a higher number of PKS clusters and differences in hybrid and RiPP-related regions, highlighting biosynthetic diversity among closely related polar isolates.

Across both strains, NRPS BGCs were the most prevalent, consistent with trends reported from other *Rhodococcus* species (Undabarrena *et al*., 2021). Among these,

the presence of BGCs predicted to biosynthesise non-alpha polyamino acids such as ε-polylysine was confirmed with high confidence (100% similarity to characterised reference clusters). ε-Polylysine is a cationic polymer with well-documented broad-spectrum antimicrobial activity. The ectoine BGC, while present in both strains, showed only 50% sequence similarity to known reference clusters, suggesting either divergence from canonical ectoine pathways or limitations in database representation. KRD197 had two BGCs that displayed >50% sequence similarity to known pathways: a mayamycin-like cluster (63% similarity) and a heterobactin B-like siderophore BGC (63% similarity). These findings align with previous reports describing these metabolites produced by *Rhodococcus* and related genera (Bosello *et al.,* 2011; Bosello *et al.,* 2013).

To contextualise these findings, the BGC repertoire of both Antarctic strains was compared to the BGCs from 21 publicly available *Rhodococcus* genomes (NCBI database) selected based on phylogenetic proximity (Figure 3.4 and Table S3.3). BGC similarity and grouping were assessed using BiG-SCAPE, which organises BGCs into Gene Cluster Families (GCFs) based on domain architecture and sequence similarity, applying a standard cutoff of 0.3 for clustering, where GCFs represent clusters with ≥70% sequence conservation. BGCs that did not cluster with any others (singletons) were interpreted as unique or strain-specific biosynthetic regions and retained for downstream analyses; however, they were excluded from the network visualisation (Fig. 3.2) to improve clarity and avoid distortion of similarity-based relationships. Across all 23 *Rhodococcus* genomes, 618 BGCs were detected, distributed as follows: NRPS (246), “Other” (butyrolactones, oligosaccharides, arylpolyenes, aminocoumarins, and includes saccharides (4) (183), terpenes (61), type I PKSs (53), RiPPs (48), PKS (18) and PKS-NRP hybrids (9). KRD162 and KRD197 had approximately half of their BGCs (8 and 9, respectively) grouped within shared GCFs (shared with other strains), while the remainder were singletons, suggesting strain-specific BGCs and a degree of novelty at the genomic level.

Only two GCFs contained BGCs with significant homology to characterised clusters from the MIBiG reference database, rhodochelin and heterobactin siderophores. The rhodochelin biosynthetic pathway was first described from *R. jostii RHA1* (Bosello *et al.,* 2011), to be a siderophore. This GCF was detected also in *R. koreensis* DSM44498, *R. opacus* DSM43205, and *R. tibetensis* FXJ9.536 strains, suggesting that rhodochelin or related siderophores may be a conserved ecological trait within

these species. Similarly, the heterobactin A BGC, known from *R. erythropolis* PR4 (Bosello *et al.,* 2013), clustered with BGCs from *R. baikonurensis*, *R. qingshengii*, and *R. jianlingiae*, highlighting widespread siderophore biosynthetic capacity of *Rhodococcus*. These results illustrate the diversity and partial conservation of siderophore biosynthesis within the genus, while also pointing to uncharacterised BGCs that warrant further exploration for novel metabolite discovery. However, unlike highly diverse secondary metabolites such as PKS- or NRPS-derived compounds, siderophores are subject to strong functional and structural constraints, as their iron-chelating activity depends on conserved chemical features. As a result, variation within siderophore families is often limited compared to other classes of secondary metabolites. It is noteworthy that, while the groups with the highest total number of BGCs were NRPs and the "other" category, the largest individual biosynthetic families were found among two BGC types: one terpene and one PKS cluster, each comprising 17 members. This suggests that BGCs belonging to the NRPs and "other" classes exhibit higher diversity, distributed across numerous smaller families, whereas terpene and PKS BGCs are organised into fewer but larger and more conserved GCFs. The widespread presence of these conserved BGCs across the 17 *Rhodococcus* strains indicates they are likely essential or play a generalist role, potentially linked to ecological adaptation.

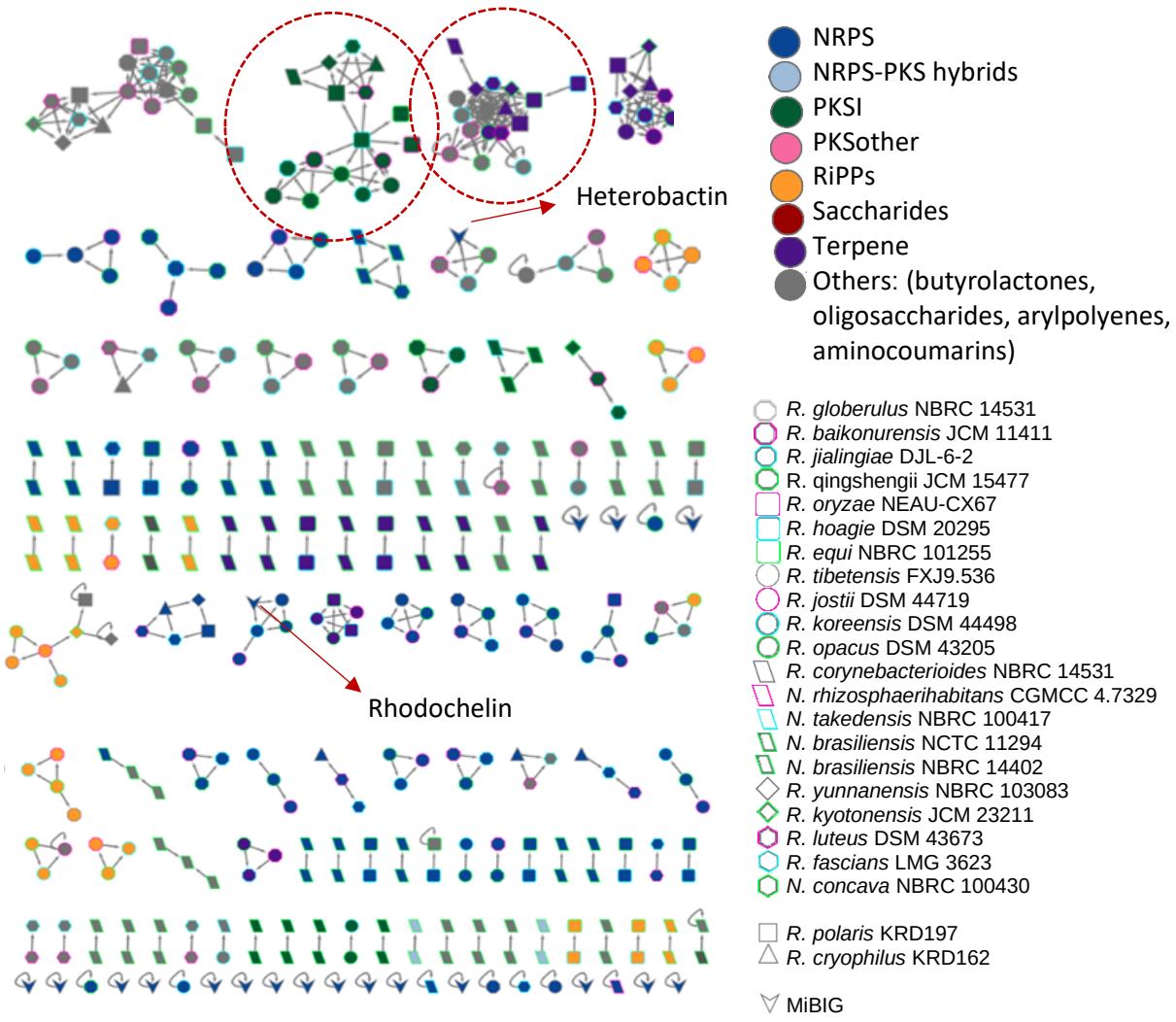

Figure 3.2. GCF network of the predicted BGCs in the genomes of KRD162 and KRD197 with 21 pylogenetically-related *Rhodococcus* strains using BiG-SCAPE and visualised with Cytoscape. Each node represents a BGC and the edges represent a correlation distance of 0.3 or higher. The node shape and border colour show *Rhodococcus* species and colour node show natural product classes. The dotted circle shows the largest families of BGSs (terpene and PKS).

Among these terpene BGCs, a putative *lycopene cyclase* gene was identified. Lycopene cyclase catalyses a key step in carotenoid biosynthesis, producing pigmented isoprenoids involved in cellular protection against oxidative stress and environmental radiation. This gene served as a marker to construct the phylogenetic tree shown in Figure 3.3, allowing comparison of the evolutionary relationships of this biosynthetic feature across strains. The resulting tree places strain KRD162 closer to *R. fascians*, while KRD197 clusters with *R. yunnanensis* and *R. kyotonensis*. This distribution largely mimics the multi-locus phylogeny derived from whole-genome analysis of the same strains (Fig. 3.4). In contrast, such correlation was not observed when analysing the gene family structure (GFS) based on the conserved PKS BGC family (Fig. S3.2), where KRD197 showed no clear relationship with *R. kyotonensis*. Additionally, only 17 of the 23 analysed strains harboured either the conserved terpene or PKS gene clusters, highlighting their limited but potentially ecologically relevant distribution.

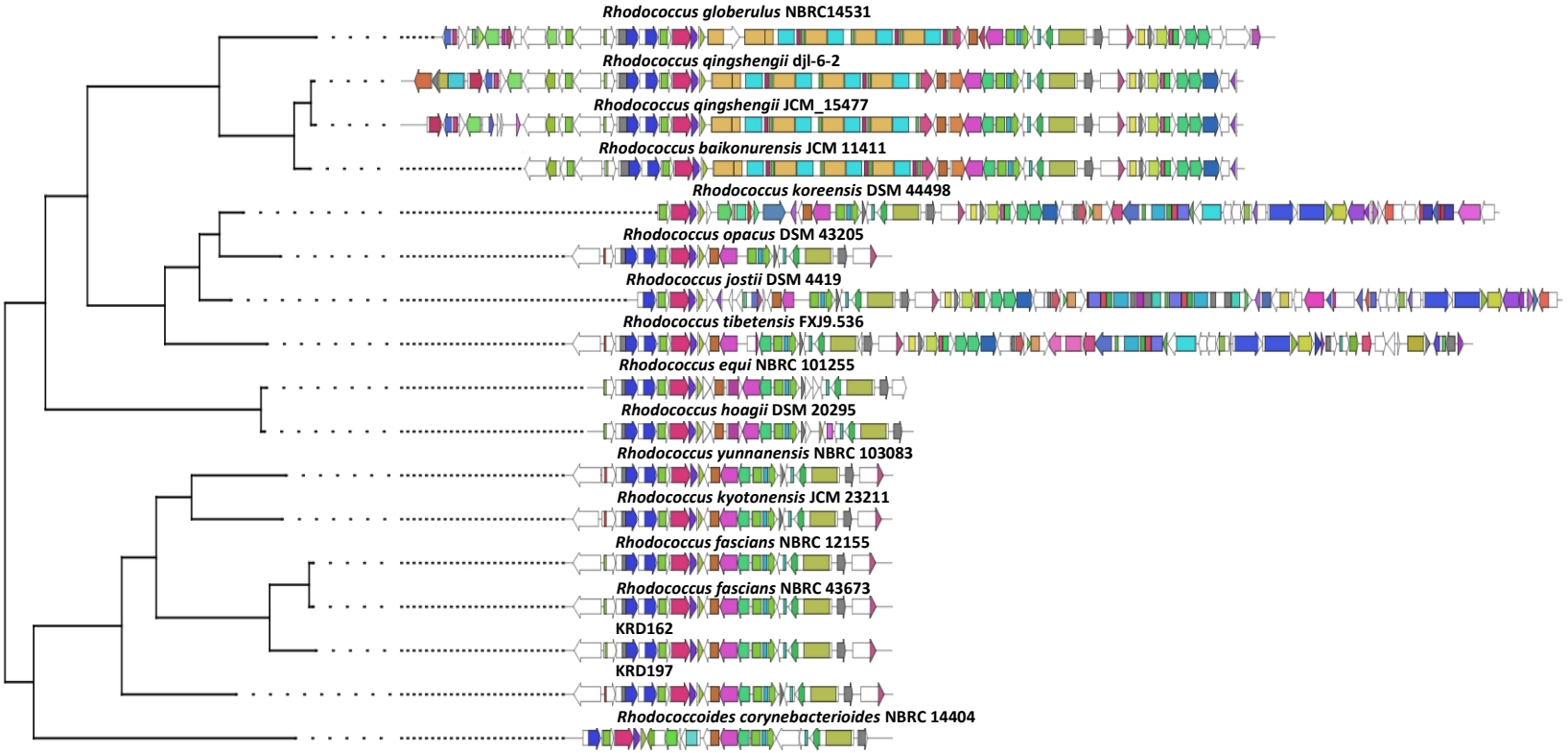

Figure 3.3. CORASON-based gene cluster tree illustrating functional and structural relationships among terpene BGCs (putative lycopene cyclase gene) detected in *Rhodococcus* KRD162, KRD197, and 15 related genomes. The tree is derived from the alignment of conserved biosynthetic domains, providing a comparative representation of cluster similarity. As CORASON does not perform statistical phylogenetic inference, bootstrap values, branch length scales and formal outgroup are not included. Gene clusters are depicted as arrows indicating gene orientation and colour-coded by function, while dotted lines represent branches without sufficient genetic content for full cluster comparison.

3.2.4 Taxonomic characterisation of *Rhodococcus* isolates KRD162 and KRD197

3.2.4.1 Phylogenetic and evolutionary relationships within the *Rhodococcus* genus

The nearly complete 16S rRNA gene sequences of isolates KRD162 and KRD197 were initially analysed to determine their phylogenetic relation within the genus *Rhodococcus*. For KRD162, the closest matches were *R. sovatensis* (NR_156055.1; 99.37% similarity) and *R. cerastii* (NR_117103.1; 99.56%), while KRD197 exhibited similarity to *R. kyotonensis* (NR_041512.1; 99.22%), *R. cercidiphylli* (NR_116275.1; 98.80%) and *R. yunnanensis* (NR_043009.1; 98.91%). A maximum likelihood phylogenetic reconstruction based on 16S rRNA gene sequences revealed that both KRD162 and KRD197 form a well-supported monophyletic clade with *R. fascians* (NR_037021.1), although each occupied a distinct, separate branch within the tree (Fig. S3.3). While 16S rRNA gene similarity remains a widely used marker for initial taxonomic placement, its limitations for species delineation are well established, particularly within Actinomycetales, where closely related species often share >99% sequence identity (Tindall *et al.,* 2010). Therefore, higher-resolution genomic comparisons are required to robustly assess taxonomic novelty.

To this end, whole-genome comparisons were performed using Average Nucleotide Identity based on BLAST (ANIb), an established approach for species-level discrimination with a generally accepted species boundary of 95% (Chun *et al.,* 2018). The ANI analysis included 22 reference genomes of *Rhodococcus* strains selected as the closest relatives to KRD162 and KRD197 based on results from the TYGS platform (https://tygs.dsmz.de) (Table S3.3). Although the selected reference genomes varied in assembly quality and contiguity, they represent the best available taxonomic framework for comparative analysis. The results revealed that KRD162 and KRD197 shared ANI values ranging from 70% to 72% when compared to all reference *Rhodococcus* genomes—well below the species delineation threshold of 95%. Furthermore, digital DNA–DNA hybridisation (dDDH) values between KRD162 and the closest reference strain, *R. fascians* NBRC 12155, were 22.3%, while for KRD197, the highest dDDH value was 24.8% with *R. yunnanensis* NBRC 103083. Both values fall significantly below the established 70% species boundary (Chun *et al.,* 2018), supporting the conclusion that these isolates represent two previously undescribed, phylogenetically distinct species within the genus *Rhodococcus*. Additionally, the ANI between KRD162 and KRD197 was 71.5%, with a corresponding dDDH value of 23.1%, confirming that they are not only distinct from known *Rhodococcus* species but also from each other (Fig. 3.4). Taken together, these genomic comparisons, despite the limitations associated with varying

assembly quality among public genomes, strongly supported the recognition of KRD162 and KRD197 as two novel, phylogenetically distinct *Rhodococcus* species.

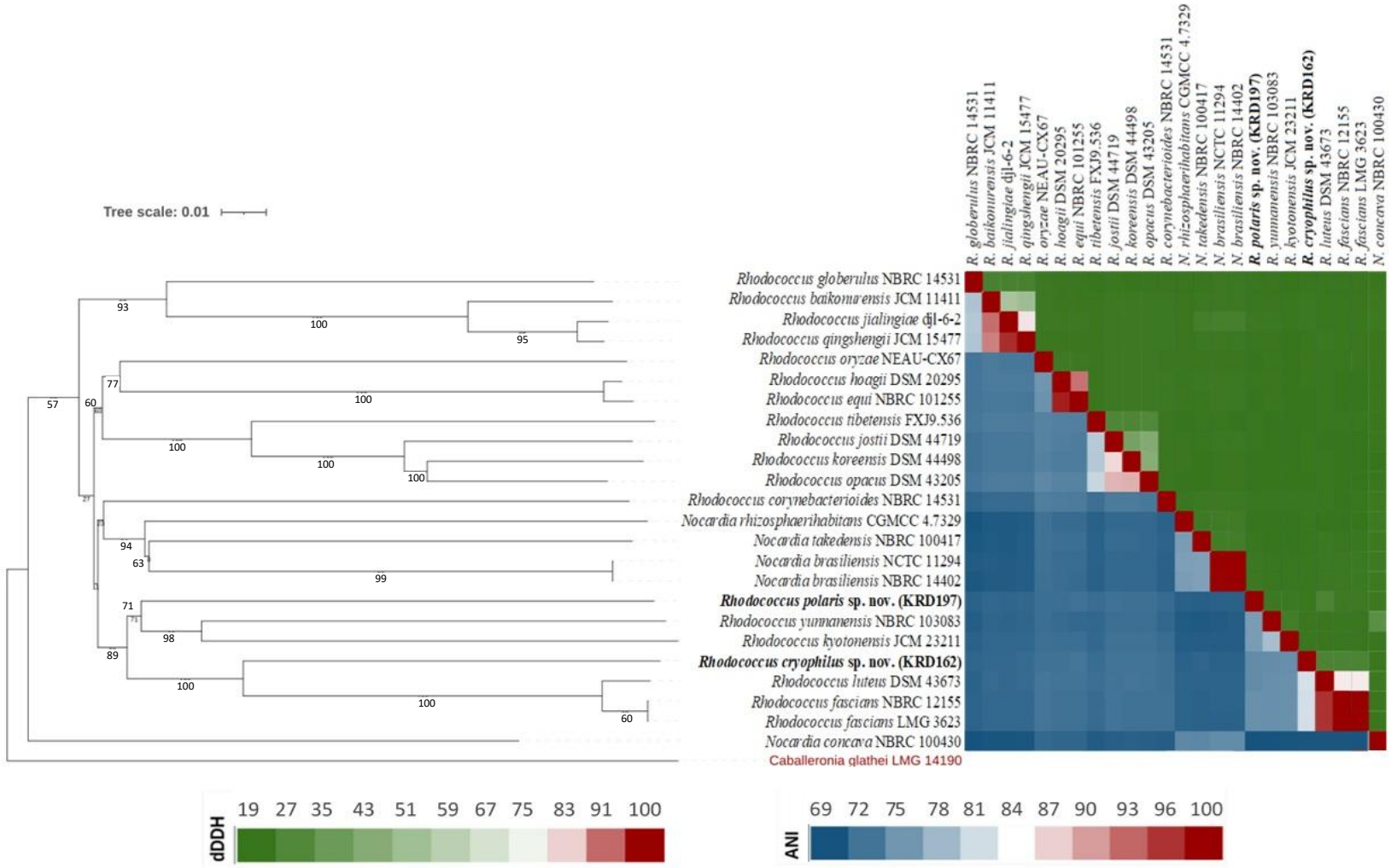

Figure 3.4. Average nucleotide identity (ANI) (blue, 69–81%; white, 84%; and red, 87–100%) and digital DNA–DNA hybridization (dDDH) (green, 19–75%; red, 83–95%) values shown as a heatmap of genomic distances between strains KRD162, KRD197, and other *Rhodococcus* strains. A whole-genome–based phylogenetic tree, reconstructed by TYGS using the Genome BLAST Distance Phylogeny (GBDP) method, is displayed alongside 22 reference strains. *Caballeronia glathei* LMG 14190 was used as an outgroup. The numbers below the branches are support values exceeding 60% of the bootstrap. Bar: 0.01 substitution per nucleotide position.

3.2.4.2 Phenotypic and chemotaxonomy properties.

As a part of the phenotypic description, the colony morphology of strains KRD162 and KRD197, together with the reference strain *R. fascians* DSM 20669^T, was examined on various ISP media (ISP2, ISP3, ISP4, ISP5). All strains formed yellow-pigmented colonies on ISP2, ISP3, and ISP5, while no growth was observed on ISP4. No production of diffusible pigments was detected (Fig. S3.4). Salinity and pH tolerance assays revealed halotolerance in both isolates, with growth occurring at NaCl concentrations of 0%, 15%, 25%, and 35%. Salt, however, was not essential for growth. Differences in pH tolerance were noted: KRD197 grew between pH 6–9, KRD162 between pH 5–8, and the reference strain across pH 5–9. SEM analysis revealed smooth rod-shaped cells in both isolates (Fig. 3.5), consistent with *Rhodococcus* species morphology (Sun *et al.,* 2023), reinforcing their taxonomic placement within this genus. Cellular fatty acid profiles (Table 3.3) showed that C16:0, C18:1 ω9c, C14:0, and 10-methyl C18:0 were predominant across all strains, consistent with reported *Rhodococcus* profiles. However, moderate levels of unsaturated and methylated fatty acids varied between strains. KRD197 exhibited elevated C16:1 ω6c and 10-methyl fatty acids compared to KRD162. Although these differences occur in less abundant fatty acids (minor components), they suggest underlying phenotypic diversity between the isolates, despite overall chemotaxonomic similarity.

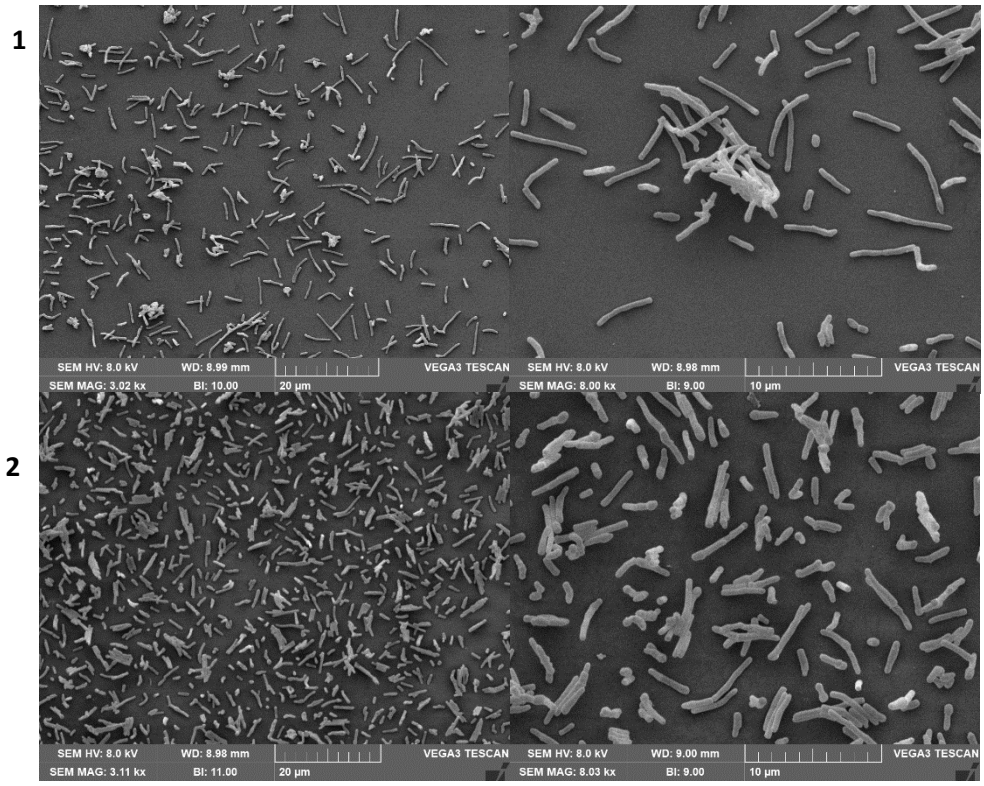

Figure 3.5. Scanning electron micrograph images of strain 1. = KRD162 and 2 = KRD197; growth on ISP2 for 3 days at 28 °C. Bar, 20 and 10 µm.

Table 3.3. Differential phenotypic characteristics and cellular fatty acid composition of strains KRD162, KRD197 and the Type strain of the most closely related species of the genus *Rhodococcus*. Strains were cultivated on ISP2 at 28 °C for 72 h. Fatty acid profiles are expressed as percentage of total cellular fatty acids and were determined by gas chromatography of fatty acid methyl esters (GC-FAME) following standard protocols. Columns represent strains: 1 = KRD162; 2 = KRD197; 3 = *R. fascians* DSM 20669T. ND: Not detected.

Morphology	1	2	3
ISP2	Yellow	Yellow	Yellow
ISP3	Yellow	Yellow	Yellow
ISP4	-	-	-
ISP5	Yellow	Yellow	Yellow
Growth at:			
NaCl (%)	0–35	0–35	0-35
pH	5-8	6-9	5-9
Fatty acid	1	2	3
Saturated:			
C12:0	ND	0.4	ND
C14:0	7.5	4.7	7.4
C15:0	1. 2	1.8	1.9
C16:0	34.9	30.2	33.3
C17:0	5.2	0.9	0.4
C18:0	2.8	2.1	1.0
C19:0	ND	0.4	ND
C20:0	0.3	ND	ND
Unsaturated:			
C14:1 ω4c	ND	ND	0.8
C15:1 ω5c	ND	ND	0.4
C15:1 ω9c	ND	ND	0.2
C16:1 ω6c	3.7	8.5	10.6
C16:1 ω7c	0.3	1.2	0.9
C16:1 ω9c	1.1	0.9	0.9
C17:1 ω8c	0.3	2.0	1.2
C18:1 ω7c	ND	0.2	ND
C18:1 ω9c	22.3	29.6	26.7
C19:1 ω9c	ND	0.9	0.8
C20:1 ω9c	ND	0.1	ND
C20:1 ω11c	ND	0.6	0.4
Hydroxy:			
C10:0 3-OH	0.4	ND	ND
Methyl:			
10-methyl C16:0	ND	0.2	0.3
10-methyl C17:0	ND	0.8	0.4
10-methyl C18:0 (TBSA)	17.8	14.3	12.3

3.2.4.3 Formal description of *Rhodococcus cryophilus* sp. nov. (KRD162) and *Rhodococcus arcticum* sp. nov. (KRD197).

- *Rhodococcus cryophilus* (cry.o'phil.us. L. masc. adj. *cryophilus*, from Gr. *kryos* meaning "cold", and L. *-philus*, meaning "loving"), referring to the organism's adaptation to cold environments, such as Antarctica, from where the Type strain was isolated.

  Cells are Gram-positive, aerobic, and rod-shaped, measuring approximately 0.4–0.6 µm in diameter and 1.5–3.5 µm in length. After 7 days of growth on ISP2 agar at 28 °C, colonies are circular, opaque, and yellow. The strain grows well on ISP2, ISP3, and ISP5 agar media, but not on ISP4. The strain grows at pH 5.0–8.0 and tolerates up to 35% (w/v) NaCl. The predominant fatty acids are C16:0 (34.9%), C18:1 ω9c (22.3%), C14:0 (7.5%), and 10-methyl C18:0 (TBSA; 17.8%). Notably, unsaturated fatty acids such as C16:1 ω6c (3.7%) and C16:1 ω7c (0.3%) were also detected in moderate abundance. The type strain is KRD162^T (DSM 119240=NCIMB 15613), isolated from marine sediment collected in Antarctica. Its genome has a size of 6.06 Mbp and a G+C content of 64.34 mol%.

- *Rhodococcus polaris (po.la'ris. L. masc. adj. polaris, of or pertaining to the pole; referring to the polar origin of the Type strain).*

  Cells are Gram-positive, aerobic, rod-shaped, and measure approximately 0.6–0.9 µm in diameter and 1.0–2.5 µm in length. After 7 days on ISP2 agar at 28 °C, colonies appear circular, opaque, and yellow. The strains grow on ISP2, ISP3, and ISP5 agar, but not on ISP4. The strain grows between pH 6.0–9.0 and tolerates up to 35% (w/v) NaCl. The major fatty acids are C16:0 (30.2%), C18:1 ω9c (29.6%), C14:0 (4.7%), and 10-methyl C18:0 (TBSA; 14.3%). Additionally, unsaturated fatty acids such as C16:1 ω6c (8.5%) and C16:1 ω7c (1.2%) were identified, along with methylated fatty acids including 10-methyl C16:0 (0.2%) and 10-methyl C17:0 (0.8%). The Type strain is KRD197^T (DSM 119478=NCIMB 15612), isolated from Antarctic marine sediment. The genome is 5.39 Mbp in size, with a G+C content of 64.13 mol%.

3.3 Discussion

One of the objectives of this study was to obtain hybrid assemblies, combining Oxford Nanopore (ONT) long reads with high-accuracy Illumina short reads, and to test whether this approach would generate highly contiguous and polished genomes for the Antarctic strains *Rhodococcus* KRD162 and KRD197. We hypothesised that this method would overcome assembly fragmentation and sequencing errors inherent to ONT technology, ultimately providing reliable resources for downstream comparative and biosynthetic analyses.

The results largely confirmed this hypothesis: both genomes reached near-complete assembly (KRD162: 5 contigs; KRD197: 2 contigs) with extremely low mismatch rates after Illumina-based polishing (Coverage: KRD162 = 271.8×, KRD197 = 296.6×). This demonstrates that, even for complex Actinomycetota genomes, hybrid assemblies can achieve accuracies comparable to those reported for prokaryotic model systems with low sequence complexity (Luan *et al.,* 2024). However, recovery of extrachromosomal elements remained incomplete: only one circular plasmid (pRKRD162-A) was obtained from KRD162, and none were fully resolved from KRD197. This underscores the need to combine sequencing with plasmid-enrichment protocols when studying extrachromosomal diversity in this group. Similar limitations in plasmid recovery have been reported for other Actinomycetota, where small plasmids are often fragmented or overlooked despite high sequencing coverage (Wick *et al.,* 2021; Johnson *et al.,* 2023). Similar limitations in plasmid recovery have been reported for other Actinomycetota. For instance, *Nocardia* sp. 107 harbors a small plasmid pXT107 (~4.3 kb) that represents one of the smallest extrachromosomal replicons described, while *Nocardia aobensis* IFM 10795 possesses a cryptic plasmid pYS1 of ≈4,326 bp. In *Amycolatopsis*, pMEA-like integrative and conjugative elements with autonomous mobile mechanisms have been described, showing the complexity of detecting small replicons even with good assembly (Xia *et al.,* 2006; te Poele *et al.,* 2008; Shibaya *et al.,* 2011). Because plasmids can harbour ecologically relevant genes, including BGCs, their incomplete detection limits our understanding of the full biosynthetic potential of these isolates. Complementary validation, for instance with pulsed-field gel electrophoresis (PFGE) or targeted plasmid sequencing, will be essential to confirm the extrachromosomal complement.

The complete genomes enabled a robust taxonomic classification and phylogenetic analysis of the Antarctic isolates. Based on their high 16S rRNA gene similarity (>99%) to known *Rhodococcus* species, one might initially assume they were close relatives of existing taxa rather than novel species. However, whole-genome comparisons contradicted this expectation, with ANI and dDDH values well below species thresholds. This reinforces the limitations of 16S rRNA as a sole taxonomic marker, a pattern reported in multiple Actinomycetota genera such as *Streptomyces* and *Nocardia*, where genome-level analyses uncovered cryptic diversity (Chun *et al.,* 2018; Nonthakaew *et al.,* 2025).

The genomic divergence was corroborated by phenotypic traits, including salinity and pH tolerance, fatty acid profiles, and colony morphology. Accordingly, two new species are proposed: *Rhodococcus cryophilus* sp. nov. (KRD162) and *Rhodococcus polaris* sp. nov. (KRD197). Phylogenomic reconstruction confirmed their placement within *Rhodococcus*, but with distinct evolutionary trajectories: KRD162 clustered near *R. fascians* LMG3623, while KRD197 grouped with *R. yunnanensis* NBRC103083 and *R. kyotonensis* JCM232111. Despite originating from the similar Antarctic sediment, these isolates followed independent diversification paths. Notably, no consistent clustering by isolation source was observed, echoing findings in other Actinomycetota where ecological adaptation often occurs via horizontal gene transfer (HGT) rather than vertical inheritance, echoing findings in other Actinomycetota such as *Salinispora* and *Micromonospora*, where ecological adaptation often occurs via HGT rather than vertical inheritance (Ziemert *et al.,* 2014; Seipke *et al.,* 2012; Mark *et al.,* 2024).

The comparative analysis of BGCs across 23 *Rhodococcus* genomes revealed both conserved and strain-specific features. Several well-characterised pathways, such as those encoding ε-poly-L-lysine, heterobactins, and rhodochelins, were detected in multiple genomes, consistent with earlier studies of conserved antimicrobial and siderophore production in this genus (Undabarrena *et al.,* 2021). Importantly, the presence of ε-poly-L-lysine BGCs in both Antarctic strains is consistent with previously proposed ecological roles of this antimicrobial polymer—based on studies primarily conducted in *Streptomyces* (Shima & Sakai, 1977)—but also suggests a broader distribution across *Rhodococcus*. This aligns with the hypothesis that certain BGCs are conserved because they provide selective advantages in resource-limited or competitive

environments such as Polar marine sediments (Jensen, 2016; Charlop-Powers *et al.,* 2015).

Conversely, BGCs typically reported in *Rhodococcus*, such as ectoine and butyrolactone, were absent from both Antarctic isolates. Since ectoines act as osmoprotectants and butyrolactones as signalling molecules (Graf *et al.,* 2008; Du *et al.,* 2011), their absence may reflect adaptation of polar lineages through alternative stress-response mechanisms. Although our study did not directly test this hypothesis, future assays exploring metabolite production under osmotic or nutrient stress could reveal functionally analogous protective compounds. Such adaptations would illustrate how BGC variation underpins niche specialisation in extreme environments. Another striking observation was the high proportion of uncharacterised BGCs (~80%) with low similarity to MIBiG references. This mirrors findings in other rare Actinomycetota, where lineage-specific clusters frequently encode previously uncharacterised metabolites (Ziemert *et al.,* 2014; Alas *et al.,* 2024). From an evolutionary perspective, these patterns point to ongoing diversification driven by selective pressures in polar environments.

This study makes two key contributions. First, it expands the taxonomic diversity of *Rhodococcus* by formally describing two new species from Antarctic sediments, reinforcing the value of genome sequencing in uncovering cryptic diversity beyond 16S-based analyses. Second, it highlights the genomic plasticity and biosynthetic versatility of the genus, showing that even closely related strains can follow independent evolutionary pathways. Together, these findings position *R. cryophilus* and *R. polaris* as promising models for exploring how rare Actinomycetota adapt and diversify in extreme environments. Nevertheless, experimental validation remains essential to connect predicted traits with ecological function. Future studies integrating metabolomic and transcriptomic profiling under polar stress conditions, as well as expanded comparative genomics across Antarctic isolates, will help clarify whether these species represent isolated cases or are part of broader endemic lineages.

4 CHAPTER 4. Assessing the effect of temperature on *Rhodococcus* metabolite production*

4.1 Introduction

Rhodococcus strains are well known for their metabolic versatility, which supports applications such as bioremediation, the degradation of organic pollutants and the production of industrially relevant compounds, such as surfactants, flocculants, amides and polymers (Kim *et al.,* 2018). However, to date, only six chemically characterised families of antimicrobial metabolites have been reported from this genus. These are depicted in Figure 4.1 and include: (i) aurachin RE, a quinoline derivative produced by *R. erythropolis* JCM 6824 with potent activity against Gram-positive bacteria (Kitagawa *et al.,* 2018); (ii) lariatins A (Fig. 4.1 [**1**]) and B (Fig. 4.1 [**2**]), macrocyclic peptides from *R. jostii* K01-B0171 active against *Mycobacterium tuberculosis* and *M. smegmatis* (Iwatsuki *et al.,* 2006; Iwatsuki *et al.,* 2007); (iii) rhodopeptins from *Rhodococcus* sp. Mer-N1033, exhibiting antifungal and antibacterial properties (Chiba *et al.,* 1999); (iv) rhodostreptomycin A and B, identified in *R. fascians* 307CO during co-cultivation with *Streptomyces padanus* (Kurosawa *et al.,* 2008); (v) a bacteriocin-like molecule from *R. erythropolis* JCM 2895 (Kitagawa *et al.,* 2018); and (vi) the humimycins A (Fig. 4.1[**3**]) and B (Fig. 4.1[**4**]), predicted from genome mining and experimentally validated for activity against *Staphylococcus* and *Streptococcus* (Chu *et al.,* 2016). Although the number of characterised *Rhodococcus* antibiotics remains limited, the presence of numerous BGCs in their genomes suggests vast potential still to be explored, with environmental modulation, or simulating environmental conditions offering a promising route to activating unknown biosynthetic pathways in the laboratory (Cappelletti *et al.,* 2020).

Among these environmental drivers, temperature emerges as one of the most influential parameters affecting microbial physiology and secondary metabolism. Adaptation to fluctuating temperatures has occurred multiple times throughout evolution (locally and globally), resulting in a wide array of molecular strategies to preserve cellular homeostasis across microbial lineages (Wani *et al.,* 2022). It has been shown to modulate enzymatic activity, membrane fluidity, and regulatory networks, ultimately determining

*Part of the content in this chapter has been previously published. See Macias-Contreras M I *et al*. Assessing the effect of temperature on *Rhodococcus* metabolite production. Microbiology (Reading). 2025;171(8):001598. Free full-text available at https://pmc.ncbi.nlm.nih.gov/articles/PMC12380520/

which metabolites are biosynthesised (Pardo-Este *et al.,* 2024). These temperature fluctuations can be ecologically relevant for microbial communities, in the Southern Ocean seawater temperatures oscillate between –2 and 10 °C due to seasonal ice dynamics, exposing microbial populations to recurrent and rapid thermal shifts (Convey *et al.,* 2014). In addition, upper-ocean microbes may experience short-term fluctuations of up to 10 °C beyond seasonal averages, highlighting their remarkable thermal tolerance (Podar *et al.,* 2020). Temperature fluctations have been shown to reconfigure metabolite profiles, for example, incubation of Antarctic microbes under lower temperatures and higher salinity (mimicking sea-ice formation) resulted in increased proline, betaine, and ectoine production even though the microbial taxa remained largely unchanged (Dawson *et al.,* 2023). Similarly, in the lactic acid bacterium *Lactococcus garvieae*, when cultured at 10–14 °C led to elevated levels of trehalose and succinylacetone, while higher temperatures increased acetate and acetoacetate concentrations and altered the balance of amino acids like betaine (Safari *et al.,* 2019). Finally, in a model of temperature upshift response, *Escherichia coli* and *Bacillus subtilis* showed that rearrangements in the metabolome mediated growth-rate adaptation over a timescale of approximately 1.5 doublings (Knapp *et al.,* 2023).

When considering the effect of temperature on *Rhodococcus*, transcriptomics work has revealed *Rhodococcus* sp. JG3, isolated from the permafrost of the Antarctic Dry Valley, could grow over a wide range of temperatures (−5 to 30 °C) and its genome harboured an expanded set of genes encoding cold shock proteins, responses to oxidative and osmotic stress, and cell wall modifications that, together, improve survival in sub-zero conditions (Goordial *et al.,* 2016; Raymond-Bouchard *et al.,* 2018). Several adaptive traits have been described, such as the production of cold-active enzymes, redundancy of metabolic genes with isoforms optimised for different temperatures, and the accumulation of compatible solutes such as trehalose, which stabilises membranes and proteins at low temperatures (Elbein *et al.,* 2003). Modulation of membrane fluidity through alterations in mycolic acid composition contributes to survival during thermal shifts (de Carvalho *et al.,* 2016). Transcriptomic studies also revealed extensive reprogramming of gene expression under cold conditions, with upregulation of pathways related to translation, amino acid uptake, siderophore biosynthesis, and defence against oxidative stress, while lipid metabolism and energy conversion were generally reduced (Raymond-Bouchard *et*

*Part of the content in this chapter has been previously published. See Macias-Contreras M I *et al*. Assessing the effect of temperature on *Rhodococcus* metabolite production. Microbiology (Reading). 2025;171(8):001598. Free full-text available at https://pmc.ncbi.nlm.nih.gov/articles/PMC12380520/

al., 2018). Similar trends have been observed from *Rhodococcus* sp. CNS16, where growth at 10–20°C induced changes in cell morphology, membrane desaturation, and antioxidant enzyme expression (Wang *et al.,* 2020). Together, these studies illustrate the versatility of *Rhodococcus* in adapting to thermal stress, underscoring its potential as a model for exploring the molecular basis of cold adaptation. Despite such advances, systematic studies on the effect of temperature on bacterial metabolomes remain scarce. Understanding how temperature impacts secondary metabolism of *Rhodococcus* is therefore essential, both for uncovering new bioactive molecules and for expanding our knowledge of microbial adaptation to environmental change. In this study, we investigated the effect of temperature on the secondary metabolite production of *Rhodococcus* strains isolated from Scottish and Polar marine sediments.

*Part of the content in this chapter has been previously published. See Macias-Contreras M I *et al*. Assessing the effect of temperature on *Rhodococcus* metabolite production. Microbiology (Reading). 2025;171(8):001598. Free full-text available at https://pmc.ncbi.nlm.nih.gov/articles/PMC12380520/

Lariatin A
$C_{94}H_{143}N_{27}O_{25}$
(1)

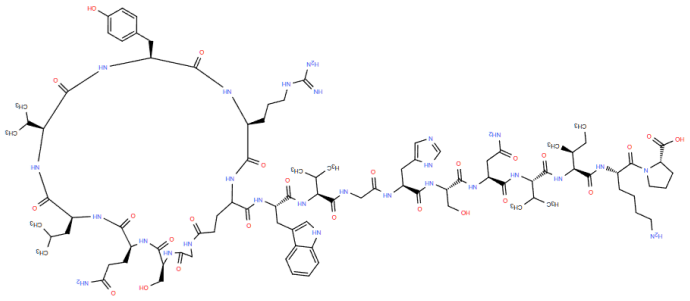

Lariatin B
$C_{10}H_{153}N_{29}O_{27}$
(2)

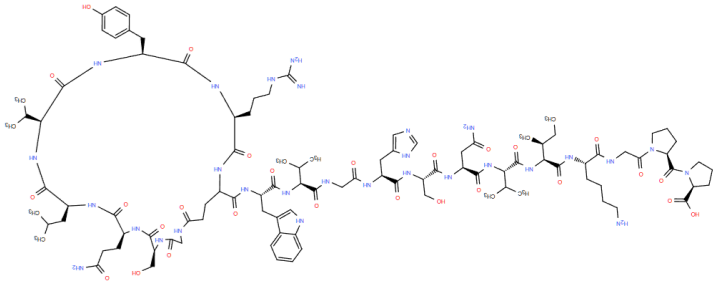

Humimycin A
$C_{58}H_{85}N_7O_{14}$
(3)

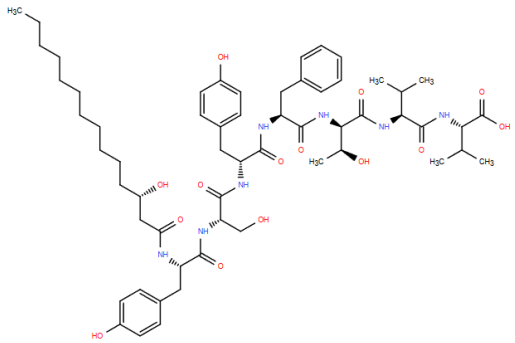

Humimycin B
$C_{59}H_{87}N_7O_{15}$
(4)

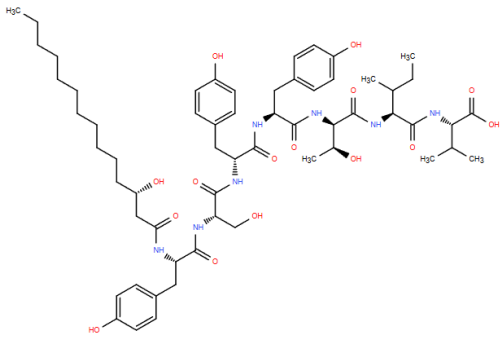

Figure 4.1. Chemical structure of Lariatin A (**1**) and B (**2**), isolated from *Rhodococcus* sp. K01−B0171 and humimycin A (**3**) and B (**4**) identified by genome analysis of *R. equi* and *R. erythropolis*.

*Part of the content in this chapter has been previously published. See Macias-Contreras M I *et al*. Assessing the effect of temperature on *Rhodococcus* metabolite production. Microbiology (Reading). 2025;171(8):001598. Free full-text available at https://pmc.ncbi.nlm.nih.gov/articles/PMC12380520/

4.2 Results

4.2.1 *Rhodococcus* phylogeny

The 16S rRNA gene-based phylogeny of the seven selected strains (Fig. 4.2), comprising five isolates from polar sediment and two from Scottish sediment (Table S4.1), revealed clustering into two well-supported clades, where the strains from the Arctic–Antarctic area clade with the type strains *Rhodococcus fascians* NR_037021.1 and *Rhodococcus yunnanensis* NR_043009.1 (bootstrap 99–100%), while the strains from Scotland form a second clade with type species such as *Rhodococcus erythropolis* NR_037024.1 and *Nocardia coeliaca* NR_104776.1 (reclassification of the latter to *Rhodococcus* has been suggested: Yarza *et al*., 2012; Ludwig *et al*., 2020) (bootstrap ≥88%). This geographic separation into two clades is noteworthy; however, it is important to emphasize that 16S rRNA gene sequences alone lack sufficient resolution to reliably resolve phylogenetic relationships within closely related actinomycetes. Additionally, the limited sample size restricts the ability to draw firm conclusions regarding species divergence based on geographic origin. Based on phylogenetic diversity and morphological characteristics, five strains of *Rhodococcus* were selected for further metabolomic and phenotypic analyses (KRD162, KRD197, KRD175, KRD226 and KRD231). As part of the strain selection process, antimicrobial activity against the ESKAPE pathogens was used as an initial screening criterion to identify promising bioactive producers. However, none of the strains exhibited detectable antimicrobial activity. This preliminary screening was conducted using agar plug assays from strains grown on ISP2 agar at 28 °C for 7 days (data not shown).

*Part of the content in this chapter has been previously published. See Macias-Contreras M I *et al*. Assessing the effect of temperature on *Rhodococcus* metabolite production. Microbiology (Reading). 2025;171(8):001598. Free full-text available at https://pmc.ncbi.nlm.nih.gov/articles/PMC12380520/

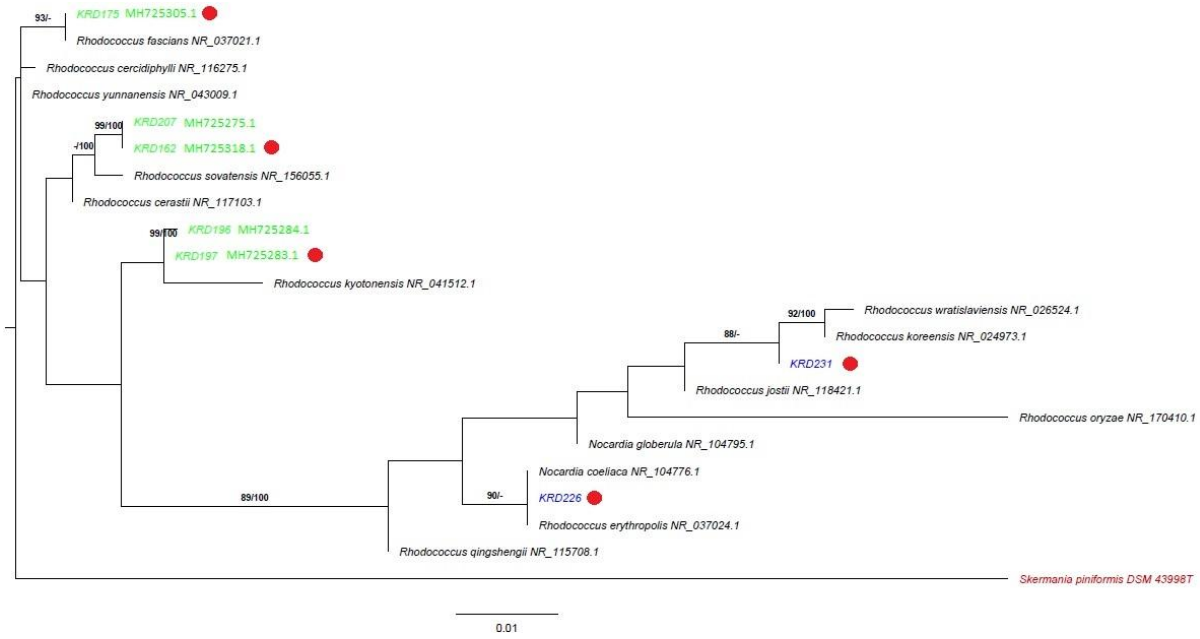

Figure 4.2. ML and MP tree based on 16S rRNA gene sequences of seven *Rhodococcus* strains isolated from the Arctic and Antarctic. This shows the genetic distance between isolates and closely related type strains (<96% similarity, NCBI accession numbers) with *Skermania piniformi*s DSM 43998 used as an outgroup. The branches are scaled in terms of the expected number of substitutions per site; the scale bar represents 0.01 substitutions per site. The numbers above the branches are support values exceeding 60% of the ML (left) and MP (right) bootstrap. Strain origin is represented by branch colours: green, Arctic/Antarctic; blue, Scotland; and red, outgroup. The red dot indicates that these strains were selected for further analysis.

4.2.2 Growth dynamics and determining stationary phase

To assess the impact of temperature on metabolite production, standardization of the extraction point was required to ensure that the growth stage was consistent across strains. For this purpose, five *Rhodococcus* strains (KRD162, KRD197, KRD175, KRD226 and KRD231) and one type strain (*R. fascians* ATCC 12974) were cultured in triplicate at three temperatures: 30, 25 and 20 °C. Although additional experiments were initially conducted at lower temperatures (10 and 15 °C), the growth of all strains – including those from polar environments – was too slow and insufficient to generate reproducible growth curves or extract metabolites for analysis. These conditions were therefore excluded from the study. All strains showed clear growth phases at all

*Part of the content in this chapter has been previously published. See Macias-Contreras M I *et al*. Assessing the effect of temperature on *Rhodococcus* metabolite production. Microbiology (Reading). 2025;171(8):001598. Free full-text available at https://pmc.ncbi.nlm.nih.gov/articles/PMC12380520/

temperatures (lag, exponential growth and stationary phases) (Fig. 4.3). In general, the lag phase lasted between 0 and 36 h, the exponential phase occurred between 4 and 132 h and the stationary phase was reached between 48 and 132 h, depending on the strain and temperature. For example, *Rhodococcus* KRD162 and KRD197 reached the stationary phase at 48 h at 30 and 25 °C, while these same strains reached the stationary phase at 20 °C at 72 and 84 h, respectively. The results showed that although strains KRD162, KRD197 and KRD175 were isolated from a Polar environment, there was no relationship between temperature and origin. For example, strains KRD197 and KRD175 reached the highest cell densities, of around OD600=0.4 x 100 = 40, while KRD162 consistently remained below 20. The calculation of the specific growth rate (%−μ/day) for each strain (Fig. S4.2), based on the natural logarithm of the linear portion of the growth curves, revealed that strains KRD197, KRD175, KRD226 and KRD231 followed the expected trend: their growth rate increased at higher temperatures, meaning that cell division occurred at a faster rate, leading to a shorter lag phase and an earlier transition to the stationary phase. In contrast, at lower temperatures, the growth rate decreased, resulting in a prolonged lag phase and a delayed entry into the stationary phase. However, strain KRD162 showed atypical behaviour, growing slower at 30 °C and reaching a higher cell density at 25 °C. Statistical analysis (t-test) showed that the specific growth rates of strains KRD162, KRD175 and KRD226 were significantly different across all three temperatures tested. KRD197 and KRD231 displayed significantly lower growth rates at 20 °C compared with 25 and 30 °C (Fig. S4.2). In contrast, strain *R. fascians* ATCC 12974 did not exhibit significant differences in growth rate across the temperatures tested. These results suggest that although these strains were isolated from cold or temperate marine regions, their temperature responses are strain-specific and do not necessarily reflect a uniform adaptation to low temperatures. With the growth established for each strain at three temperatures, the metabolite extraction point was set at 24 h after reaching the stationary phase, ensuring that all strains would be in the same growth phase for comparison of their specialized metabolites. According to several reports, the production of antibiotics by actinomycetes occurs mainly after the stationary phase is reached, and as such, this was chosen to maximize chemical diversity.

*Part of the content in this chapter has been previously published. See Macias-Contreras M I *et al*. Assessing the effect of temperature on *Rhodococcus* metabolite production. Microbiology (Reading). 2025;171(8):001598. Free full-text available at https://pmc.ncbi.nlm.nih.gov/articles/PMC12380520/

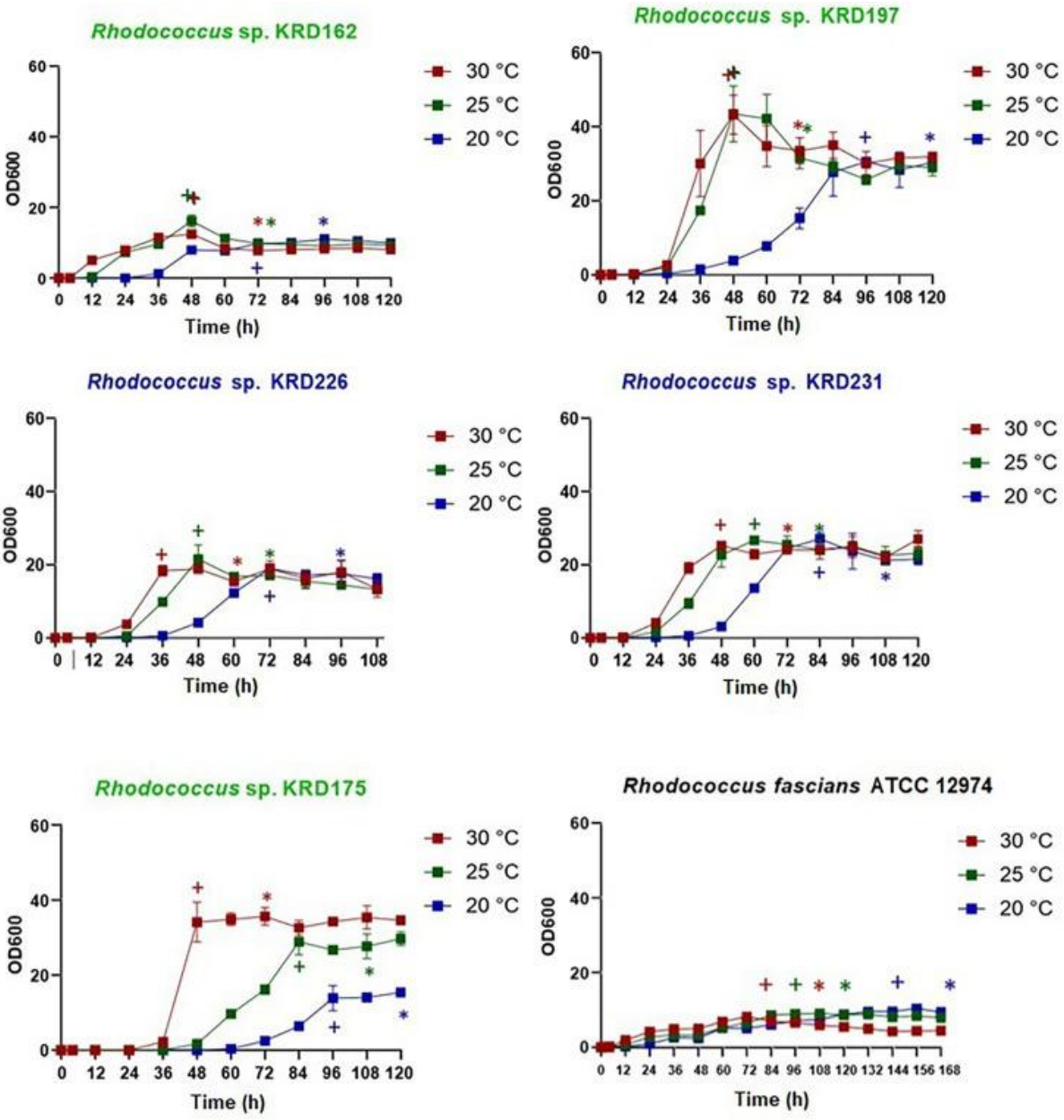

Figure 4.3. OD over time of six *Rhodococcus* strains (KRD162, KRD197, KRD226, KRD231, KRD175 and *R. fascians* ATCC 12974) cultured at 20 °C, 25 °C and 35 °C in ISP2 medium. The time (hours) is on the x-axis and OD at 600 nm on the y-axis. Data points represent the average value of three replicates. Error bars represent the Standard Deviation of triplicate cultures. The origin of the strains is represented by the colour of the graph title: green, Arctic/Antarctic; blue, Scotland; and black, *Rhodococcus* type strain. A cross indicates the start of the stationary phase and an asterisk the selected extraction point.

*Part of the content in this chapter has been previously published. See Macias-Contreras M I *et al*. Assessing the effect of temperature on *Rhodococcus* metabolite production. Microbiology (Reading). 2025;171(8):001598. Free full-text available at https://pmc.ncbi.nlm.nih.gov/articles/PMC12380520/

4.2.3 Molecular network analysis of *Rhodococcus* strains highlights the distinct metabolic profile of KRD197

Metabolite extracts were obtained from the cultures of all six strains after 24 h in the stationary phase and analysed by LC-HRMS/MS in positive ionization mode. The resulting MS-MS data were uploaded to the GNPS platform for molecular networking analysis. The molecular network constructed from this data consisted of 1,280 features (i.e. distinct molecular ions) (Fig. 4.4), organized into 86 molecular families (groups of 2 or more nodes connected by edges due to similar fragmentation patterns). These features were classified into seven biosynthetic categories, alkaloids, aa and peptides, carbohydrates, fatty acids, polyketides, shikimates and phenylpropanoids and terpenoids, using CANOPUS (Dührkop *et al*., 2021) and the NPClassifier ontology (Kim *et al*., 2021). It should be noted that the metabolite profiles obtained in this study reflect only the compounds extractable with ethyl acetate under the conditions used. As such, the analysis is inherently biassed towards moderately polar to lipophilic metabolites and may exclude highly polar or volatile compounds. Additionally, while the HP-20 resin has shown high affinity for a broad range of bacterial metabolites in previous studies (Santoyo-Garcia *et al.,* 2022; Bogdanov *et al,* 2024), its capture efficiency was not directly evaluated here. These methodological choices were made to prioritize the detection of drug-like small molecules and ensure consistency with our laboratory's established workflows. Among these, the fatty acid pathways represented the largest proportion of features, accounting for 18.5% of the total. Additionally, 467 features (36.5%) were identified as singletons (fragmentation patterns not correlated with others), suggesting the presence of chemical diversity within the samples. In contrast, 434 features (33.9%) were present in both media and solvent controls (grey nodes), indicating that they originated from media components. Among the analysed *Rhodococcus* strains, KRD197, KRD226 and KRD175 had the highest number of features, with 1,095 (85.5%), 565 (44.14%) and 513 (40.07%) features, respectively. Notably, KRD197 exhibited 632 exclusive features, underscoring its distinct metabolic profile (Fig. S4.3). However, the distribution of features across all strains did not follow a defined pattern in relation to temperature, suggesting that metabolite production by *Rhodococcus* is primarily species-specific, rather than phylogenetic or geographical. For example, strains from Arctic–Antarctic environments shared 364 features with their most closely related type strain, *R.*

*Part of the content in this chapter has been previously published. See Macias-Contreras M I *et al*. Assessing the effect of temperature on *Rhodococcus* metabolite production. Microbiology (Reading). 2025;171(8):001598. Free full-text available at https://pmc.ncbi.nlm.nih.gov/articles/PMC12380520/

fascians, while strains isolated from Scotland shared 385 features with this species, despite being more distantly related.

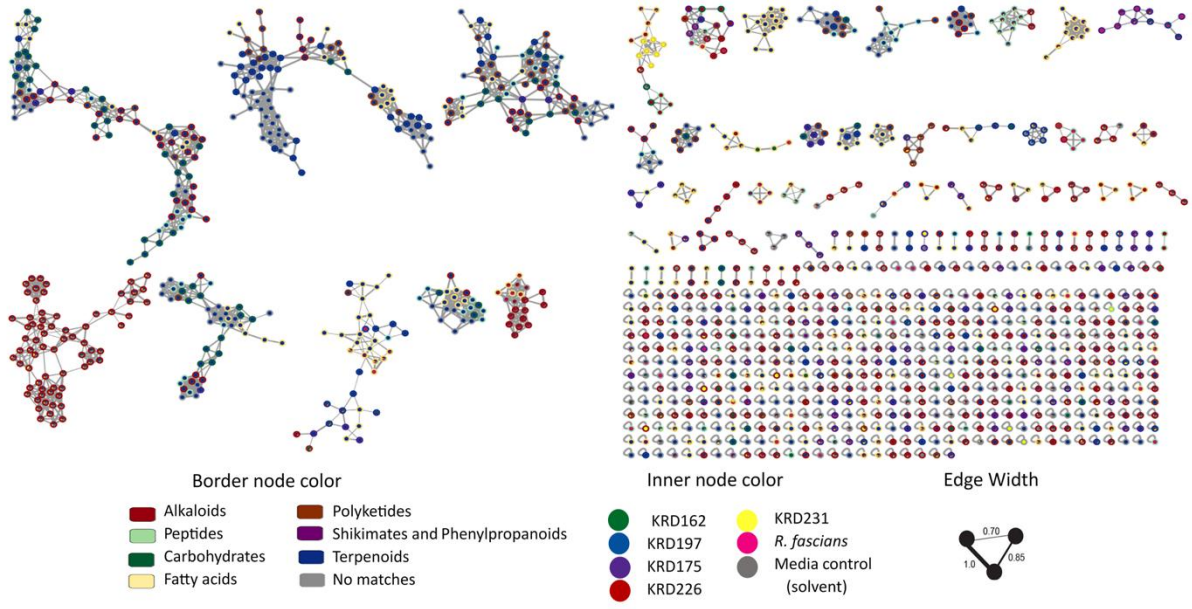

Figure 4.4. Feature-based molecular networking (FBMN) of six *Rhodococcus* strains at 20, 25 and 30 °C. Inner pie chart node colour represents the presence of each feature across the strains, and grey represents features present in the culture solvent/media controls. Border node colour represents the chemical class annotation, and parent ions without matches are coloured grey.

4.2.4 Temperature-dependent metabolite production by *Rhodococcus* KRD197

Rhodococcus KRD197 exhibited the highest number of features (1,095) among the analysed strains (Fig. S4.7A) and was therefore selected to evaluate the effect of temperature on metabolite production. The molecular network generated from this particular strain had 1,095 features, distributed across 57 molecular families (68.6%) and 344 singletons (31.4%), highlighting its chemical diversity. The majority of these features (819) were observed at 20 °C, followed by 416 at 30 °C and 374 at 25 °C (Fig. S4.7B). The higher number of features at lower temperatures suggests that the strain may activate defensive metabolic pathways in response to stress induced by colder environments. In general, the proportions of natural product categories varied with temperature. Carbohydrates and polyketides showed a marked increase as the

temperature decreased, with their proportions rising from 1% and 7%, respectively, at 30 °C, to 11% and 12%, respectively, at 20 °C. Peptides also increased from 6% at 30 °C to 10% at 20 °C (Fig. S4.6). This activation of the carbohydrate biosynthetic pathway has been associated with enhanced stress resistance in other species. Interestingly, KRD197 was the only strain that showed an increase in the number of features as the temperature decreased (Fig. S4.4). This strain also exhibited a higher proportion of features across all chemical classes compared with other strains, which maintained a similar number of features across chemical classes regardless of their geographical origin (Scottish or Polar, Fig. S4.5). These findings suggest that KRD197 may possess adaptive mechanisms that respond to temperature-induced stress, potentially activating biosynthetic pathways that lead to the production of a broader range of metabolites.

4.2.5 *Rhodococcus* KRD197 showed metabolic shifts induced by temperature

The metabolomic profile of *Rhodococcus* KRD197 varied significantly with temperature. Hierarchical clustering of the top 250 features showed that profiles grouped primarily by temperature, with biological replicates displaying similar profiles ($P>0.05$), while significant differences were observed between temperatures and controls ($P<0.05$, Fig. 4.5). The heat map further revealed temperature-specific metabolite patterns: at 30 °C, features linked to fatty acid pathways were predominant; at 25 °C, only a small set of fatty acid-related features was present; and at 20 °C, an enrichment of carbohydrate pathways was observed. However, most features were shared between 30 and 25 °C, indicating a more distinct metabolic shift at 20 °C. Volcano plot analysis confirmed these trends, highlighting significant metabolite abundance changes across temperatures ($P<0.1$, fold change >2.0). Although FBMN indicated an overall increase in the number of features at lower temperatures, volcano plots revealed that higher temperatures (30 °C) led to a greater number of significantly increased metabolites (163 features at 30 °C vs. 4 features at 20 °C, Fig. S4.8B). Notably, 19% of the elevated features were associated with fatty acid metabolism, and features that vary with temperature accounted for 65% of the total

*Part of the content in this chapter has been previously published. See Macias-Contreras M I *et al*. Assessing the effect of temperature on *Rhodococcus* metabolite production. Microbiology (Reading). 2025;171(8):001598. Free full-text available at https://pmc.ncbi.nlm.nih.gov/articles/PMC12380520/

(163 of 250), suggesting a substantial shift in specialized metabolite production driven by temperature changes.

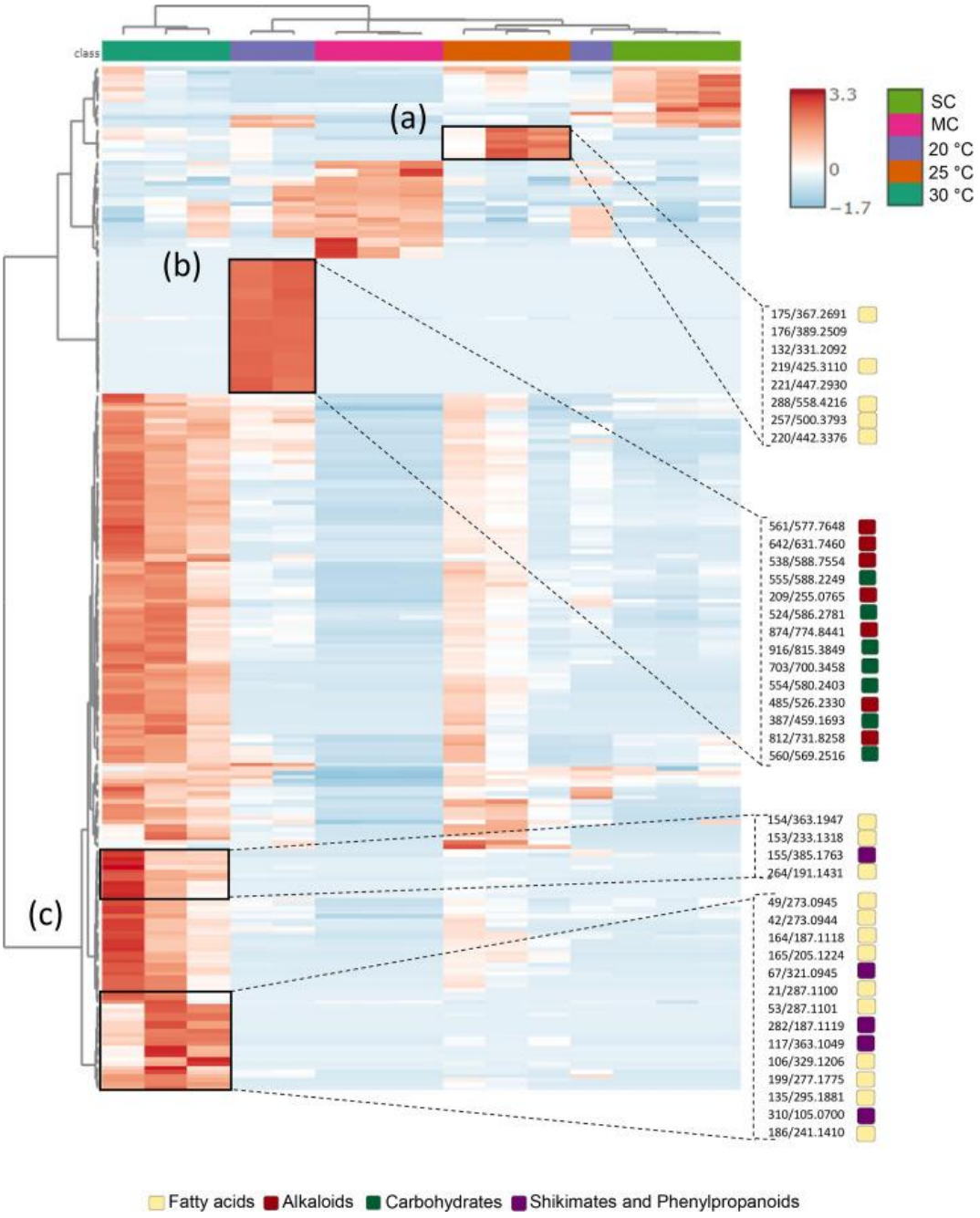

Figure 4.5. Hierarchical cluster and heat map of KRD197 metabolites when cultured at 30 °C, 25 °C and 20 °C (SC, solvent control; MC, media control) ranked by ANOVA. Each row represents a metabolite feature, and each column represents a sample condition (in triplicate). The top 250 metabolite features that vary significantly

*Part of the content in this chapter has been previously published. See Macias-Contreras M I *et al*. Assessing the effect of temperature on *Rhodococcus* metabolite production. Microbiology (Reading). 2025;171(8):001598. Free full-text available at https://pmc.ncbi.nlm.nih.gov/articles/PMC12380520/

(P<0.05) across the 3 temperatures are shown and clustered. The red colour of the tile indicates high abundance, and blue indicates low abundance. Highlighted in (**a**), (**b**) and (**c**) are features (*m/z*) of interest at each temperature with coloured boxes, indicating chemical classes.

4.2.6 Temperature-dependent production of antimicrobial compounds

Through molecular networking and dereplication using GNPS (Nothias *et al.,* 2020) and DEREPLICATOR (Mohimani *et al.,* 2018), several metabolites were annotated, including cyclo-(Leu-Phe) and cyclo-(Val-Phe), among others. To support these annotations, additional analysis was performed using SIRIUS (Dührkop *et al.,* 2019). Mass accuracy is reported as the median mass error (ppm) calculated by SIRIUS, which summarises the deviation between observed and theoretical masses across all candidate molecular formulae evaluated for a given feature. This analysis validated the possible presence of compounds such as cyclo-(Leu-Phe) ($C_{15}H_{20}N_2O_2$, [M+H]+, median mass error: –0.300 p.p.m.) and cyclo-(l-Val-l-Leu) ($C_{11}H_{20}N_2O_2$, [M+H]+, median mass error: 1.290 p.p.m.). Notably, the analysis also revealed the presence of fatty acids such as lauric acid ($C_{12}H_{24}O_2$, [M+H]+, median mass error: 0.448 p.p.m.) and 8-methylhexadecanoic acid ($C_{17}H_{34}O_2$, [M+H]+, median mass error: 1.545 p.p.m.) (Fig. S4.9), detected exclusively in the strain KRD197 extract cultured at 20 °C. Lauric acid, in particular, has previously been associated with antimicrobial activity (Matsue *et al.,* 2019). For most other metabolites, no significant matches were found in public databases, suggesting that these strains may produce structurally diverse or novel metabolites. However, since this annotation was based solely on computational predictions and no authentic standard was used for confirmation, the identification remains tentative and further experimental validation would be necessary to confirm the presence of these metabolites.

4.3 Discussion

The phylogenetic analysis led to the selection of five *Rhodococcus* strains, whose growth was characterized through OD measurements at 600 nm. The growth curves showed expected phases, with stationary phases reached between 48 and 132 h at 30 and 25 °C. Similar growth behaviours have been observed by *Rhodococcus* sp. NAM 81 (stationary phase at 42 h; Mohammad *et al.,* 2016) and *R. opacus* MITGM-173 (72 h; Kurosawa *et*

*Part of the content in this chapter has been previously published. See Macias-Contreras M I *et al*. Assessing the effect of temperature on *Rhodococcus* metabolite production. Microbiology (Reading). 2025;171(8):001598. Free full-text available at https://pmc.ncbi.nlm.nih.gov/articles/PMC12380520/

al., 2015). *R. fascians*, in particular, exhibited growth patterns consistent with previous reports, where the stationary phase was reached on the third day at an OD600 of ~1.75 in glycerol medium (Vereecke *et al.,* 2002).

Given that secondary metabolite production is commonly associated with the stationary phase, metabolite extraction was standardized to occur 24 h after the onset of the stationary phase. This approach is supported by previous studies that reported peak antibiotic production during this phase, for instance, *Streptomyces coelicolor* producing undecylprodigiosin and actinorhodin (Manteca *et al.,* 2008) and *Streptomyces goldiniensis* producing aurodox (McHugh *et al.,* 2023).

Metabolomic analysis revealed that *Rhodococcus* KRD197 exhibits a temperature-dependent metabolite profile, with a notable increase in metabolic diversity at lower temperatures. This shift was characterized by a significant enrichment of carbohydrate-associated features, a pattern consistent with studies on psychrotolerant fungi (*Atradidymella* sp.), which showed increased metabolite production at 4 °C (Ulaganathan *et al.,* 2017). In other microorganisms, such as algae, an increased carbohydrate output has been associated with osmotic stress regulation, as observed from Chlamydomonas reinhardtii, where extracellular carbohydrate and polymeric substance production contribute to cold adaptation (Aslam *et al.,* 2012; Liu *et al.,* 2023). In this study, temperature-dependent metabolic modulation was also observed, and branched-chain fatty acids with reported antimicrobial activity were detected exclusively at 20 °C, which could indicate that cold stress could also trigger biosynthetic pathways related to antimicrobial production. Branched-chain fatty acids have been reported to disrupt bacterial membranes, inhibit protein synthesis and affect gene replication (Casillas-Vargas *et al.,* 2021). These findings suggest that cold tolerance in KRD197 is a complex process, potentially integrating osmotic regulation, membrane stability and antimicrobial metabolite production as adaptive mechanisms.

In contrast, higher temperatures (particularly at 30 °C) exhibited a significant increase in fatty acids, which – though typically considered primary metabolites – may play adaptive roles under thermal stress. This is consistent with findings from *Caenorhabditis elegans*, where fatty acid metabolism plays a role in heat resistance, osmotic balance and

*Part of the content in this chapter has been previously published. See Macias-Contreras M I *et al*. Assessing the effect of temperature on *Rhodococcus* metabolite production. Microbiology (Reading). 2025;171(8):001598. Free full-text available at https://pmc.ncbi.nlm.nih.gov/articles/PMC12380520/

oxidative stress response (Horikawa & Sakamoto, 2009). The composition of membrane fatty acids is tightly regulated by temperature, with cold stress promoting increased unsaturation to maintain membrane fluidity, while thermophilic bacteria exhibit low unsaturated fatty acid content to enhance membrane stability (Zhang & Rock, 2008; Nordström & Laakso, 1992).

In summary, *Rhodococcus* KRD197 appears to exhibit a dual metabolic adaptation strategy in response to temperature. At lower temperatures, the strain showed increased carbohydrate production and the possible selective biosynthesis of antimicrobial metabolite, suggesting roles in osmotic regulation and chemical defense. Conversely, at higher temperatures, a shift towards fatty acid metabolism likely contributed to membrane stability and enhanced stress tolerance. These findings provide insight into the temperature-driven metabolic plasticity of *Rhodococcus* KRD197 and highlight its biotechnological potential in diverse and variable environmental conditions.

While this study provides a comprehensive metabolomic profile of *Rhodococcus* KRD197, future research should focus on integrating genomic and metabolomic approaches to further elucidate its biosynthetic capabilities. Whole-genome sequencing and comparative genomic analyses could facilitate the identification of BGCs associated with the production of specialized metabolites, particularly those that are temperature regulated, thereby advancing our understanding of the genetic basis for environmental adaptation and natural product biosynthesis in this promising strain.

*Part of the content in this chapter has been previously published. See Macias-Contreras M I *et al*. Assessing the effect of temperature on *Rhodococcus* metabolite production. Microbiology (Reading). 2025;171(8):001598. Free full-text available at https://pmc.ncbi.nlm.nih.gov/articles/PMC12380520/

5 CHAPTER 5. Exploring the metabolomic and genomic potential of *Micromonospora* sp. KRD324

5.1 Introduction

The bacterial genus *Micromonospora* belongs to the family *Micromonosporaceae*, within the class Actinomycetes, phylum Actinomycetota and was first proposed by Ørskov in 1923 (Trujillo *et al.,* 2014; Parte *et al.,* 2025). The strains are Gram-positive, aerobic and primarily saprotrophic and are characterised by their ability to form branched mycelia and produce spores, although they typically lack aerial mycelium (Trujillo *et al.,* 2014; Lee *et al.,* 2022). Their spores are usually brown or black and develop directly on the substrate mycelium in grouped arrangements (Yan *et al.,* 2022), and they can produce carotenoid pigments in shades of orange, red, yellow, brown, violet, or black. Although, as shown by environmental DNA (eDNA) sequencing, their relative abundance in environmental microbiomes is typically low, often less than one percent of bacterial communities in soil and sediments (Delgado-Baquerizo *et al.,* 2018). *Micromonospora* species have been recovered from a broad range of terrestrial and aquatic environments, including peatlands in Thailand, forest soils in China, and mangrove habitats in Hainan (Qiu *et al.,* 2008; Songsumanus *et al.,* 2011). Specific species have been isolated from well-defined sites, such as *M. sedimentincola* from Thai coastal areas and *M. profundi* from the Black Sea (Supong *et al.,* 2012; Veyisoglu *et al.,* 2016). They have also been reported from plant-associated niches such as wheat endophytes (Coombs & Franco, 2003; Trujillo *et al.,* 2015). This wide ecological range, combined with selective isolation methods, has led to studies investigating *Micromonospora* secondary metabolites.

Since the first antimicrobial compound produced by *Micromonospora* was reported in 1947 (Waksman *et al.,* 1947), this genus has been investigated for antibiotics, but it was really the discovery of gentamicin (Fig. 5.1 [**1**]) in 1963, that really showed success. Gentamicin is an aminoglycoside antibiotic produced by *Micromonospora purpurea* (Weinstein *et al.,* 1963), and 80 years latter it remains a critically important medicine (WHO, 2023), used to treat infections such as meningitis, pneumonia, and gonorrhoea. In fact, at least 11 secondary metabolites or derivatives are in clinical use from this genus, including netilmicin (Stewart *et al.,* 1977), isepamicin (SmithKline & French Laboratories,

1995), neomycin (Fig. 5.1 [**2**]) (Waksman and Lechevalier, 1949), and sisomicin (Weinstein *et al.,* 1976). Moreover, the genus has shown potential for producing bioactive compounds beyond antibacterial activity. For instance, turbinmicin, produced by *Micromonospora* WMMC-415, exhibits broad-spectrum antifungal activity against multidrug-resistant pathogens such as *Candida auris* and *Aspergillus fumigatus*, and is currently in pre-clinical development with promising *in vivo* efficacy in murine models (Zhao *et al.,* 2021; Alas *et al*., 2024). In addition, crude extracts of *Micromonospora* sp. M2, have been shown to induce apoptosis of cancer cell through oxidative stress, with lobosamide D identified as the principal active compound (Jeong *et al.,* 2024). However, despite these successes, genome sequencing has revealed that the genus' biosynthetic capacity far exceeds the number of characterised metabolites (Hifnawy *et al.,* 2020). This is also reflected in the NCBI (National Center for Biotechnology Information) database, which, as of June 2025, listed 948 *Micromonospora* genomes (112 of which are complete or at the chromosomal level), and 1,541 biosynthetic gene clusters (BGCs) reported by antiSMASH. These data continue to reflect a discrepancy between the predicted biosynthetic capacity, and the number of compounds characterised to date, suggesting that a considerable portion of the metabolic potential of the genus remains unexplored or unverified experimentally.

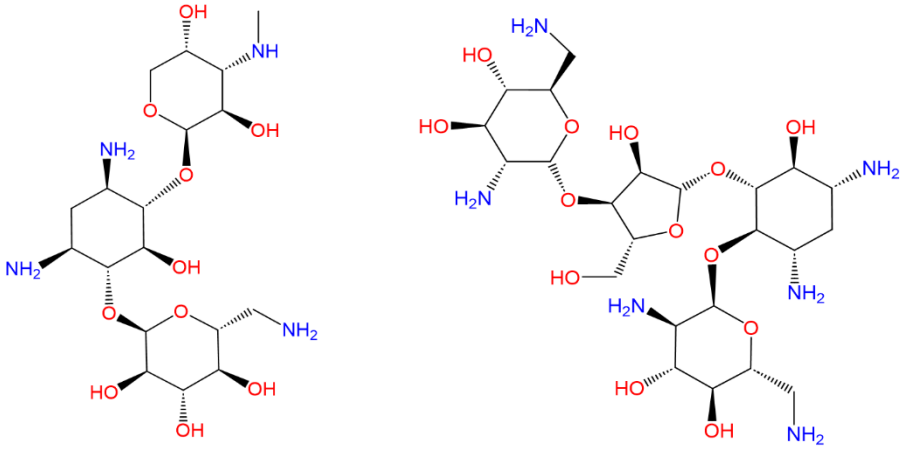

Gentamicin
$C_{18}H_{36}N_4O_{10}$
(1)

Neomycin
$C_{23}H_{46}N_6O_{13}$
(2)

Figure 5.1. Chemical structures of gentamicin (1) and neomycin (2), that are representative aminoglycosides produced by *Micromonospora* species.

Among the BGCs annotated in *Micromonospora* genomes, those coding for macrolide-type polyketides stand out due to their structural diversity and pharmacological relevance (Hifnawy *et al.,* 2020). Macrolides are polyketide-derived secondary metabolites whose biosynthesis iuses modular polyketide synthase (PKS) enzymes. These are broadly classified into three categories: classical macrolides, spirotetronates, and other macrolide subclasses (Yan *et al.,* 2022). Among these, classical macrolides are the most represented, with 16-membered macrolides constituting the predominant subclass isolated from *Micromonospora* species. These compounds have found applications mainly in veterinary medicine, with only a few examples translated into clinical use in humans. Notable naturally occurring macrolides include josamycin (Fig. 5.2 [**3**]) (Osono *et al.,* 1967), spiramycin (PinnertSindico, 1954), tylosin (Hamill *et al.,* 1961), and midecamycin (Neu, 1983), alongside semi-synthetic derivatives such as miokamycin (Fig. 5.2 [**4**]) (Yokota, 1984), rokitamycin (Cinco *et al.,* 1995), tilmicosin (Ose, 1987), and tildipirosin (Andersen *et al.,* 2012).

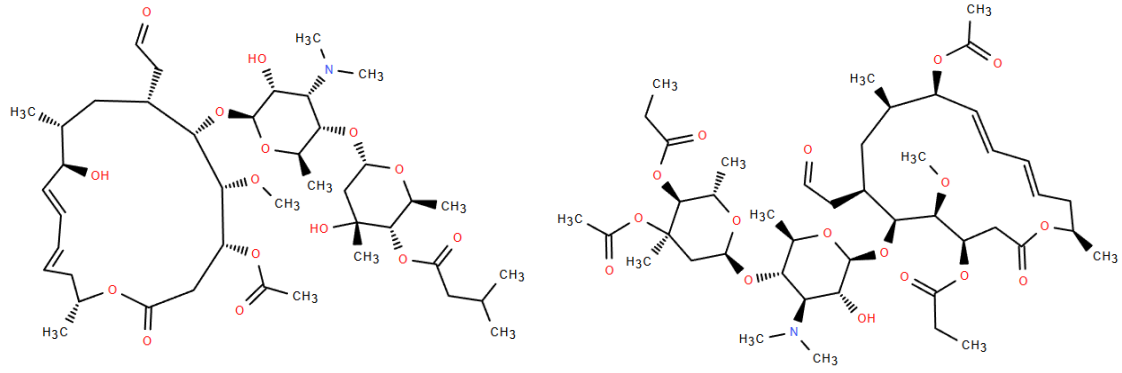

Josamycin
$C_{42}H_{69}NO_{15}$
(3)

Miokamycin
$C_{45}H_{71}O_{17}$
(4)

Figure 5.2. Chemical structures of the naturally occurring macrolides josamycin (3) and miokamycin (4).

One of the earliest macrolides to be structurally characterised from *Micromonospora* was rosamicin (Fig. 5.3 [**5**]), a 16-membered ring compound originally isolated from *Micromonospora rosaria* (Wagman *et al.,* 1972). Since then, related metabolites such as juvenimicin A1–A4 and B1–B4, produced by *Micromonospora chalcea* var. *izumensis*, have been described, with juvenimicin A3 confirmed to be structurally identical to rosamicin (Kishi *et al.,* 1976). More recently, juvenimicin C (Fig. 5.3 [**6**]) was reported from the marine-derived strain *Micromonospora* sp. CNJ-878 (Carlson *et al.,* 2013). These macrolides exhibit broad-spectrum antibacterial activity, particularly against Gram-positive bacteria such as *Staphylococcus aureus* and *Bacillus subtilis* (Hatano *et al.,* 1976). In addition to these, structurally related metabolites have also been elucidated, such as SCH 23831 (Fig. 5.3 [**7**]), produced by *Micromonospora rosaria*, which shares the 16-membered macrolide scaffold but includes distinctive substitutions, such as a pyridine ring (Puar *et al.,* 1979) (Table 5.1). Although their precise mechanisms of action remain poorly characterised, their structural resemblance to rosamicin-type macrolides suggests a potentially related biological role.

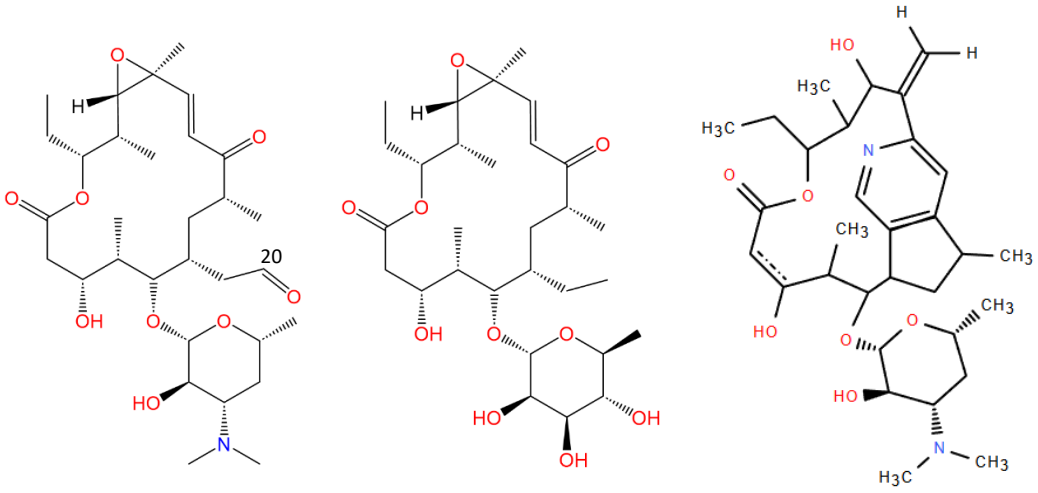

Figure 5.3. Chemical structures of the 16-membered macrolides rosamicin (5), juvenimicin C (6) and SCH 23831 (7) isolated from *Micromonospora* species.

Table 5.1. Summary of reported 16-membered macrolides within the juvenimicin family, including structurally related metabolite SCH 23831. The table presents molecular formula, monoisotopic mass, and observed protonated ion $[M+H]^+$ values for each metabolite.

Metabolite	Molecular formula	Monoisotopic mass (Da)	[M+H]+ (*m/z*)	Reference
Juvenimicin A1	Not described	—	—	Kishi *et al.,* (1976) [PMID:993104]
Juvenimicin A2	$C_{30}H_{51}NO_8$	553.3611	554.3687	Kishi *et al.,* (1976)
Juvenimicin A3 (rosamicin)	$C_{31}H_{51}NO_9$	581.3564	582.3637	Kishi *et al.,* (1976)
Juvenimicin A4	$C_{33}H_{53}NO_{10}$	625.3733	626.3806	Kishi *et al.,* (1976)
Juvenimicin B1	$C_{31}H_{53}NO_8$	567.3766	568.3844	Kishi *et al.,* (1976)
Juvenimicin B2	$C_{31}H_{53}NO_9$	583.3715	584.3788	Kishi *et al.,* (1976)
Juvenimicin B3	$C_{33}H_{53}NO_{11}$	641.3682	642.3755	Kishi *et al.,* (1976)
Juvenimicin B4	Not described	—	—	Kishi *et al.,* (1976)
Juvenimicin C	$C_{29}H_{48}O_{10}$	556.3247	557.3321	Carlson, *et al*. (2013)
6108 A1	$C_{31}H_{51}NO_9$	581.3587	582.366	Funaishi *et al.,*1990
6108 B	$C_{32}H_{53}NO_9$	595.3744	596.3817	Funaishi *et al.,*1990
6108 C	$C_{33}H_{53}NO_{10}$	625.3733	626.3806	Funaishi *et al.,*1990
6108 D	$C_{32}H_{53}NO_8$	579.3638	580.3711	Funaishi *et al.,*1990
Sch 23831	$C_{31}H_{48}N_2O_7$	560.3461	561.3535	Puar *et al.,* 1979

Despite the important bioactivity of these macrolides, complete experimental characterisation of the BGCs responsible for their biosynthesis remains limited. Genome mining was used to propose the rosamicin BGC from the genome of *Micromonospora rosaria* (MIBiG BGC0002086) (Kautsar *et al.,* 2020), but only partial pathway elucidation was achieved. Iizaka *et al.* (2013) identified two genes, *rosC* and *rosD*, encoding cytochrome P450 enzymes involved in late-stage rosamicin oxidation reactions in rosamicin biosynthesis, with the latter catalysing multi-step oxidation at the C20 position (as numbered in Fig. 5.3), converting rosamicin into its oxidised analogues including 20-carboxyrosamicin. These findings imply two biosynthetic branches — one leading to rosamicin and the other to its oxidised analogue — though the full pathway remains unresolved. Interestingly, a homologous BGC found in the genome of *Salinispora pacifica*, was linked to salinipyrone and pacificanone polyketide production, likely arising from divergent post-PKS tailoring adaptations (Awakawa *et al.,* 2015). While such

divergence has not yet been experimentally confirmed for *Micromonospora*, the genomic similarity and conserved biosynthetic logic suggest comparable biosynthetic flexibility. Together, these insights highlight the potential for re-examining ‘known’ rosamycin-like BGCs to uncover their full biosynthetic potential.

These biosynthetic capacities can be explored through changes in abiotic factors, as discussed in Chapter 1 and 3 (temperature). One of the most relevant for marine environments is salinity**,** as *Micromonospora* species are frequently adapted to saline conditions, which can modulate their secondary metabolite production. Several studies have demonstrated that salinity not only influences growth but also affects the production of secondary metabolites, including antibiotics, pigments, and cytotoxic compounds. For instance, rifamycin production by *Salinispora arenicola*, was found to double under low (1%) NaCl concentrations compared to media containing 3% NaCl (Ng *et al.,* 2014). In another case, *Streptomyces coelicolor*, exposed to salt stress led to the accumulation of osmoprotectants such as ectoine, alanine, glycine, and proline, as well as di- and tri-peptides (Kol *et al.,* 2010). Similarly, halophilic *Streptomyces* isolates from Indian saltpans showed an increase in antibiotic production under NaCl concentrations of up to 15%, with enhanced antimicrobial activity (Jenifer *et al.,* 2015). These examples support the idea that osmotic stress induced by salinity can activate otherwise silent biosynthetic pathways in Actinomycetal bacteria, triggering the production of secondary metabolites that would remain undetected under standard conditions.

In this context, the present chapter investigates the effect of salinity as an abiotic factor influencing secondary metabolite production by *Micromonospora* strains isolated from two contrasting environments: a hypersaline lagoon in Mexico and coastal sediments from Scotland. Through an integrated metabolomic and genomic approach, this study explored the metabolic plasticity of these strains, aiming to identify differentially produced metabolites in response to salinity variations.

5.2 Results.

5.2.1 Phylogenetic relationship and antibacterial activity.

A total of 10 *Micromonospora* strains were included in this study, of which seven were isolated from marine sediment collected in the Ojo de Liebre Lagoon, Mexico, and three from coastal sediment around Scotland (Table 5.2). The Mexican strains (KRD321, KRD322, KRD323, KRD324, KRD325, KRD326, and KRD327) displayed orange colonies on ISP2 medium, with a hard, irregular surface and no aerial mycelium. Black pigmentation, associated with spore formation, appeared after approximately two to three weeks, except in strain KRD321, which developed white sporulation (Fig. S5.1). In contrast, the Scottish strains KRD319 and KRD320 consistently produced black spores, while KRD236 displayed orange colonies with no evidence of sporulation within the same timeframe.

16S rRNA gene sequencing revealed that all seven Mexican strains shared 100% identity with the Type strain *Micromonospora spongicola* NR169445, while the Scottish strains exhibited high similarity (99.45–100%) to *Micromonospora aurantiaca* NR074415 (Table S5.1). The phylogenetic tree (Fig. 5.4), reconstructed from ~470 bp partial 16S rRNA sequences for the Mexican and one Scottish strain (KRD236), and ~1500 bp fragments for the remaining Scottish strains (KRD319 and KRD320), revealed two major clades: (a) the *Actinoplanes–Paractinoplanes–Micromonospora* group, and (b) the *Micromonospora–Plantactinospora* cluster. Within clade (b), a well-supported subclade (b1) included all seven Mexican isolates and one Scottish strain (KRD326), forming a distinct lineage with 100% bootstrap support. In contrast, the remaining Scottish strains KRD319 and KRD320 clustered within clade (a), along with type strains such as *Micromonospora aurantiaca* NR074415 and *Micromonospora maritima NR109311*. Notably, within the subclade (b1), the Mexican isolates split into two groups: one composed of KRD321, KRD322, KRD323, KRD324, and KRD325, as well as KRD326 and KRD236 (Scottish strain), all closely related to *Micromonospora spongicola* NR169445; and another formed solely of KRD327, which appeared as a sister branch. This substructuring may reflect genomic divergence among local populations. However, due to amplification issues with universal 16S rRNA primers, the phylogenetic analysis

for Mexican isolates was limited to a ~470 bp sequence obtained with genus-specific primers. While this approach reliably confirmed genus-level identity, the reduced sequence length may have compromised the phylogenetic resolution. Therefore, bootstrap support and branch topology — especially among closely related isolates — should be interpreted with caution.

To explore potential functional differences among these strains, antibacterial bioassays (plug assay) were conducted. Only strain KRD324 exhibited inhibition against the tested pathogens *Enterococcus faecalis* and *Bacillus subtilis*, with inhibition zones of 18 mm and 26 mm, respectively (Fig. S5.2). Based on this bioactivity, along with observed morphological variation and phylogenetic distribution, six strains were selected for further metabolomic analysis: KRD236, KRD319, KRD320, KRD321, KRD324 and KRD327.

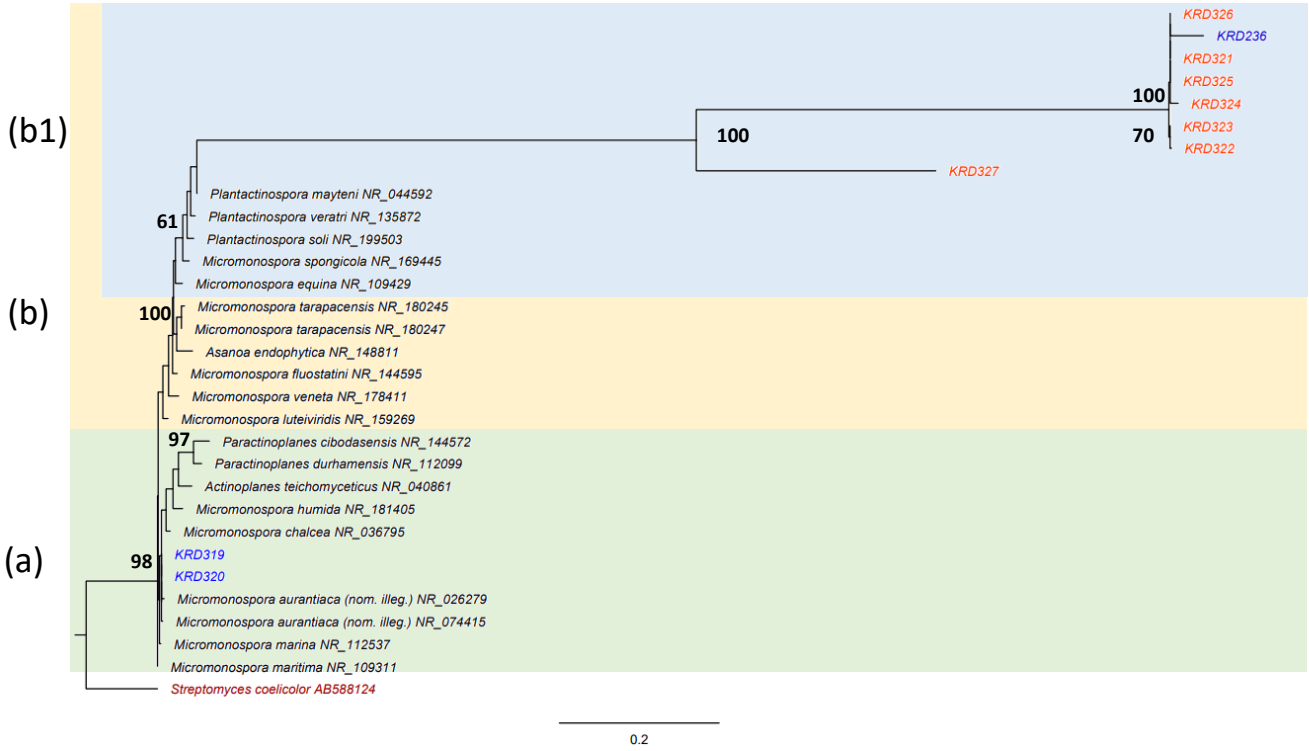

Figure 5.4. Maximum likelihood (ML) tree based on the partial and complete 16S rRNA gene (~450 bp and and ~1500 bp) sequences of *Micromonospora* strains isolated from Mexico and Scotland. This shows the genetic distance between isolates and closely related type strains (<96% similarity, NCBI accession numbers) with *Streptomyces coelicolor* AB588124 used as an outgroup. Branches were scaled by the

expected number of substitutions per site (scale bar, 0.02 nucleotides). The numbers next to the branches are support values exceeding 60% of the ML bootstrap. The origin of the strains is represented by colours, Orange: Mexico, blue: Scotland and red: outgroup**.**

Table 5.2. *Micromonospora* strains from Mexico and Scotland isolated as part of this work and strains from the Duncan Lab bacterial culture collection. Isolation media are indicated for each strain. SC: Starch casein agar, CC: Colloidal chitin agar, G1: Gause's No. 1, 10%A1: A1 (modified starch-casein seawater medium). The shaded strains correspond to those selected for metabolite analysis.

Genus	Strain ID	Phylogeny	Isolation place	Isolation media	Antibacterial activity	Morphology	Selected
Micromonospora sp.	KRD236	Subclade b1	Scotland	SC	-	Black spores	✓
	KRD319	Clade a	Scotland	CC	-	Black spores	✓
	KRD320	Clade a	Scotland	G1	-	Black spores	✓
	KRD321	Subclade b1	Mexico	10% A1	-	White spores	✓
	KRD322	Subclade b1	Mexico	10% A1	-	Black spores	X
	KRD323	Subclade b1	Mexico	10% A1	-	Black spores	X
	KRD324	Subclade b1	Mexico	10% A1	✓	Black spores	✓
	KRD325	Subclade b1	Mexico	10% A1	-	Black spores	X
	KRD326	Subclade b1	Mexico	10% A1	-	Black spores	X
	KRD327	Subclade b1	Mexico	10% A1	-	Black spores	✓

5.2.2 Metabolomic insights into salinity adaptation

Given that the Mexican strains were isolated from a hypersaline lagoon, salinity — at varying concentrations — was evaluated as a key abiotic factor that may influence metabolite production. However, it was observed that the six strains selected for metabolomic analysis (three from Mexico: KRD321, KRD324, KRD327; and three from Scotland: KRD236, KRD319, KRD320) did not exhibit consistent growth in liquid A1 medium, consequently, A1 agar plates were used. However, due to the strains slow growth (21 days), fungal contamination was observed on 11 plates, which resulted in only 94 out of the 105 planned plates (Table S5.2) available for metabolite extraction and LC-HRMS/MS analysis. To assess the LC-MS/MS data, a molecular network was generated

from these 94 metabolite extracts (six strains and three media controls), each cultured in triplicate under five salinities (0 ‰, 15 ‰, 25 ‰, 35 ‰, and 40 ‰ of sea salt [w/v]), resulting, in a total of 1,296 molecular features, organised into 119 molecular families and 672 singletons (Fig. 5.5). Interestingly, despite being phylogenetically distinct, the Scottish strain KRD319 and the Mexican strain KRD324 exhibited the highest number of features, with 4451 and 8911 in total across all salinities, respectively (Table S5.2). A total of 30 matches with reference compounds were obtained from the GNPS spectral library across all strains (data not shown), a number that increased to 115 when using DEREPLICATOR+. Among these putative identifications were several known or potentially bioactive compounds, including salinilactam A (*m/z* 470.29), cespihypotin W (*m/z* 321.206), dysifragilisin A (*m/z* 307.19), antibiotic SCH 23831 (*m/z* 560.346), rifamycin S (*m/z* 696.302), mikanifuran (*m/z* 287.237), cirramycin A (*m/z* 598.359), amycolactam (*m/z* 315.17), and rosamicin (*m/z* 581.356), among others (Table S5.3). The tentative identification of these compounds, many of which belong to antibiotic, antifungal, or cytotoxic families, highlights the presence of chemically diverse and pharmacologically promising metabolites across the analysed strains. Particularly, the detection of macrolide-type structures such as juvenimicin and rosamicin suggests that some of these strains may activate polyketide synthase (PKS) gene clusters, known for their role in the biosynthesis of clinically relevant antibiotics. Further annotation using SIRIUS (v.5.8.6) agreed with several of these matches, including rosamicin (parent ion: 584.38 Da; median mass error: 0.243 ppm, $[M+H]^+$), juvenimicin A2 (parent ion: 554.37 Da; median mass error: 0.328 ppm, $[M+H]^+$), and sporeamicin B (parent ion: 700.43 Da; median mass error: 0.204 ppm, $[M+H]^+$), and also revealed the possible presence of saliniketal A (parent ion: 418.26 Da; median mass error: -1.081 ppm, $[M+Na]^+$) and salinipyronone A (parent ion: 293.17 Da; median mass error: -0.243 ppm, $[M+H]^+$). Notably, all these latter annotations (except saliniketal A) were exclusively detected from the extract of the Mexican strain KRD324, which was the only bioactive strain (Fig. 5.4).

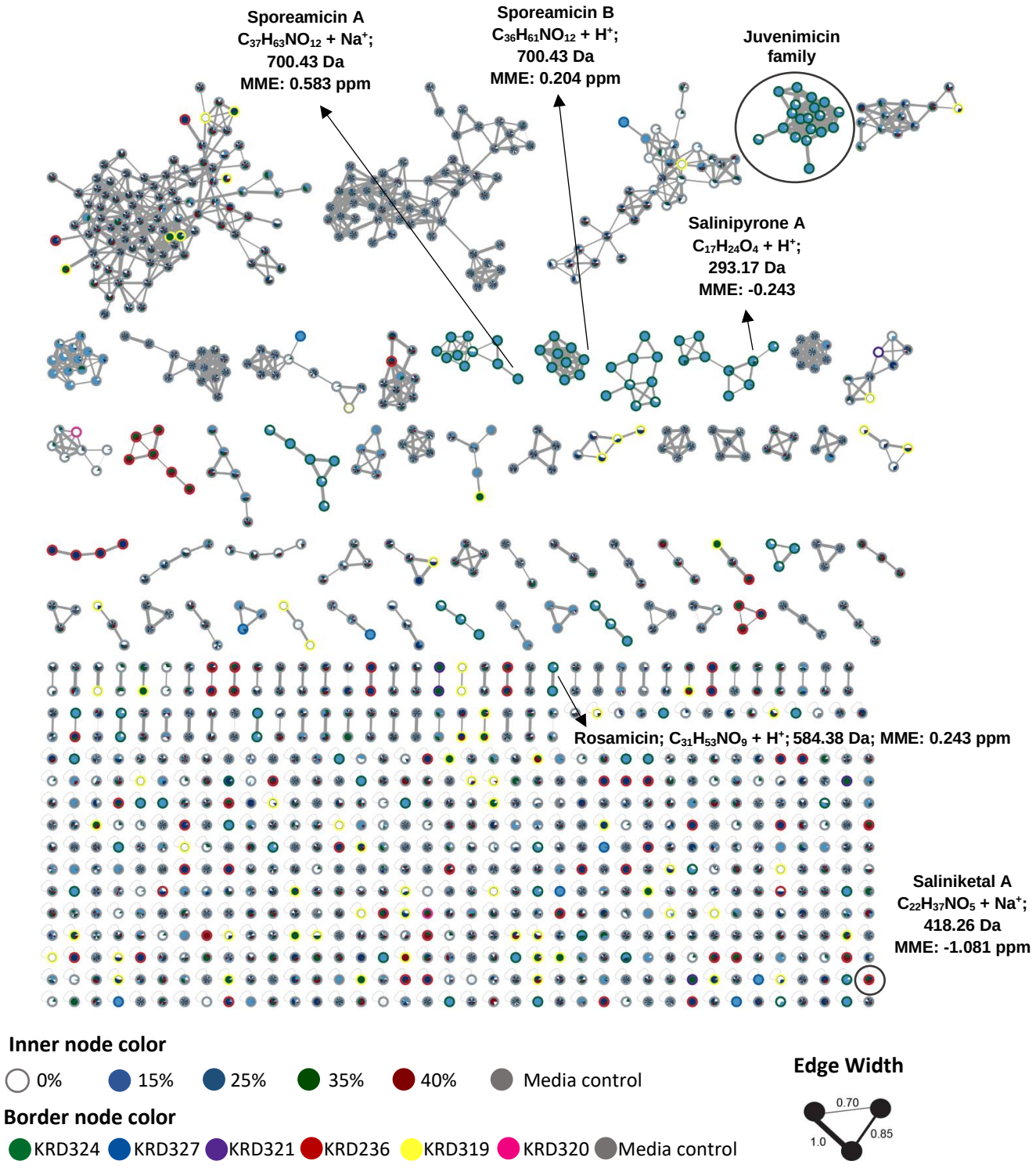

Figure 5.5. Metabolite profiles (Feature Base Molecular Networking) of six *Micromonospora* strains at 0, 15, 25, 35, and 40 ‰ salinity. Inner node colours

represent salinity levels; border node colours indicate bacterial strain origin; grey nodes correspond to metabolites detected in the culture media control. Highlighted metabolites include: Salinipyrone A ($C_{17}H_{24}O_4$ + $[M+H]^+$; 293.17 Da; MME: -0.243 ppm), Rosamycin ($C_{31}H_{53}NO_9$ + $[M+H]^+$; 584.38 Da; MME: 0.243 ppm), and Saliniketal *A* ($C_{22}H_{37}NO_5$ + $[M+Na]^+$; 418.26 Da; MME: -1.081 ppm).

Although fungal contamination prevented robust statistical comparisons across all strains and salinity conditions (which had been a primary aim), clear trends were still observed through qualitative inspection of the molecular network data. Notably, the Mexican strain KRD324 exhibited a peak in metabolite production at 15 ‰ sea salt (467 nodes on average), followed by a decline at higher salinities (reaching just 269 nodes at 40 ‰ on average). This pattern suggests that moderate salt stress may trigger secondary metabolite production in KRD324.This may be part of an ecological or defensive response, while higher salinities may suppress this activity, potentially due to a metabolic reallocation toward maintaining osmotic balance. In contrast, strain KRD321 (also Mexican) displayed a more stable metabolite output across the salinity gradient (ranging between 260–330 nodes), indicating a less sensitive or differently regulated metabolic response. The Scottish strains did not show any consistent trends, further supporting the idea that strain-specific regulatory mechanisms — rather than geographic origin alone — may shape secondary metabolism under osmotic stress. While these observations are based on limited sample numbers and require further validation, they highlight the potential influence of salinity as a modulating factor of metabolite diversity by marine-derived *Micromonospora*.

Based on its comparatively high number of molecular features and the preliminary annotation of several putative antibiotics via GNPS and SIRIUS — including rosamicin- and juvenimicin-like compounds — *Micromonospora* sp. KRD324 was selected for further chemical investigation. GNPS yielded 53 spectral matches to reference compounds in this strain, which increased to 67 with the inclusion of DEREPLICATOR+. Among these, compounds tentatively assigned to known antibiotic classes were identified, including rosamicin (*m/z* 582.364), antibiotic SCH 23831 (*m/z* 560.346), cirramycin A (*m/z* 598.359), juvenimicin B (*m/z* 584.379), and sporeamicin C (*m/z* 686.411) (Table S5.3). Subsequent annotation using SIRIUS (v.6.2.0) supported the presence of several of

these candidates based on predicted molecular formulas, including rosamicin (parent ion: 584.38 Da; median mass error: 0.243 ppm, $[M+H]^+$), juvenimicin A2 (parent ion: 554.37 Da, median mass error: 0.328 ppm), saliniketal A (parent ion: 418.26 Da; median mass error: -1.081 ppm, $[M+Na]^+$), and salinipyrone A (parent ion: 293.17 Da; median mass error: -0.243 ppm, $[M+H]^+$) (Fig. 5.4). While these annotations remain putative, they suggest the presence of bioactive macrolide-like structures in the metabolite extracts of KRD324.

In the case of juvenimicin-related metabolites, a dense molecular subnetwork comprising 19 features was observed (Fig. 5.6). These nodes shared similar MS/MS fragmentation patterns and were primarily detected under 0‰ and 15‰ salinity conditions. The shared fragmentation patterns among these related metabolites include neutral losses consistent with cleavage of a glycosidic moiety, a fragmentation behaviour commonly reported for glycosidylated macrolides such as juvenimicins. Two nodes within the cluster had high similarity scores to known compounds — for instance, juvenimicin A2 (parent ion: 554.37 Da, median mass error: 0.328 ppm) and juvenimicin B2 (parent ion: 584.38 Da, median mass error: 0.258 ppm) according to SIRIUS (v.6.2.0). Additionally, one node was tentatively annotated as rosamicin (parent ion: 584.38 Da; median mass error: 0.243 ppm, $[M+H]^+$), a compound previously reported to be structurally identical to juvenimicin A3 (Kishi *et al.,* 1976). These results suggest that strain KRD324 may produce previously undescribed analogues of the juvenimicin/rosamicin family. Notably, the detection of this macrolide subnetwork was only at 15‰ salinity which suggests that this condition may selectively induce the expression of relevant BGC. This observation aligns with the previously noted peak in metabolite diversity at the same salinity. Possible explanations include: (1) increased competition at moderate salinity triggering an antibiotic response; (2) physiological optimisation at 15‰, allowing energy investment into secondary metabolism; or (3) a synergistic effect of ecological pressure and cellular readiness promoting secondary metabolite biosynthesis. Further transcriptomic or gene cluster activation studies would be required to validate these hypotheses.

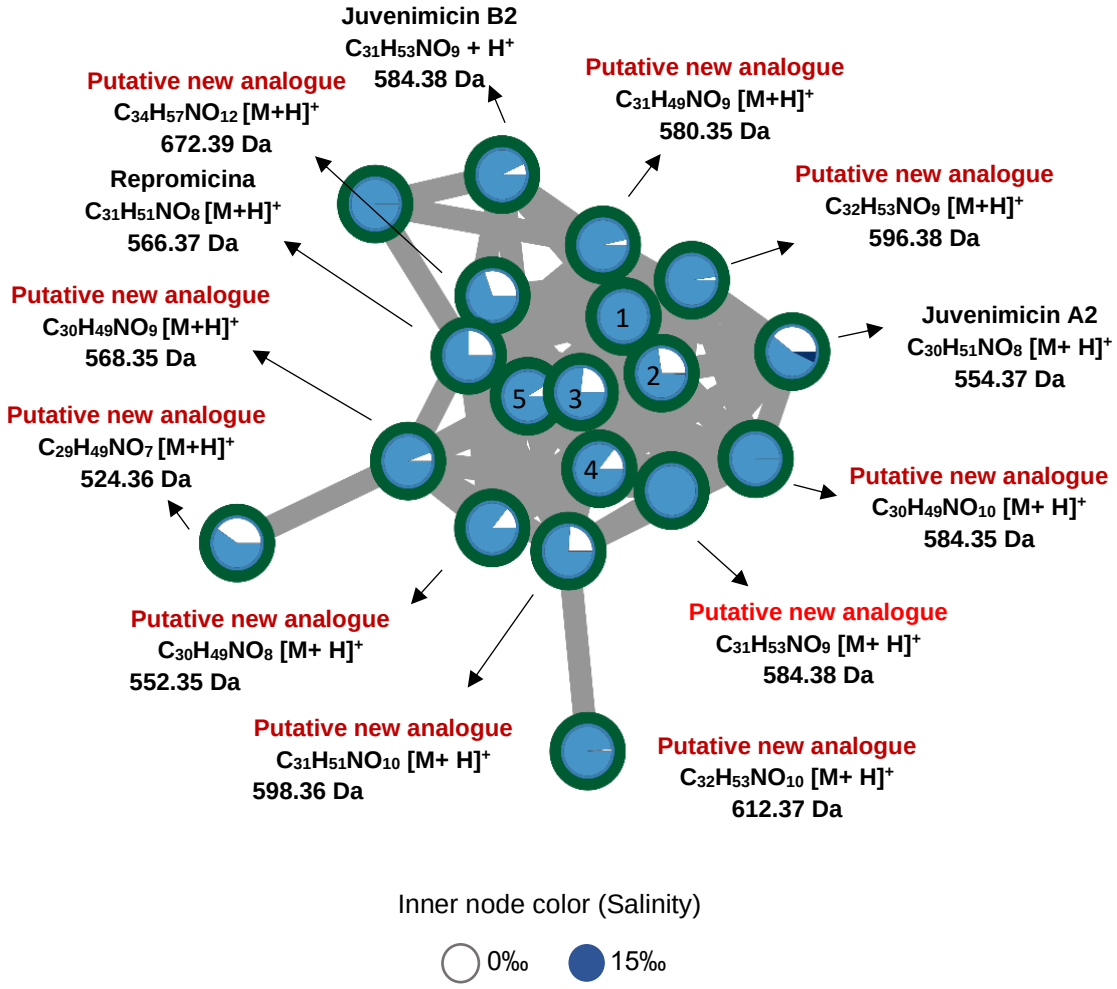

Node ID	Molecular formula	*m/z* (Da)	Adduct	Annotation (SIRIUS)
1	$C_{32}H_{53}NO_9$	596.38	[M+H]+	Putative new analogue
2	$C_{31}H_{53}NO_{10}$	600.37	[M+H]+	Putative new analogue
3	$C_{31}H_{51}NO_9$	582.36	[M+H]+	Rosamicin
4	$C_{31}H_{51}NO_{10}$	598.36	[M+H]+	Putative new analogue
5	$C_{31}H_{53}NO_9$	584.38	[M+H]+	Putative new analogue

Figure 5.6. Molecular family of compounds predicted to be related to juvemicins from strain KRD324 at 0, 15, 25, 35, and 40 ‰ salinity. Node fill colours indicate the salinity condition under which each feature was detected. Numbered nodes correspond to features listed in the accompanying table, which summarises precursor *m/z* values, adducts, and SIRIUS-based annotations. Nodes highlighted in red represent features with no match to public databases and are therefore considered putative new juvenimicin-like analogues, based on shared MS/MS fragmentation patterns and network connectivity.

Following the detection of putative juvenimicin-like metabolites at 15‰ salinity in agar extracts, the study was extended to include targeted purification efforts of these compounds. Although initial detection occurred from agar-grown cultures, scale-up and fractionation procedures are more feasible in liquid media. Therefore, strain KRD324 was cultivated in triplicate in A1 broth supplemented with 15‰ sea salt, as a preliminary test of liquid media to support production. Moderately polar to lipophilic metabolites were extracted using ethyl acetate, and the resulting extracts were analysed by UHPLC-MS/MS in positive ionisation mode. Representative MS^2 spectra are shown in Figure 5.7, which support the presence of key juvenimicin-like macrolides previously observed in solid media. These include features with exact mass matches and fragmentation profiles consistent with rosamicin (*m/z* 582.36) and juvenimicin B1 (*m/z* 568.38), as predicted by SIRIUS (v.6.0.4). A third feature displays a closely related precursor mass (m/z 600.37 $[M+H]^+$) and shares several diagnostic fragment ions characteristic of glycosylated macrolides, including fragments consistent with loss of the amino sugar moiety. However, distinct differences in the relative intensities and presence of secondary fragment ions distinguish this feature from the annotated juvenimicins, suggesting structural variation in peripheral functional groups rather than in the macrolide core itself. Together, these MS/MS similarities and differences indicate the production of a small family of juvenimicin-related metabolites, comprising both known compounds and at least one unannotated analogue. These findings indicate that juvenimicin-related metabolites are also produced under liquid broth conditions, reinforcing the reproducibility of secondary metabolite expression across culture formats.

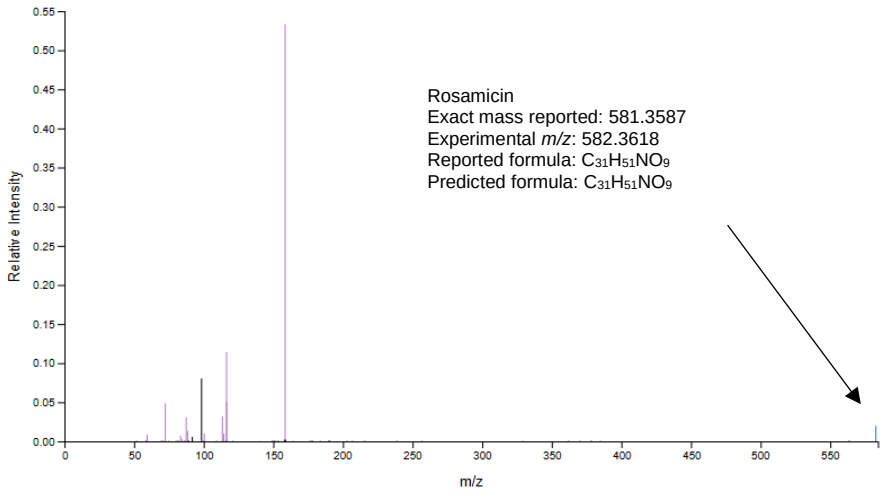

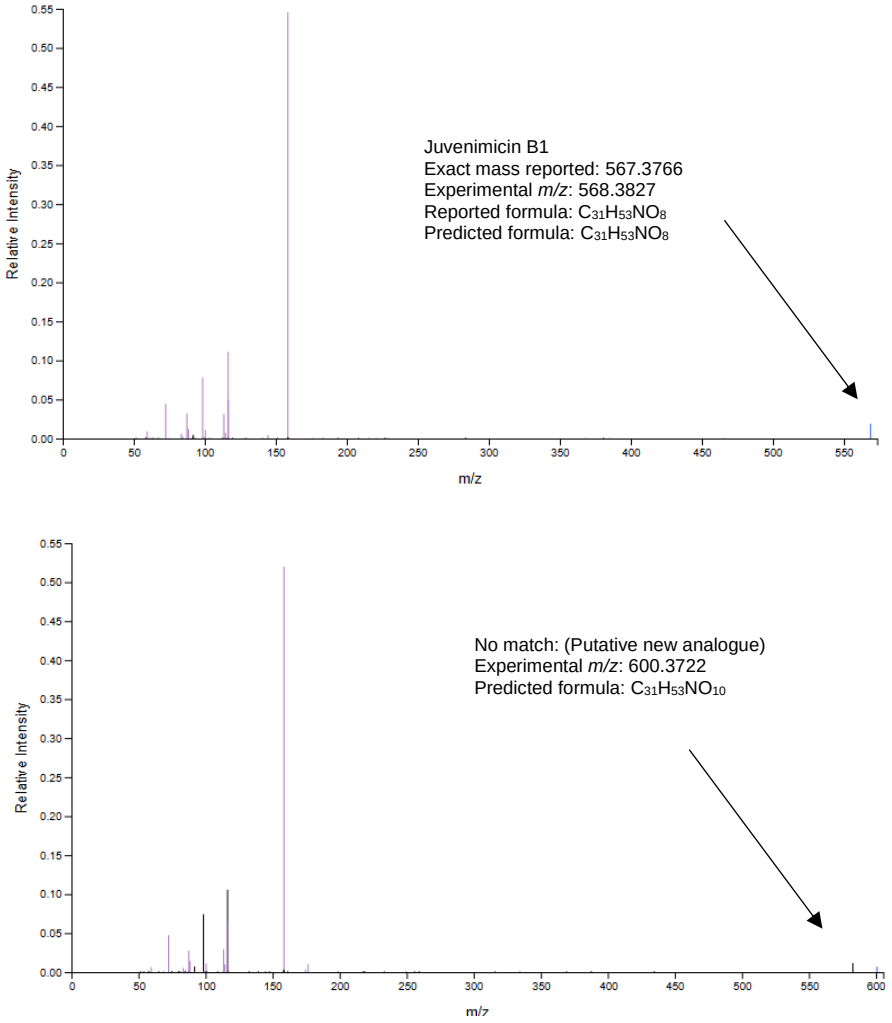

Figure 5.7. MS2 spectra acquired by UHPLC-Orbitrap MS/MS in positive mode from ethyl acetate extracts of *Micromonospora* sp. KRD324 cultured in A1 broth with 15‰ sea salt. Spectra putatively identified by SIRIUS as (a) **Rosamicin** (*m/z* [M + H]$^+$ 582.3618), (b) **Juvenimicin B1** (*m/z* [M + H]$^+$ 568.3827), and (c) a **putative new analogue** (*m/z* [M + H]$^+$ 600.3722). All spectra display shared fragmentation features consistent with glycosylated macrolides, including a prominent fragment around m/z ~157, tentatively attributed to cleavage of the amino sugar moiety. Structural assignments remain tentative in the absence of NMR confirmation.

All features associated with this cluster and their spectral details are summarised in Table 5.3. This table show MS/MS-based annotations, as predicted by SIRIUS (v.6.0.4), and revealed a common mass range among all putative compounds, with [M+H]+ parent ions

ranging from 552.35 to 624.38 Da. Retention times varied between 3.74 and 4.64 min, suggesting moderate structural variation (e.g., in polarity or functional groups). The mass accuracy was high, with median mass errors ranging from –2.06 to –0.52 ppm, (absolute values ≤ 2 ppm), which is within the accepted range for high-resolution MS and supports confidence in the predicted molecular formulas. Among the features, two known antibiotics were putatively annotated: rosamicin (*m/z* 582.36, [M+H]+, median mass error –1.62 ppm) and juvenimicin B1 (*m/z* 568.38, [M+H]+, median mass error –1.22 ppm). The remaining ten features exhibited highly similar MS/MS fragmentation patterns, including diagnostic ions associated with the macrolide backbone and glycosidic cleavage, yet did not match any entries in public spectral or structural databases. The combination of shared precursor mass range, closely clustered retention times, and conserved fragmentation behaviour strongly suggests that these features belong to the same juvenimicin-related molecular family, while differences in exact mass and minor fragmentation patterns point to structural diversification through modifications such as oxidation, reduction, or substituent variation. Although definitive structural assignment is not possible without isolation and spectroscopic characterisation, these data support the presence of multiple unannotated juvenimicin-related analogues produced by strain KRD324 under hypersaline conditions.

Table 5.3. Summary of MS/MS-based annotation for 19 features (plus five structurally related singletons) matching juvenimicin-like macrolides detected in *Micromonospora* sp. KRD324 cultivated at 15‰ salinity (A1 medium), based on SIRIUS predictions (v.6.0.4). The table includes molecular formula, adduct type, parent *m/z*, retention time (RT), the most similar structure proposed, and match similarity. Cell colours correspond to the Ion Identity Molecular Network in Fig. S5.5: blue indicates key features forming the core of the juvenimicin-like molecular family; yellow and red indicate sodium and potassium adduct variants, respectively, while grey nodes in the network represent putative new analogues (PNA) with no matches in databases (SIRIUS, GNPS and NPAtlas).

Experimental data (Broth crude extract)				SIRIUS v.6.0.4 prediction		
Feature number	Adduct	Parent mass (Da)	RT	Formula	Median mass error (ppm)	Match similarity
161	[M+H]+	582.36	3.94	$C_{31}H_{51}NO_9$	-1.62	Rosamicin; Juvenimicin A3
162	[M+H]+	600.37	3.94	$C_{31}H_{53}NO_{10}$	-1.279	

201	[M+H]+	568.38	4.18	$C_{31}H_{53}NO_8$	-1.221	Juvenimicin B1
232	[M+H]+	552.39	4.44	$C_{31}H_{53}NO_7$	-1.42	
203	[M+Na]+	590.36	4.19	$C_{31}H_{53}NO_8$	-0.519	
164	[M+Na]+	604.34	3.94	$C_{31}H_{51}NO_9$	-1.477	Rosamicin
231	[M+Na]+	574.37	4.43	$C_{31}H_{53}NO_7$	-0.685	
168	-	-	-	-	-	-
113	[M+H]+	624.38	3.74	$C_{32}H_{53}N_3O_9$	-0.915	PNA
125	[M+H]+	568.35	3.83	$C_{30}H_{49}NO_9$	-0.746	PNA
131	[M+Na]+	598.36	3.86	$C_{29}H_{53}NO_{10}$	-1.685	PNA
189	[M+H]+	554.37	4.08	$C_{30}H_{51}NO_8$	-1.363	PNA
154	[M+H]+	568.35	3.92	$C_{30}H_{49}NO_9$	-1.221	PNA
210	[M+H]+	538.37	4.3	$C_{30}H_{51}NO_7$	-1.018	PNA
245	[M+H]+	566.4	4.64	$C_{32}H_{55}NO_7$	-1.537	PNA
188	[M+H]+	596.38	4.08	$C_{32}H_{53}NO_9$	-1.354	PNA
181	[M+Na]+	552.35	4.03	$C_{28}H_{51}NO_8$	-2.055	PNA
214	[M+H]+	582.40	4.32	$C_{32}H_{55}NO_8$	-1.137	PNA
147	[M+?]+	597.37	3.88	$C_{27}H_{48}N_8O_7$	-0.837	PNA
167	-	-	-	-	-	-

To determine whether these features represented distinct molecules or adduct/isotope variants of the same compound, Ion Identity Molecular Networking (IIMN) was applied (Fig. 5.8). This approach integrates MS^2 spectral similarity with MS^1 adduct correlation. The resulting network consisted of 21 interconnected nodes, comprising: four main features with [M+H]+ ions (including two compounds matching rosamicin and juvenimicin B1); four adduct-related variants of these main features (three with *in-silico* predictions; one feature 168, remained unannotated). Importantly, twelve additional nodes clustered within the same molecular family but showed no ion identity links consistent with adduct or isotopic forms, indicating that they represent structurally related yet distinct molecular species. The separation of these nodes from known adduct patterns, combined with their conserved MS/MS fragmentation behaviour, supports the interpretation that they correspond to genuine juvenimicin-related analogues rather than artefacts. Although most of these features could not be matched to known compounds in public databases, their close association with annotated juvenimicin macrolides in the IIMN network suggests diversification around a shared macrolide scaffold. Collectively, these results

demonstrate that strain KRD324 produces a suite of structurally related juvenimicin-like metabolites, extending beyond previously characterised members of this family.

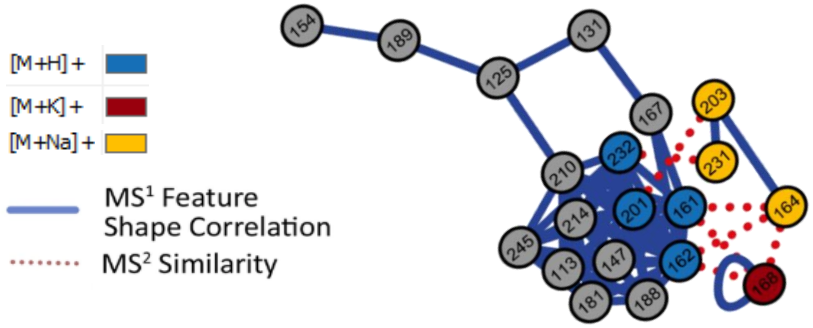

Figure 5.8. Ion identity molecular network of *Micromonospora* sp. KRD324 cultured in A1 broth with 15‰ sea salt. The network contains MS2 similarity edges from molecular networking as solid blue lines combined with MS1 ion identity networking edges as dotted red line.

5.2.3 Scale-up and targeted fractionation of Juvenimicin-like Macrolides from *Micromonospora* sp. KRD324.

To enable further characterisation and potential purification of the juvenimicin-like metabolites identified via Ion Identity Molecular Networking (IIMN), *Micromonospora* KRD324 was scaled up under optimised saline conditions. The strain was cultured in 13 flasks (1 L Erlenmeyer; 200 mL A1 medium with 15‰ sea salt), yielding a total culture volume of 2.6 L. Due to equipment constraints, larger flasks were not used, although they might have improved yield and simplified handling. To account for medium-derived compounds, three sterile A1 control flasks were extracted in parallel. Ethyl acetate extraction of the inoculated cultures yielded between 22–39 mg of crude extract per flask, compared to 3–7 mg from controls. This protocol generated sufficient material for chromatographic fractionation, and one representative crude extract was selected for pilot

fractionation. Initially, a silica-based column was used to reduce polar matrix interference and concentrate macrolides; however, UHPLC-MS/MS analysis showed that juvenimicin-like compounds were not recovered (data not shown). This likely reflects either compound loss due to adsorption on the silica or instability under the chromatographic conditions—both are known issues for labile macrolides. Subsequently, a reverse-phase C18 column was used with a gradient elution with water and acetonitrile, yielding eight fractions, wish were analysed by UHPLC-MS/MS (positive ESI mode).

A total of nine features were annotated as putative juvenimicin-like macrolides (Table 5.4) and supported by SIRIUS (v.6.0.4) prediction. Retention times ranged from 3 to 4.6 min, consistent with moderate hydrophobicity and indicative of partial chromatographic separation of related analogues. Among these, two features matched previously reported macrolides: juvenimicin A2 and juvenimicin B1, both with high annotation confidence and low mass errors. One early-eluting feature (RT 0.70 min) displayed unusually high polarity, which is not typical for macrolides. This may reflect a polar metabolite, an artefact, or an annotation error due to algorithmic limitations. Notably, feature *m/z* 561.353, $C_{31}H_{48}N_2O_7$ (feature ID 1598), initially considered a new analogue due to its nitrogen-rich composition, was found to match Sch 23831, a known macrolide with antibacterial properties previously isolated from *Micromonospora rosaria* (Puar *et al.,* 1979). In addition, feature 1339 was detected at *m/z* 600.374, is consistent with a dehydrated protonated ion $[M-H_2O+H]^+$ from a neutral molecule with the formula $C_{31}H_{53}NO_{10}$. This may result from in-source fragmentation or reflect the presence of a naturally occurring dehydrated variant. Overall, fewer putative new analogues were detected in the fractions compared to the crude extract. This may be due to metabolite degradation or concentrations near the detection threshold. Conversely, certain features (e.g., 1598) became more prominent after fractionation, likely due to reduced matrix complexity or improved enrichment during purification.

Table 5.4. Summary of MS/MS-based experimental data annotation for nine features matching juvenimicin-like macrolides detected in fractions of *Micromonospora* sp. KRD324 crude extract cultivated at 15‰ salinity (A1 medium). The annotations were also supported by SIRIUS analysis (v.6.2.0). The table includes reference numbers (related to figure S5.4), predicted molecular formulas, ion adducts, observed and theoretical *m/z* values, retention times, mass errors, SIRIUS confidence scores, and explained peaks. The latter indicates the number of experimental MS/MS

fragment peaks that can be rationalised by the candidate molecular structure, relative to the total peaks observed.

#	ID number	Molecular formula	Adduct	RT (min)	*m/z* observed	*m/z* theoretical	Exact mass reported (Da)	Median mass error (ppm)	Peaks exp.	Match
1	1513	$C_{30}H_{51}NO_8$	[M+H]+	4.06	554.369	554.369	553.73	-0.436	7/7	Juvenimicin A2
2	1598	$C_{31}H_{48}N_2O_7$	[M+H]+	4.15	561.353	561.353	560.35	-0.441	8/8	Sch 23831
3	1612	$C_{31}H_{53}NO_8$	[M+H]+	4.17	568.384	568.384	567.37	-0.448	10/10	Juvenimicin B1
4	258	$C_{32}H_{47}N_5O_5$	[M+H]+	0.70	582.364	582.365	PNMA	-0.484	2/2	No
5	1239	$C_{31}H_{51}NO_{10}$	[M+H]+	3.83	598.358	598.357	PNMA	0.060	5/5	No
6	1339	$C_{31}H_{53}NO_{10}$	[M+H]+	3.91	600.374	600.374	PNMA	-0.588	2/2	No
7	1340	$C_{31}H_{53}NO_{10}$	$[M-H_2O+H]+$	3.92	582.363	582.364	PNMA	-0.497	5/5	No (dehydrated version of compound 6)
8	1431	$C_{32}H_{53}NO_{10}$	[M+H]+	3.99	612.374	612.374	PNMA	-0.361	2/2	No
9	1750	$C_{32}H_{55}NO_8$	[M+H]+	4.30	582.4	582.4	PNMA	-0.276	3/3	No

*PNMA: Putative New Macrolide Analogue

A feature-based molecular network was constructed using the metabolite extracts from eight C18 fractions to visualise the distribution of juvenimicin-like metabolites. The network comprised 917 nodes, of which ten features were annotated as putative juvenimicin-like macrolides based on their MS/MS fragmentation patterns (Fig. S5.3) with five forming a molecular family and five singleton nodes. These metabolites were only detected in the 40%, 50%, 60% and 80% acetonitrile fractions consistent with the expected retention behaviour of moderately hydrophobic macrolides using C18 for separation. To complement this network-based analysis, the raw UHPLC-MS/MS chromatogram data files were assessed using mzMine 3 to independently identify the ions (Fig. 5.9 and Fig. S5.4). In fraction 3 (40% acetonitrile), feature 582.3627 *m/z* with formula $C_{31}H_{53}NO_{10}$ (feature ID 1340) showed the highest signal (1.1×10^9), while Sch 23831 (feature 561.353 *m/z* with formula $C_{31}H_{48}N_2O_7$, feature ID 1598) was detected at lower intensity (1.7×10^8), alongside minor signals such as feature 582.3993 *m/z* (formula $C_{32}H_{55}NO_8$; signal 1.07×10^7, feature ID 1750). In fraction 4, feature 582.3627 *m/z* (feature ID 1340) decreased notably, and Sch 23831 was no longer detectable, suggesting both compounds was at a maximum intensity in fraction 3. In contrast,

juvenimicin B1 appeared in fraction 4, accompanied by a threefold increase in feature 582.3993 *m/z* (feature ID 1750) (3.0×10^7). This compound continued to rise across subsequent fractions, peaking in fraction 6 (80% acetonitrile) at 6.0×10^7. Fractions 7 and 8 retained low but detectable signals, likely corresponding to residual washout of macrolide metabolites during the gradient elution (Fig. S5.4). Notably, feature 582.3993 *m/z* (feature ID 1750) consistently displayed a split peak in all relevant chromatograms, which may reflect either chromatographically separable isomers or interactions with the stationary phase affecting retention time. While further structural elucidation is required, this observation underscores the microheterogeneity within this metabolite group.

In summary, due to limited time, further purification remains to be achieved. Fractions 3 and 6 should be prioritised for subsequent isolation and characterisation efforts based on detection of juvenimicin-like analogues with predicted molecular formulas $C_{31}H_{53}NO_{10}$ (feature ID 1340) and $C_{32}H_{55}NO_8$ (feature ID 1750), respectively. These findings provide additional support for the chemical diversity and biosynthetic potential of *Micromonospora* sp. KRD324 under hypersaline conditions.

(A)

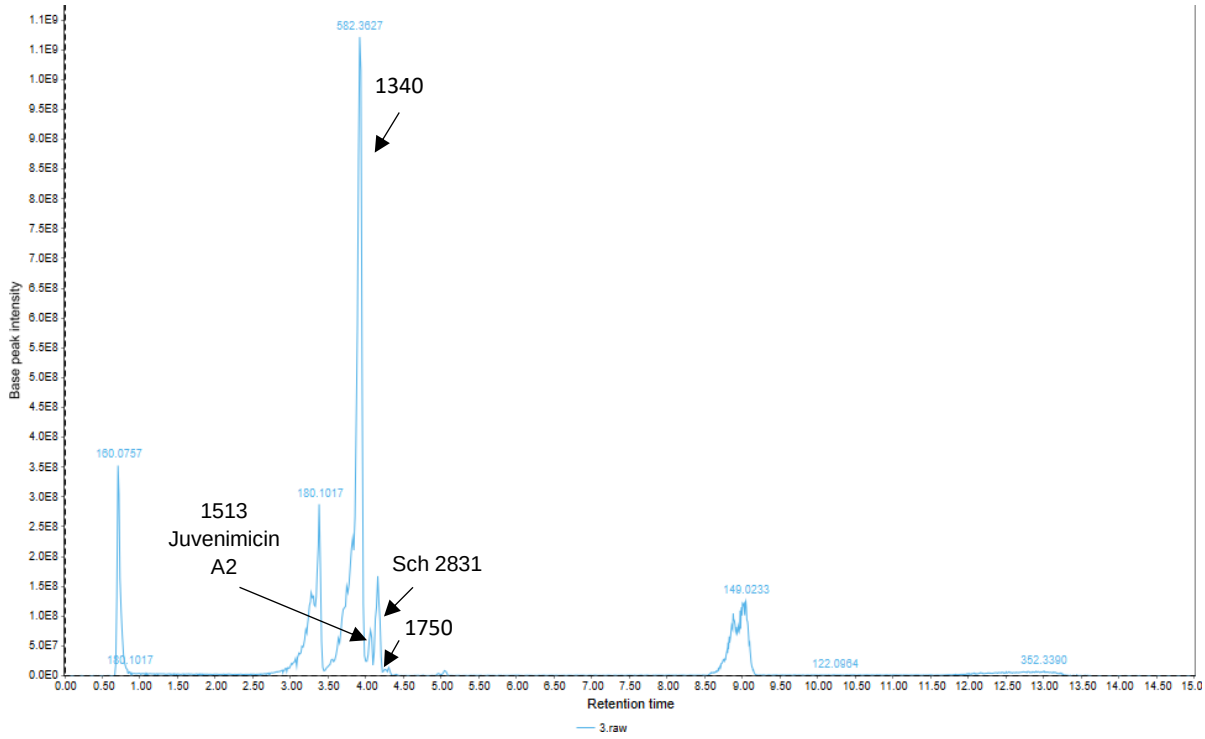

(B)

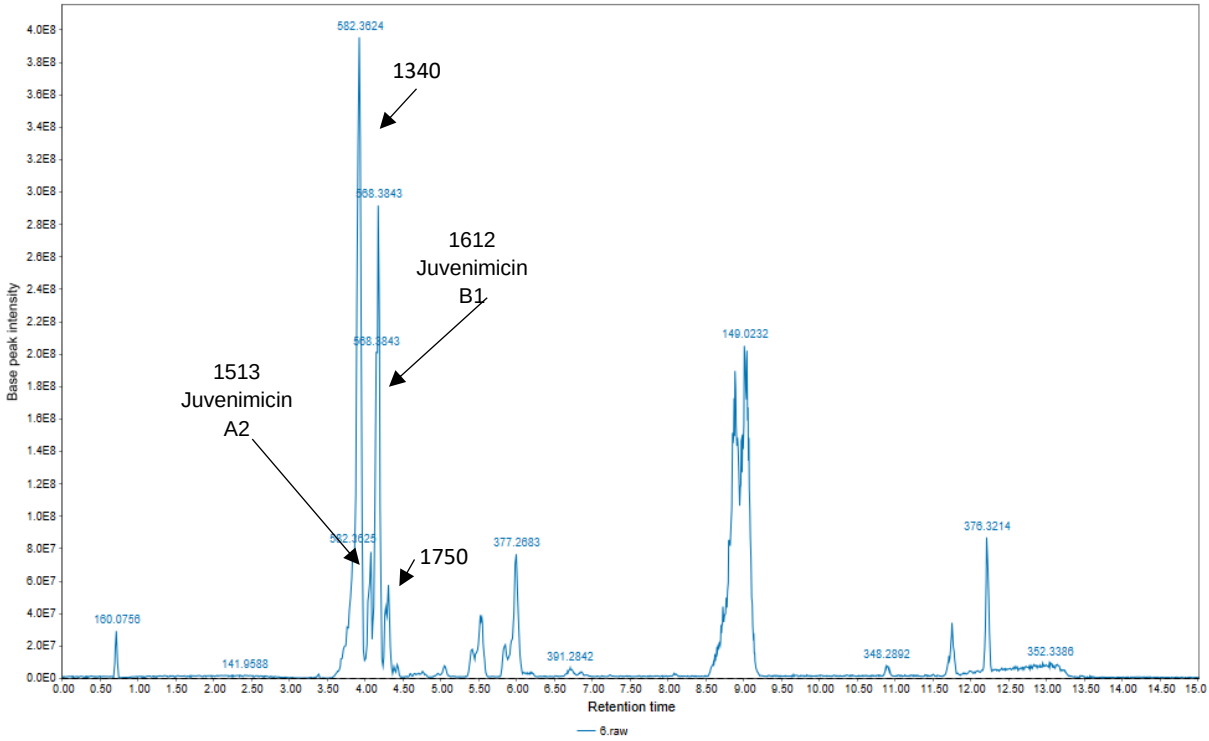

Figure 5.9. HR-LC chromatograms of selected fractions from the semi-preparative C18 fractionation of *Micromonospora* sp. KRD324 crude extract grown at 15% salinity. (A) Fraction 3 (eluted with H_2O–MeCN 60:40); (B) Fraction 6 (eluted with H_2O–MeCN 20:80). Both chromatograms were acquired in positive ionisation mode using UHPLC-HRMS. Retention times and intensity profiles are shown for macrolide-type features identified as juvenimicin analogues based on SIRIUS predictions (see Table 5.3). Peaks marked correspond to the features with parent *m/z* values of 582.3627 (feature ID 1340), Sch 2831 (561.3534), 582.3992 (feature ID 1750), Juvenimicin A2 (554.3682), and juvenamicin B1 (568.3845).

5.2.4 Genomic insight into the biosynthetic capacity of *Micromonospora* sp. KRD324

To complement the metabolomic evidence for rosamycin-like and other macrolide compounds, the genome of *Micromonospora* sp. KRD324 was sequenced. Assembly metrics such as genome size, GC content, N50, and completeness were determined following the workflow described in Chapter 3. In brief, a hybrid assembly approach was applied, combining short-read Illumina and long-read Nanopore sequencing. This strategy enabled a high-contiguity genome assembly with improved structural resolution

that minimised assembly artefacts and provided confidence for BGC detection. The complete genome of strain KRD324 was 6.26 Mbp in size, with a GC content of 70.67%, a low sequence error rate of 0.16 mismatches per 100 Kbp, and an estimated completeness of 99.4%, as assessed by BUSCO (v. 5.8.0) (Table 5.5). These features are consistent with reported genome characteristics of the genus *Micromonospora*, known for large, GC-rich genomes and extensive biosynthetic potential (Yan *et al.,* 2022). Genome annotation predicted 5,667 protein-coding sequences (CDSs), alongside 17 non-coding RNAs, 47 tRNAs, and six rRNA operons, further supporting the completeness and functional richness of the assembly. No plasmids were detected using MOB-suite, suggesting a primarily chromosomal genome architecture in this strain.

Table 5.5. Assembly metrics for *Micromonospora* strains KRD324. Hybrid assembly strategies using Nanopore and Illumina reads polished with Pilon. Metrics include the number of contigs, total assembly length (in base pairs), size of the largest contig, average coverage (rounded to nearest decimal), N50 (a measure of assembly continuity), and completeness based on BUSCO analysis (using the Busco v5 Linage Datasets (2023-05-02)).

Parameter	KRD324
Number of contigs	1
Total length (bp)	6266434
Largest contig	6266434
Average coverage	240.86
GC%	70.67
N50 (bp)	6266434
Mismatches per 100 Kbp	0.16
Busco (complete single-copy genes)	99.4
Plasmids	0
Annotation results[b]	
Number of CDSs (protein)	5,667
Number of ncRNAs regions	17
Number of tRNAs	47
Number of rRNAs	6

[a]The presence of plasmids in the genome sequences was inferred using MOB-Recon and plasflow in Galaxy Europe (https://usegalaxy.eu/)
[b]Genome annotation was performed using the Bakta tool through Proksee platforms (https://proksee.ca/).

Genome mining identified 20 BGCs (Fig. 5.10A), comprising five PKS, five terpene, three RiPP-like peptide, four hybrid BGCs, one NAGGN, one lantipeptide-class I, and one siderophore BGC. The absence of nonribosomal peptide synthetase (NRPS) clusters is notable, although *Micromonospora* strains are known to prioritise polyketide and terpene biosynthesis (Yan *et al.,* 2022). Among the identified BGCs, one PKS displayed 100% gene-level homology to the well-characterised rosamicin BGC (BGC0002086) from *Micromonospora carbonacea* (Kautsar *et al.,* 2020), strongly supporting the hypothesis that strain KRD324 possesses the biosynthetic machinery required to produce rosamicin or structurally related macrolides. In the genome of KRD324, the putative rosamicin-like BGC spans approximately 21 Kbp, located between positions 2,892,312 and 2,913,358 nt on the main contig. This region is notably smaller than the canonical rosamicin BGC reported in the MIBiG database (60.2 Kbp) (Fig. 5.10B). Given the high-quality, circular genome assembly obtained for KRD324, with minimal mismatches and 99.4% completeness, this size difference is unlikely to be an artefact of sequencing or assembly but may reflect genuine structural divergence. Such streamlining of biosynthetic gene clusters could be an adaptive mechanism to optimise metabolite production. Interestingly, although rosamicin was detected in the crude extract, fractionation efforts revealed that the better (stronger) ionising macrolide corresponded to a putative new analogue, with no detectable peak for rosamicin itself. This observation raises the possibility that evolutionary modifications within the BGC may have redirected the biosynthetic output of KRD324 towards structurally related, but distinct, macrolide analogues, rather than the canonical rosamicin. In addition to the rosamicin BGC, several other clusters of interest were detected, including those showing similarity to neocarzilin (28% similarity), isoenerietane (25%), frankiamicin (28%), sporolides (21%) and various terpenes and RiPP-like peptides, although with lower confidence scores. The low similarity scores observed for these clusters highlight the limitations of structure prediction based solely on genome mining, as partial gene-level homology reflects shared biosynthetic logic rather than direct correspondence to known chemical structures. Consequently, such predictions should be interpreted as indicative of biosynthetic potential rather than definitive evidence of specific metabolite production, reinforcing the need for complementary metabolomic and experimental validation.

(A)

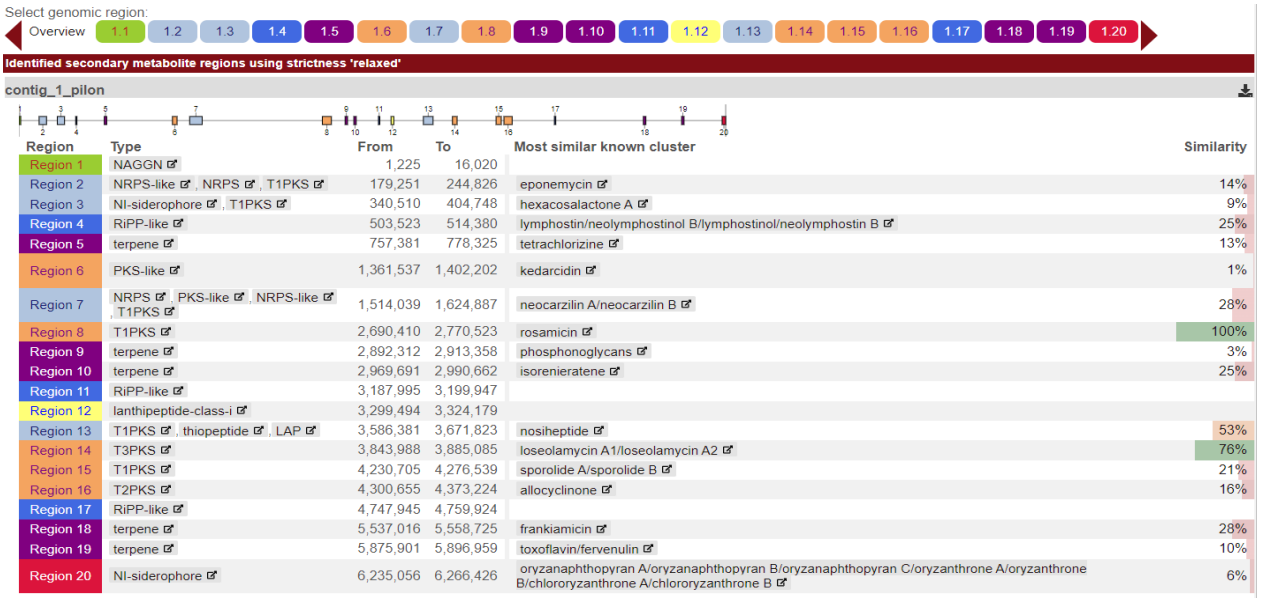

Region	Type	From	To	Most similar known cluster	Similarity
Region 1	NAGGN	1,225	16,020		
Region 2	NRPS-like, NRPS, T1PKS	179,251	244,826	eponemycin	14%
Region 3	NI-siderophore, T1PKS	340,510	404,748	hexacosalactone A	9%
Region 4	RiPP-like	503,523	514,380	lymphostin/neolymphostinol B/lymphostinol/neolymphostin B	25%
Region 5	terpene	757,381	778,325	tetrachlorizine	13%
Region 6	PKS-like	1,361,537	1,402,202	kedarcidin	1%
Region 7	NRPS, PKS-like, NRPS-like, T1PKS	1,514,039	1,624,887	neocarzilin A/neocarzilin B	28%
Region 8	T1PKS	2,690,410	2,770,523	rosamicin	100%
Region 9	terpene	2,892,312	2,913,358	phosphonoglycans	3%
Region 10	terpene	2,969,691	2,990,662	isorenieratene	25%
Region 11	RiPP-like	3,187,995	3,199,947		
Region 12	lanthipeptide-class-i	3,299,494	3,324,179		
Region 13	T1PKS, thiopeptide, LAP	3,586,381	3,671,823	nosiheptide	53%
Region 14	T3PKS	3,843,988	3,885,085	loseolamycin A1/loseolamycin A2	76%
Region 15	T1PKS	4,230,705	4,276,539	sporolide A/sporolide B	21%
Region 16	T2PKS	4,300,655	4,373,224	allocyclinone	16%
Region 17	RiPP-like	4,747,945	4,759,924		
Region 18	terpene	5,537,016	5,558,725	frankiamicin	28%
Region 19	terpene	5,875,901	5,896,959	toxoflavin/fervenulin	10%
Region 20	NI-siderophore	6,235,056	6,266,426	oryzanaphthopyran A/oryzanaphthopyran B/oryzanaphthopyran C/oryzanthrone A/oryzanthrone B/chlororyzanthrone A/chlororyzanthrone B	6%

(B)

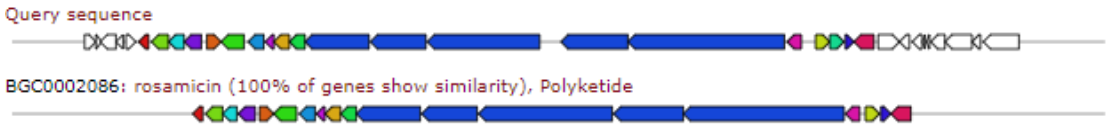

Figure 5.10. Overview of BGCs predicted in the genome of *Micromonospora* KRD324 by antiSMASH. A) shows the complete BGC landscape identified in the genome of strain KRD324 using relaxed detection parameters. A total of 20 regions with predicted biosynthetic potential were detected, including hybrid NRPS-PKS, PKS-like, terpenes, siderophores, RiPPs, and lanthipeptides, among others. Notably, region eight corresponds to a T1PKS cluster with 100% gene similarity to the rosamicin BGC (BGC0002086) deposited in the MIBiG database, highlighted in green in the similarity column. B) Shows the synteny comparison between the rosamicin-like cluster of strain KRD324 (query sequence) and the canonical rosamicin BGC, showing conserved gene architecture and gene identity.

Interestingly, genome mining with the Antibiotic Resistant Target Seeker (ARTS) (Mehmet *et al.,* 2020) tool revealed putative resistance determinants within the KRD324 genome. ARTS predicts self-resistance genes based on the detection of conserved resistance markers, gene duplications, and proximity to BGCs, which are known indicators of self-protection mechanisms in secondary metabolite-producing microorganisms. Among the 30 predicted resistance models identified in this genome,

high-confidence predictions included an ABC-efflux transporters (E-value 1.4e-77; Bit-scores 259.9) and a putative Erm23S_rRNA_methyltransferase (E-value: 3.2e-94; Bit-score: 313.3) (Table 5.6). The latter is associated with ribosomal methylation, a well-characterised mechanism conferring resistance to macrolide antibiotics, including rosamicin and juvenimicin-like compounds, while the former may facilitate the export of bioactive compounds, contributing to self-protection mechanisms in the producer strain. The detection of high-confidence self-resistance markers supports the hypothesis that *Micromonospora* sp. KRD324 harbours intrinsic defence mechanisms that may have co-evolved alongside the biosynthetic pathways responsible for juvenimycin-like macrolide production, further reinforcing its potential as a producer of these bioactive secondary metabolites. However, experimental validation of these resistance elements remains necessary to confirm their functionality.

In addition, phylogenetic reconstruction of the ARTS-predicted rRNA methyltransferase gene (Fig. S5.5) revealed that *Micromonospora* sp. KRD324 clusters closely with *Salinispora tropica* and *Salinispora arenicola*, two marine actinomycetes known for their specialised metabolite biosynthesis. Notably, a homologous BGC to the rosamicin cluster has been described from *Salinispora pacifica* (BGC0001830), which produces not only rosamycin-like macrolides but also additional metabolites, including salinipyrone A and pacificanone (Awakawa *et al.,* 2015). These findings raise the possibility that *Micromonospora* sp. KRD324 possesses the genetic potential to produce a broader array of structurally diverse bioactive compounds beyond rosamicin and juvenimicin analogues.

Table 5.6. Predicted antibiotic resistance markers from the *Micromonospora* sp. KRD324 genome identified using ARTS (Antibiotic Resistant Target Seeker). The analysis reports the total number of detected genes, core genes (essential single-copy genes), BGC-associated hits, and genes predicted as resistance markers based on duplication events or proximity to BGCs. The table summarises 15 selected resistance-related hits from a total of 30 predicted by ARTS. For each hit, the corresponding gene model, description, sequence ID, E-value, and Bit-score are provided. Lower E-values and higher Bit-scores indicate higher confidence in the predicted homology.

Total genes	5672	Gene duplication	11
Core	367	BGC proximity	30
Total BGC hits	20		
Known resistance models hits	30		

Model	Description	Sequence id	E-value	Bit-score
PF00044.19	Gp_dh_N	504	3.50E-56	188
PF00183.13	HSP90	3869	8.60E-132	438.8
PF00183.13	HSP90	4594	6.90E-07	26.6
PF00185.19	OTCace	5344	9.90E-49	163.8
PF00204.20	DNA_gyraseB	2755	5.50E-60	200.1
PF00227.21	Proteasome	5529	3.40E-32	109.9
PF00364.17	Biotin_lipoyl	887	2.00E-46	154.1
PF00521.15	DNA_topoisoIV	2756	8.20E-149	494.6
PF01039.17	Carboxyl_trans	3890	1.60E-206	685
PF13599.1	Pentapeptide_4	2032	6.10E-24	82.2
RF0007	ABC_efflux	430	1.40E-77	259.9
RF0054	ClassB	412	4.40E-27	93.3
RF0067	Erm23S_rRNA_methyltrans	2376	3.20E-94	313.3
RF0174	ArmA_Rmt	3011	3.50E-55	185.4
TIGR02013	TIGR02013	2169	0	1733.9

5.3 Discussion

The integration of phylogenetic, morphological, and antimicrobial screening enabled the selection of six *Micromonospora* strains for comparative metabolomic analysis. Among these, KRD324 emerged as a particularly promising candidate, displaying reproducible antimicrobial activity against *Enterococcus faecalis* and *Bacillus subtilis*, with HPLC-MS/MS evidence for multiple macrolides, including rosamicin- and juvenimicin-type derivatives. These findings are consistent with the known chemistry of *Micromonospora*, which has long been recognised as a source of macrolide and juvenimicin analogues

(Kishi, 1976; Carlson et al., 2013), and with recent genomic surveys that highlight rich BGC diversity within Micromonosporaceae (Alas et al., 2024; Hifnawy et al., 2020).

Remarkably, metabolites historically associated with *Salinispora* — including rifamycin-related polyketides and salinipyrone-type compounds — were also detected in KRD324 (cf. rifamycin reports in *Salinispora*; Matsuda et al., 2009; Oh *et al.,* 2008). This overlap expands the recognised chemical space of *Micromonospora* and raises two testable evolutionary scenarios: (i) horizontal gene transfer (HGT) of intact or partial BGCs between lineages (a process documented across actinobacteria and implicated in the patchy distribution of many PKS/NRPS clusters: Nett *et al.,* 2009; Doroghazi & Metcalf, 2013; Seshadri *et al.,* 2022), or (ii) convergent evolution of similar biosynthetic solutions driven by shared ecological pressures in marine habitats. Both possibilities are supported in the literature — numerous studies document lateral acquisition and exchange of BGCs (e.g., Doroghazi & Metcalf, 2013; Nett *et al.,* 2009), whereas others emphasise convergent functional outcomes without recent transfer (contrasting examples in McDonald & Currie, 2017).

The metabolomic profile under variable salinity revealed that the production of juvenimicin-like compounds by KRD324 was strongly condition-dependent, with a distinct molecular family detected almost exclusively at 15‰ salinity. This pattern is consistent with previous reports showing that osmotic stress can enhance metabolite yields by marine actinomycetes — for instance, *Salinispora arenicola* M413 doubled rifamycin production at 1% NaCl compared to 3% artificial sea salt (Ng *et al.,* 2014). Additional metabolomic work showed that *Salinispora* grown under different salinities altered not only yield but the whole secondary-metabolite profile (Bose *et al.,* 2015). Soil actinomycetes isolated under higher salinity conditions likewise exhibited significantly increased production of antibacterial compounds compared to those from lower-salinity soils (Basilo *et al.,* 2003). Interestingly, while KRD324 exhibited a sharp decline in metabolite diversity with increasing salinity, this pattern was not consistent across the other strains tested. This strain-specific response highlights the importance of considering both abiotic factors and genomic background when studying secondary metabolism. It also suggests that environmental modulation may act as a strain-targeted trigger of cryptic biosynthetic pathways, rather than as a generalised response across the genus.

Genome sequencing of KRD324 revealed a rosamicin-like PKS cluster, concordant with the concurrent detection of rosamicin and juvenimicin metabolites. The organisation of this BGC resembles rosamicin pathways described in *Micromonospora carbonacea* and *Salinispora pacifica* (Awakawa et al., 2015; Kautsar et al., 2020), suggesting a conserved PKS core with variable tailoring enzymes. Such architectural conservation frequently explains observed chemodiversity: post-PKS tailoring (oxidation, glycosylation, methylation) often generates analogues from a shared backbone (Doroghazi & Metcalf, 2013; Nett *et al.,* 2009). To distinguish HGT from convergence here, targeted analyses are required — for example, phylogenetic reconstruction of KS domains, comparison of flanking mobile elements, and dot-plot synteny analyses. These approaches have been successfully applied to demonstrate HGT of entire antibiotic clusters (e.g., streptomycete rifamycin-related transfers; Belknap *et al.,* 2020; Doroghazi & Metcalf, 2013).

The scale-up of KRD324 cultures corroborated the production of multiple juvenimicins (A2, B1, Sch 23831), alongside at least two uncharacterised analogues. Notably, one of these analogues (582.3627 *m/z*) represented the detected at the highest levels metabolite under the tested conditions, suggesting it could be the main driver of the antibacterial activity. This finding not only validates the potential of KRD324 potential as a source of bioactive macrolides but also illustrates the effectiveness of scaling experiments in prioritising strains for detailed chemical characterisation. Future work should include structural elucidation and bioactivity-guided fractionation to confirm whether these compounds indeed represent new juvenimicin derivatives and to assess their therapeutic or ecological roles.

Together, these results demonstrate how integrating phylogenetics, metabolomics, and genomics can uncover new secondary metabolites in underexplored microbial taxa. Specifically, this study (i) expands the known metabolic repertoire of *Micromonospora* by linking it to metabolites previously thought to be genus-specific to *Salinispora*, (ii) shows that salinity can act as a selective trigger for juvenimicin production, (iii) provides genomic evidence for tailoring-driven diversification of macrolides via a rosamicin-like BGC, and (iv) identifies KRD324 as a candidate producer of new juvenimicin analogues. Beyond its immediate findings, the study illustrates how rare Actinomycetota from contrasting

environments can serve as models to investigate the interplay between environmental cues, genomic plasticity, and chemical innovation.

6 CHAPTER 6. Final discussion and future perspectives.

6.1 Critical reflections

Antimicrobial resistance (AMR) continues to represent one of the greatest challenges to global health (Ahmed *et al.,* 2024). Decades after the discovery of penicillin, the rise of multidrug-resistant pathogens has dramatically reduced the efficacy of existing antibiotics, underscoring the urgent need for new chemical scaffolds with novel modes of action (Jacobowski *et al.,* 2025). In this context, natural product discovery remains one of the most promising avenues for identifying bioactive molecules with therapeutic potential (Mullowney *et al.,* 2023). However, the classical sources — particularly *Streptomyces* — have been extensively mined, and many biosynthetic gene clusters (BGCs) remain silent under laboratory conditions (Sharma *et al.,* 2021). I believe that overcoming this stagnation requires both the exploration of underexplored microbial taxa and the recreation of environmental conditions that trigger the expression of their latent biosynthetic capacity. In this thesis, I aimed to contribute to this broader effort by investigating rare actinomycetes from contrasting and underexplored environments and assessing how environmental parameters influence their metabolomic profiles. By integrating genomic and metabolomic analyses, I sought to reveal the hidden chemical diversity in these bacteria and identify potential metabolites with biological relevance. In this way, my work contributes to antibiotic discovery through a new perspective by showing that ecology can be a powerful driver of metabolic diversification.

The concept underlying my approach aligns with the principles of the One Strain–Many Compounds (OSMAC) strategy, which posits that varying culture conditions can activate different biosynthetic pathways within the same organism. Although my focus was not strictly OSMAC-driven, the controlled manipulation of abiotic factors such as temperature and salinity reflect a similar rationale — modifying environmental cues to mimic natural

stressors and stimulate otherwise silent metabolic pathways. Some previous studies using nickel as environmental perturbations for instance, induced the biosynthesis of the new antibiotics estremycins A and B in *Streptomyces pratensis* NA-ZhouS1 (Akhter, 2018), while a similar approach was used for *Vibrio* spp., under elevated salinity and resulted in an increase in prodigiosin, a bioactive pigment metabolite (Gallardo *et al.,* 2016). One of the main methodological challenges at the beginning of this work was ensuring that the metabolomic variations observed truly reflected the influence of abiotic parameter across strains, rather than differences in physiological state. One critical step and the first objective of the thesis was to normalise growth to enable this comparison to be achieved. It is well established that bacterial metabolism varies markedly across growth phases (Moreno & Rojo, 2022), with secondary metabolites typically accumulating during the stationary phase as part of stress or nutrient-limitation responses. This was detected studying *Streptomyces coelicolor,* where the biosynthesis of metabolites such as albaflavenone and actinorhodin appeared only after 48 h (sporulation/stationary phase) (Čihák *et al.,* 2017), or in a general study of three environmental bacteria (*Burkholderiathailandensis* E264, *Chromobacterium violaceum* ATCC 31532, and *Pseudomona ssyringae pv.tomat*o DC3000), where it was found that most of the metabolites released varied with the strain, but that in general there was metabolic redirection to a metabolite accumulation in the stationary phase. Therefore, I selected the stationary phase for metabolite extraction to capture the highest diversity of bioactive compounds and to minimise growth-related variability.

Growth conditions were standardised for all *Rhodococcus* strains based on optical density, ensuring that metabolite extraction occurred at comparable physiological stages. This standardisation was crucial to confirm that temperature was the only variable influencing metabolite production, allowing for a more accurate interpretation of the observed changes in metabolic profiles. Under these controlled conditions, *Rhodococcus* KRD197 displayed clear temperature-dependent metabolomic changes. Several fatty acid derivatives with potential bioactivity were detected exclusively at 20 °C, suggesting that lower temperatures could activate specific lipid-associated biosynthetic pathways that remain inactive under standard culture conditions.

In contrast, the standardisation process for *Micromonospora* proved more challenging. Only a subset of the isolated strains grew consistently in liquid culture, requiring adaptation to solid media and extended incubation periods. Therefore, a 21-day growth period was adopted as a reference, although this limitation prevented complete physiological standardisation across conditions. Despite these constraints, *Micromonospora* KRD324 displayed a distinct metabolomic profile at varying salinities, with molecular features consistent with the production of rosamicin-like macrolides, including potential juvenimicin analogues. Interestingly, these metabolites were biosynthesised almost exclusively at 15‰ salinity. This observation was particularly revealing when considered in the context of the strain's natural habitat — the Ojo de Liebre Lagoon — where salinity fluctuates seasonally and geographically between approximately 35‰ and 39‰ due to evaporation and tidal exchange (Aguila Ramírez *et al.*, 2003). This suggests that the environmental conditions under which the strain naturally thrives may not favour the active production of these macrolides. Instead, the 15‰ condition appears to represent a suboptimal, low-stress environment that temporarily releases metabolic constraints, allowing secondary metabolism to proceed. In highly saline habitats, much of the cellular energy is likely channeled into osmotic balance and maintenance of macromolecular stability, limiting the energetic availability for complex biosynthetic pathways (Schink *et al.,* 2021).

This interpretation supports the idea that metabolite induction is not necessarily maximised under native or extreme environmental conditions but may emerge under transitional or stress-relief states. A similar phenomenon has been reported in other microorganisms, such as *Escherichia coli*, where moderate stress induces (p)ppGpp-mediated metabolic reallocation, balancing growth and adaptation (Zhu *et al.,* 2024). In this sense, the 15‰ condition may represent an artificial "window of opportunity" for *Micromonospora* KRD324 — one that unmasks cryptic biosynthetic potential otherwise repressed under its natural osmotic regime. While members of this genus are known to produce antimicrobial metabolites (Hifnawy *et al.,* 2020), the salinity-dependent activation observed here may reflect a latent ecological capacity that is not expressed *in situ*. However, confirming this hypothesis would require analyses across a broader set of *Micromonospora* strains and environmental gradients to determine whether this represents a strain-specific response or a wider adaptive trend within the genus.

6.2 Future perspectives

The primary objective of this work was to evaluate how environmental parameters influence secondary metabolism in rare marine actinomycetes. While this goal was achieved, the experimental design allowed for the assessment of only a single variable per genus — temperature for *Rhodococcus* and salinity for *Micromonospora*. Nevertheless, the results provided clear evidence that even subtle changes in abiotic conditions can markedly reshape metabolomic profiles. Future studies should therefore explore the combined effects of multiple environmental stressors to more closely approximate the complexity of natural habitats.

The next logical step would be to implement multifactorial experimental designs that simultaneously vary parameters such as temperature, salinity, and pH, while also testing the role of trace metals as biosynthetic cofactors. Such approaches would make it possible to detect interactive effects (e.g., temperature × salinity) and identify optimal “ecological windows” for metabolite induction. Similar multifactorial strategies have already proven successful in microbial secondary metabolism research. For instance, simultaneous variation of temperature and salinity in marine microbial communities revealed distinct metabolomic shifts associated with osmoadaptation and stress-response pathways (Dawson *et al.,* 2023). Likewise, controlled chemostat studies with *Streptomyces* demonstrated that concurrent adjustments of temperature and pH significantly influence both growth rate and antibiotic production profiles (James *et al.,* 1991). Additionally, factorial and response-surface optimisation methods combining salinity, pH, and nutrient composition have enhanced secondary metabolite yields in *Streptomyces* and related Actinomycetota, confirming that environmental factors interact synergistically to modulate biosynthetic output (Ahsan *et al.,* 2017; Yun *et al.,* 2018).

Another promising parameter to investigate is hydrostatic pressure, particularly relevant for marine or deep-sediment isolates. Although technically demanding, recent advances in pressurised bioreactor and isobaric culture systems now allow the simulation of oceanic pressures up to several hundred bars. For example, *Thermococcus aciditolerans* exhibited adaptive metabolic responses when cultured under high-pressure conditions (Jiao *et al.,* 2025), while studies on the deep-sea bacterium *Shewanella eurypsychrophilus* YLB-09 demonstrated pressure-induced modulation of metabolite

profiles (Qiu & Tang, 2023). Incorporating pressure as an experimental variable could therefore provide valuable insights into how microbial metabolism adapts to depth-related stress and might reveal unique metabolites linked to these extreme conditions. In summary, applying multifactorial and environmentally realistic approaches will enable a more comprehensive understanding of microbial adaptation and secondary metabolism. By recreating ecological complexity in the laboratory, future work can uncover novel metabolites that remain silent under single-variable perturbations, further bridging the gap between environmental microbiology and natural product discovery.

A practical improvement to the current experimental setup would be to transition from Erlenmeyer flask cultures to microtiter plates for high-throughput growth curves and metabolite monitoring. Microplate-based approaches allow simultaneous testing of multiple conditions, reducing culture volume, and increasing experimental efficiency. For example, studies on *Streptomyces* and other Actinomycetota have successfully used 24- and 96-well plate formats to generate precise growth curves, assess nutrient effects, and screen for secondary metabolite production under diverse environmental conditions (Minas *et al.,* 2000; Liu *et al.,* 2023). Applying this strategy to *Rhodococcus* and *Micromonospora* would not only streamline data collection but also facilitate systematic investigation of combinatorial stressors and enable correlations between growth dynamics and metabolomic profiles.

Finally, one clear step should be the integration of transcriptomic analyses to uncover the regulatory mechanisms linking environmental stress to secondary metabolism. In *Rhodococcus jostii* RHA1, one of the few microorganisms whose global response to desiccation stress has been analyzed, microarray-based transcriptomic profiling revealed extensive transcriptional reprogramming, with 380 up-regulated and 371 down-regulated genes under low relative humidity (LeBlanc *et al.,* 2008). These included regulators and genes involved in lipid metabolism, cell envelope modification, and DNA repair, illustrating how environmental stress can trigger complex regulatory networks. Similarly, Amos, *et al*. (2017) demonstrated in *Salinispora* that transcriptomic profiling across different growth stages can explain temporal patterns of metabolite production, bioinformatically linking BGCs identified to biosynthetic output (Amos *et al.,* 2017). Extending such analyses to *Rhodococcus* and *Micromonospora* could clarify how temperature or salinity stress

modulates biosynthetic gene expression, identify previously silent pathways, and guide the rational design of culture conditions to enhance metabolite discovery. Moreover, transcriptomics can be combined with metabolomics to establish mechanistic connections between gene expression, growth dynamics, and secondary metabolite accumulation, providing a more comprehensive picture of microbial adaptation.

6.3 Conclusions

In summary, this work confirmed that environmental parameters such as temperature and salinity can markedly influence the secondary metabolism of rare marine actinomycetes, supporting the initial hypothesis that abiotic factors modulate metabolomic expression. By standardising growth conditions to isolate the effect of temperature, I demonstrated that *Rhodococcus* KRD197 exhibited distinct metabolomic profiles across temperatures, with several fatty acid derivatives of putative bioactive potential detected exclusively at 20 °C. Similarly, *Micromonospora* KRD324 responded to variations in salinity by producing rosamicin-like macrolides, including potential juvenimicin analogues, which were biosynthesised almost exclusively at 15‰ salinity. These findings suggest that moderate environmental stress — rather than extreme conditions — can act as a regulatory signal for activating secondary metabolism in marine actinomycetes.

Beyond these specific outcomes, these results highlight the ecological relevance of environmental modulation in shaping microbial chemical diversity. The study reinforces the importance of exploring underrepresented taxa and environmental gradients to uncover new natural products and highlights the power of a combined metabologenomics approach to compare strains. Overall, this work provides a foundation for future investigations into how multifactorial environmental pressures — such as temperature, salinity, and metal availability — jointly influence biosynthetic pathways, offering new directions for natural product discovery from rare actinomycetes.

Bibliography

1. Abdel-Razek AS, El-Naggar ME, Allam A, Morsy OM, Othman SI. Microbial natural products in drug discovery. *Processes*. 2020;8(4):470. doi: 10.3390/pr8040470.
2. Abdi G, Tarighat MA, Jain M, Tendulkar R, Tendulkar M, Barwant M. Revolutionizing genomics: exploring the potential of next-generation sequencing. In: Singh V, Kumar A, editors. *Advances in Bioinformatics*. Singapore: Springer; 2024. p. 1–25. doi: 10.1007/978-981-99-8401-5_1.
3. Abraham EP, Chain E. An enzyme from bacteria able to destroy penicillin. *Rev Infect Dis*. 1988;10(4):677–8. (Reprinted from *Nature*. 1940).
4. Adamek M, Alanjary M, Sales-Ortells H, et al. Comparative genomics reveals phylogenetic distribution patterns of secondary metabolites in *Amycolatopsis* species. *BMC Genomics*. 2018;19:426. doi:10.1186/s12864-018-4809-4.
5. Adnani N, Chevrette MG, Adibhatla SN, Zhang F, Yu Q, Braun DR, et al. Coculture of marine invertebrate-associated bacteria and interdisciplinary technologies enable biosynthesis and discovery of a new antibiotic, Keyicin. *ACS Chem Biol*. 2017;12(12):3093–102. doi:10.1021/acschembio.7b00688.
6. Agarwal H, Bajpai S, Mishra A, Kohli I, Varma A, Fouillaud M, et al. Bacterial pigments and their multifaceted roles in contemporary biotechnology and pharmacological applications. *Microorganisms.* 2023;11(3):614. doi: 10.3390/microorganisms11030614. PMID: 36985186; PMCID: PMC10053885.
7. Aguila Ramírez RN, Casas Valdez M, Ortega García S, et al. Spatial and seasonal variation of macroalgal biomass in Laguna Ojo de Liebre, Baja California Sur, Mexico. *Hydrobiologia*. 2003;501:207–214. doi: 10.1023/A:1026210312362.
8. Ahmad N, Joji RM, Kumar V, Pagani L, Shahid M. Editorial: Evolution, molecular mechanisms and the strategies to combat antimicrobial resistance (AMR): a One Health approach. *Front Cell Infect Microbiol*. 2025 Jun 2;15:1582613. doi: 10.3389/fcimb.2025.1582613. PMID: 40529308; PMCID: PMC12171209.
9. Ahmed L, Jensen PR, Freel KC, Brown R, Jones AL, et al. *Salinispora pacifica* sp. nov., an actinomycete from marine sediments. *Antonie Van Leeuwenhoek*. 2013;103:1069–78. doi:10.1007/s10482-013-9884-6.

10. Ahmed SK, Hussein S, Qurbani K, Ibrahim RH, Fareeq A, Mahmood KA, Mohamed MG. Antimicrobial resistance: impacts, challenges, and future prospects. *J Med Surg Public Health*. 2024;2:100081. doi:10.1016/j.glmedi.2024.100081.
11. Ahsan T, Chen J, Wu Y, Irfan M, Shafiq M, Lin S, et al. Application of response surface methodology for optimization of medium components for the production of secondary metabolites by *Streptomyces diastatochromogenes* KX852460. *AMB Expr*. 2017;7:96. doi: 10.1186/s13568-017-0388-z.
12. Akhter N, Liu Y, Auckloo BN, Shi Y, Wang K, Chen J, et al. Stress-driven discovery of new angucycline-type antibiotics from a marine *Streptomyces pratensis* NA-ZhouS1. *Mar Drugs*. 2018;16(9):331. doi:10.3390/md16090331. PMID:30213076; PMCID:PMC6163593.
13. Alam K, Mazumder A, Sikdar S, Zhao YM, Hao J, Song C, et al. Streptomyces: The biofactory of secondary metabolites. *Front Microbiol*. 2022;13:968053. doi:10.3389/fmicb.2022.968053.
14. Alam K, Mazumder A, Sikdar S, Zhao YM, Hao J, Song C, et al. *Streptomyces*: The biofactory of secondary metabolites. *Front Microbiol*. 2022;13:968053. doi: 10.3389/fmicb.2022.968053.
15. Alanjary M, Steinke K, Ziemert N. AutoMLST: an automated web server for generating multi-locus species trees highlighting natural product potential. *Nucleic Acids Res*. 2019;47(W1):W276–82. doi:10.1093/nar/gkz282.
16. Alarcon-Barrera JC, Kostidis S, Ondo-Mendez A, Giera M. Recent advances in metabolomics analysis for early drug development. *Drug Discov Today.* 2022 Jun;27(6):1763–73. doi:10.1016/j.drudis.2022.02.018. PMID: 35218927.
17. Alas I, Braun DR, Ericksen SS, Salamzade R, Kalan L, Rajski SR, Bugni TS. Micromonosporaceae biosynthetic gene cluster diversity highlights the need for broad-spectrum investigations. *Microb Genom*. 2024;10(1):001167. doi:10.1099/mgen.0.001167. PMID:38175683; PMCID:PMC10868606.
18. Alas I, Braun DR, Ericksen SS, Salamzade R, Kalan L, Rajski SR, Bugni TS. Micromonosporaceae biosynthetic gene cluster diversity highlights the need for broad-spectrum investigations. *Microb Genom.* 2024;10(1):001167. doi:10.1099/mgen.0.001167.
19. Allen F, Pon A, Wilson M, Greiner R, Wishart D. CFM-ID: a web server for annotation, spectrum prediction and metabolite identification from tandem mass

spectra. *Nucleic Acids Res.* 2014 Jul;42(Web Server issue):W94–9. doi:10.1093/nar/gku436. PMID: 24895432; PMCID: PMC4086103.

20. Amos GCA, Awakawa T, Tuttle RN, Letzel AC, Kim MC, Kudo Y, et al. Comparative transcriptomics as a guide to natural product discovery and biosynthetic gene cluster functionality. *Proc Natl Acad Sci U S A*. 2017 Dec 26;114(52):E11121-E11130. doi: 10.1073/pnas.1714381115. PMID: 29229817; PMCID: PMC5748202.
21. Van der Geize R, Dijkhuizen L. Harnessing the catabolic diversity of *Rhodococcus* for environmental and biotechnological applications. Microbiology. 2004;7(3):255–61.
22. Anand S, Prasad MV, Yadav G, Kumar N, Shehara J, Ansari MZ, Mohanty D. SBSPKS: structure-based sequence analysis of polyketide synthases. *Nucleic Acids Res*. 2010;38(Web Server issue):W487–96. doi:10.1093/nar/gkq340.
23. Andersen NM, Poehlsgaard J, Warrass R, Douthwaite S. Inhibition of protein synthesis on the ribosome by tildipirosin compared with other veterinary macrolides. *Antimicrob Agents Chemother.* 2012;56(11):6033–6. doi:10.1128/AAC.01250-12.
24. Arnison PG, Bibb MJ, Bierbaum G, Bowers AA, Bugni TS, Bulaj G, et al. Ribosomally synthesized and post-translationally modified peptide natural products: overview and recommendations for a universal nomenclature. *Nat Prod Rep*. 2013;30(1):108–60. doi:10.1039/c2np20085f.
25. Aslam SN, Cresswell-Maynard T, Thomas DN, Underwood GJC. Production and characterization of the Intra- and Extracellular Carbohydrates and Polymeric Substances (EPS) of three sea-ice diatom species, and evidence for a cryoprotective role for EPS. J Phycol. 2012;48:1494–1509. doi: 10.1111/jpy.12004.
26. Aston, F. W. (1920). Isotopes and atomic weights. In: Nature Publishing Group UK London.
27. Auch AF, von Jan M, Klenk HP, Göker M. Digital DNA-DNA hybridization for microbial species delineation by means of genome-to-genome sequence comparison. *Stand Genomic Sci*. 2010 Jan 28;2(1):117-34. doi: 10.4056/sigs.531120. PMID: 21304684; PMCID: PMC3035253.

28. Awakawa T, Crüsemann M, Munguia J, Ziemert N, Nizet V, Fenical W, et al. Salinipyrone and Pacificanone are biosynthetic by-products of the rosamicin polyketide synthase. *Chembiochem.* 2015;16(10):1443–7. doi:10.1002/cbic.201500177.
29. Bachmann BO, Van Lanen SG, Baltz RH. Microbial genome mining for accelerated natural products discovery: is a renaissance in the making? *J Ind Microbiol Biotechnol*. 2014;41(2):175–84. doi:10.1007/s10295-013-1389-9.
30. Bagger FO, Borgwardt L, Jespersen AS, Hansen AR, Bertelsen B, Kodama M, Nielsen FC. Whole genome sequencing in clinical practice. *BMC Med Genomics*. 2024;17(1):39. doi:10.1186/s12920-024-01795-w. PMID:38287327; PMCID:PMC10823711.
31. Balleux G, Höfte M, Arguelles-Arias A, Deleu M, Ongena M. *Bacillus* lipopeptides as key players in rhizosphere chemical ecology. *Trends Microbiol.* 2025;33(1):80–95. doi: 10.1016/j.tim.2024.08.001. PMID: 39214821.
32. Balouiri M, Sadiki M, Ibnsouda SK. Methods for in vitro evaluating antimicrobial activity: A review. *J Pharm Anal*. 2016;6(2):71–9. doi:10.1016/j.jpha.2015.11.005.
33. Baltz RH. Natural product drug discovery in the genomic era: realities, conjectures, misconceptions, and opportunities. *J Ind Microbiol Biotechnol*. 2019;46(3–4):281–99. doi:10.1007/s10295-018-2115-4.
34. Banić Tomišić Z. The story of azithromycin. *Kemija u industriji*. 2011;60(12):603–617. Disponible en: https://hrcak.srce.hr/74687
35. Barka EA, Vatsa P, Sanchez L, Gaveau-Vaillant N, Jacquard C, Meier-Kolthoff JP, et al. Correction for Barka et al., Taxonomy, Physiology, and Natural Products of Actinobacteria. *Microbiol Mol Biol Rev*. 2016;80(4):iii. doi:10.1128/MMBR.00044-16.
36. Baron S, editor. *Medical Microbiology*. 4th ed. Galveston: The University of Texas Medical Branch at Galveston; 1996.
37. Basilio A, González I, Vicente MF, Gorrochategui J, Cabello A, González A, Genilloud O. Patterns of antimicrobial activities from soil actinomycetes isolated under different conditions of pH and salinity. *J Appl Microbiol*. 2003;95(4):814-23. doi:10.1046/j.1365-2672.2003.02049.x. PMID:12969296.
38. Becerril-Espinosa A, Freel KC, Jensen PR, Soria-Mercado IE. Marine actinobacteria from the Gulf of California: diversity, abundance and secondary

metabolite biosynthetic potential. *Antonie Van Leeuwenhoek*. 2013;103(4):809–19. doi:10.1007/s10482-012-9861-2.

39. Belknap KC, Park CJ, Barth BM, Andam CP. Genome mining of biosynthetic and chemotherapeutic gene clusters in Streptomyces bacteria. *Sci Rep*. 2020 Feb 6;10(1):2003. doi: 10.1038/s41598-020-58904-9. PMID: 32029878; PMCID: PMC7005152.
40. Benhadj M, Gacemi-Kirane D, Menasria T, Guebla K, Ahmane Z. Screening of rare actinomycetes isolated from natural wetland ecosystem (Fetzara Lake, northeastern Algeria) for hydrolytic enzymes and antimicrobial activities. *J King Saud Univ Sci*. 2019;31(4):706–12. doi: 10.1016/j.jksus.2018.03.008.
41. Bérdy J. Thoughts and facts about antibiotics: where we are now and where we are heading. *J Antibiot (Tokyo)*. 2012;65(8):385–95. doi: 10.1038/ja.2012.27.
42. Bertani G. Studies on lysogenesis. I. The mode of phage liberation by lysogenic *Escherichia coli*. *J Bacteriol*. 1951;62(3):293–300. doi:10.1128/jb.62.3.293-300.1951.
43. Bibb MJ. Regulation of secondary metabolism in streptomycetes. *Curr Opin Microbiol*. 2005;8(2):208–15. doi:10.1016/j.mib.2005.02.016.
44. Blin K, Shaw S, Augustijn HE, Reitz ZL, Biermann F, Alanjary M, et al. antiSMASH 7.0: new and improved predictions for detection, regulation, chemical structures, and visualisation. *Nucleic Acids Res*. 2023;51(W1):W46–51. doi:10.1093/nar/gkad344.
45. Blin K, Shaw S, Kloosterman AM, Charlop-Powers Z, van Wezel GP, Medema MH, Weber T. antiSMASH 6.0: improving cluster detection and comparison capabilities. *Nucleic Acids Res*. 2021;49(W1):W29–35. doi:10.1093/nar/gkab335.
46. Blin K, Shaw S, Vader L, Szenei J, Reitz ZL, Augustijn HE, et al. antiSMASH 8.0: extended gene cluster detection capabilities and analyses of chemistry, enzymology, and regulation. *Nucleic Acids Res*. 2025;53(W1):W32–8. doi:10.1093/nar/gkaf334.
47. Blin K, Shaw S, Vader L, Szenei J, Reitz ZL, Augustijn HE, et al. antiSMASH 8.0: capacidades extendidas de detección de grupos de genes y análisis de química, enzimología y regulación. Nucleic Acids Res. 2025;53(W1):W32–W38.

48. Böcker S, Letzel MC, Lipták Z, Pervukhin A. SIRIUS: decomposing isotope patterns for metabolite identification. *Bioinformatics.* 2009 Jan 15;25(2):218–24. doi:10.1093/bioinformatics/btn603. PMID: 19015140; PMCID: PMC2639009.
49. Bogaerts B, Van den Bossche A, Verhaegen B, Delbrassinne L, Mattheus W, Nouws S, et al. Closing the gap: Oxford Nanopore Technologies R10 sequencing allows comparable results to Illumina sequencing for SNP-based outbreak investigation of bacterial pathogens. *J Clin Microbiol*. 2024 May 8;62(5):e0157623. doi: 10.1128/jcm.01576-23. Epub 2024 Mar 5. PMID: 38441926; PMCID: PMC11077942.
50. Bogdanov A, Salib MN, Chase AB, Hammerlindl H, Muskat MN, et al. Small-molecule in situ resin capture provides a compound-first approach to natural product discovery. *Nat Commun.* 2024;15:5230. doi:10.1038/s41467-024-45230-4.
51. Bogdanov A, Salib MN, Chase AB, Hammerlindl H, Muskat MN, Luedtke S, et al. Small molecule in situ resin capture – a compound-first approach to natural product discovery. *bioRxiv* [Preprint]. 2023 May 30:2023.03.02.530684. doi:10.1101/2023.03.02.530684. Update in: *Nat Commun.* 2024 Jun 19;15(1):5230. doi:10.1038/s41467-024-49367-x. PMID: 37398257; PMCID: PMC10312467.
52. Bonifaz-Trujillo J. General properties of actinomycetes. In: *Basic Medical Mycology*. 5th ed. New York: McGraw Hill; 2015. Available from: https://accessmedicina.mhmedical.com/content.aspx?bookid=1529&sectionid=98865575.
53. Bose U, Hewavitharana AK, Ng YK, Shaw PN, Fuerst JA, Hodson MP. LC-MS-based metabolomics study of marine bacterial secondary metabolite and antibiotic production in *Salinispora arenicola*. *Mar Drugs*. 2015;13(1):249–66. doi:10.3390/md13010249.
54. Bose U, Hewavitharana AK, Ng YK, Shaw PN, Fuerst JA, Hodson MP. LC-MS-based metabolomics study of marine bacterial secondary metabolite and antibiotic production in *Salinispora arenicola*. *Mar Drugs*. 2015;13(1):249-66. doi:10.3390/md13010249. PMID:25574739; PMCID:PMC4306935.
55. Bosello M, Robbel L, Linne U, Xie X, Marahiel MA. Biosynthesis of the siderophore rhodochelin requires the coordinated expression of three independent gene

clusters in *Rhodococcus jostii* RHA1. *J Am Chem Soc*. 2011;133:4587–4595. doi:10.1021/ja1109453.

56. Bosello M, Zeyadi M, Kraas FI, Linne U, Xie X, et al. Structural characterization of the heterobactin siderophores from *Rhodococcus erythropolis* PR4 and elucidation of their biosynthetic machinery. *J Nat Prod*. 2013;76:2282–2290. doi:10.1021/np4006579.
57. Bosello M. Structural characterization of the siderophore rhodochelin from *Rhodococcus jostii* RHA1 and elucidation of its biosynthetic machinery [dissertation]. Marburg: Philipps-Universität Marburg; 2012. doi:10.17192/z2012.0767.
58. Bredholdt H, Galatenko OA, Engelhardt K, Fjærvik E, Terekhova LP, Zotchev SB. Rare actinomycete bacteria from the shallow water sediments of the Trondheim fjord, Norway: isolation, diversity and biological activity. *Environ Microbiol*. 2007;9(11):2756. doi:10.1111/j.1462-2920.2007.01387.x.
59. Caicedo-Montoya C, Manzo-Ruiz M, Ríos-Estepa R. Pan-genome of the genus *Streptomyces* and prioritization of biosynthetic gene clusters with potential to produce antibiotic compounds. Front Microbiol. 2021;12:677558.
60. Camponovo CR, García CP. *Rhodococcus equi*. Rev Chil Infectol. 2006;23(2):155–6.
61. Cappelletti M, Presentato A, Piacenza E, et al. Biotechnology of *Rhodococcus* for the production of valuable compounds. Appl Microbiol Biotechnol. 2020;104:8567–94.
62. Cappelletti M, Presentato A, Piacenza E, Firrincieli A, Turner RJ, Zannoni D. Biotechnology of *Rhodococcus* for the production of valuable compounds. *Appl Microbiol Biotechnol.* 2020 Oct;104(20):8567–94. doi:10.1007/s00253-020-10861-z. PMID: 32918579; PMCID: PMC7502451.
63. Carlson S, Marler L, Nam SJ, Santarsiero BD, Pezzuto JM, Murphy BT. Potential chemopreventive activity of a new macrolide antibiotic from a marine-derived Micromonospora sp. *Mar Drugs.* 2013;11(4):1152–61. doi:10.3390/md11041152.
64. Carro L, Golińska P, Saati-Santamaría Z, Igual JM, Klenk HP, Goodfellow M. Atacama desert is a source of new *Micromonospora* strains: description of

Micromonospora sicca sp. nov. *Syst Appl Microbiol*. 2024;47(5):126542. doi:10.1016/j.syapm.2024.126542.

65. Casillas-Vargas G, Ocasio-Malavé C, Medina S, Morales-Guzmán C, Del Valle RG, et al. Antibacterial fatty acids: an update of possible mechanisms of action and implications in the development of the next-generation of antibacterial agents. Prog Lipid Res. 2021;82:101093. doi: 10.1016/j.plipres.2021.101093.
66. Cawoy H, Debois D, Franzil L, De Pauw E, Thonart P, Ongena M. Lipopeptides as main ingredients for inhibition of fungal phytopathogens by *Bacillus subtilis*/*amyloliquefaciens*. *Microb Biotechnol*. 2015;8(2):281–95. doi:10.1111/1751-7915.12238.
67. Chambers MC, Maclean B, Burke R, Amodei D, Ruderman DL, Neumann S, et al. A cross-platform toolkit for mass spectrometry and proteomics. *Nat Biotechnol*. 2012;30(10):918–20. doi:10.1038/nbt.2377.
68. Charlop-Powers Z, Owen JG, Reddy BVB, Ternei MA, Guimarães DO, de Frias UA, et al. Global biogeographic sampling of bacterial secondary metabolism. *eLife*. 2015;4:e05048.
69. Chater KF, Losick R. Mycelial life style of *Streptomyces coelicolor* A3(2) and its relatives. In: Shapiro JA, Dworkin M, editors. *Bacteria as Multicellular Organisms*. New York: Oxford University Press; 1997. p. 149–82.
70. Chebotar I, Kuleshov K, Bocharova J, Mayanskiy N. Experimental evolution of cefiderocol resistance in *Pseudomonas aeruginosa*. *Heliyon*. 2025;11(13):e43681. doi:10.1016/j.heliyon.2025.e43681.
71. Cheema MT, Ponomareva LV, Liu T, Voss SR, Thorson JS, Shaaban KA, Sajid I. Taxonomic and metabolomics profiling of Actinobacteria strains from Himalayan collection sites in Pakistan. *Curr Microbiol.* 2021 Aug;78(8):3044–57. doi:10.1007/s00284-021-02557-y. PMID: 34125273; PMCID: PMC10716794.
72. Chen H, Cui J, Wang P, Wang X, Wen J. Enhancement of bleomycin production in *Streptomyces verticillus* through global metabolic regulation of N-acetylglucosamine and assisted metabolic profiling analysis. *Microb Cell Fact*. 2020;19(1):32. doi:10.1186/s12934-020-01301-8.
73. Chen YJ, Takahashi CN, Organick L, et al. Quantifying molecular bias in DNA data storage. *Nat Commun*. 2020;11:3264. doi:10.1038/s41467-020-16958-3.

74. Chevrette MG, Gutiérrez-García K, Selem-Mojica N, Aguilar-Martínez C, Yañez-Olvera A, Ramos-Aboites HE, et al. Evolutionary dynamics of natural product biosynthesis in bacteria. *Nat Prod Rep.* 2020;37(4):566–599. doi:10.1039/c9np00048h.
75. Chevrette MG, Handelsman J. Needles in haystacks: reevaluating old paradigms for the discovery of bacterial secondary metabolites. *Nat Prod Rep*. 2021;38(11):2083–99.
76. Chhalodia AK, Xu H, Tabekoueng GB, Gu B, Taizoumbe KA, Lauterbach L, et al. Functional characterisation of twelve terpene synthases from actinobacteria. *Beilstein J Org Chem*. 2023;19:1386–98. doi:10.3762/bjoc.19.100.
77. Chiba H, Agematu H, Kaneto R, Terasawa T, Sakai K, Dobashi K, Yoshioka T. Rhodopeptins (Mer-N1033), novel cyclic tetrapeptides with antifungal activity from *Rhodococcus* sp. I. Taxonomy, fermentation, isolation, physico-chemical properties and biological activities. *J Antibiot (Tokyo).* 1999 Aug;52(8):695–9. doi:10.7164/antibiotics.52.695. PMID: 10580382.
78. Christianson DW. Structural and chemical biology of terpenoid cyclases. *Chem Rev.* 2017;117(17):11570–648. doi: 10.1021/acs.chemrev.7b00287. Erratum in: *Chem Rev.* 2018;118(24):11795. PMID: 28841019; PMCID: PMC5599884.
79. Chu J, Vila-Farres X, Inoyama D, Ternei M, Cohen LJ, Gordon EA, et al. Discovery of MRSA active antibiotics using primary sequence from the human microbiome. *Nat Chem Biol.* 2016 Dec;12(12):1004–6. doi:10.1038/nchembio.2207. PMID: 27748750; PMCID: PMC5117632.
80. Chun J, Oren A, Ventosa A, Christensen H, Arahal DR, da Costa MS, et al. Proposed minimal standards for the use of genome data for the taxonomy of prokaryotes. *Int J Syst Evol Microbiol*. 2018 Jan;68(1):461–6. doi: 10.1099/ijsem.0.002516. PMID: 29292687.
81. Chun J, Oren A, Ventosa A, Christensen H, Arahal DR, da Costa MS, et al. Proposed minimal standards for the use of genome data for the taxonomy of prokaryotes. *Int J Syst Evol Microbiol*. 2018;68:461–6. doi:10.1099/ijsem.0.002516.
82. Chun J, Oren A, Ventosa A, Christensen H, Arahal DR, da Costa MS, et al. Proposed minimal standards for the use of genome data for the taxonomy of prokaryotes. *Int J Syst Evol Microbiol*. 2018;68:461–466.

83. Church DL, Cerutti L, Gürtler A, Griener T, Zelazny A, Emler S. Performance and application of 16S rRNA gene cycle sequencing for routine identification of bacteria in the clinical microbiology laboratory. *Clin Microbiol Rev*. 2020;33(4):e00053-19. doi: 10.1128/cmr.00053-19.
84. Ciapina EMP, Melo WC, Santa Anna LMM, et al. Biosurfactant production by *Rhodococcus erythropolis* grown on glycerol as sole carbon source. Appl Biochem Biotechnol. 2006;131:880–6.
85. Čihák M, Kameník Z, Šmídová K, Bergman N, Benada O, Kofroňová O, et al. Secondary metabolites produced during the germination of *Streptomyces coelicolor*. *Front Microbiol*. 2017 Dec 13;8:2495. doi: 10.3389/fmicb.2017.02495. PMID: 29326665; PMCID: PMC5733532.
86. Cimermancic P, Medema MH, Claesen J, Kurita K, Wieland Brown LC, Mavrommatis K, et al. Insights into secondary metabolism from a global analysis of prokaryotic biosynthetic gene clusters. *Cell.* 2014 Jul 17;158(2):412–21. doi:10.1016/j.cell.2014.06.034. PMID: 25036635; PMCID: PMC4123684.
87. Cinco M, Padovan D, Stinco G, Trevisan G. In vitro activity of rokitamycin, a new macrolide, against Borrelia burgdorferi. *Antimicrob Agents Chemother.* 1995;39(5):1185–6. doi:10.1128/AAC.39.5.1185.
88. Clardy J, Fischbach MA, Currie CR. The natural history of antibiotics. *Curr Biol*. 2009;19(11):R437–41.
89. Claverías FP, Undabarrena A, González M, Seeger M, Cámara B. Culturable diversity and antimicrobial activity of actinobacteria from marine sediments in Valparaíso bay, Chile. *Front Microbiol*. 2015;6:737. doi:10.3389/fmicb.2015.00737.
90. Claydon MA, Davey SN, Edwards-Jones V, Gordon DB. The rapid identification of intact microorganisms using mass spectrometry. *Nat Biotechnol.* 1996 Nov;14(11):1584–6. doi:10.1038/nbt1196-1584.
91. Clish CB. Metabolomics: an emerging but powerful tool for precision medicine. *Cold Spring Harb Mol Case Stud.* 2015;1(1):a000588. doi:10.1101/mcs.a000588.
92. Collins JA, Osheroff N. Gyrase and Topoisomerase IV: recycling old targets for new antibacterials to combat fluoroquinolone resistance. *ACS Infect Dis*. 2024;10(4):1097–1115. doi: 10.1021/acsinfecdis.4c00128.

93. Conville PS, Witebsky FG. Nocardia, Rhodococcus, Gordonia, Actinomadura, Streptomyces, and other aerobic actinomycetes. In: *Manual of Clinical Microbiology*. Washington (DC): ASM Press; 2015. doi:10.1128/9781555816728.ch27.
94. Coombs JT, Franco CM. Isolation and identification of actinobacteria from surface-sterilized wheat roots. *Appl Environ Microbiol.* 2003;69(9):5603–8. doi:10.1128/AEM.69.9.5603-5608.2003.
95. Covington BC, Xu F, Seyedsayamdost MR. A natural product chemist's guide to unlocking silent biosynthetic gene clusters. *Annu Rev Biochem*. 2021;90:763-88. doi:10.1146/annurev-biochem-081420-102432. PMID:33848426; PMCID:PMC9148385.
96. Danecek P, Bonfield JK, Liddle J, Marshall J, Ohan V, Pollard MO, et al. Twelve years of SAMtools and BCFtools. *Gigascience*. 2021;10(2):giab008. doi:10.1093/gigascience/giab008.
97. Danecek P, Bonfield JK, Liddle J, Marshall J, Ohan V, Pollard MO, et al. Twelve years of SAMtools and BCFtools. *Gigascience*. 2021;10(2):giab008. doi:10.1093/gigascience/giab008.
98. Daniels T, So T. Fidaxomicin for the treatment of *Clostridium difficile* infection in the pediatric population - not quite so soon yet. *Gastroenterology Research*. 2011;4:1–5.
99. Dawson HM, Connors E, Erazo NG, et al. Microbial metabolomic responses to changes in temperature and salinity along the western Antarctic Peninsula. *ISME J.* 2023;17:2035–46. doi:10.1038/s41396-023-01475-0.
100. Dawson HM, Connors E, Erazo NG, Sacks JS, Mierzejewski V, Rundell SM, et al. Microbial metabolomic responses to changes in temperature and salinity along the western Antarctic Peninsula. *ISME J*. 2023 Nov;17(11):2035-46. doi: 10.1038/s41396-023-01475-0. Epub 2023 Sep 15. PMID: 37709939; PMCID: PMC10579395.
101. de Andrade CP, Lacerda CD, Valente RA, Rocha LSH, de Souza ATF, Pereira DIM, et al. An OSMAC strategy for the production of antimicrobial compounds by the Amazonian fungi *Talaromyces pinophilus* CCM-UEA-F0414 and *Penicillium paxilli* CCM-UEA-F0591. *Antibiotics (Basel).* 2025;14(8):756. doi:10.3390/antibiotics14080756.

102. de Carvalho CCCR, Fischer MA, Kirsten S, Wurz B, Wick LY, Heipieper HJ. Adaptive response of *Rhodococcus opacus* PWD4 to salt and phenolic stress on the level of mycolic acids. *AMB Express.* 2016;6:66. doi:10.1186/s13568-016-0240-6.
103. de Carvalho CCCR. Adaptation of *Rhodococcus* to organic solvents. In: Alvarez HM, editor. *Biology of Rhodococcus*. 2nd ed. Cham: Springer Nature; 2019. p. 103–35.
104. Debono M, Barnhart M, Carrell CB, Hoffmann JA, Occolowitz JL, Abbott BJ, et al. A21978C, a complex of new acidic peptide antibiotics: isolation, chemistry, and mass spectral structure elucidation. *J Antibiot (Tokyo)*. 1987;40(6):761–77. doi: 10.7164/antibiotics.40.761.
105. Delahaye C, Nicolas J. Sequencing DNA with nanopores: troubles and biases. *PLoS One*. 2021 Oct 1;16(10):e0257521. doi: 10.1371/journal.pone.0257521. PMID: 34597327; PMCID: PMC8486125.
106. Demain AL, Fang A. The natural functions of secondary metabolites. *Adv Biochem Eng Biotechnol*. 2000;69:1–39. doi:10.1007/3-540-44964-7_1.
107. Depuydt S, De Veylder L, Holsters M, Vereecke D. Eternal youth, the fate of developing *Arabidopsis* leaves upon *Rhodococcus fascians* infection. Plant Physiol. 2009;149:1387–98.
108. Dettmer K, Nurnberger N, Kaspar H, Gruber MA, Almstetter MF, Oefner PJ. Metabolite extraction from adherently growing mammalian cells for metabolomics studies: optimization of harvesting and extraction protocols. *Anal Bioanal Chem.* 2011;399(3):1127–39. doi:10.1007/s00216-010-4425-x.
109. Devanshi S, Shah KR, Arora S, Saxena S. Actinomycetes as an environmental scrubber. In: Abdel-Raouf ME, El-Keshawy MH, editors. *Crude Oil - New Technologies and Recent Approaches*. London: IntechOpen; 2021. doi:10.5772/intechopen.99187.
110. Deveau A, Bonito G, Uehling J, Paoletti M, Becker M, Bindschedler S, et al. Bacterial–fungal interactions: ecology, mechanisms and challenges. *FEMS Microbiol Rev*. 2018;42(3):335–52. doi:10.1093/femsre/fuy008.
111. Díaz-Corrales FJ, Serrano JA. *Rhodococcus equi* en humanos. Aspectos clínicos y terapéuticos. Rev Soc Ven Microbiol. 2003;23(2):131–4. Disponible en:

http://ve.scielo.org/scielo.php?script=sci_arttext&pid=S1315-25562003000200006&lng=es

112. Domagk G. Ein Beitrag zur Chemotherapie der bakteriellen Infektionen. *Dtsch Med Wochenschr*. 1935;61:250–253.
113. Donkor ES. Sequencing of bacterial genomes: principles and insights into pathogenesis and development of antibiotics. *Genes (Basel)*. 2013 Oct 14;4(4):556–72. doi: 10.3390/genes4040556. PMID: 24705262; PMCID: PMC3927574.
114. Donovick R, Pagano JF, Stout HA, Weinstein MJ. Thiostrepton, a new antibiotic. I. In vitro studies. *Antibiot Annu*. 1955–1956;3:554–9.
115. Doroghazi JR, Metcalf WW. Comparative genomics of actinomycetes with a focus on natural product biosynthetic genes. *BMC Genomics*. 2013 Sep 11;14:611. doi: 10.1186/1471-2164-14-611. PMID: 24020438; PMCID: PMC3848822.
116. dos Santos HRM, Argolo CS, Argôlo-Filho RC, Loguercio LL. A 16S rDNA PCR-based theoretical to actual delta approach on culturable mock communities revealed severe losses of diversity information. *BMC Microbiol*. 2019;19:74. doi: 10.1186/s12866-019-1446-2.
117. Du R, Xiong W, Xu L, et al. Metagenomics reveals the habitat specificity of biosynthetic potential of secondary metabolites in global food fermentations. *Microbiome*. 2023;11:115. doi:10.1186/s40168-023-01536-8.
118. Du YE, Bae ES, Lim Y, Cho JC, Nam SJ, Shin J, et al. Svalbamides A and B, pyrrolidinone-bearing lipodipeptides from Arctic *Paenibacillus* sp. *Mar Drugs*. 2021;19(4):229. doi:10.3390/md19040229.
119. Du YL, Shen XL, Yu P, Bai LQ, Li YQ. Gamma-butyrolactone regulatory system of *Streptomyces chattanoogensis* links nutrient utilization, metabolism, and development. *Appl Environ Microbiol*. 2011;77(23):8415–8426. doi:10.1128/AEM.05898-11.
120. Duban M, Cociancich S, Leclère V. Nonribosomal Peptide Synthesis Definitely Working Out of the Rules. *Microorganisms*. 2022;10(3):577. doi:10.3390/microorganisms10030577.
121. Duca D, Lorv J, Patten CL, Rose D, Glick BR. Indole-3-acetic acid in plant-microbe interactions. *Antonie Van Leeuwenhoek*. 2014;106(1):85–125. doi:10.1007/s10482-013-0095-y.

122. Dührkop K, Fleischauer M, Ludwig M, Aksenov AA, Melnik AV, et al. SIRIUS 4: a rapid tool for turning tandem mass spectra into metabolite structure information. *Nat Methods.* 2019;16(4):299–302. doi:10.1038/s41592-019-0344-8.
123. Dührkop K, Fleischauer M, Ludwig M, Aksenov AA, Melnik AV, Meusel M, et al. SIRIUS 4: a rapid tool for turning tandem mass spectra into metabolite structure information. *Nat Methods*. 2019;16(4):299–302. doi:10.1038/s41592-019-0344-8.
124. Dührkop K, Nothias LF, Fleischauer M, Reher R, Ludwig M, et al. Systematic classification of unknown metabolites using high-resolution fragmentation mass spectra. *Nat Biotechnol.* 2021;39(4):462–71. doi:10.1038/s41587-020-0740-8.
125. Dührkop K, Nothias LF, Fleischauer M, Reher R, Ludwig M, Hoffmann MA, et al. Systematic classification of unknown metabolites using high-resolution fragmentation mass spectra. *Nat Biotechnol*. 2021;39(4):462–71. doi:10.1038/s41587-020-0740-8.
126. Dührkop K, Shen H, Meusel M, Rousu J, Böcker S. Searching molecular structure databases with tandem mass spectra using CSI:FingerID. *Proc Natl Acad Sci U S A*. 2015;112(41):12580–5. doi:10.1073/pnas.1509788112.
127. Dunkel M, Fullbeck M, Neumann S, Preissner R. SuperNatural: a searchable database of available natural compounds. *Nucleic Acids Res.* 2006;34(Database issue): D678–83. doi:10.1093/nar/gkj132.
128. Dutta S, Whicher JR, Hansen DA, Hale WA, Chemler JA, Congdon GR, et al. Structure of a modular polyketide synthase. *Nature*. 2014;510(7506):512–7. doi:10.1038/nature13423.
129. Edgar RC. MUSCLE: multiple sequence alignment with high accuracy and high throughput. *Nucleic Acids Res*. 2004;32:1792–7. doi:10.1093/nar/gkh340.
130. Ekpanyaskun P. Transcriptomic Analysis of Rhodococcus sp. RHA1 Responses to Heat Shock and Osmotic Stress. Master thesis. University of British Columbia, Vancouver, BC, Canada; 2006.
131. Elbein AD, Pan YT, Pastuszak I, Carroll D. New insights on trehalose: a multifunctional molecule. *Glycobiology.* 2003;13(4):17R–27R. doi:10.1093/glycob/cwg047.
132. Electron Microscopy Research Services (EMRS), Newcastle University. Scanning electron microscopy sample preparation protocol. Newcastle, UK; 2024. Unpublished protocol.

133. Elshamy AA, Aboshanab KM. A review on bacterial resistance to carbapenems: epidemiology, detection and treatment options. *Future Sci OA*. 2020;6(3):FSO438. doi: 10.2144/fsoa-2019-0098. PMID: 32140243; PMCID: PMC7050608.
134. Engelhardt K, Degnes KF, Kemmler M, Bredholt H, Fjaervik E, Klinkenberg G, et al. Production of a new thiopeptide antibiotic, TP-1161, by a marine *Nocardiopsis* species. *Appl Environ Microbiol*. 2010;76(15):4969–76. doi:10.1128/AEM.00741-10.
135. Ernstmeyer K, Christman E, editors. *Nursing Pharmacology* [Internet]. 2nd ed. Eau Claire (WI): Chippewa Valley Technical College; 2023. Chapter 3 Antimicrobials. Available from: https://www.ncbi.nlm.nih.gov/books/NBK594998/
136. Ezeobiora CE, Igbokwe NH, Amin DH, et al. Uncovering the biodiversity and biosynthetic potentials of rare actinomycetes. *Futur J Pharm Sci*. 2022;8:23. doi:10.1186/s43094-022-00410-y.
137. Fan Y, Wang C, Wang L, Chairoungdua A, Piyachaturawat P, Fu P, et al. New ansamycins from the deep-sea-derived bacterium *Ochrobactrum* sp. OUCMDZ-2164. *Mar Drugs*. 2018;16(8):282. doi:10.3390/md16080282.
138. Fang BZ, Salam N, Han MX, Jiao JY, Cheng J, Wei DQ, et al. Insights on the effects of heat pretreatment, pH, and calcium salts on isolation of rare actinobacteria from karstic caves. *Front Microbiol*. 2017;8:1535. doi:10.3389/fmicb.2017.01535.
139. Feeney MA, Newitt JT, Addington E, Algora-Gallardo L, Allan C, et al. ActinoBase: tools and protocols for researchers working on *Streptomyces* and other filamentous actinobacteria. *Microb Genom*. 2022;8(7):mgen000824. doi:10.1099/mgen.0.000824.
140. Feling RH, Buchanan GO, Mincer TJ, Kauffman CA, Jensen PR, Fenical W. Salinosporamide A: a highly cytotoxic proteasome inhibitor from a novel microbial source, a marine bacterium of the new genus *Salinospora*. *Angew Chem Int Ed Engl*. 2003;42:355–7.
141. Fernández M, Sánchez J. Nuclease activities and cell death processes associated with the development of surface cultures of *Streptomyces antibioticus*. *Microbiology*. 2002;148:405–12. doi:10.1099/00221287-148-2-405.
142. Fleischmann RD, Adams MD, White O, Clayton RA, Kirkness EF, Kerlavage AR, et al. Whole-genome random sequencing and assembly of *Haemophilus*

influenzae Rd. *Science*. 1995 Jul 28;269(5223):496–512. doi: 10.1126/science.7542800. PMID: 7542800.

143. Fleming A. On the antibacterial action of cultures of a *Penicillium*, with special reference to their use in the isolation of *B. influenzae*. *Br J Exp Pathol*. 1929;10(3):226–36.
144. Freese HM, Meier-Kolthoff JP, Sardà Carbasse J, Afolayan AO, Göker M. TYGS and LPSN in 2025: a global core biodata resource for genome-based classification and nomenclature of prokaryotes within DSMZ Digital Diversity. *Nucleic Acids Res.* 2025;53(Database issue):gkaf1110. doi:10.1093/nar/gkaf1110.
145. Fukuda TTH, Helfrich EJN, Mevers E, Melo WGP, Van Arnam EB, Andes DR, et al. Specialized metabolites reveal evolutionary history and geographic dispersion of a multilateral symbiosis. *ACS Cent Sci*. 2021;7(2):292-9. doi:10.1021/acscentsci.0c00978. PMID:33615194; PMCID:PMC7889630.
146. Funaishi K, Kawamura K, Satoh F, Hiramatsu M, Hagiwara M, Okanishi M. New analogues of rosaramicin isolated from a *Micromonospora* strain. I. Taxonomy, fermentation, isolation and physico-chemical and biological properties. *J Antibiot (Tokyo).* 1990;43(8):938–47. doi:10.7164/antibiotics.43.938.
147. Fuqua WC, Winans SC, Greenberg EP. Quorum sensing in bacteria: the LuxR-LuxI family of cell density-responsive transcriptional regulators. *J Bacteriol.* 1994;176(2):269–75.
148. Galinski EA, Pfeiffer HP, Trüper HG. 1,4,5,6-Tetrahydro-2-methyl-4-pyrimidinecarboxylic acid: a novel cyclic amino acid from halophilic phototrophic bacteria of the genus *Ectothiorhodospira*. *Eur J Biochem.* 1985;149(1):135–9. doi: 10.1111/j.1432-1033.1985.tb08903.x.
149. Gallardo K, Candia JE, Remonsellez F, Escudero LV, Demergasso CS. The ecological coherence of temperature and salinity tolerance interaction and pigmentation in a non-marine *Vibrio* isolated from Salar de Atacama. *Front Microbiol*. 2016;7:1943. doi:10.3389/fmicb.2016.01943. PMID:27990141; PMCID:PMC5130992.
150. Gamaleldin NM, Bahr HS, Mostafa YA, McAllister BF, El Zawily A, Ngwa CJ, et al. Metabolomic profiling, in vitro antimalarial investigation and in silico modeling of the marine actinobacterium strain *Rhodococcus* sp. UR111 associated with the

soft coral *Nephthea* sp. *Antibiotics (Basel).* 2022;11(11):1631. doi:10.3390/antibiotics11111631.

151. Ganesh SK, Subathra Devi C. Molecular and therapeutic insights of rapamycin: a multi-faceted drug from *Streptomyces hygroscopicus*. *Mol Biol Rep*. 2023;50(4):3815–33. doi:10.1007/s11033-023-08283-x.
152. Gao B, Gupta RS. Phylogenetic framework and molecular signatures for the main clades of the phylum Actinobacteria. *Microbiol Mol Biol Rev*. 2012;76(1):66–112.
153. Gehring AM, Bradley KA, Walsh CT. Enterobactin biosynthesis in *Escherichia coli*: isochorismate lyase (EntB) is a bifunctional enzyme that is phosphopantetheinylated by EntD and then acylated by EntE using ATP and 2,3-dihydroxybenzoate. *Biochemistry*. 1997;36(28):8495–503. doi:10.1021/bi970453p.
154. Genilloud O. Mining actinomycetes for novel antibiotics in the omics era: are we ready to exploit this new paradigm? *Antibiotics (Basel)*. 2018;7(4):85. doi:10.3390/antibiotics7040085.
155. Gerber NN, Lechevalier HA. Geosmin, an earthly-smelling substance isolated from actinomycetes. *Appl Microbiol*. 1965;13(6):935–8. doi:10.1128/am.13.6.935-938.1965.
156. Ghilchik MW, Morris AS, Reeves DS. Immunosuppressive powers of the antibacterial agent trimethoprim. *Nature*. 1970;227(5256):393–4.
157. Gil JA, Campelo-Diez AB. Candicidin biosynthesis in *Streptomyces griseus*. *Appl Microbiol Biotechnol*. 2003;60(6):633–42. doi:10.1007/s00253-002-1163-9.
158. Glick R, Gilmour C, Tremblay J, Satanower S, Avidan O, Déziel E, et al. Increase in rhamnolipid synthesis under iron-limiting conditions influences surface motility and biofilm formation in *Pseudomonas aeruginosa*. *J Bacteriol.* 2010;192(12):2973–80. doi: 10.1128/JB.01601-09. PMID: 20154129; PMCID: PMC2901684.
159. Goers L, Freemont P, Polizzi KM. Co-culture systems and technologies: taking synthetic biology to the next level. *J R Soc Interface*. 2014;11(96):20140065. doi:10.1098/rsif.2014.0065. PMID:24829281; PMCID:PMC4032528.
160. Goethals K, Vereecke D, Jaziri M, Van Montagu M, Holsters M. Leafy gall formation by *Rhodococcus fascians*. Annu Rev Phytopathol. 2001;39:27–52.

161. Gohlke RS, McLafferty FW. Time-of-flight mass spectrometry and gas-liquid partition chromatography. *Anal Chem*. 1959;31:535–41. doi:10.1021/ac50164a024.
162. Goldstein SL, Klassen JL. *Pseudonocardia* symbionts of fungus-growing ants and the evolution of defensive secondary metabolism. *Front Microbiol*. 2020;11:621041. doi: 10.3389/fmicb.2020.621041.
163. Goloboff PA, Farris JS, Nixon KC. TNT, a free program for phylogenetic analysis. *Cladistics*. 2008;24:774–86. doi:10.1111/j.1096-0031.2008.00217.x.
164. Gonçalves T, Vasconcelos U. Colour me blue: the history and the biotechnological potential of pyocyanin. *Molecules.* 2021;26(4):927. doi: 10.3390/molecules26040927.
165. Gong XW, Yang JK, Duan YQ, Dong JY, Zhe W, Wang L, et al. Isolation and characterization of *Rhodococcus* sp. Y22 and its potential application to tobacco processing. Res Microbiol. 2009;160(3):200–4.
166. Gontang EA, Fenical W, Jensen PR. Phylogenetic diversity of Gram-positive bacteria cultured from marine sediments. *Appl Environ Microbiol*. 2007;73:3272–82. doi:10.1128/AEM.02811-06.
167. Goodfelow M, Anderson G. The actinomycete-genus *Rhodococcus*: a home for the “rhodochrous” complex. J Gen Microbiol. 1977;100:99–122.
168. Goordial J, Raymond-Bouchard I, Zolotarov Y, de Bethencourt L, Ronholm J, Shapiro N, et al. Cold adaptive traits revealed by comparative genomic analysis of the eurypsychrophile *Rhodococcus* sp. JG3 isolated from high-elevation McMurdo Dry Valley permafrost, Antarctica. *FEMS Microbiol Ecol.* 2016;92(2):fiv154. doi:10.1093/femsec/fiv154.
169. Goris J, Konstantinidis KT, Klappenbach JA, Coenye T, Vandamme P, Tiedje JM. DNA-DNA hybridization values and their relationship to whole-genome sequence similarities. *Int J Syst Evol Microbiol*. 2007 Jan;57(Pt 1):81-91. doi: 10.1099/ijs.0.64483-0. PMID: 17220447.
170. Gourevitch A, Hunt GA, Pursiano TA, Carmack CC, Moses AJ, Lein J. Microbiological evaluation of 5-methyl-3-phenyl-4-isoxazolyl penicillin. *Antibiot Chemother (Northfield)*. 1961;11:780–9.

171. Graf R, Anzali S, Buenger J, Pfluecker F, Driller H. The multifunctional role of ectoine as a natural cell protectant. *Clin Dermatol*. 2008;26(4):326–333. doi:10.1016/j.clindermatol.2008.01.002.
172. GraphPad Prism, version 8.0.0. San Diego (CA): GraphPad Software; 2018.
173. Grebe SK, Singh RJ. LC-MS/MS in the clinical laboratory: where to from here? *Clin Biochem Rev*. 2011;32(1):5–31.
174. Gurevich A, Saveliev V, Vyahhi N, Tesler G. QUAST: quality assessment tool for genome assemblies. *Bioinformatics*. 2013 Apr 15;29(8):1072-5. doi: 10.1093/bioinformatics/btt086. Epub 2013 Feb 19. PMID: 23422339; PMCID: PMC3624806.
175. Gürtler H, Pedersen R, Anthoni U, Christophersen C, Nielsen PH, Wellington EM, et al. Albaflavenone, a sesquiterpene ketone with a zizaene skeleton produced by a streptomycete with a new rope morphology. *J Antibiot (Tokyo)*. 1994;47(4):434–9. doi:10.7164/antibiotics.47.434.
176. Hall RJ, Whelan FJ, McInerney JO, Ou Y, Domingo-Sananes MR. Horizontal Gene Transfer as a Source of Conflict and Cooperation in Prokaryotes. *Front Microbiol*. 2020;11:1569. doi:10.3389/fmicb.2020.01569.
177. Hall TA. BioEdit: a user-friendly biological sequence alignment editor and analysis program for Windows 95/98/NT. *Nucleic Acids Symp Ser*. 1999;41:95–8.
178. Hamed AA, Mohamed OG, Aboutabl EA, Fathy FI, Fawzy GA, El-Shiekh RA, et al. Identification of antimicrobial metabolites from the Egyptian soil-derived *Amycolatopsis keratiniphila* revealed by untargeted metabolomics and molecular docking. *Metabolites.* 2023;13(5):620. doi:10.3390/metabo13050620. PMID: 37233661; PMCID: PMC10221244.
179. Hamill RL, Haney ME Jr, Stamper M, Wiley PF. Tylosin, a new antibiotic: II. Isolation, properties, and preparation of desmycosin, a microbiologically active degradation product. *Antibiot Chemother.* 1961;11:328–34.
180. Han SW, Won HS. Advancements in the Application of Ribosomally Synthesized and Post-Translationally Modified Peptides (RiPPs). *Biomolecules*. 2024;14(4):479. doi:10.3390/biom14040479.
181. Harir M, Bendif H, Bellahcene M, Fortas Z, Pogni R. Streptomyces secondary metabolites. *Basic Biol Appl Actinobacteria*. 2018;6:99–122.

182. Harrigan WF, McCance ME. Composition of culture media. In: Harrigan WF, McCance ME, editors. *Laboratory Methods in Microbiology*. Academic Press; 1966. p. 36–45. doi:10.1016/B978-1-4832-3205-8.50015-5.
183. Hassler HB, Walters W, Schadt CW, Campbell JH, Hofmockel KS, Lemons A, et al. Challenges and perspectives for 16S rRNA gene amplicon sequencing in environmental microbiome studies. *Microbiome*. 2022;10:170. doi: 10.1186/s40168-022-01337-4.
184. Hatano K, Higashide E, Shibata M. Studies on juvenimicin, a new antibiotic. I. Taxonomy, fermentation and antimicrobial properties. *J Antibiot (Tokyo).* 1976;29(11):1163–70. doi:10.7164/antibiotics.29.1163.
185. Hayakawa I, Hiramitsu Y, Tanaka Y. A new class of potent quinolone antibacterial agents. I. Synthesis and structure-activity relationships of 9-fluoro-3-methyl-10-(4-methyl-1-piperazinyl)-7-oxo-2,3-dihydro-7H-pyrido[1,2,3-de]-1,4-benzoxazine-6-carboxylic acid derivatives. *Antimicrob Agents Chemother*. 1986;29(1):163–168.
186. Hayakawa M, Nomura S. Humic acid-vitamin agar. A new medium for the selective isolation of soil actinomycetes. *J Ferment Technol*. 1987;65:501–9. doi:10.1016/0385-6380(87)90108-7.
187. He H, Ding WD, Bernan VS, Richardson AD, Ireland CM, Greenstein M, et al. Lomaiviticins A and B, potent antitumor antibiotics from *Micromonospora lomaivitiensis*. *J Am Chem Soc*. 2001;123(22):5362–3. doi: 10.1021/ja010129o.
188. Heald SC, Brandão PF, Hardicre R, Bull AT. Physiology, biochemistry and taxonomy of deep-sea nitrile metabolising *Rhodococcus* strains. Antonie Van Leeuwenhoek. 2001;80(2):169–83.
189. Heather JM, Chain B. The sequence of sequencers: the history of sequencing DNA. *Genomics*. 2016 Jan;107(1):1–8. doi: 10.1016/j.ygeno.2015.11.003. Epub 2015 Nov 10. PMID: 26554401; PMCID: PMC4727787.
190. Hertweck C, Luzhetskyy A, Rebets Y, Bechthold A. Type II polyketide synthases: gaining a deeper insight into enzymatic teamwork. *Nat Prod Rep*. 2007;24(1):162–90. doi:10.1039/b507395m.
191. Hibbing ME, Fuqua C, Parsek MR, Peterson SB. Bacterial competition: surviving and thriving in the microbial jungle. *Nat Rev Microbiol*. 2010;8(1):15–25. doi:10.1038/nrmicro2259.

192. Hifnawy MS, Fouda MM, Sayed AM, Mohammed R, Hassan HM, AbouZid SF, et al. The genus *Micromonospora* as a model microorganism for bioactive natural product discovery. *RSC Adv*. 2020 Jun 8;10(35):20939-59. doi: 10.1039/d0ra04025h. PMID: 35517724; PMCID: PMC9054317.
193. Hifnawy MS, Fouda MM, Sayed AM, Mohammed R, Hassan HM, AbouZid SF, et al. The genus *Micromonospora* as a model microorganism for bioactive natural product discovery. RSC Adv. 2020;10(35):20939–59.
194. Hifnawy MS, Fouda MM, Sayed AM, Mohammed R, Hassan HM, AbouZid SF, et al. The genus Micromonospora as a model microorganism for bioactive natural product discovery. *RSC Adv.* 2020;10(35):20939–59. doi:10.1039/d0ra04025h.
195. Hobbs G, Frazer CM, Gardner DCJ, Cullum JA, Oliver SG. Dispersed growth of *Streptomyces* in liquid culture. *Appl Microbiol Biotechnol*. 1989;31(3):272–7. doi:10.1007/BF00258437.
196. Hoffmann MA, Nothias LF, Ludwig M, Fleischauer M, Gentry EC, Witting M, et al. High-confidence structural annotation of metabolites absent from spectral libraries. *Nat Biotechnol*. 2022;40(3):411–21. doi:10.1038/s41587-021-01159-1.
197. Holmes AH, Moore LS, Sundsfjord A, Steinbakk M, Regmi S, Karkey A, Guerin PJ, Piddock LJ. Understanding the mechanisms and drivers of antimicrobial resistance. *Lancet*. 2016;387(10014):176–87. doi:10.1016/S0140-6736(15)00473-0. PMID:26603922.
198. Homann VV, Sandy M, Tincu JA, Templeton AS, Tebo BM, Butler A. Loihichelins A-F, a suite of amphiphilic siderophores produced by the marine bacterium *Halomonas* LOB-5. *J Nat Prod*. 2009;72(5):884-8. doi:10.1021/np800640h. PMID:19320498; PMCID:PMC2891265.
199. Hong K, Gao AH, Xie QY, Gao H, Zhuang L, Lin HP, et al. Actinomycetes for marine drug discovery isolated from mangrove soils and plants in China. *Mar Drugs*. 2009;7:24–44.
200. Horai H, Arita M, Kanaya S, Nihei Y, Ikeda T, Suwa K, et al. MassBank: a public repository for sharing mass spectral data for life sciences. *J Mass Spectrom*. 2010;45(7):703–14. doi:10.1002/jms.1777.
201. Horikawa M, Sakamoto K. Fatty-acid metabolism is involved in stress-resistance mechanisms of Caenorhabditis elegans. Biochem Biophys Res Commun. 2009;390:1402–1407. doi: 10.1016/j.bbrc.2009.11.006

202. Horinouchi S, Beppu T. Hormonal control by A-factor of morphological development and secondary metabolism in *Streptomyces*. *Proc Jpn Acad Ser B Phys Biol Sci*. 2007;83(9-10):277-95. doi:10.2183/pjab/83.277. PMID:24367152; PMCID:PMC3859367.
203. Hoskisson PA, Seipke RF. Cryptic or silent? The known unknowns, unknown knowns, and unknown unknowns of secondary metabolism. *mBio*. 2020;11:e02642-20. doi:10.1128/mbio.02642-20.
204. Hover BM, Kim SH, Katz M, Charlop-Powers Z, Owen JG, Ternei MA, et al. Culture-independent discovery of the malacidins as calcium-dependent antibiotics with activity against multidrug-resistant Gram-positive pathogens. *Nat Microbiol*. 2018;3(4):415-22. doi:10.1038/s41564-018-0110-1. PMID:29459710.
205. Hover BM, Kim SH, Katz M, et al. Culture-independent discovery of the malacidins as calcium-dependent antibiotics with activity against multidrug-resistant Gram-positive pathogens. *Nat Microbiol*. 2018;3:415–22. doi: 10.1038/s41564-018-0110-1.
206. Howarth TT, Brown AG, King TJ. Clavulanic acid, a novel β-lactam isolated from *Streptomyces clavuligerus*; X-ray crystal structure analysis. *J Chem Soc Chem Commun*. 1976;266b–267b.
207. Hsu SC, Lockwood JL. Powdered chitin agar as a selective medium for enumeration of actinomycetes in water and soil. *Appl Microbiol*. 1975;29(3):422–6. doi:10.1128/am.29.3.422-426.1975.
208. Hu B, Gao S, Zhang H, et al. Whole-genome sequencing and pathogenicity analysis of *Rhodococcus equi* isolated in horses. BMC Vet Res. 2024;20:362.
209. Hu GA, Song Y, Liu SY, Yu WC, Yu YL, Chen JW, et al. Exploring the diversity and specificity of secondary biosynthetic potential in *Rhodococcus*. Mar Drugs. 2024;22(9):409.
210. Hu X, Wang Y, Zhao C, Li S, Hu X, You X, et al. Mintaimycins, a group of novel peptide metabolites from *Micromonospora* sp. C-3509. *Molecules.* 2022 Feb 9;27(4):1150. doi:10.3390/molecules27041150. PMID: 35208940; PMCID: PMC8877661.
211. Hug JJ, Bader CD, Remškar M, Cirnski K, Müller R. Concepts and methods to access novel antibiotics from actinomycetes. *Antibiotics (Basel)*. 2018;7(2):44. doi: 10.3390/antibiotics7020044.

212. Iizaka Y, Higashi N, Ishida M, Oiwa R, Ichikawa Y, Takeda M, et al. Function of cytochrome P450 enzymes RosC and RosD in the biosynthesis of rosamicin macrolide antibiotic produced by *Micromonospora rosaria*. *Antimicrob Agents Chemother.* 2013;57(3):1529–31. doi:10.1128/AAC.02092-12.
213. International Human Genome Sequencing Consortium. Initial sequencing and analysis of the human genome. *Nature*. 2001;409:860–921. doi: 10.1038/35057062.
214. Ivanov YV, Linz B, Register KB, Newman JD, Taylor DL, Boschert KR, et al. Identification and taxonomic characterization of *Bordetella pseudohinzii* sp. nov. isolated from laboratory-raised mice. *Int J Syst Evol Microbiol*. 2016 Dec;66(12):5452–9. doi: 10.1099/ijsem.0.001540. Epub 2016 Oct 4. PMID: 27707434; PMCID: PMC5244500.
215. Iwatsuki M, Tomoda H, Uchida R, Gouda H, Hirono S, Omura S. Lariatins, antimycobacterial peptides produced by *Rhodococcus* sp. K01-B0171, have a lasso structure. J Am Chem Soc. 2006;128:7487.
216. Iwatsuki M, Uchida R, Takakusagi Y, Matsumoto A, Jiang CL, Takahashi Y, et al. Lariatins, novel anti-mycobacterial peptides with a lasso structure, produced by *Rhodococcus jostii* K01-B0171. J Antibiot. 2007;60:357–63.
217. Jacobowski AC, Boleti APA, Cruz MV, Santos KFDP, de Andrade LRM, Frihling BEF, et al. Combating antimicrobial resistance: innovative strategies using peptides, nanotechnology, phages, quorum sensing interference, and CRISPR-Cas systems. *Pharmaceuticals*. 2025;18(8):1119. doi: 10.3390/ph18081119.
218. Jagannathan SV, Manemann EM, Rowe SE, Callender MC, Soto W. Marine actinomycetes, new sources of biotechnological products. *Mar Drugs*. 2021;19(7):365. doi:10.3390/md19070365.
219. Jakimowicz D, van Wezel GP. Cell division and DNA segregation in *Streptomyces*: how to build a septum in the middle of nowhere? *Mol Microbiol*. 2012;85(3):393–404. doi:10.1111/j.1365-2958.2012.08107.x.
220. James AT, Martin AJP. Gas-liquid partition chromatography: the separation and micro-estimation of volatile fatty acids. *Biochem J*. 1952;50(5):679–90. doi:10.1042/bj0500679.

221. James PD, Edwards C, Dawson M. The effects of temperature, pH and growth rate on secondary metabolism in *Streptomyces thermoviolaceus* grown in a chemostat. *J Gen Microbiol*. 1991 Jul;137(7):1715-20. doi: 10.1099/00221287-137-7-1715. PMID: 1683400.
222. Janda JM, Abbott SL. Bacterial identification for publication: when is enough enough? *J Clin Microbiol*. 2002;40(6):1887–91. doi: 10.1128/JCM.40.6.1887-1891.2002.
223. Jenifer JS, Donio MB, Michaelbabu M, Vincent SG, Citarasu T. Haloalkaliphilic *Streptomyces* spp. AJ8 isolated from solar salt works and its pharmacological potential. *AMB Express.* 2015;5(1):143. doi:10.1186/s13568-015-0143-2.
224. Jensen PR, Gontang E, Mafnas C, Mincer TJ, Fenical W. Culturable marine actinomycete diversity from tropical Pacific Ocean sediments. *Environ Microbiol*. 2005;7:1039–48.
225. Jensen PR, Gontang E, Mafnas C, Mincer TJ, Fenical W. Culturable marine actinomycete diversity from tropical Pacific Ocean sediments. *Environ Microbiol*. 2005;7:1039–48. doi:10.1111/j.1462-2920.2005.00785.x.
226. Jensen PR. Microbe Profile: *Salinispora tropica*: natural products and the evolution of a unique marine bacterium. *Microbiology (Reading)*. 2022;168(4):001163. doi:10.1099/mic.0.001163.
227. Jensen PR. Natural products and the gene cluster revolution. *Trends Microbiol*. 2016;24(12):968–977. doi:10.1016/j.tim.2016.07.006.
228. Jeong GH, Bak DH, Lee H, Cho JY, Kang SH, Chung BY, Park S, Bai HW. Anti-cancer effects of plant-derived Micromonospora sp. M2 against A549 and MCF-7 cell lines. *Biosci Biotechnol Biochem.* 2024;88(6):608–19. doi:10.1093/bbb/zbae036.
229. Jevons MP. “Celbenin”-resistant Staphylococci. *Br Med J*. 1961;1(5219):124–5.
230. Jiao ZX, Li XG, Zhang WJ, Zhang GY, Bai SJ, Fu L, Wu LF. High hydrostatic pressure enhanced the growth of deep-sea *Thermococcus aciditolerans* by promoting the reduction of elemental sulfur. *Front Microbiol*. 2025 Aug 18;16:1643593. doi: 10.3389/fmicb.2025.1643593. PMID: 40901076; PMCID: PMC12401011.

231. Johnson J, Soehnlen M, Blankenship HM. Long read genome assemblers struggle with small plasmids. *Microb Genom*. 2023;9(5):mgen001024. doi:10.1099/mgen.0.001024.
232. Jose PA, Jebakumar SRD. Diverse actinomycetes from Indian coastal solar salterns - a resource for antimicrobial screening. *J Pure Appl Microbiol*. 2013;7:2569–75.
233. Kahan JS, Kahan FM, Goegelman R, Currie SA, Jackson M, Stapley EO, et al. Thienamycin, a new β-lactam antibiotic. I. Discovery, taxonomy, isolation and physical properties. *J Antibiot (Tokyo)*. 1979;32(1):1–12.
234. Katsuyama Y, Ohnishi Y. Type III polyketide synthases in microorganisms. *Methods Enzymol.* 2012;515:359–77. doi: 10.1016/B978-0-12-394290-6.00017-3. PMID: 22999182.
235. Kaufmann KW. Fitting and using growth curves. *Oecologia*. 1981;49(3):293–9. doi:10.1007/BF00347591.
236. Kautsar SA, van der Hooft JJJ, de Ridder D, Medema MH. BiG-SLiCE: a highly scalable tool maps the diversity of 1.2 million biosynthetic gene clusters. *Gigascience*. 2021;10(1):giaa154. doi:10.1093/gigascience/giaa154.
237. Kautsar SA, Blin K, Shaw S, Navarro-Muñoz JC, Terlouw BR, van der Hooft JJ, et al. MIBiG 2.0: a repository for biosynthetic gene clusters of known function. *Nucleic Acids Res.* 2020;48(D1):D454–8. doi:10.1093/nar/gkz882.
238. Kettenring JK, Maiabarba A, Vekey K, Cavalleri B. Sequence determination of actagardine, a novel lantibiotic, by homonuclear 2D NMR spectroscopy. *J Antibiot*. 1990;43:1082.
239. Khilyas IV, Sorokina AV, Markelova MI, et al. Genomic and phenotypic analysis of siderophore-producing *Rhodococcus qingshengii* strain S10 isolated from an arid weathered serpentine rock environment. Arch Microbiol. 2021;203:855–60.
240. Kieser T, Bibb MJ, Buttner MJ, Chater KF, Hopwood DA. *Practical Streptomyces genetics*. Norwich: John Innes Foundation; 2000.
241. Kim D, Choi KY, Yoo M, Zylstra GJ, Kim E. Biotechnological potential of *Rhodococcus* biodegradative pathways. *J Microbiol Biotechnol.* 2018 Jul 28;28(7):1037–51. doi:10.4014/jmb.1712.12017. PMID: 29913546.

242. Kim HW, Wang M, Leber CA, Nothias LF, Reher R, et al. NPClassifier: a deep neural network-based structural classification tool for natural products. *J Nat Prod.* 2021;84(9):2795–807. doi:10.1021/acs.jnatprod.1c00399.
243. Kim HW, Wang M, Leber CA, Nothias LF, Reher R, Kang KB, et al. NPClassifier: a deep neural network-based structural classification tool for natural products. *J Nat Prod*. 2021;84(11):2795–807. doi:10.1021/acs.jnatprod.1c00399.
244. Kim SJ, Matsuoka S, Patti GJ, Schaefer J. Vancomycin derivative with damaged D-Ala-D-Ala binding cleft binds to cross-linked peptidoglycan in the cell wall of *Staphylococcus aureus*. *Biochemistry*. 2008;47(12):3822–31. doi: 10.1021/bi702232a.
245. Kim TK, Hewavitharana AK, Shaw PN, Fuerst JA. Discovery of a new source of rifamycin antibiotics in marine sponge actinobacteria by phylogenetic prediction. *Appl Environ Microbiol*. 2006;72(3):2118–25. doi:10.1128/AEM.72.3.2118-2125.2006.
246. Kishi T, Harada S, Yamana H, Miyake A. Studies on juvenimicin, a new antibiotic. II. Isolation, chemical characterization and structures. *J Antibiot (Tokyo).* 1976;29(11):1171–81.
247. Kitagawa W, Mitsuhashi S, Hata M, Tamura T. Identification of a novel bacteriocin-like protein and structural gene from *Rhodococcus erythropolis* JCM 2895 using suppression-subtractive hybridization. *J Antibiot (Tokyo).* 2018 Oct;71(10):872–9. doi:10.1038/s41429-018-0078-3. PMID: 29980745.
248. Kitagawa W, Tamura T. A quinoline antibiotic from *Rhodococcus erythropolis* JCM 6824. *J Antibiot (Tokyo).* 2008;61(11):680–2. doi:10.1038/ja.2008.96.
249. Klein EY, Impalli I, Poleon S, Denoel P, Cipriano M, Van Boeckel TP, Pecetta S, Bloom DE, Nandi A. Global trends in antibiotic consumption during 2016–2023 and future projections through 2030. *Proc Natl Acad Sci U S A*. 2024;121(49):e2411919121. doi:10.1073/pnas.2411919121. PMID:39556760; PMCID:PMC11626136.
250. Knapp BD, Willis L, Gonzalez C, Vashistha H, Touma JJ, Tikhonov M, et al. Metabolomic rearrangement controls the intrinsic microbial response to temperature changes. *bioRxiv* [Preprint]. 2023 Aug 30:2023.07.22.550177. doi:10.1101/2023.07.22.550177. PMID: 37546722; PMCID: PMC10401945.

251. Kol S, Merlo ME, Scheltema RA, de Vries M, Vonk RJ, Kikkert NA, et al. Metabolomic characterization of the salt stress response in *Streptomyces coelicolor*. *Appl Environ Microbiol.* 2010;76(8):2574–81. doi:10.1128/AEM.01992-09.
252. Kolmogorov M, Yuan J, Lin Y, Pevzner PA. Assembly of long, error-prone reads using repeat graphs. *Nat Biotechnol*. 2019;37:540–546. doi: 10.1038/s41587-019-0072-8.
253. Kolmogorov M, Yuan J, Lin Y, Pevzner PA. Assembly of long, error-prone reads using repeat graphs. *Nat Biotechnol*. 2019;37(5):540–546. doi:10.1038/s41587-019-0072-8.
254. Koren S, Harhay GP, Smith TPL, Bono JL, Harhay DM, McVey SD, et al. Reducing assembly complexity of microbial genomes with single-molecule sequencing. *Genome Biol*. 2013;14(9):R101. doi: 10.1186/gb-2013-14-9-r101. PMID: 24034426; PMCID: PMC4053942.
255. Koren S, Schatz MC, Walenz BP, Martin J, Howard JT, Ganapathy G, et al. Hybrid error correction and *de novo* assembly of single-molecule sequencing reads. *Nat Biotechnol*. 2012 Jul 1;30(7):693–700. doi: 10.1038/nbt.2280. PMID: 22750884; PMCID: PMC3707490.
256. Koyama Y, Kurosasa A, Tsuchiya A, Takakuta K. A new antibiotic 'colistin' produced by spore-forming soil bacteria. *J Antibiot*. 1950;3:457–458.
257. Kramer J, Özkaya Ö, Kümmerli R. Bacterial siderophores in community and host interactions. *Nat Rev Microbiol*. 2020;18:152–63. doi:10.1038/s41579-019-0284-4.
258. Krawczyk PS, Lipinski L, Dziembowski A. PlasFlow: predicting plasmid sequences in metagenomic data using genome signatures. *Nucleic Acids Res*. 2018;46(6):e35. doi:10.1093/nar/gkx1321.
259. Kremer LS, Bader DM, Mertes C, Kopajtich R, Pichler G, Iuso A, et al. Genetic diagnosis of Mendelian disorders via RNA sequencing. *Nat Commun*. 2017 Jun 12;8:15824. doi: 10.1038/ncomms15824. PMID: 28604674; PMCID: PMC5499207.
260. Kudo Y, Konoki K, Yotsu-Yamashita M. Identification of γ-butyrolactone signalling molecules in diverse actinomycetes using resin-assisted isolation and

chemoenzymatic synthesis. *RSC Chem Biol*. 2025;6(4):630–41. doi:10.1039/d5cb00007f.

261. Kügler S, Cooper RE, Boessneck J, Küsel K, Wichard T. Rhizobactin B is the preferred siderophore by a novel *Pseudomonas* isolate to obtain iron from dissolved organic matter in peatlands. *Biometals*. 2020;33(6):415–33. doi:10.1007/s10534-020-00258-w.
262. Kumar H, Vijayakumar S, Shintre N, Tamhane V, Deshpande N, Joshi T, et al. In silico exploration of biosynthetic gene clusters in marine *Streptomyces* sp. and *Nocardiopsis* sp. from the western coast of India: Genome-based profiling using whole genome sequencing. *J Genet Eng Biotechnol*. 2025;23(2):100483. doi:10.1016/j.jgeb.2025.100483.
263. Kumar RR, Jadeja VJ. Isolation of Actinomycetes: a complete approach. *Int J Curr Microbiol Appl Sci*. 2016;5(5):606–18.
264. Kurosawa K, Ghiviriga I, Sambandan TG, Lessard PA, Barbara JE, Rha C, Sinskey AJ. Rhodostreptomycins, antibiotics biosynthesized following horizontal gene transfer from *Streptomyces padanus* to *Rhodococcus fascians*. *J Am Chem Soc.* 2008 Jan 30;130(4):1126–7. doi:10.1021/ja077821p. PMID: 18179219.
265. Kurosawa K, Radek A, Plassmeier JK, Sinskey AJ. Improved glycerol utilization by a triacylglycerol-producing Rhodococcus opacus strain for renewable fuels. Biotechnol Biofuels. 2015;8:31. doi: 10.1186/s13068-015-0209-z.
266. Küster E, Williams S. Selection of media for isolation of streptomycetes. *Nature*. 1964;202:928–9. doi:10.1038/202928a0.
267. Kuvarina AE, Roshka YA, Rogozhin EA, et al. Antimicrobial properties and the effect of temperature on the formation of secondary metabolites in psychrophilic micromycetes. *Appl Biochem Microbiol*. 2022;58:243-50. doi:10.1134/S0003683822030085.
268. Langmead B, Salzberg SL. Fast gapped-read alignment with Bowtie 2. *Nat Methods*. 2012;9(4):357–9. doi:10.1038/nmeth.1923.
269. Langmead B, Salzberg SL. Fast gapped-read alignment with Bowtie 2. *Nat Methods*. 2012;9(4):357–359. doi:10.1038/nmeth.1923.
270. Laponogov I, Sadawi N, Galea D, Mirnezami R, Veselkov KA. ChemDistiller: an engine for metabolite annotation in mass spectrometry. *Bioinformatics.* 2018 Jun

15;34(12):2096–102. doi:10.1093/bioinformatics/bty080. PMID: 29447341; PMCID: PMC9881669.

271. Larkin MJ, Kulakov LA, Allen CCR. Genomes and plasmids in *Rhodococcus*. In: Álvarez HM, editor. Biology of *Rhodococcus*. Microbiology Monographs. Vol. 16. Berlin Heidelberg: Springer-Verlag; 2010. p. 73–90.
272. Lawson PA, Citron DM, Tyrrell KL, Finegold SM. Reclassification of *Clostridium difficile* as *Clostridioides difficile* (Hall and O'Toole 1935) Prévot 1938. *Anaerobe*. 2016 Aug;40:95-9. doi: 10.1016/j.anaerobe.2016.06.008. PMID: 27370902.
273. LeBlanc JC, Gonçalves ER, Mohn WW. Global response to desiccation stress in the soil actinomycete *Rhodococcus jostii* RHA1. *Appl Environ Microbiol*. 2008;74:2627–36.
274. Lechevalier MP. Genus *Nocardia*. In: Williams ST, Sharpe ME, Holt JG, editors. Bergey's Manual of Systematic Bacteriology. Vol. 4. Baltimore (MD): Williams & Wilkins; 1989. p. 2348–61.
275. Lee TH, Brittin NJ, Alas I, Roberts CD, Chanana S, Braun DR, Ericksen SS, Guo S, Rajski SR, Bugni TS. Discovery of new everninomicin analogs from a marine-derived *Micromonospora* sp. by metabolomics and genomics approaches. *Mar Drugs.* 2025;23(8):316. doi:10.3390/md23080316.
276. Leinweber A, Weigert M, Kümmerli R. The bacterium *Pseudomonas aeruginosa* senses and gradually responds to interspecific competition for iron. *Evolution*. 2018;72(7):1515–28. doi:10.1111/evo.13491. PMID:29665015; PMCID:PMC6314444.
277. Leisner JJ. The diverse search for synthetic, semisynthetic and natural product antibiotics from the 1940s and up to 1960 exemplified by a small pharmaceutical player. *Front Microbiol*. 2020;11:976.
278. Lewin GR, Carlos C, Chevrette MG, Horn HA, McDonald BR, Stankey RJ, et al. Evolution and ecology of actinobacteria and their bioenergy applications. *Annu Rev Microbiol*. 2016;70:235–54. doi:10.1146/annurev-micro-102215-095748.
279. Li H. Minimap and miniasm: fast mapping and de novo assembly for noisy long sequences. *Bioinformatics*. 2016;32(14):2103–2110. doi:10.1093/bioinformatics/btw152.

280. Li J, Zhao GZ, Long LJ, Wang FZ, Tian XP, Zhang S, et al. *Rhodococcus nanhaiensis* sp. nov., an actinobacterium isolated from marine sediment. Int J Syst Evol Microbiol. 2012;62(10):2517–21.
281. Li MH, Ung PM, Zajkowski J, et al. Automated genome mining for natural products. *BMC Bioinformatics*. 2009;10:185. doi:10.1186/1471-2105-10-185.
282. Li Y, Gong N, Zhou L, Yang Z, Zhang H, Gu Y, et al. OSMAC-based discovery and biosynthetic gene clusters analysis of secondary metabolites from marine-derived *Streptomyces globisporus* SCSIO LCY30. *Mar Drugs*. 2024;22(1):21. doi:10.3390/md22010021.
283. Lianza M, Leroy R, Machado Rodrigues C, Borie N, Sayagh C, Remy S, et al. The three pillars of natural product dereplication: alkaloids from the bulbs of *Urceolina peruviana* as a preliminary test case. *Molecules.* 2021;26(3):637. doi:10.3390/molecules26030637.
284. Lichman BR. The scaffold-forming steps of plant alkaloid biosynthesis. *Nat Plants*. 2021;7(1):1–13. doi:10.1038/s41577-020-00400-4.
285. Liigand P, Kaupmees K, Haav K, Liigand J, Leito I, Girod M, et al. Think negative: finding the best electrospray ionization/MS mode for your analyte. *Anal Chem*. 2017;89(11):5665–8. doi:10.1021/acs.analchem.7b00096.
286. Lin Y, Yuan J, Kolmogorov M, Shen MW, Chaisson M, Pevzner PA. Assembly of long error-prone reads using de Bruijn graphs. *Proc Natl Acad Sci U S A*. 2016;113(52):E8396–405. doi:10.1073/pnas.1604560113.
287. Lin Z, Li F, Krug PJ, et al. The polyketide to fatty acid transition in the evolution of animal lipid metabolism. *Nat Commun*. 2024;15:236. doi:10.1038/s41467-023-44497-0.
288. Ling LL, Schneider T, Peoples AJ, Spoering AL, Engels I, Conlon BP, et al. A new antibiotic kills pathogens without detectable resistance. *Nature*. 2015;517(7535):455-9. doi:10.1038/nature14098. PMID:25561178.
289. Little RF, Hertweck C. Correction: Chain release mechanisms in polyketide and non-ribosomal peptide biosynthesis. *Nat Prod Rep*. 2022;39(1):206–7. doi:10.1039/d1np90038b.
290. Liu CW, Murray JD. The role of flavonoids in nodulation host-range specificity: an update. *Plants (Basel)*. 2016;5(3):33. doi:10.3390/plants5030033. PMID:27529286; PMCID:PMC5039741.

291. Liu SW, Zhai XX, Liu D, Liu YY, Sui LY, Luo KK, et al. Bioprospecting of actinobacterial diversity and antibacterial secondary metabolites from the sediments of four saline lakes on the Northern Tibetan Plateau. *Microorganisms*. 2023;11(10):2475. doi: 10.3390/microorganisms11102475.
292. Liu W, Cong B, Lin J, Liu S, Deng A, et al. Taxonomic identification and temperature stress tolerance mechanisms of Aequorivita marisscotiae sp. nov. Commun Biol . 2023;6:1186. doi: 10.1038/s42003-023-05559-7.
293. Liu YY, Wang Y, Walsh TR, Yi LX, Zhang R, Spencer J, et al. Emergence of plasmid-mediated colistin resistance mechanism MCR-1 in animals and human beings in China: a microbiological and molecular biological study. *Lancet Infect Dis*. 2016;16(2):161–8. doi:10.1016/S1473-3099(15)00424-7.
294. Lode H. Safety and tolerability of commonly prescribed oral antibiotics for the treatment of respiratory tract infections. *Am J Med*. 2010;123(4 Suppl):S26–38.
295. Long A, Sokal RR, Sneath PHA. *Principles of Numerical Taxonomy*. San Francisco and London: W. H. Freeman and Co.; 1963. 359 p.
296. Long Y, Jiang J, Hu X, Zhou J, Hu J, Zhou S. Actinobacterial community in Shuanghe Cave using culture-dependent and -independent approaches. *World J Microbiol Biotechnol*. 2019;35:1–12. doi: 10.1007/s11274-019-2713-y.
297. Luan T, Commichaux S, Hoffmann M, et al. Benchmarking short and long read polishing tools for nanopore assemblies: achieving near-perfect genomes for outbreak isolates. *BMC Genomics*. 2024;25:679. doi:10.1186/s12864-024-10582-x.
298. Ludwig W, Viver T, Westram R, Gago JF, Bustos-Caparros E, et al. Release LTP_12_2020: a new ARB alignment and improved 16S rRNA tree for prokaryotic type strains. *Syst Appl Microbiol.* 2021;44(5):126218. doi:10.1016/j.syapm.2021.126218.
299. Luimstra VM, Schuurmans JM, Hellingwerf KJ, Matthijs HCP, Huisman J. Blue light induces major changes in the gene expression profile of the cyanobacterium *Synechocystis* sp. PCC 6803. *Physiol Plant*. 2020;170(1):10-26. doi:10.1111/ppl.13086. PMID:32141606; PMCID:PMC7496141.
300. Ma Y, Galinski EA, Grant WD, Oren A, Ventosa A. Halophiles 2010: Life in Saline Environments. *Appl Environ Microbiol*. 2010;76:. doi:10.1128/AEM.01868-10.

301. Maldonado LA, Fragoso-Yáñez D, Pérez-García A, Rosellón-Druker J, Quintana ET. Actinobacterial diversity from marine sediments collected in Mexico. *Antonie Van Leeuwenhoek*. 2009;95(2):111–20. doi:10.1007/s10482-008-9294-3.
302. Manteca A, Alvarez R, Salazar N, Yagüe P, Sanchez J. Mycelium differentiation and antibiotic production in submerged cultures of Streptomyces coelicolor. Appl Environ Microbiol. 2008;74:3877–3886. doi: 10.1128/AEM.02715-07.
303. Mao D, Okada BK, Wu Y, Xu F, Seyedsayamdost MR. Recent advances in activating silent biosynthetic gene clusters in bacteria. *Curr Opin Microbiol*. 2018;45:156-63. doi:10.1016/j.mib.2018.05.001. PMID:29883774; PMCID:PMC6281788.
304. Margulies M, Egholm M, Altman W, Attiya S, Bader JS, Bemben LA, et al. Genome sequencing in microfabricated high-density picolitre reactors. *Nature*. 2005;437:376–80. doi: 10.1038/nature03959.
305. Mark DR, Tucker NP, Herron PR. Chromosome architecture as a determinant for biosynthetic diversity in *Micromonospora*. *Microb Genomics*. 2024;10(11):mgen001313. doi:10.1099/mgen.0.001313.
306. Matsuda S, Adachi K, Matsuo Y, et al. Salinisporamycin, a novel metabolite from *Salinispora arenicola*. *J Antibiot (Tokyo).* 2009;62(10):519–26. doi:10.1038/ja.2009.75.
307. Matsuda S, Adachi K, Matsuo Y, Nukina M, Shizuri Y. Salinisporamycin, a novel metabolite from *Salinispora arenicola*. *J Antibiot (Tokyo)*. 2009;62(9):519–26. doi:10.1038/ja.2009.75.
308. Matsue M, Mori Y, Nagase S, Sugiyama Y, Hirano R, et al. Measuring the antimicrobial activity of lauric acid against various bacteria in human gut microbiota using a new method. *Cell Transplant.* 2019;28(11):1528–41. doi:10.1177/0963689719881366.
309. Mauduit M, Derrien M, Grenier M, Greff S, Molinari S, Chevaldonné P, Simmler C, Pérez T. In situ capture and real-time enrichment of marine chemical diversity. *ACS Cent Sci.* 2023 Nov 8;9(11):2084–95. doi:10.1021/acscentsci.3c00661. PMID: 38033807; PMCID: PMC10683479.
310. Mauduit M, Derrien M, Grenier M, Greff S, Molinari S, Chevaldonné P, et al. In situ capture and real-time enrichment of marine chemical diversity. *ACS Cent Sci*.

2023;9(11):2084-95. doi:10.1021/acscentsci.3c00661. PMID:37939460; PMCID:PMC10631183.

311. McDonald BR, Currie CR. Lateral Gene Transfer Dynamics in the Ancient Bacterial Genus Streptomyces. *mBio*. 2017 Jun 6;8(3):e00644-17. doi: 10.1128/mBio.00644-17. PMID: 28588130; PMCID: PMC5472806.
312. McGuire JM, Bunch RL, Anderson RC, Boaz HE, Flynn EH, Powell HM, Smith JW. Ilotycin, a new antibiotic. *Antibiot Chemother (Northfield)*. 1952;2(6):281–3.
313. McHugh RE, Giard J, Braes RE, McKean I, Roe AJ, et al. Optimisation of aurodox production by Streptomyces goldiniensis. Access Microbiol. 2023 doi: 10.1099/acmi.0.000572.v1.
314. Medema M, Kottmann R, Yilmaz P, et al. Minimum information about a biosynthetic gene cluster. *Nat Chem Biol*. 2015;11:625–31. doi:10.1038/nchembio.1890.
315. Medema MH, Blin K, Cimermancic P, de Jager V, Zakrzewski P, Fischbach MA, et al. antiSMASH: rapid identification, annotation and analysis of secondary metabolite biosynthesis gene clusters in bacterial and fungal genome sequences. *Nucleic Acids Res*. 2011;39(Web Server issue):W339–46. doi:10.1093/nar/gkr466.
316. Meier-Kolthoff JP, Auch AF, Klenk HP, Göker M. Genome sequence-based species delimitation with confidence intervals and improved distance functions. *BMC Bioinformatics*. 2013 Feb 21;14:60. doi: 10.1186/1471-2105-14-60. PMID: 23432962; PMCID: PMC3665452.
317. Meier-Kolthoff JP, Carbasse JS, Peinado-Olarte RL, Göker M. TYGS and LPSN: a database tandem for fast and reliable genome-based classification and nomenclature of prokaryotes. *Nucleic Acids Res*. 2021;50(D1):D801–7. doi:10.1093/nar/gkab902.
318. Meier-Kolthoff JP, Hahnke RL, Petersen J, Scheuner C, Michael V, et al. Complete genome sequence of DSM 30083T, the type strain (U5/41T) of *Escherichia coli*, and a proposal for delineating subspecies in microbial taxonomy. *Stand Genomic Sci*. 2014;10:2. doi:10.1186/1944-3277-10-2.
319. Melander RJ, Zurawski DV, Melander C. Narrow-spectrum antibacterial agents. *Medchemcomm*. 2018;9(1):12–21. doi:10.1039/C7MD00528H. PMID:29527285; PMCID:PMC5839511.

320. Mikheenko A, Prjibelski A, Saveliev V, Antipov D, Gurevich A. Versatile genome assembly evaluation with QUAST-LG. *Bioinformatics*. 2018;34(13):i142–50. doi:10.1093/bioinformatics/bty266.
321. Millán-Aguiñaga N, Soldatou S, Brozio S, Munnoch JT, Howe J, et al. Awakening ancient polar *Actinobacteria*: diversity, evolution and specialized metabolite potential. *Microbiology*. 2019;165(11):1169–80. doi:10.1099/mic.0.000858.
322. Minas W, Bailey JE, Duetz W. *Streptomycetes* in micro-cultures: growth, production of secondary metabolites, and storage and retrieval in the 96-well format. *Antonie Van Leeuwenhoek*. 2000;78:297–305. doi: 10.1023/A:1010254013352.
323. Mirete S, Sánchez-Costa M, Díaz-Rullo J, González de Figueras C, Martínez-Rodríguez P, González-Pastor JE. Metagenome-Assembled Genomes (MAGs): advances, challenges, and ecological insights. *Microorganisms*. 2025;13(5):985. doi:10.3390/microorganisms13050985.
324. Mohammad Nawawi N, Ahmad A, Nallapan Maniyam M, Ibrahim A. Biotransformation of phenol by the resting cells of Rhodococcus sp. NAM 81. Indian J Fundam Appl Life Sci. 2016;6:101–107.
325. Mohanty B, Majedi SM, Pavagadhi S, Te SH, Boo CY, Gin KY, Swarup S. Effects of light and temperature on the metabolic profiling of two habitat-dependent bloom-forming cyanobacteria. *Metabolites*. 2022;12(5):406. doi:10.3390/metabo12050406. PMID:35629910; PMCID:PMC9146292.
326. Mohimani H, Gurevich A, Shlemov A, Mikheenko A, Korobeynikov A, Cao L, et al. Dereplication of microbial metabolites through database search of mass spectra. *Nat Commun*. 2018;9(1):4035. doi:10.1038/s41467-018-06082-8.
327. Mohimani H, Gurevich A, Shlemov A, Mikheenko A, Korobeynikov A, et al. Dereplication of microbial metabolites through database search of mass spectra. *Nat Commun.* 2018;9:4035. doi:10.1038/s41467-018-06082-8.
328. Mohimani H, Gurevich A, Shlemov A, Mikheenko A, Korobeynikov A, et al. Dereplication of microbial metabolites through database search of mass spectra. *Nat Commun.* 2018;9:4035. doi:10.1038/s41467-018-06082-8.
329. Moreno R, Rojo F. The importance of understanding the regulation of bacterial metabolism. *Environ Microbiol*. 2023 Jan;25(1):54-8. doi: 10.1111/1462-2920.16123. Epub 2022 Jul 20. PMID: 35859345; PMCID: PMC10084369.

330. Mukai A, Fukai T, Hoshino Y, et al. Nocardithiocin, a novel thiopeptide antibiotic, produced by pathogenic *Nocardia pseudobrasiliensis* IFM 0757. *J Antibiot*. 2009;62:613–9. doi: 10.1038/ja.2009.90.
331. Mukherjee D, Mukherjee A, Ghosh TC. Evolutionary rate heterogeneity of primary and secondary metabolic pathway genes in *Arabidopsis thaliana*. *Genome Biol Evol*. 2015;8(1):17–28. doi:10.1093/gbe/evv217. PMID:26556590; PMCID:PMC4758233.
332. Mukherjee PK. LC–MS: a rapid technique for understanding the plant metabolite analysis. In: Mukherjee PK, editor. *Quality Control and Evaluation of Herbal Drugs*. Amsterdam: Elsevier; 2019. p. 459–79. doi:10.1016/B978-0-12-813374-3.00011-9.
333. Mullowney MW, Duncan KR, Elsayed SS, et al. Artificial intelligence for natural product drug discovery. *Nat Rev Drug Discov*. 2023;22:895–916. doi: 10.1038/s41573-023-00774-7.
334. Murray CJL, Ikuta KS, Sharara F, Swetschinski L, Robles Aguilar G, Gray A, et al. Global burden of bacterial antimicrobial resistance in 2019: a systematic analysis. *Lancet*. 2022;399(10325):629–55. doi:10.1016/S0140-6736(21)02724-0.
335. Murray RGE, Holt JG. The prokaryotes: an evolving electronic resource for the microbiological community. In: Bergey's Manual of Systematic Bacteriology. 2nd ed. Vol 2. New York: Springer; 2005. p. 287–99.
336. Muscatello G, Leadon DP, Klayt M, Ocampo-Sosa A, Lewis DA, Fogarty U, et al. *Rhodococcus equi* infection in foals: the science of 'rattles'. Equine Vet J. 2007;39(5):470–8.
337. Myers OD, Sumner SJ, Li S, Barnes S, Du X. One step forward for reducing false positive and false negative compound identifications from mass spectrometry metabolomics data: new algorithms for constructing extracted ion chromatograms and detecting chromatographic peaks. *Anal Chem*. 2017;89(17):8696–703. doi:10.1021/acs.analchem.7b00947.
338. Nasser AA, Bizri AR. Chronic scalp wound infection due to *Rhodococcus equi* in an immunocompetent patient. J Infect. 2001;42:67–78.
339. National Center for Biotechnology Information (NCBI) [Internet]. Bethesda (MD): National Library of Medicine (US), National Center for Biotechnology Information; 1988 [cited 2023 Nov 11]. Available from: https://www.ncbi.nlm.nih.gov/

340. Navarro-Muñoz JC, Selem-Mojica N, Mullowney MW, et al. A computational framework to explore large-scale biosynthetic diversity. *Nat Chem Biol*. 2019;15:1009–16. doi:10.1038/s41589-019-0400-9.
341. Navarro-Muñoz JC, Selem-Mojica N, Mullowney MW, Kautsar SA, Tryon JH, Parkinson EI, et al. A computational framework to explore large-scale biosynthetic diversity. *Nat Chem Biol*. 2020;16(1):60–8. doi:10.1038/s41589-019-0400-9.
342. Navarro-Muñoz JC, Selem-Mojica N, Mullowney MW, Kautsar SA, Tryon JH, Parkinson EI, et al. A computational framework to explore large-scale biosynthetic diversity. Nat Chem Biol. 2020;16(1):60–8.
343. Nazari B, Forneris CC, Gibson MI, Moon K, Schramma KR, Seyedsayamdost MR. Nonomuraea sp. ATCC 55076 harbours the largest actinomycete chromosome to date and the kistamicin biosynthetic gene cluster. *Medchemcomm*. 2017;8(4):780–8. doi:10.1039/c6md00637j.
344. Neave M, Rachmawati R, Xun L, et al. Differential specificity between closely related corals and abundant *Endozoicomonas* endosymbionts across global scales. *ISME J*. 2017;11:186–200. doi:10.1038/ismej.2016.95.
345. Nett M, Ikeda H, Moore BS. Genomic basis for natural product biosynthetic diversity in the actinomycetes. *Nat Prod Rep*. 2009 Nov;26(11):1362–84. doi: 10.1039/b817069j. Epub 2009 Sep 1. PMID: 19844637; PMCID: PMC3063060.
346. Neu HC. In vitro activity of midecamycin, a new macrolide antibiotic. *Antimicrob Agents Chemother.* 1983;24(3):443–4.
347. Ng YK, Hodson MP, Hewavitharana AK, Bose U, Shaw PN, Fuerst JA. Effects of salinity on antibiotic production in sponge-derived *Salinispora* actinobacteria. *J Appl Microbiol.* 2014;117(1):109–25. doi:10.1111/jam.12507.
348. Ngamcharungchit C, Chaimusik N, Panbangred W, Euanorasetr J, Intra B. Bioactive metabolites from terrestrial and marine actinomycetes. *Molecules*. 2023;28(15):5915. doi:10.3390/molecules28155915.
349. Nonthakaew N, Sharkey LKR, Pidot SJ. The genus *Nocardia* as a source of new antimicrobials. *NPJ Antimicrob Resist*. 2025;3:5. doi:10.1038/s44259-025-00075-6.
350. Nordström KM, Laakso SV. Effect of growth temperature on fatty acid composition of ten thermus strains. Appl Environ Microbiol. 1992;58:1656–1660. doi: 10.1128/aem.58.5.1656-1660.1992.

351. Nothias LF, Petras D, Schmid R, Dührkop K, Rainer J, et al. Feature-based molecular networking in the GNPS analysis environment. *Nat Methods.* 2020;17(9):905–8. doi:10.1038/s41592-020-0933-6.
352. Nouioui I, Sangal V. Advanced prokaryotic systematics: the modern face of an ancient science. *New Microbes New Infect*. 2022 Nov 11;49-50:101036. doi: 10.1016/j.nmni.2022.101036. PMID: 36425013; PMCID: PMC9678754.
353. Núñez M, Naciff A, Cuadros F, Rojas C, Carvallo G, Yáñez C. Adapting to UV: integrative genomic and structural analysis in bacteria from Chilean extreme environments. *Int J Mol Sci.* 2025;26(12):5842. doi: 10.3390/ijms26125842. PMID: 40565314; PMCID: PMC12192789.
354. Nurk S, Koren S, Rhie A, Rautiainen M, Bzikadze AV, Mikheenko A, et al. The complete sequence of a human genome. *Science*. 2022;376:44–53. doi: 10.1126/science.abj6987.
355. Olsen JV, de Godoy LM, Li G, Macek B, Mortensen P, Pesch R, et al. Parts per million mass accuracy on an Orbitrap mass spectrometer via lock mass injection into a C-trap. *Mol Cell Proteomics.* 2005 Dec;4(12):2010–21. doi:10.1074/mcp.T500030-MCP200. PMID: 16249172.
356. Omura S, Iwai Y, Hirano A, Nakagawa A, Awaya J, Tsuchya H, et al. A new alkaloid AM-2282 OF *Streptomyces* origin. Taxonomy, fermentation, isolation and preliminary characterization. *J Antibiot (Tokyo)*. 1977;30(4):275–82. doi:10.7164/antibiotics.30.275.
357. Onaka H, Mori Y, Igarashi Y, Furumai T. Mycolic acid-containing bacteria induce natural-product biosynthesis in Streptomyces species. *Appl Environ Microbiol*. 2011;77(2):400-6. doi:10.1128/AEM.01337-10. PMID:21097597; PMCID:PMC3020563.
358. Ongena M, Jacques P. *Bacillus* lipopeptides: versatile weapons for plant disease biocontrol. *Trends Microbiol.* 2008;16(3):115–25. doi: 10.1016/j.tim.2007.12.009. PMID: 18289856.
359. Oren A. Industrial and environmental applications of halophilic microorganisms. *Environmental Technology*. 2010;31(8–9):825–34. doi:10.1080/09593330903370026.
360. Orlandi VT, Martegani E, Giaroni C, Baj A, Bolognese F. Bacterial pigments: a colorful palette reservoir for biotechnological applications. *Biotechnol Appl*

Biochem. 2022;69(3):981–1001. doi: 10.1002/bab.2170. PMID: 33870552; PMCID: PMC9544673.

361. Osama N, Bakeer W, Raslan M, Soliman HA, Abdelmohsen UR, Sebak M. Anti-cancer and antimicrobial potential of five soil *Streptomycetes*: a metabolomics-based study. *R Soc Open Sci*. 2022;9(2):211509. doi:10.1098/rsos.211509.
362. Ose EE. In vitro antibacterial properties of EL-870, a new semi-synthetic macrolide antibiotic. *J Antibiot (Tokyo).* 1987;40(2):190–4.
363. Osono T, Oka Y, Watanabe S, Okami Y, Umezawa H. A new antibiotic, josamycin. I. Isolation and physico-chemical characteristics. *J Antibiot.* 1967;20(3):174–80.
364. Padhi C, Field CM, Forneris CC, Olszewski D, Fraley AE, Sandu I, et al. Metagenomic study of lake microbial mats reveals protease-inhibiting antiviral peptides from a core microbiome member. *Proc Natl Acad Sci U S A*. 2024;121(49):e2409026121. doi:10.1073/pnas.2409026121. PMID:39585984; PMCID:PMC11626197.
365. Paoli L, Ruscheweyh HJ, Forneris CC, Hubrich F, Kautsar S, Bhushan A, et al. Biosynthetic potential of the global ocean microbiome. *Nature*. 2022;607(7917):111-8. doi:10.1038/s41586-022-04862-3. PMID:35794336.
366. Pardo-Esté C, Cortés J, Castro-Severyn J, Pérez V, Henriquez-Aedo K, Cuadros F, et al. Secondary metabolites with antimicrobial activity produced by thermophilic bacteria from a high-altitude hydrothermal system. *Front Microbiol.* 2024 Sep 30;15:1477458. doi:10.3389/fmicb.2024.1477458. PMID: 39411441; PMCID: PMC11474921.
367. Parra J, Beaton A, Seipke RF, Wilkinson B, Hutchings MI, Duncan KR. Antibiotics from rare actinomycetes, beyond the genus *Streptomyces*. *Curr Opin Microbiol*. 2023;76:102385. doi: 10.1016/j.mib.2023.102385.
368. Parsek MR, Greenberg EP. Acyl-homoserine lactone quorum sensing in gram-negative bacteria: a signaling mechanism involved in associations with higher organisms. *Proc Natl Acad Sci U S A*. 2000;97(16):8789–93. doi:10.1073/pnas.97.16.8789.
369. Parte AC, Sardà Carbasse J, Meier-Kolthoff JP, Reimer LC, Göker M. List of Prokaryotic names with Standing in Nomenclature (LPSN) – Actinomycetes [Internet]. Available from: https://lpsn.dsmz.de/class/actinomycetes [Accessed June 2025].

370. Pathom-Aree W, Stach JE, Ward AC, Horikoshi K, Bull AT, Goodfellow M. Diversity of actinomycetes isolated from Challenger Deep sediment (10,898 m) from the Mariana Trench. *Extremophiles*. 2006;10(3):181–9. doi:10.1007/s00792-005-0482-z.
371. Pattengale ND, Alipour M, Bininda-Emonds ORP, Moret BME, Stamatakis A. How many bootstrap replicates are necessary?. *J Comput Biol*. 2010;17:337–54. doi:10.1089/cmb.2009.0179.
372. Peek J, Lilic M, Montiel D, Milshteyn A, Woodworth I, Biggins JB, et al. Rifamycin congeners kanglemycins are active against rifampicin-resistant bacteria via a distinct mechanism. *Nat Commun*. 2018;9:4147. doi: 10.1038/s41467-018-06587-2.
373. Petersen JSPG, Grohe K, Zeiler HJ, Metzger KG. (□S,□S)- and (□R,□R)-1-Cyclopropyl-6-fluoro-1,4-dihydro-8-methoxy-7-(octahydro-6H-pyrrolo[3,4-b]pyridin-6-yl)-4-oxo-3-quinolinecarboxylic acids. *U.S. Patent* 4,990,517. 1991 Feb 12.
374. Pinnert-Sindico S, Pellerat J. Un nouvel antibiotique: la spiramycine étude de son activité in vitro. *Therapie.* 1956;11(2):308–23.
375. Pita L, Rix L, Slaby BM, et al. The sponge holobiont in a changing ocean: from microbes to ecosystems. *Microbiome*. 2018;6:46. doi:10.1186/s40168-018-0428-1.
376. Pitt JJ. Mass spectrometry in the analysis of microbial natural products—current status and future prospects. *J Microbiol Methods*. 2009;78(2):1–13. doi:10.1016/j.mimet.2009.07.010.
377. Poorinmohammad N, Bagheban-Shemirani R, Hamedi J. Genome mining for ribosomally synthesised and post-translationally modified peptides (RiPPs) reveals undiscovered bioactive potentials of actinobacteria. *Antonie Van Leeuwenhoek*. 2019;112(10):1477–99. doi:10.1007/s10482-019-01276-6.
378. Pop M. Genome assembly reborn: recent computational challenges. *Brief Bioinform*. 2009 Jul;10(4):354–66. doi: 10.1093/bib/bbp026. Epub 2009 May 29. PMID: 19482960; PMCID: PMC2691937.
379. Procópio RE, Silva IR, Martins MK, Azevedo JL, Araújo JM. Antibiotics produced by *Streptomyces*. *Braz J Infect Dis*. 2012;16(5):466–71. doi:10.1016/j.bjid.2012.08.014.

380. Puar MS, Brambilla R, Bartner P, Schumacher D, Jaret RS. Sch 23831, a novel macrolide from Micromonospora rosaria. *Tetrahedron Lett.* 1979;20:2767–70.
381. Punitha C, Sampathkumar P. Evaluation of antibacterial activity on bioactive compounds from *Dunaliella salina* by GC–MS analysis. *Int J Biol Pharm Allied Sci.* 2022;11(5):5712–5720. doi:10.31032/ijbpas/2022/11.5.5712.
382. Putnam ML, Miller ML. *Rhodococcus fascians* in herbaceous perennials. Plant Dis. 2007;91:1064–76.
383. Qiu D, Ruan J, Huang Y. Selective isolation and rapid identification of members of the genus *Micromonospora*. *Appl Environ Microbiol*. 2008;74(17):5593–7. doi:10.1128/AEM.00303-08.
384. Qiu D, Ruan J, Huang Y. Selective isolation and rapid identification of members of the genus Micromonospora. *Appl Environ Microbiol.* 2008;74(17):5593–7. doi:10.1128/AEM.00303-08.
385. Qiu X, Tang X. Metabolic adaptations of *Shewanella eurypsychrophilus* YLB-09 for survival in the high-pressure environment of the deep sea. *Front Microbiol*. 2024 Oct 17;15:1467153. doi: 10.3389/fmicb.2024.1467153. PMID: 39483757; PMCID: PMC11527400.
386. Quinn GA, Dyson PJ. Going to extremes: progress in exploring new environments for novel antibiotics. *npj Antimicrob Resist*. 2024;2:8. doi: 10.1038/s44259-024-00025-8.
387. Rambaut A. FigTree version 1.4.3 [Internet]. 2009. Available from: http://tree.bio.ed.ac.uk
388. Ramsrud AL, LaFrentz SA, LaFrentz BR, Cain KD, Call DR. Differentiating 16S rRNA alleles of *Flavobacterium psychrophilum* using a simple PCR assay. *J Fish Dis*. 2007 Mar;30(3):175–80. doi: 10.1111/j.1365-2761.2007.00795.x. PMID: 17352793.
389. Raoult D, Ogata H, Audic S, Robert C, Suhre K, Drancourt M, et al. Tropheryma whipplei Twist: a human pathogenic Actinobacteria with a reduced genome. *Genome Res*. 2003;13(8):1800–9. doi:10.1101/gr.1474603.
390. Rashad FM, Fathy HM, El-Zayat AS, Elghonaimy AM. Isolation and characterization of multifunctional *Streptomyces* species with antimicrobial,

nematicidal and phytohormone activities from marine environments in Egypt. *Microbiol Res*. 2015;175:34–47. doi:10.1016/j.micres.2015.03.002.

391. Rateb ME, Houssen WE, Arnold M, Abdelrahman MH, Deng H, Harrison WT, Okoro CK, Asenjo JA, Andrews BA, Ferguson G, Bull AT, Goodfellow M, Ebel R, Jaspars M. Chaxamycins A-D, bioactive ansamycins from a hyper-arid desert *Streptomyces* sp. *J Nat Prod*. 2011;74(6):1491-9. doi:10.1021/np200320u. PMID:21553813.
392. Raymond-Bouchard I, Tremblay J, Altshuler I, Greer CW, Whyte LG. Comparative transcriptomics of cold growth and adaptive features of a eury- and steno-psychrophile. *Front Microbiol.* 2018;9:1565. doi:10.3389/fmicb.2018.01565.
393. Raymond-Bouchard J, Tremblay I, Altshuler CW, Greer LG, Whyte LG. Comparative transcriptomics of cold growth and adaptive features of a eury- and steno-psychrophile. *Front Microbiol*. 2018;9:1565.
394. Reinhart AA, Oglesby-Sherrouse AG. Regulation of *Pseudomonas aeruginosa* virulence by distinct iron sources. *Genes.* 2016;7(12):126. doi: 10.3390/genes7120126.
395. Reynolds WF. Chapter 29 – Natural product structure elucidation by NMR spectroscopy. In: Badal S, Delgoda R, editors. *Pharmacognosy*. Boston: Academic Press; 2017. p. 567–96.
396. Richter M, Rosselló-Móra R. Shifting the genomic gold standard for the prokaryotic species definition. *Proc Natl Acad Sci U S A*. 2009 Nov 10;106(45):19126–31. doi: 10.1073/pnas.0906412106. Epub 2009 Oct 23. PMID: 19855009; PMCID: PMC2776425.
397. Richter M, Rosselló-Móra R. Shifting the genomic gold standard for the prokaryotic species definition. *Proc Natl Acad Sci U S A*. 2009 Nov 10;106(45):19126-31. doi: 10.1073/pnas.0906412106. Epub 2009 Oct 23. PMID: 19855009; PMCID: PMC2776425.
398. Robertson J, Nash JHE. MOB-suite: software tools for clustering, reconstruction and typing of plasmids from draft assemblies. *Microb Genom*. 2018;4(8):e000206. doi:10.1099/mgen.0.000206.
399. Rodríguez J, Pavía P, Montilla M, et al. Identifying triatomine symbiont *Rhodococcus rhodnii* as intestinal bacteria from *Rhodnius ecuadoriensis* (Hemiptera: Reduviidae) laboratory insects. Int J Trop Insect Sci. 2011;31:34–7.

400. Romano S, Jackson SA, Patry S, Dobson ADW. Extending the “One Strain Many Compounds” (OSMAC) Principle to Marine Microorganisms. *Mar Drugs*. 2018;16(7):244. doi:10.3390/md16070244.
401. Román-Ponce B, Millán-Aguiñaga N, Guillen-Matus D, Chase AB, Ginigini JGM, Soapi K, Feussner KD, Jensen PR, Trujillo ME. Six novel species of the obligate marine actinobacterium *Salinispora*: *S. cortesiana* sp. nov., *S. fenicalii* sp. nov., *S. goodfellowii* sp. nov., *S. mooreana* sp. nov., *S. oceanensis* sp. nov. and *S. vitiensis* sp. nov., and emended description of the genus *Salinispora*. *Int J Syst Evol Microbiol*. 2020;70(8):4668–82. doi:10.1099/ijsem.0.004330.
402. Ron EZ, Rosenberg E. Natural roles of biosurfactants. *Environ Microbiol.* 2001;3(4):229–36. doi: 10.1046/j.1462-2920.2001.00190.x. PMID: 11359505.
403. Roth B, Falco EA, Hitchings GH, Bushby SRM. 5-Benzyl-2,4-diaminopyrimidines as antibacterial agents. I. Synthesis and antibacterial activity in vitro. *J Med Pharm Chem*. 1962;5:1103–1123.
404. Rutledge P, Challis G. Discovery of microbial natural products by activation of silent biosynthetic gene clusters. *Nat Rev Microbiol*. 2015;13:509–23. doi:10.1038/nrmicro3496.
405. Rutledge PJ, Challis GL. Discovery of microbial natural products by activation of silent biosynthetic gene clusters. *Nat Rev Microbiol*. 2015;13(8):509-23. doi:10.1038/nrmicro3496.
406. Ruttkies C, Neumann S, Posch S. Improving MetFrag with statistical learning of fragment annotations. *BMC Bioinformatics.* 2019;20(1):376. doi:10.1186/s12859-019-2954-7. PMID: 31277571; PMCID: PMC6612146.
407. Safari Alighialo N, Rahimi R, Hajirezaee S, Nikookhah F. 1H NMR-based metabolomics approach to understanding the temperature-dependent pathogenicity of *Lactococcus garvieae*. *Int J Aquat Biol.* 2019;7(4):224–32. doi:10.22034/ijab.v7i4.609.
408. Saito S, Kato W, Ikeda H, et al. Discovery of “heat shock metabolites” produced by thermotolerant actinomycetes in high-temperature culture. *J Antibiot*. 2020;73:203–10. doi: 10.1038/s41429-020-0279-4.
409. Salam MA, Al-Amin MY, Salam MT, Pawar JS, Akhter N, Rabaan AA, et al. Antimicrobial resistance: a growing serious threat for global public health. *Healthcare (Basel)*. 2023;11(13):1946.

410. Salzberg SL, Phillippy AM, Zimin A, Puiu D, Magoc T, Koren S, et al. GAGE: a critical evaluation of genome assemblies and assembly algorithms. *Genome Res*. 2012 Mar;22(3):557–67. doi: 10.1101/gr.131383.111. Erratum in: *Genome Res*. 2012 Jun;22(6):1196. PMID: 22147368; PMCID: PMC3290791.
411. Sánchez Carrillo R, Guerra Ramírez P. *Pseudomonas spp.* benéficas en la agricultura. *Rev Mex Cienc Agríc*. 2022;13(4):715–25. doi:10.29312/remexca.v13i4.2799.
412. Sánchez N, Sandoval AH, Díaz-Corrales F, Serrano JA. El género *Rhodococcus*. Una revisión didáctica. Rev Soc Ven Microbiol. 2004;24(1–2):24–33.
413. Sanchez S, Demain AL. Metabolic regulation and overproduction of primary metabolites. *Microb Biotechnol*. 2008;1(4):283–319. doi:10.1111/j.1751-7915.2007.00015.x. PMID:21261849; PMCID:PMC3815394.
414. Sanders CC. Ciprofloxacin: in vitro activity, mechanism of action, and resistance. *Rev Infect Dis*. 1988;10(3):516–27.
415. Sanger F, Nicklen S, Coulson AR. DNA sequencing with chain-terminating inhibitors. *Proc Natl Acad Sci U S A*. 1977;74(12):5463–7. doi: 10.1073/pnas.74.12.5463.
416. Santamaria G, Liao C, Lindberg C, Chen Y, Wang Z, Rhee K, Pinto FR, Yan J, Xavier JB. Evolution and regulation of microbial secondary metabolism. *Elife*. 2022;11:e76119. doi:10.7554/eLife.76119. PMID:36409069; PMCID:PMC9708071.
417. Santos H, et al. Bacterial melanin: production, roles, and applications. *FEMS Microbiol Lett.* 2016;363(7):fnw070.
418. Santoyo-Garcia JH, Walls LE, Nowrouzi B, Galindo-Rodriguez GR, Ochoa-Villarreal M, et al. In situ solid–liquid extraction enhances recovery of taxadiene from engineered *Saccharomyces cerevisiae* cell factories. *Sep Purif Technol.* 2022;290:120880. doi:10.1016/j.seppur.2022.120880.
419. Sasser MC. Identification of bacteria by gas chromatography of cellular fatty acids. Technical Note # 1012001. Newark (DE): MIDI Inc.
420. Sayed AM, Hassan MH, Alhadrami HA, Hassan HM, Goodfellow M, Rateb ME. Extreme environments: microbiology leading to specialized metabolites. *J Appl Microbiol*. 2020;128:630–57. doi:10.1111/jam.14386.

421. Sayers EW, Beck J, Bolton EE, Brister JR, Chan J, Comeau DC, et al. Database resources of the National Center for Biotechnology Information. *Nucleic Acids Res*. 2024;52(D1):D33–43. doi:10.1093/nar/gkad1044. PMID:37994677; PMCID:PMC10767890.
422. Saygin H, Sahin N, Goodfellow M. Karakum desert: a unique source of cultivable novel and rare actinomycetes with a remarkable biosynthetic potential. *World J Microbiol Biotechnol*. 2025;41:202. doi: 10.1007/s11274-025-04399-3.
423. Schaffert L, Albersmeier A, Winkler A, et al. Complete genome sequence of the actinomycete *Actinoalloteichus hymeniacidonis* type strain HPA 177T isolated from a marine sponge. *Stand Genomic Sci*. 2016;11:91. doi:10.1186/s40793-016-0213-3.
424. Schalk IJ, Guillon L. Pyoverdine biosynthesis and secretion in *Pseudomonas aeruginosa*: implications for metal homeostasis. *Environ Microbiol.* 2013;15(6):1661–73. doi: 10.1111/1462-2920.12013. PMID: 23126435.
425. Schatz A, Bugie E, Waksman SA. Streptomycin, a substance exhibiting antibiotic activity against gram-positive and gram-negative bacteria. *Proc Soc Exp Biol Med*. 1944;55(1):66–69.
426. Schatz A, Bugie E, Waksman SA. Streptomycin, a substance exhibiting antibiotic activity against gram-positive and gram-negative bacteria. *Proc Soc Exp Biol Med*. 1944;55:66–9.
427. Schatz A, Waksman SA. Strain specificity and production of antibiotic substances: IV. Variations among actinomycetes, with special reference to *Actinomyces griseus*. *Proc Natl Acad Sci U S A*. 1945;31(5):129–37. doi:10.1073/pnas.31.5.129.
428. Schatz MC, Delcher AL, Salzberg SL. Assembly of large genomes using second-generation sequencing. *Genome Res*. 2010 Sep;20(9):1165-73. doi: 10.1101/gr.101360.109. Epub 2010 May 27. PMID: 20508146; PMCID: PMC2928494.
429. Schink S, Polk M, Athaide E, Mukherjee A, Ammar C, Liu X, et al. The energy requirements of ion homeostasis determine the lifespan of starving bacteria. *bioRxiv*. 2021 Nov 22. doi: 10.1101/2021.11.22.469587.
430. Schlimpert S, Elliot MA. The best of both worlds—*Streptomyces coelicolor* and *Streptomyces venezuelae* as model species for studying antibiotic production and

bacterial multicellular development. *J Bacteriol*. 2023;205(7):e0015323. doi:10.1128/jb.00153-23

431. Schmid R, Heuckeroth S, Korf A, Smirnov A, Myers O, Dyrlund TS, et al. Integrative analysis of multimodal mass spectrometry data in MZmine 3. *Nat Biotechnol*. 2023;41(4):447–9. doi:10.1038/s41587-023-01772-1.
432. Schorn MA, Alanjary MM, Aguinaldo K, Korobeynikov A, Podell S, Patin N, et al. Sequencing rare marine actinomycete genomes reveals high density of unique natural product biosynthetic gene clusters. *Microbiology (Reading)*. 2016;162(12):2075–86. doi:10.1099/mic.0.000386.
433. Schwecke T, Aparicio JF, Molnár I, König A, Khaw LE, Haydock SF, et al. The biosynthetic gene cluster for the polyketide immunosuppressant rapamycin. *Proc Natl Acad Sci U S A*. 1995;92(17):7839–43. doi:10.1073/pnas.92.17.7839.
434. Schwichtenberg AH. A new semisynthetic penicillin: sodium nafcillin. *JAMA*. 1965;191:930–1.
435. Segaran G, Sundar RDV, Settu S, Shankar S, Sathiavelu M. A review on endophytic actinomycetes and their applications. *J Chem Pharm Res*. 2017;9:152–8.
436. Seipke RF, Kaltenpoth M, Hutchings MI. *Streptomyces* as symbionts: an emerging and widespread theme? *FEMS Microbiol Rev*. 2012;36(4):862–876. doi:10.1111/j.1574-6976.2011.00313.x.
437. Seong CN, Choi JH, Baik KS. An improved selective isolation of rare actinomycetes from forest soil. *J Microbiol*. 2001;39(1):17–23.
438. Serna-Cardona N, Zamora-Leiva L, Sánchez-Carvajal E, Claverías FP, Cumsille A, Pentón KA, et al. Unveiling metabolo-genomic insights of potent antitumoral and antibiotic activity in *Streptomyces* sp. VB1 from Valparaíso Bay. *Front Microbiol*. 2024;15:1463911. doi:10.3389/fmicb.2024.1463911.
439. Seshadri R, Roux S, Huber KJ, Wu D, Yu S, Udwary D, et al. Expanding the genomic encyclopedia of Actinobacteria with 824 isolate reference genomes. *Cell Genom*. 2022 Nov 11;2(12):100213. doi: 10.1016/j.xgen.2022.100213. PMID: 36778052; PMCID: PMC9903846.
440. Seung KJ, Keshavjee S, Rich ML. Multidrug-resistant tuberculosis and extensively drug-resistant tuberculosis. *Cold Spring Harb Perspect Med*. 2015;5(9):a017863. doi:10.1101/cshperspect.a017863. PMID:25918181; PMCID:PMC4561400.

441. Shannon P, Markiel A, Ozier O, Baliga NS, Wang JT, Ramage D, et al. Cytoscape: a software environment for integrated models of biomolecular interaction networks. *Genome Res*. 2003;13(11):2498–504. doi:10.1101/gr.1239303.
442. Sharma P, Dutta J, Thakur D. Future prospects of actinobacteria in health and industry. In: Singh BP, Gupta VK, editors. *Actinobacteria: diversity and biotechnological applications*. Amsterdam: Elsevier; 2018. p.403–14.
443. Sharma V, Kaur R, Salwan R. *Streptomyces*: host for refactoring of diverse bioactive secondary metabolites. *3 Biotech*. 2021 Jul;11(7):340. doi: 10.1007/s13205-021-02872-y. Epub 2021 Jun 16. PMID: 34221811; PMCID: PMC8209132.
444. Shibayama Y, Dabbs ER, Yazawa K, Mikami Y. Functional analysis of a small cryptic plasmid pYS1 from *Nocardia*. *Plasmid*. 2011;66(1):26–37. doi:10.1016/j.plasmid.2011.04.001.
445. Shirling EB, Gottlieb D. Methods for characterization of *Streptomyces* species. *Int J Syst Evol Microbiol*. 1966;16:313–40.
446. Shukla R, Peoples AJ, Ludwig KC, Maity S, Derks MGN, De Benedetti S, et al. An antibiotic from an uncultured bacterium binds to an immutable target. *Cell*. 2023;186(19):4059-73.e27. doi:10.1016/j.cell.2023.07.038. PMID:37634690.
447. Simão FA, Waterhouse RM, Ioannidis P, Kriventseva EV, Zdobnov EM. BUSCO: assessing genome assembly and annotation completeness with single-copy orthologs. *Bioinformatics*. 2015 Oct 1;31(19):3210-2. doi: 10.1093/bioinformatics/btv351. Epub 2015 Jun 9. PMID: 26059717.
448. Simão FA, Waterhouse RM, Ioannidis P, Kriventseva EV, Zdobnov EM. BUSCO: assessing genome assembly and annotation completeness with single-copy orthologs. *Bioinformatics*. 2015;31(19):3210–2. doi:10.1093/bioinformatics/btv351.
449. Simão FA, Waterhouse RM, Ioannidis P, Kriventseva EV, Zdobnov EM. BUSCO: assessing genome assembly and annotation completeness with single-copy orthologs. *Bioinformatics*. 2015;31(19):3210–3212. doi:10.1093/bioinformatics/btv351.
450. Singhal N, Kumar M, Kanaujia PK, Virdi JS. MALDI-TOF mass spectrometry: an emerging technology for microbial identification and diagnosis. *Front Microbiol.* 2015;6:791. doi:10.3389/fmicb.2015.00791.

451. SmithKline & French Laboratories Ltd. Aminoglycoside antibiotic SCH 21420 and process for preparation thereof. US patent 5,442,047. 1995 Aug 15.
452. Soldatou S, Eldjarn GH, Ramsay A, van der Hooft JJJ, Hughes AH, Rogers S, et al. Comparative metabologenomics analysis of polar actinomycetes. *Mar Drugs*. 2021;19(2):77. doi:10.3390/md19020077.
453. Songsumanus A, Tanasupawat S, Thawai C, Suwanborirux K, Kudo T. Micromonospora humi sp. nov., isolated from peat swamp forest soil. *Int J Syst Evol Microbiol.* 2011;61(Pt 5):1176–81.
454. Stach JE, Bull AT. Estimating and comparing the diversity of marine Actinobacteria. *Antonie Van Leeuwenhoek*. 2005;87:3–9.
455. Stackebrandt E, Ebers J. Taxonomic parameters revisited: tarnished gold standards. *Microbiol Today*. 2006;33:152–5.
456. Stamatakis A. RAxML version 8: a tool for phylogenetic analysis and post-analysis of large phylogenies. *Bioinformatics*. 2014;30:1312–3. doi:10.1093/bioinformatics/btu033.
457. Starcevic A, Zucko J, Simunkovic J, Long PF, Cullum J, Hranueli D. ClustScan: an integrated program package for the semi-automatic annotation of modular biosynthetic gene clusters and in silico prediction of novel chemical structures. *Nucleic Acids Res*. 2008;36(21):6882–92. doi:10.1093/nar/gkn685.
458. Steenbergen JN, Alder J, Thorne GM, Tally FP. Daptomycin: a lipopeptide antibiotic for the treatment of serious Gram-positive infections. *J Antimicrob Chemother*. 2005;55(3):283–8. doi: 10.1093/jac/dkh546.
459. Stephens CR, et al. Preparation of 6-Deoxytetracyclines. *J Am Chem Soc*. 1958;80(19):5324–5325.
460. Stewart D, Bodey GP, LeBlanc B. In vitro studies on netilmicin, a new aminoglycoside antibiotic. *Antimicrob Agents Chemother.* 1977;11(6):1017–20. doi:10.1128/AAC.11.6.1017.
461. Strepparava N, Wahli T, Segner H, Petrini O. Detection and quantification of *Flavobacterium psychrophilum* in water and fish tissue samples by quantitative real-time PCR. *BMC Microbiol*. 2014 Apr 26;14:105. doi: 10.1186/1471-2180-14-105. PMID: 24767577; PMCID: PMC4005812.

462. Subramani R, Aalbersberg W. Culturable rare actinomycetes: diversity, isolation and marine natural product discovery. *Appl Microbiol Biotechnol*. 2013;97(21):9291–321. doi:10.1007/s00253-013-5229-7.
463. Subramani R, Sipkema D. Marine rare actinomycetes: A promising source of structurally diverse and unique novel natural products. *Mar Drugs*. 2019;17(5):249. doi:10.3390/md17050249.
464. Sugimoto Y, Camacho FR, Wang S, Chankhamjon P, Odabas A, Biswas A, et al. A metagenomic strategy for harnessing the chemical repertoire of the human microbiome. *Science*. 2019;366(6471):eaax9176. doi:10.1126/science.aax9176. PMID:31727833.
465. Sun M, Zhu B, Liu J, Qin K, Peng F. *Rhodococcus antarcticus* sp. nov., isolated from a till sample of Collins glacier front, Antarctica. *Int J Syst Evol Microbiol*. 2023;73(7).
466. Supong K, Suriyachadkun C, Tanasupawat S, Suwanborirux K, Pittayakhajonwut P, Kudo T, Thawai C. Micromonospora sediminicola sp. nov., isolated from marine sediment. *Int J Syst Evol Microbiol.* 2013;63(Pt 2):570–5. Veyisoglu A, Carro L, Cetin D, Guven K, Spröer C, Pötter G, et al. Micromonospora profundi sp. nov., isolated from deep marine sediment. *Int J Syst Evol Microbiol.* 2016;66(11):4735–43.
467. Swofford DL. *PAUP*: Phylogenetic analysis using parsimony (*and other methods*). Version 4.0b10. Sunderland: Sinauer Associates; 2002.
468. Tacconelli E, Carrara E, Savoldi A, Harbarth S, Mendelson M, Monnet DL, et al. Discovery, research, and development of new antibiotics: the WHO priority list of antibiotic-resistant bacteria and tuberculosis. *Lancet Infect Dis*. 2018;18(3):318–27.
469. Takahashi Y, Nakashima T. Actinomycetes, an inexhaustible source of naturally occurring antibiotics. *Antibiotics (Basel)*. 2018;7(2):45. doi:10.3390/antibiotics7020045.
470. Taurino C, Frattini L, Marcone GL, et al. *Actinoplanes teichomyceticus* ATCC 31121 as a cell factory for producing teicoplanin. *Microb Cell Fact*. 2011;10:82. doi: 10.1186/1475-2859-10-82.
471. te Poele EM, Samborskyy M, Oliynyk M, Leadlay PF, Bolhuis H, Dijkhuizen L. Actinomycete integrative and conjugative pMEA-like elements of *Amycolatopsis*

and *Saccharopolyspora* decoded. *Plasmid*. 2008;59(3):202–216. doi:10.1016/j.plasmid.2008.01.003.

472. Thomson JJ. Bakerian Lecture: Rays of positive electricity. *Proc R Soc Lond A*. 1913;89:1–20. doi:10.1098/rspa.1913.0057.
473. Tian S, Wang D, Yang L, et al. A systematic review of 1-Deoxy-D-xylulose-5-phosphate synthase in terpenoid biosynthesis in plants. *Plant Growth Regul*. 2022;96:221–35. doi:10.1007/s10725-021-00784-8.
474. Tindall BJ, Rossello-Mora R, Busse HJ, Ludwig W, Kämpfer P. Notes on the characterization of prokaryote strains for taxonomic purposes. *Int J Syst Evol Microbiol*. 2010;60:249–266. doi:10.1099/ijs.0.016949-0.
475. Torres-del-Pliego E, Delgado-Mejía E, Gil-Alonso L, del Mar-Periáñez-Párraga L. Primer caso de administración de ceftazidima/avibactam en hospitalización a domicilio. Bacteriemia por Klebsiella pneumoniae BLEE multirresistente. *Enferm Infecc Microbiol Clin*. 2017;35:322–3.
476. Traxler MF, Seyedsayamdost MR, Clardy J, Kolter R. Interspecies modulation of bacterial development through iron competition and siderophore piracy. *Mol Microbiol.* 2012;86(3):628–44. doi: 10.1111/mmi.12008. PMID: 22931126; PMCID: PMC3481010.
477. Traxler MF, Seyedsayamdost MR, Clardy J, Kolter R. Interspecies modulation of bacterial development through iron competition and siderophore piracy. *Mol Microbiol*. 2012;86(3):628-44. doi:10.1111/mmi.12008. PMID:22931126; PMCID:PMC3481010.
478. Traxler MF, Watrous JD, Alexandrov T, Dorrestein PC, Kolter R. Interspecies interactions stimulate diversification of the *Streptomyces coelicolor* secreted metabolome. *mBio.* 2013;4(4):e00459–13. doi: 10.1128/mBio.00459-13. PMID: 23963177; PMCID: PMC3747584.
479. Trujillo ME, Hong K, Genilloud O. Family Micromonosporaceae. In: Rosenberg E, DeLong EF, Lory S, Stackebrandt E, Thompson F, editors. *The Prokaryotes: The Actinobacteria.* Heidelberg: Springer; 2014. p. 499–569. doi:10.1007/978-3-642-30138-4_196.
480. Trujillo ME, Riesco R, Benito P, Carro L. Endophytic actinobacteria and the interaction of Micromonospora and nitrogen fixing plants. *Front Microbiol.* 2015;6:1341. doi:10.3389/fmicb.2015.01341.

481. Tsugawa H, Kind T, Nakabayashi R, Yukihira D, Tanaka W, Cajka T, et al. Hydrogen rearrangement rules: computational MS/MS fragmentation and structure elucidation using MS-FINDER software. *Anal Chem.* 2016 Aug 16;88(16):7946–58. doi:10.1021/acs.analchem.6b00770. PMID: 27419259; PMCID: PMC7063832.
482. Tsunakawa M, Hu SL, Hoshino Y, Detlefson DJ, Hill SE, Furumai T, et al. Siamycins I and II, new anti-HIV peptides: I. Fermentation, isolation, biological activity and initial characterization. *J Antibiot (Tokyo)*. 1995;48(5):433–4. doi:10.7164/antibiotics.48.433.
483. Tuttle RN, Demko AM, Patin NV, Kapono CA, Donia MS, Dorrestein P, et al. Detection of natural products and their producers in ocean sediments. *Appl Environ Microbiol*. 2019;85(8):e02830-18. doi:10.1128/AEM.02830-18. PMID:30718318; PMCID:PMC6467651.
484. Ulaganathan Y, Weber J-F, Convey P, Rizman-Idid M, Alias SA. Antimicrobial properties and the influence of temperature on secondary metabolite production in cold environment soil fungi. Polar Sci. 2017;13:34–42.
485. Undabarrena A, Valencia R, Cumsille A, Zamora-Leiva L, Castro-Nallar E, Barona-Gomez F, Cámara B. *Rhodococcus* comparative genomics reveals a phylogenomic-dependent non-ribosomal peptide synthetase distribution: insights into biosynthetic gene cluster connection to an orphan metabolite. *Microb Genom*. 2021;7(7):000621. doi:10.1099/mgen.0.000621.
486. Undabarrena A, Valencia R, Cumsille A, Zamora-Leiva L, Castro-Nallar E, Barona-Gomez F, Cámara B. *Rhodococcus* comparative genomics reveals a phylogenomic-dependent non-ribosomal peptide synthetase distribution: insights into biosynthetic gene cluster connection to an orphan metabolite. Microb Genom. 2021;7(7):000621.
487. van Bergeijk DA, Terlouw BR, Medema MH, van Wezel GP. Ecology and genomics of Actinobacteria: new concepts for natural product discovery. *Nat Rev Microbiol*. 2020;18(9):546–58. doi:10.1038/s41579-020-0379-y.
488. van der Hooft JJJ, Mohimani H, Bauermeister A, Dorrestein PC, Duncan KR, Medema MH. Linking genomics and metabolomics to chart specialized metabolic diversity. *Chem Soc Rev.* 2020 Jun 7;49(11):3297–314. doi:10.1039/D0CS00162G.

489. van der Hooft JJJ, Mohimani H, Bauermeister A, Dorrestein PC, Duncan KR, Medema MH. Linking genomics and metabolomics to chart specialized metabolic diversity. *Chem Soc Rev.* 2020 Jun 7;49(11):3297–314. doi:10.1039/D0CS00162G.
490. van der Meij A, Worsley SF, Hutchings MI, van Wezel GP. Chemical ecology of antibiotic production by actinomycetes. *FEMS Microbiol Rev*. 2017;41(3):392–416.
491. van Wezel GP, McDowall KJ. The regulation of the secondary metabolism of *Streptomyces*: new links and experimental advances. *Nat Prod Rep*. 2011;28:1311–33.
492. Ventola CL. The antibiotic resistance crisis: part 1: causes and threats. *P T*. 2015;40(4):277–83. PMID:25859123; PMCID:PMC4378521.
493. Vereecke D, Cornelis K, Temmerman W, Jaziri M, Van Montagu M, et al. Chromosomal locus that affects pathogenicity of Rhodococcus fascians. J Bacteriol. 2002;184:1112–1120. doi: 10.1128/jb.184.4.1112-1120.2002.
494. Větrovský T, Baldrian P. The variability of the 16S rRNA gene in bacterial genomes and its consequences for bacterial community analyses. *PLoS One*. 2013;8(2):e57923. doi: 10.1371/journal.pone.0057923.
495. Visick KL, Ruby EG. *Vibrio fischeri* and its host: it takes two to tango. *Curr Opin Microbiol*. 2006;9(6):632-8. doi:10.1016/j.mib.2006.10.001. PMID:17049299.
496. Wada N, Sakamoto T, Matsugo S. Multiple roles of photosynthetic and sunscreen pigments in cyanobacteria focusing on the oxidative stress. *Metabolites*. 2013;3(2):463–83. doi:10.3390/metabo3020463.
497. Waksman SA, Geiger WB, Bugie E. Micromonosporin, an antibiotic substance from a little-known group of microorganisms. *J Bacteriol.* 1947;53(3):355–7. doi:10.1128/jb.53.3.355-357.1947.
498. Waksman SA, Woodruff HB. Bacteriostatic and bactericidal substances produced by a soil *Actinomyces*. *Proc Soc Exp Biol Med*. 1940;45:609. doi: 10.3181/00379727-45-11768.
499. Waksman SA, Woodruff HB. Selective antibiotic action of various substances of microbial origin. *J Bacteriol*. 1942;44:373–84.
500. Waksman SA, Lechevalier HA. Neomycin, a new antibiotic active against streptomycin-resistant bacteria, including tuberculosis organisms. *Science.* 1949;109(2830):305–7.

501. Wali AF, Talath S, Sridhar SB, Shareef J, Goud M, Rangraze IR, Alaani NN, Mohamed OI. A comprehensive review on bioactive molecules and advanced microorganism management technologies. *Curr Issues Mol Biol*. 2024;46:13223–51. doi:10.3390/cimb46110789.
502. Walker BJ, Abeel T, Shea T, Priest M, Abouelliel A, Sakthikumar S, et al. Pilon: an integrated tool for comprehensive microbial variant detection and genome assembly improvement. *PLoS One*. 2014;9(11):e112963. doi:10.1371/journal.pone.0112963.
503. Walker BJ, Abeel T, Shea T, Priest M, Abouelliel A, Sakthikumar S, et al. Pilon: an integrated tool for comprehensive microbial variant detection and genome assembly improvement. *PLoS One*. 2014;9(11):e112963. doi:10.1371/journal.pone.0112963.
504. Waller DG, Sampson AP. Chemotherapy of infections. In: Waller DG, Sampson AP, editors. *Medical Pharmacology and Therapeutics*. 5th ed. Amsterdam: Elsevier; 2018. p. 581–629.
505. Walsh C. Where will new antibiotics come from? *Nat Rev Microbiol*. 2003;1(1):65–70.
506. Walter JD, Hunter M, Cobb M, Traeger G, Spiegel PC. Thiostrepton inhibits stable 70S ribosome binding and ribosome-dependent GTPase activation of elongation factor G and elongation factor 4. *Nucleic Acids Res*. 2012;40(1):360–70. doi:10.1093/nar/gkr623.
507. Wang DS, Xue QH, Zhu WJ, Zhao J, Duan JL, Shen GH. Microwave irradiation is a useful tool for improving isolation of actinomycetes from soil. *Mikrobiologiia*. 2013;82(1):106–14. doi:10.7868/s0026365612060183.
508. Wang H, Ding H. Dereplication of secondary metabolites from *Sophora flavescens* using an LC–MS/MS-based molecular networking strategy. *Sci Rep.* 2025;15:10148. doi:10.1038/s41598-025-94958-3.
509. Wang L, Zhang L, Zhang X, Zhang S, Yang L, Yuan H, et al. *Rhodococcus daqingensis* sp. nov., isolated from petroleum-contaminated soil. *Antonie Van Leeuwenhoek*. 2019;112(5):695–702. doi:10.1007/s10482-018-1201-y.
510. Wang M, Carver JJ, Phelan VV, Sanchez LM, Garg N, Peng Y, et al. Sharing and community curation of mass spectrometry data with Global Natural Products Social Molecular Networking. *Nat Biotechnol.* 2016;34(8):828–37. doi:10.1038/nbt.3597.

511. Wang Y, Sholeh M, Yang L, Shakourzadeh MZ, Beig M, Azizian K. Global trends of ceftazidime-avibactam resistance in gram-negative bacteria: systematic review and meta-analysis. *Antimicrob Resist Infect Control*. 2025;14(1):10. doi:10.1186/s13756-025-01518-5. PMID:39934901; PMCID:PMC11818042.
512. Wang Y, Xie J, Feng Z, Ma L, Wu W, Guo C, et al. Genomic insights into the cold adaptation and secondary metabolite potential of *Pseudoalteromonas* sp. WY3 from Antarctic krill. *Front Microbiol*. 2024;15:1459716. doi:10.3389/fmicb.2024.1459716.
513. Wang YX, Wang HB, Zhang YQ, Xu LH, Jiang CL, Li WJ. *Rhodococcus kunmingensis* sp. nov., an actinobacterium isolated from a rhizosphere soil. Int J Syst Evol Microbiol. 2008;58(6):1467–71.
514. Wang Z, Forelli N, Hernandez Y, Ternei M, Brady SF. Lapcin, a potent dual topoisomerase I/II inhibitor discovered by soil metagenome guided total chemical synthesis. *Nat Commun*. 2022;13(1):829. doi:10.1038/s41467-022-28292-0. PMID:35140156; PMCID:PMC8834480.
515. Wani AK, Akhtar N, Sher F, Navarrete AA, Américo-Pinheiro JHP. Microbial adaptation to different environmental conditions: molecular perspective of evolved genetic and cellular systems. *Arch Microbiol.* 2022 Jan 19;204(2):144. doi:10.1007/s00203-022-02757-5. PMID: 35044532.
516. Ward AL, Reddyvari P, Borisova R, Shilabin AG, Lampson BC. An inhibitory compound produced by a soil isolate of *Rhodococcus* has strong activity against the veterinary pathogen *R. equi*. PLoS One. 2018;13(12):e0209275.
517. Waters Corporation. Mass accuracy and resolution in mass spectrometry [Internet]. [cited 2025 Sep 30]. Available from: https://www.waters.com/nextgen/us/en/education/primers/the-mass-spectrometry-primer/mass-accuracy-and-resolution.htm
518. Weber T, Blin K, Duddela S, Krug D, Kim HU, Bruccoleri R, et al. antiSMASH 3.0: a comprehensive resource for the genome mining of biosynthetic gene clusters. *Nucleic Acids Res*. 2015;43(W1):W237–43. doi:10.1093/nar/gkv437.
519. Webster G, Jones C, Mullins AJ, Mahenthiralingam E. A rapid screening method for the detection of specialised metabolites from bacteria: induction and suppression of metabolites from *Burkholderia* species. *J Microbiol Methods*.

2020;178:106057. doi:10.1016/j.mimet.2020.106057. PMID:32941961; PMCID:PMC7684528.

520. Weinstein M, Wagman G, Waitz J. Discovery and isolation of sisomicin. *Infection.* 1976;4(Suppl 4):S285–8. doi:10.1007/BF01646951.
521. Wick RR, Judd LM, Wyres KL, Holt KE. Recovery of small plasmid sequences via Oxford Nanopore sequencing. *Microb Genom*. 2021;7(8):000631. doi:10.1099/mgen.0.000631.
522. Wick RR. Filtlong. 2017. Available from: https://github.com/rrwick/Filtlong
523. Wilson M, Mori T, Rückert C, et al. An environmental bacterial taxon with a large and distinct metabolic repertoire. *Nature*. 2014;506:58–62. doi:10.1038/nature12959.
524. Winker S, Woese CR. A definition of the domains Archaea, Bacteria and Eucarya in terms of small subunit ribosomal RNA characteristics. *Syst Appl Microbiol*. 1991;14(3):305–10. doi: 10.1016/S0723-2020(11)80303-6.
525. Wise R, Andrews JM, Edwards LJ. In vitro activity of Bay 09867, a new quinoline derivative, compared with those of other antimicrobial agents. *Antimicrob Agents Chemother*. 1983;23(4):559–64.
526. Wishart DS. Emerging applications of metabolomics in drug discovery and precision medicine. *Nat Rev Drug Discov.* 2016 Jul;15(7):473–84. doi:10.1038/nrd.2016.32.
527. World Health Organization. *WHO bacterial priority pathogens list 2024: bacterial pathogens of public health importance to guide research, development and strategies to prevent and control antimicrobial resistance*. Geneva: WHO; 2024. Available from: https://www.who.int/publications/i/item/9789240093461
528. Wu C, Shang Z, Lemetre C, Ternei MA, Brady SF. Cadasides, calcium-dependent acidic lipopeptides from the soil metagenome that are active against multidrug-resistant bacteria. *J Am Chem Soc*. 2019;141(9):3910-9. doi:10.1021/jacs.8b12087. PMID:30776889.
529. Wu JY, Srinivas P, Pogue JM. Cefiderocol: a novel agent for the management of multidrug-resistant gram-negative organisms. *Infect Dis Ther*. 2020;9(1):17–40. doi:10.1007/s40121-020-00286-6. PMID:32072491; PMCID:PMC7054475.

530. Wu W, Zong Z. Genome analysis-based reclassification of *Lelliottia aquatilis* as a later heterotypic synonym of *Lelliottia jeotgali*. *Int J Syst Evol Microbiol*. 2019 Apr;69(4):998-1000. doi: 10.1099/ijsem.0.003256. PMID: 30702416.
531. Xia HY, Tian YQ, Zhang R, Lin KC, Qin ZJ. Characterization of *Nocardia* plasmid pXT107. *Acta Biochim Biophys Sin (Shanghai)*. 2006;38(9):620–624. doi:10.1111/j.1745-7270.2006.00207.x.
532. Xu C, Sun X, Jin M, Zhang X. A Novel Benzoquinone Compound Isolated from Deep-Sea Hydrothermal Vent Triggers Apoptosis of Tumor Cells. *Mar Drugs*. 2017;15(7):200. doi:10.3390/md15070200.
533. Xu C, Xue C, Hou M, Geng Y, Zang R, Wu H, Zhang M. Nanopore/Illumina hybrid genome sequence resource for *Corynespora cassiicola* strain XJ infecting rubber tree in China. *Plant Dis*. 2021 Nov;105(11):3727–31. doi: 10.1094/PDIS-03-21-0458-A. Epub 2021 Nov 18. PMID: 34018814.
534. Yan S, Zeng M, Wang H, Zhang H. Micromonospora: A prolific source of bioactive secondary metabolites with therapeutic potential. *J Med Chem.* 2022;65(13):8735–71. doi:10.1021/acs.jmedchem.2c00626.
535. Yan X, Ge H, Huang T, Hindra, Yang D, Teng Q, et al. Strain prioritization and genome mining for enediyne natural products. *MBio*. 2016;7:e02104–16. doi: 10.1128/mBio.0210416.
536. Yang B, Wang Y, Qian PY. Sensitivity and correlation of hypervariable regions in 16S rRNA genes in phylogenetic analysis. *BMC Bioinformatics*. 2016;17:135. doi: 10.1186/s12859-016-0992-y.
537. Yang T, Yamada K, Zhou T, Harunari E, Igarashi Y, Terahara T, et al. Akazamicin, a cytotoxic aromatic polyketide from marine-derived *Nonomuraea* sp. *J Antibiot (Tokyo)*. 2019;72(4):202–9. doi:10.1038/s41429-018-0139-7.
538. Yarza P, Spröer C, Swiderski J, Mrotzek N, Spring S, et al. Sequencing Orphan Species initiative (SOS): filling the gaps in the 16S rRNA gene sequence database for all species with validly published names. *Syst Appl Microbiol.* 2013;36(2):69–73. doi:10.1016/j.syapm.2012.12.006.
539. Yeak KYC, Perko M, Staring G, Fernandez-Ciruelos BM, Wells JM, Abee T, Wells-Bennik MHJ. Lichenysin Production by *Bacillus licheniformis* Food Isolates and Toxicity to Human Cells. *Front Microbiol*. 2022;13:831033. doi:10.3389/fmicb.2022.831033.

540. Yokota M, Takeda U, Odaki M, Sasaki H, Niizato T, Kawaoto H, et al. Toxicological studies on a new macrolide antibiotic, midecamycin acetate (miokamycin). Part III-1. Chronic toxicity in rats. *Jpn J Antibiot.* 1984;37(7):1355–75.
541. Yuan M, Yu Y, Li HR, Dong N, Zhang XH. Phylogenetic diversity and biological activity of actinobacteria isolated from the Chukchi Shelf marine sediments in the Arctic Ocean. *Mar Drugs*. 2014;12(3):1281–97. doi: 10.3390/md12031281.
542. Yun TY, Feng RJ, Zhou DB, Pan YY, Chen YF, Wang F, et al. Optimization of fermentation conditions through response surface methodology for enhanced antibacterial metabolite production by *Streptomyces* sp. 1-14 from cassava rhizosphere. *PLoS One*. 2018 Nov 14;13(11):e0206497. doi: 10.1371/journal.pone.0206497. PMID: 30427885; PMCID: PMC6241123.
543. Zamora-Quintero AY, Torres-Beltrán M, Guillén Matus DG, Oroz-Parra I, Millán-Aguiñaga N. Rare actinobacteria isolated from the hypersaline Ojo de Liebre Lagoon as a source of novel bioactive compounds with biotechnological potential. *Microbiology (Reading)*. 2022;168(2):001144. doi:10.1099/mic.0.001144.
544. Zamora-Quintero AY, Torres-Beltrán M, Guillén-Matus DG, Oroz-Parra I, Millán-Aguiñaga N. Rare actinobacteria isolated from the hypersaline Ojo de Liebre Lagoon as a source of novel bioactive compounds with biotechnological potential. *Microbiology*. 2022;168(2):001144.
545. Zdouc MM, Blin K, Louwen NLL, Navarro J, Loureiro C, Bader CD, et al. MIBiG 4.0: advancing biosynthetic gene cluster curation through global collaboration. *Nucleic Acids Res*. 2025;53(D1):D678–90. doi:10.1093/nar/gkae1115.
546. Zdouc MM, van der Hooft JJJ, Medema MH. Metabolome-guided genome mining of RiPP natural products. *Trends Pharmacol Sci*. 2023;44(8):532–41. doi:10.1016/j.tips.2023.06.004.
547. Zeng X, Zou Y, Zheng J, Qiu S, Liu L, Wei C. Quorum sensing-mediated microbial interactions: mechanisms, applications, challenges and perspectives. *Microbiol Res.* 2023;273:127414. doi: 10.1016/j.micres.2023.127414. PMID: 37236065.
548. Zhang F, Braun DR, Chanana S, Rajski SR, Bugni TS. Phallusialides A–E, pyrrole-derived alkaloids discovered from a marine-derived *Micromonospora* sp. bacterium using MS-based metabolomics approaches. *J Nat Prod.* 2019 Dec

27;82(12):3432–9. doi:10.1021/acs.jnatprod.9b00808. PMID: 31794218; PMCID: PMC7784719.

549. Zhang YM, Rock CO. Membrane lipid homeostasis in bacteria. Nat Rev Microbiol. 2008;6:222–233. doi: 10.1038/nrmicro1839.

550. Zhang Z, Pan HX, Tang GL. New insights into bacterial type II polyketide biosynthesis [version 1; peer review: 2 approved]. *F1000Research*. 2017;6(F1000 Faculty Rev):172. doi:10.12688/f1000research.10466.1.

551. Zhao M, Zhang F, Zarnowski R, Barns K, Jones R, et al. Turbinmicin inhibits Candida biofilm growth by disrupting fungal vesicle-mediated trafficking. *J Clin Invest.* 2021;131:e145123. doi:10.1172/JCI145123.

552. Zhen C, Ge XF, Lu YT, Liu WZ. Chemical structure, properties and potential applications of surfactin, as well as advanced strategies for improving its microbial production. *AIMS Microbiol.* 2023;9(2):195–217. doi: 10.3934/microbiol.2023012. PMID: 37091822; PMCID: PMC10113169.

553. Zhou Y, Sun YB, He HW, Feng JT, Zhang X, Han LR. Optimization of medium compositions to improve a novel glycoprotein production by *Streptomyces kanasenisi* ZX01. *AMB Express*. 2017;7(1):6. doi:10.1186/s13568-016-0319-0.

554. Zhu M, Mu H, Dai X. Integrated control of bacterial growth and stress response by (p)ppGpp in *Escherichia coli*: a seesaw fashion. *iScience*. 2024 Jan 9;27(2):108818. doi: 10.1016/j.isci.2024.108818. PMID: 38299113; PMCID: PMC10828813.

555. Ziemert N, Lechner A, Wietz M, Millán-Aguinaga N, Chavarria KL, Jensen PR. Diversity and evolution of secondary metabolism in the marine actinomycete genus *Salinispora*. *Proc Natl Acad Sci U S A*. 2014;111:E1130–E1139. doi:10.1073/pnas.1324161111.

556. Ziemert N, Lechner A, Wietz M, Millán-Aguiñaga N, Chavarria KL, Jensen PR. Diversity and evolution of secondary metabolism in the marine actinomycete genus *Salinispora*. *Proc Natl Acad Sci U S A*. 2014;111:E1130–E1139.

557. Zong Z. Genome-based taxonomy for bacteria: a recent advance. *Trends Microbiol*. 2020 Nov;28(11):871-4. doi: 10.1016/j.tim.2020.09.007. Epub 2020 Sep 24. PMID: 32980201.

558. Zurenko GE, Yagi BH, Schaadt RD, Allison JW, Kilburn JO, Glickman SE, et al. In vitro activities of U-100592 and U-100766, novel oxazolidinone antibacterial agents. *Antimicrob Agents Chemother*. 1996;40(4):839–45.

Appendices

Table S3.1. Genome assembly and annotation statistics for *Rhodococcus* strains KRD162 and KRD197, obtained through hybrid assemblies combining Nanopore long reads polished with Illumina short reads. Assembly metrics include contig number, genome size, largest contig, sequencing coverage, GC content, N50, and mismatch rates. Completeness was assessed using BUSCO, and plasmid content was inferred with MOB-Recon and plasflow. Annotation was performed using Bakta via the Proksee platform, reporting coding sequences (CDSs), non-coding RNAs, tRNAs, and rRNAs. GenBank, BioSample, and BioProject accession numbers for each strain are also provided.

Genome assembly	**Flye (V.2.9.5) + Pilon tool (V. 1.20)**	
Parameter	**KRD162**	**KRD197**
Number of contigs	5	2
Total length (bp)	6060008	5393249
Largest contig (bp)	5148399	5275250
Coverage	271.77	296.61
GC%	64.34	64.13
N50 (bp)	5148399	5275250
Mismatches per 100 Kbp	0	0
Busco (complete single-copy genes)	100	100
Plasmid[a]	3	1
Genome Annotation results (Bakta pipeline)[b]		
Number of CDSs (protein)	2,237	4,860
Number of ncRNAs regions	14	13
Number of tRNAs	46	47
Number of rRNAs	12	12
GenBank accession number		
BioSample accession number	SAMN48147892	SAMN48148000
BioProject accession number	PRJNA1255561	PRJNA1255572
Complete genome assembly accession number	CP190354	CP190355

[a]The presence of plasmids in the genome sequences was inferred using MOB-Recon and plasflow in Galaxy Europe (https://usegalaxy.eu/)
[b]Genome annotation was performed using the Bakta tool through Proksee platforms (https://proksee.ca/).

a)

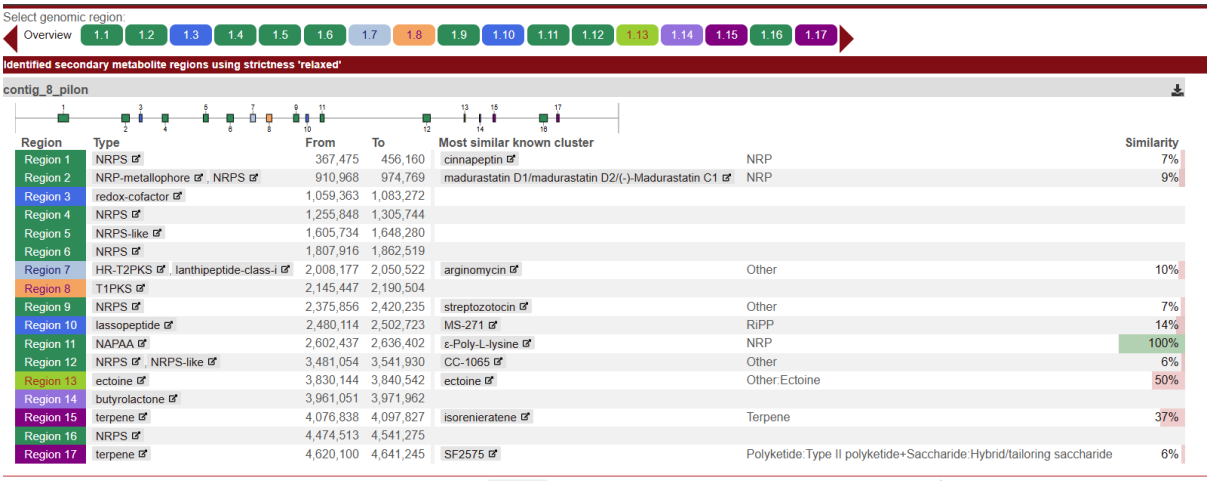

Region	Type	From	To	Most similar known cluster		Similarity
Region 1	NRPS	367,475	456,160	cinnapeptin	NRP	7%
Region 2	NRP-metallophore, NRPS	910,968	974,769	madurastatin D1/madurastatin D2/(-)-Madurastatin C1	NRP	9%
Region 3	redox-cofactor	1,059,363	1,083,272			
Region 4	NRPS	1,255,848	1,305,744			
Region 5	NRPS-like	1,605,734	1,648,280			
Region 6	NRPS	1,807,916	1,862,519			
Region 7	HR-T2PKS, lanthipeptide-class-i	2,008,177	2,050,522	arginomycin	Other	10%
Region 8	T1PKS	2,145,447	2,190,504			
Region 9	NRPS	2,375,856	2,420,235	streptozotocin	Other	7%
Region 10	lassopeptide	2,480,114	2,502,723	MS-271	RiPP	14%
Region 11	NAPAA	2,602,437	2,636,402	ε-Poly-L-lysine	NRP	100%
Region 12	NRPS, NRPS-like	3,481,054	3,541,930	CC-1065	Other	6%
Region 13	ectoine	3,830,144	3,840,542	ectoine	Other:Ectoine	50%
Region 14	butyrolactone	3,961,051	3,971,962			
Region 15	terpene	4,076,838	4,097,827	isorenieratene	Terpene	37%
Region 16	NRPS	4,474,513	4,541,275			
Region 17	terpene	4,620,100	4,641,245	SF2575	Polyketide:Type II polyketide+Saccharide:Hybrid/tailoring saccharide	6%

b)

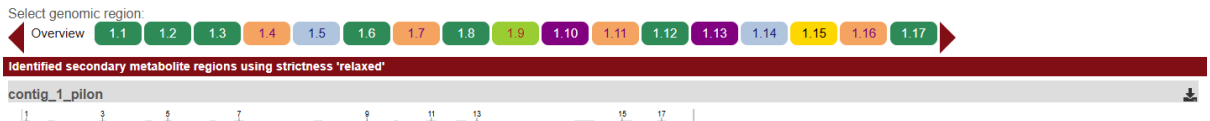

Region	Type	From	To	Most similar known cluster		Similarity
Region 1	NRPS-like	16,638	59,247			
Region 2	NRPS	208,174	257,887			
Region 3	NRPS-like	615,396	657,987			
Region 4	T1PKS	975,024	1,020,000	rubrolone A/rubrolone B	Alkaloid	11%
Region 5	NRPS, butyrolactone	1,122,885	1,173,186			
Region 6	NAPAA	1,479,377	1,519,270	ε-Poly-L-lysine	NRP	100%
Region 7	T2PKS	1,671,066	1,743,545	mayamycin	Polyketide	63%
Region 8	NRPS	2,296,661	2,354,276	CC-1065	Other	6%
Region 9	ectoine	2,706,771	2,717,169	ectoine	Other:Ectoine	50%
Region 10	terpene	2,927,281	2,948,309	isorenieratene	Terpene	42%
Region 11	PKS-like, T1PKS, arylpolyene	3,180,106	3,253,606	petrichorin A/petrichorin B	NRP	2%
Region 12	NRPS	3,417,574	3,484,333	chloramphenicol	NRP	11%
Region 13	terpene	3,563,139	3,584,317	SF2575	Polyketide:Type II polyketide+Saccharide:Hybrid/tailoring saccharide	6%
Region 14	NRPS, redox-cofactor	4,342,215	4,489,642	cinnapeptin	NRP	7%
Region 15	LAP	4,702,497	4,725,771	streptamidine	RiPP:Other	16%
Region 16	hglE-KS	4,741,109	4,787,567	vazabitide A	NRP	10%
Region 17	NRP-metallophore, NRPS	4,992,851	5,054,359	heterobactin B/heterobactin S2	NRP	63%

Figure S3.1. Predicted BGCs in the genomes of *Rhodococcus* strains (a) KRD162 and (b) KRD197 as identified by antiSMASH v8.0 (Blin *et al.,* 2025)**.** Each coloured block represents a predicted coding sequence, with annotations corresponding to biosynthetic domains or gene functions. The tables indicate the BGC type, genomic coordinates, and similarity to known clusters in the MIBiG reference database. Percent similarity reflects the degree of similarity between the predicted cluster and its closest characterised counterpart.

Table S3.2. Summary statistics for plasmid pRKRD162-A from KRD162 using Prokka tool through Proksee platforms (https://proksee.ca/). The table highlights genes predicted to be associated with plasmid stability (e.g., *parA*), antimicrobial resistance (e.g., *qacA*), mobile genetic elements (*IS110*, *IS21*, *Tn3*), recombination (e.g., *xerC*), and toxin–antitoxin systems (*higA2*, *higB2*). These features collectively suggest that pRKRD162-A may play a role in horizontal gene transfer, adaptive responses to environmental stress, and maintenance within bacterial populations.

Gene	COG	Product	Functional category
parA	–	Chromosome partitioning protein ParA	Partitioning / stability
qacA_1	COG0477	Antiseptic resistance protein	Antimicrobial resistance
qacA_2	COG0477	Antiseptic resistance protein	Antimicrobial resistance
–	–	IS110 family transposase ISMpa1	Mobile element
–	–	IS21 family transposase IS1415	Mobile element
–	–	Tn3 family transposase ISXc4	Mobile element
xerC_1	–	Tyrosine recombinase XerC	Recombination
xerC_3	COG0582	Tyrosine recombinase XerC	Recombination
higA2	–	Putative antitoxin HigA2	Toxin-antitoxin (antitoxin)
higB2	COG4683	Putative toxin HigB2	Toxin-antitoxin (toxin)

Table S3.3. Overview of the *Rhodococcus* genome assemblies that were used for comparative genomics.

Organism name	Strain	Assembly	Level	# contig/scaffold	Size megabases (Mb)	GC%
Rhodococcus globerulus	NBRC 14531	ASM189480v1	Contig	30	6.7	61.5
Rhodococcus baikonurensis	JCM 11411	ASM4048927v1	Contig	72	8.8	62.5
Rhodococcus jialingiae (*Rhodococcus qingshengii*)	DJL-6-2	ASM289396v1	Complete	4	6.7	62.5
Rhodococcus qingshengii	JCM 15477	ASM131344v1	Contig	459	7.3	62.5
Rhodococcus oryzae	NEAU-CX67	ASM504923v1	Contig	31	5.4	69
Rhodococcus hoagie (*Prescottella equi*)	DSM 20295	ASM164664v1	Contig	279	5	69
Rhodococcus equi (*Prescottella equi*)	NBRC 101255	ASM155257v1	Contig	48	5.2	69
Rhodococcus tibetensis	FXJ9.536	ASM2443803v1	Contig	63	5.8	66
Rhodococcus jostii	DSM 44719	GCA_900105375.1	Contig	6	9.9	67
Rhodococcus koreensis	DSM 44498	GCA_900105905.1	Contig	9	10.3	67.5
Rhodococcus opacus	DSM 43205	ASM4828834v1	Complete	6	9.1	67
Rhodococcus corynebacterioides	NBRC 14531	ASM189476v1	Contig	14	4	70.5
Nocardia rhizosphaerihabitans	CGMCC 4.7329	ASM1464629v1	Scaffold	26	7.7	68.5
Nocardia takedensis	NBRC 100417	ASM30869v1	Contig	266	8	69.5
Nocardia brasiliensis	NCTC 11294	49642_B01	Contig	9	8.9	68
Nocardia brasiliensis	NBRC 14402	ASM30847v2	Contig	115	8.9	68
Rhodococcus yunnanensis	NBRC 103083	ASM189500v1	Contig	68	6.4	64
Rhodococcus kyotonensis	JCM 23211	IMG-taxon 2675903021	Scaffold	50	6.3	64
Rhodococcus luteus	DSM 43673	ASM3081381v1	Contig	3	5.5	64.5
**Rhodococcus fascians*	NBRC 12155	ASM189478v1	Contig	36	5.8	64.5
Rhodococcus fascians	LMG 3623	R_fas_LMG3623	Scaffold	30	5.8	64.5
Nocardia concava	NBRC 100430	ASM30881v1	Contig	206	8.9	67.5
Rhodococcus polaris	KRD197	CP190355	Complete	5	6.0	64.13
Rhodococcus cryophilus	KRD162	CP190354	Complete	2	5.3	64.34

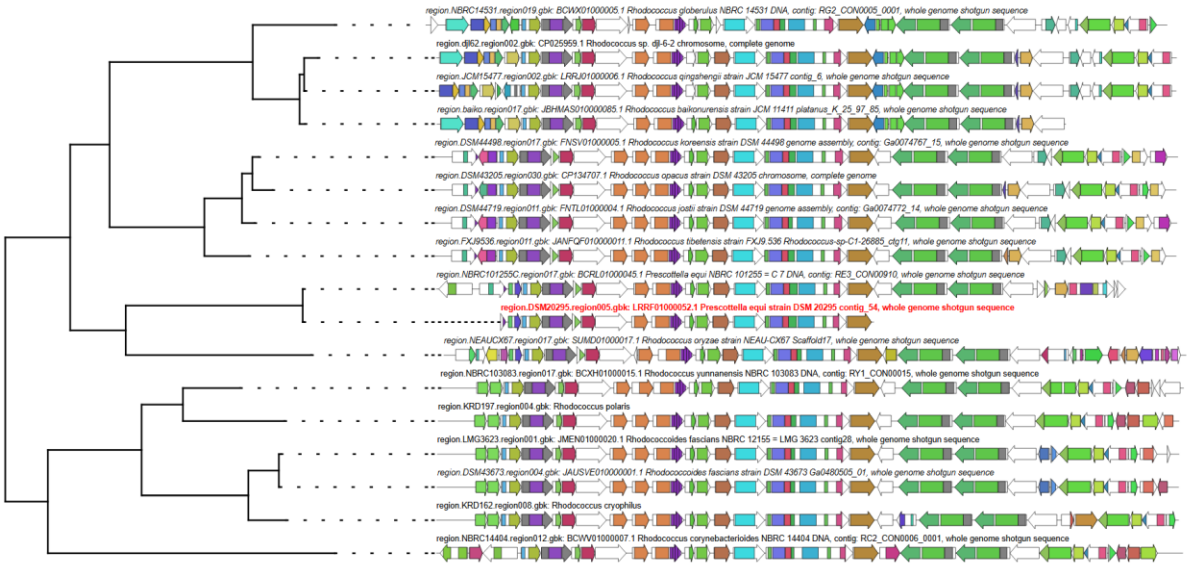

Figure S3.2. CORASON-based gene cluster tree illustrating functional and structural relationships among type I polyketide synthase (T1PKS) BGCs detected in *Rhodococcus* KRD162, KRD197, and 15 related genomes. The tree is derived from the alignment of conserved biosynthetic domains, providing a comparative representation of cluster similarity. As CORASON does not perform statistical phylogenetic inference, bootstrap values, branch length scales and formal outgroup are not included. Gene clusters are depicted as arrows indicating gene orientation and colour-coded by function, while dotted lines represent branches without sufficient genetic content for full cluster comparison.

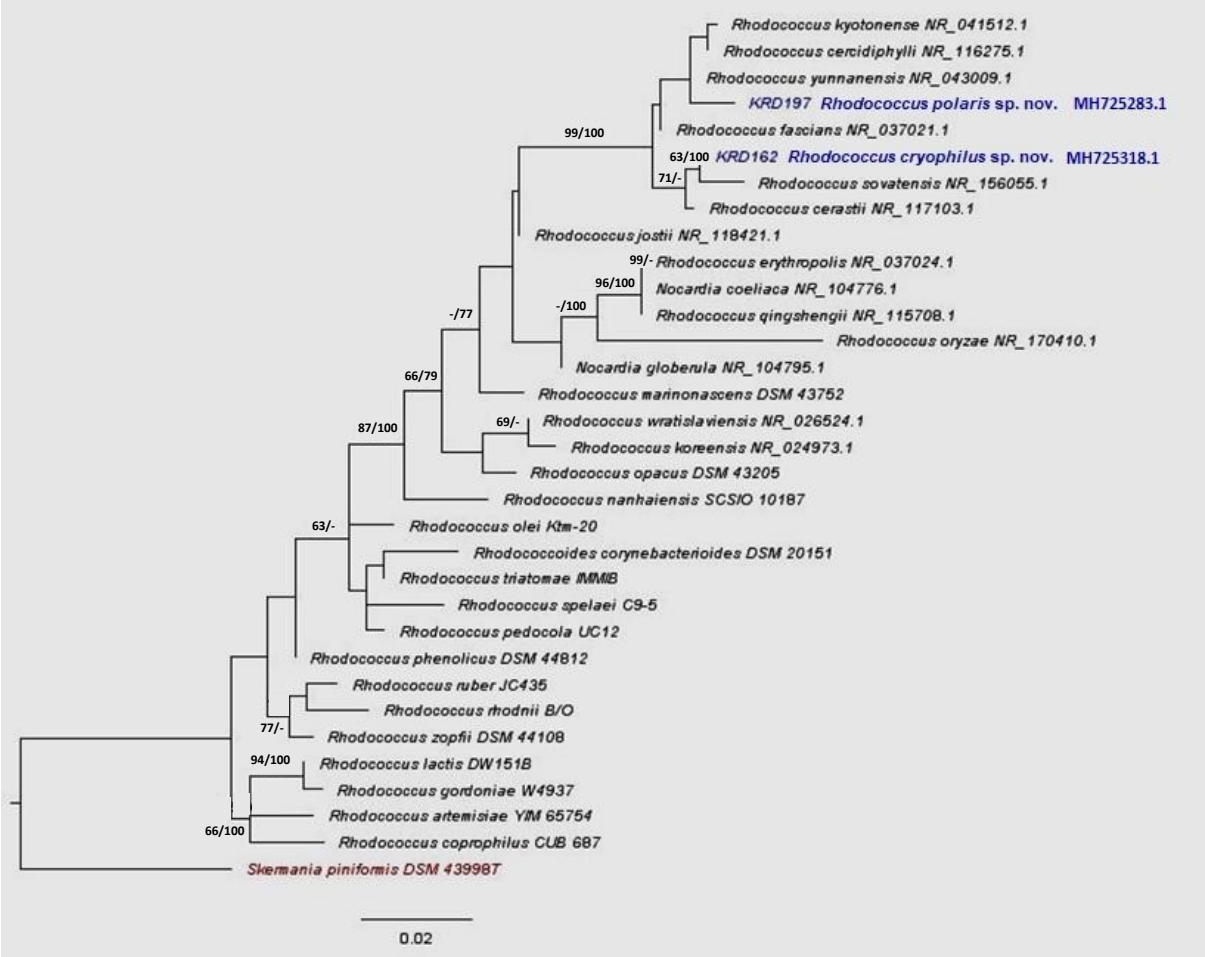

Figure S3.3. Maximum likelihood (ML) and maximum parsimony (MP) tree based on 16S rRNA gene sequences of KRD162T and KRD197T (blue) and representative members of the *Rhodococcus* genus. This shows the genetic distance between isolates and closely related Type strains (<96% similarity, NCBI accession numbers) with *Skerminia pinifornis* (red) used as an out-group. Branches are scaled in terms of the expected number of substitutions per site (scale bar, 2 nucleotides). The numbers below the branches are support values exceeding 60% of the ML (left) and MP (right) bootstrap.

Figure S3.4. Colony morphology of *Rhodococcus* strains KRD162 and KRD197 on ISP2, ISP3, and ISP5 media, compared to the reference strain *R. fascians* DSM 20669T. All strains were incubated for 7 days at 28 °C. Both Antarctic strains (KRD162 and KRD197) exhibited consistent yellow pigmentation across media, particularly on ISP2. Colony morphology was generally smooth, with less pronounced growth observed on ISP3 and ISP5, and no growth on ISP4. The reference strain showed comparable growth and pigmentation patterns, supporting the phenotypic similarity among the strains.

Strain	ISP2	ISP3	ISP5
KRD162			
KRD197	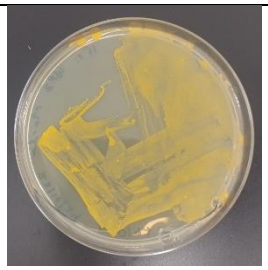		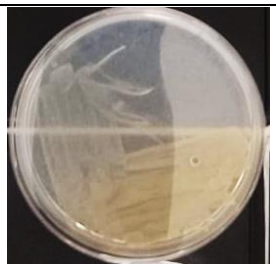
R. fascians DSM 20669^{T}			

Table S4.1. Overview of the seven *Rhodococcus* strains selected for phylogenetic and metabolomic analyses. The table details strain identifiers, geographic origin, GPS coordinates of sampling sites, and the specific isolation media employed. Five strains were obtained from Polar marine sediments and two from Scottish sediments. These strains were used to assess phylogenetic relationships and to explore metabolomic profiles under variable culture conditions.

Strain ID	Isolation location	GPS Coordinates	Isolation media	Reference
KRD162 MH725318.1	Antarctic	62 57.68S, 27 53.51W	A1	Mincer, *et al*. 2002
KRD175 MH725305.1	Arctic	79 00.01N, 06 56.84E	A1	Mincer, *et al*. 2002
KRD196 MH725284.1	Antarctic	62 11.420S, 49 29.45W	A1	Mincer, *et al.* 2002
KRD197 MH725283.1	Antarctic	58 16.15S, 24 54.26W	A1	Mincer, *et al*. 2002
KRD207	Antarctic	62 57.68S, 27 53.51W	SC	Mohseni, *et al*. 2013
KRD226	Scotland	-56° 27’ 13” N, 5° 23’ 39” W	SC	Mohseni, *et al*. 2013
KRD231	Scotland	- 56° 29’ 24” N, 5° 26’ 37” W	SC	Mohseni, *et al*. 2013

Table S4.2. *Rhodococcus* strains selected for phylogenetic analysis with closest hits in the NCBI database showing, percent identity (%ID), query cover (%QC) and sequence length.

Strain	NCBI reference strains with accession number	Percent identity	Query cover	Sequence length (base pair)
KRD162				
	Rhodococcus sovatensis NR_156055.1	99.37	99	1414
	Rhodococcus yunnanensis NR_043009.1	99.06	98	1466
	Rhodococcus cercidiphylli NR_116275.1	98.96	98	1480
	Rhodococcus jostii NR_118421.1	97.49	99	1420
	Rhodococcus spelaei NR_180470.1	96.04	99	1429
KRD175				
	Rhodococcus fascians NR_037021.1	99.89	99	1424
	Rhodococcus yunnanensis NR_043009.1	99.56	100	1466
	Rhodococcus cercidiphylli NR_116275.1	99.45	100	1480
	Nocardia globerula NR_104795.1	97.01	100	1507
	Rhodococcus pedocola NR_149270.1	96.46	99	1472
KRD196				
	Rhodococcus kyotonensis NR_041512.1	99.02	99	1420
	Rhodococcus yunnanensis NR_043009.1	98.91	99	1466
	Rhodococcus sovatensis NR_156055.1	98.37	99	1414
	Rhodococcus qingshengii NR_115708.1	97.29	99	1489
	Rhodococcus spelaei NR_180470.1	96.19	99	1429
KRD197				
	Rhodococcus yunnanensis NR_043009.1	98.91	100	1466
	Rhodococcus cercidiphylli NR_116275.1	98.80	100	1480
	Rhodococcus kyotonensis NR_041512.1	99.22	98	1420
	Rhodococcus jostii NR_118421.1	97.06	100	1420
	Rhodococcus olei NR_179708.1	96.07	100	1455
KRD207				
	Rhodococcus cerastii NR_117103.1	99.56	97	1337
	Rhodococcus sovatensis NR_156055.1	99.24	99	1414
	Rhodococcus cercidiphylli NR_116275.1	99.03	100	1480
	Rhodococcus koreensis NR_024973.1	97.28	100	1473
	Rhodococcus nanhaiensis NR_109481.1	96.09	99	1400
KRD226				
	Nocardia coeliaca NR_104776.1	99.89	100	1507
	Rhodococcus qingshengii NR_115708.1	99.89	100	1489
	Rhodococcus erythropolis NR_037024.1	99.89	100	1476
	Rhodococcus jostii NR_118421.1	98.12	100	1420
	Rhodococcus oryzae NR_170410.1	97.00	100	1474
KRD231				
	Nocardia coeliaca NR_104776.1	98.47	100	1507
	Rhodococcus jostii NR_118421.1	98.40	100	1420
	Rhodococcus spelaei NR_180470.1	97.02	99	1429
	Rhodococcus corynebacterioides NR_041873.1	96.01	100	1494
	Rhodococcus kyotonensis NR_041512.1	95.56	99	1420

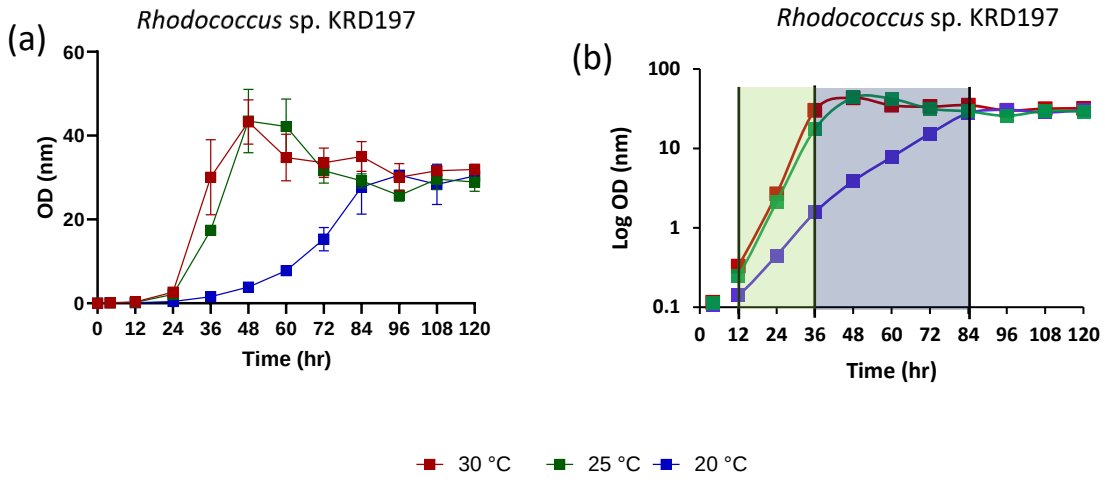

Figure S4.1. *Rhodococcus* KRD197 cell density over time when cultivated at 20 °C, 25 °C, and 30 °C in ISP2 medium. Data points represent the mean of three biological replicates, and error bars indicate the standard deviation. (a) Growth curve: time (hours) is plotted on the x-axis, and optical density at 600 nm (OD_{600}) on the y-axis. (b) Logarithmic growth curve: time (hours) is on the x-axis, and the logarithmic scale of OD_{600} on the y-axis. Green and blue shading highlight the exponential growth phase, occurring between 12–36 h at 30 °C and 25 °C, and 12–84 h at 20 °C, respectively.

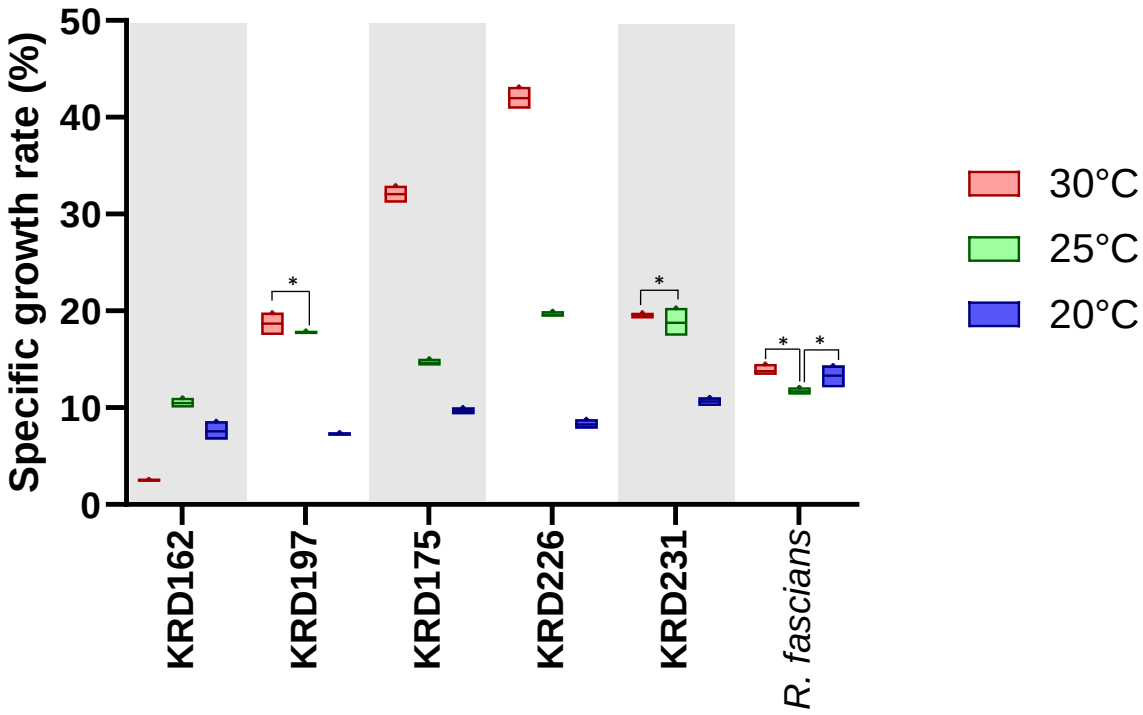

Figure S4.2. Box plots showing the specific growth rates of the six *Rhodococcus* strains (KRD162, KRD197, KRD175, KRD226, KRD231 and *R. fascians*) grown at three different temperatures: 30 °C (red), 25 °C (green) and 20 °C (blue). Boxplots show the range from 5 to 95% with the mean values as thick lines. P values are based on a between-temperatures t test. The asterisk and the lines mark the temperatures that do NOT show significant P values (P>0.05).

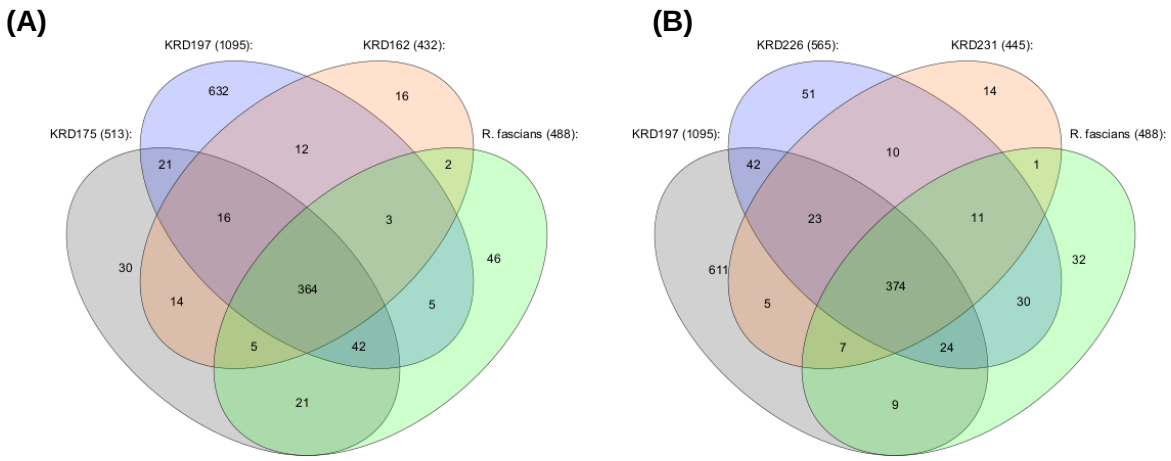

Figure S4.3. Euler diagram depicting the distribution of features detected across all *Rhodococcus* metabolites extracts. Specific and shared features among (A) Arctic/Antarctic *Rhodococcus* strains and (B) KRD197 compared with Scottish *Rhodococcus* strains. Specific features represent metabolites unique to individual strains, whereas shared features correspond to metabolites detected in multiple strains.

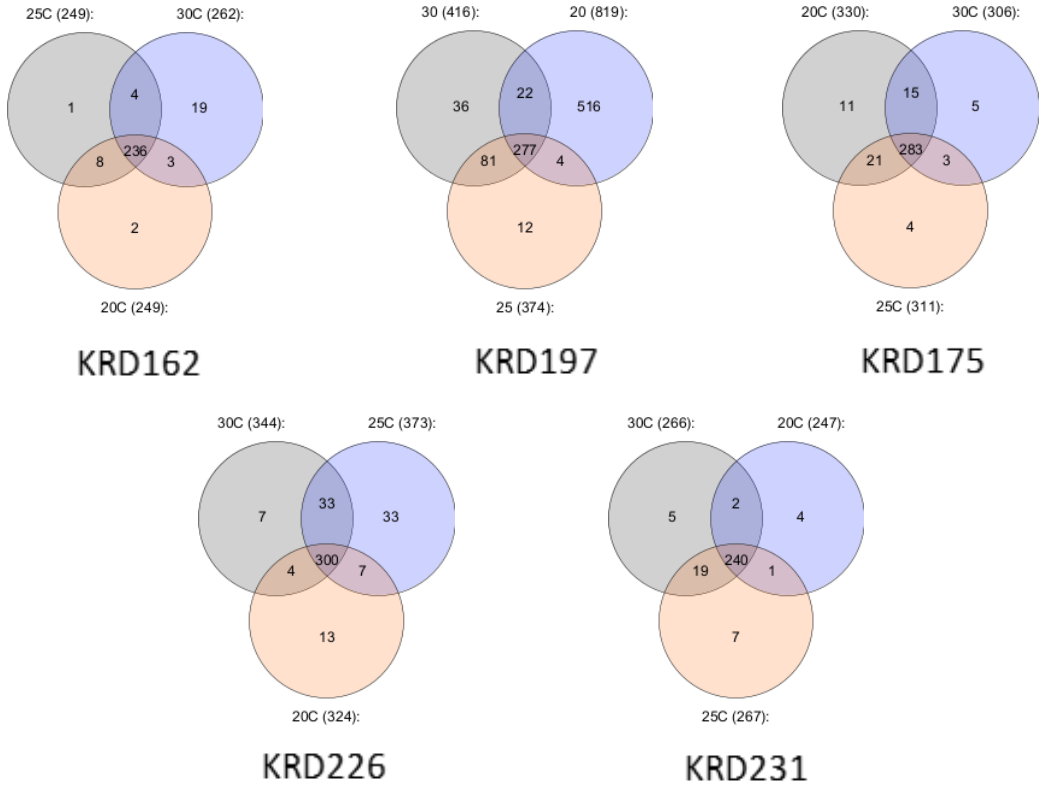

Figure S4.4. **Venn diagrams showing the distribution of metabolites produced by *Rhodococcus* strains (KRD162, KRD197, KRD175, KRD226, KRD231) at three different temperatures (20 °C, 25 °C, and 30 °C).** Strain-specific and shared metabolites are represented and colours indicate temperature: grey (30 °C), pink (25 °C), and purple (20 °C).

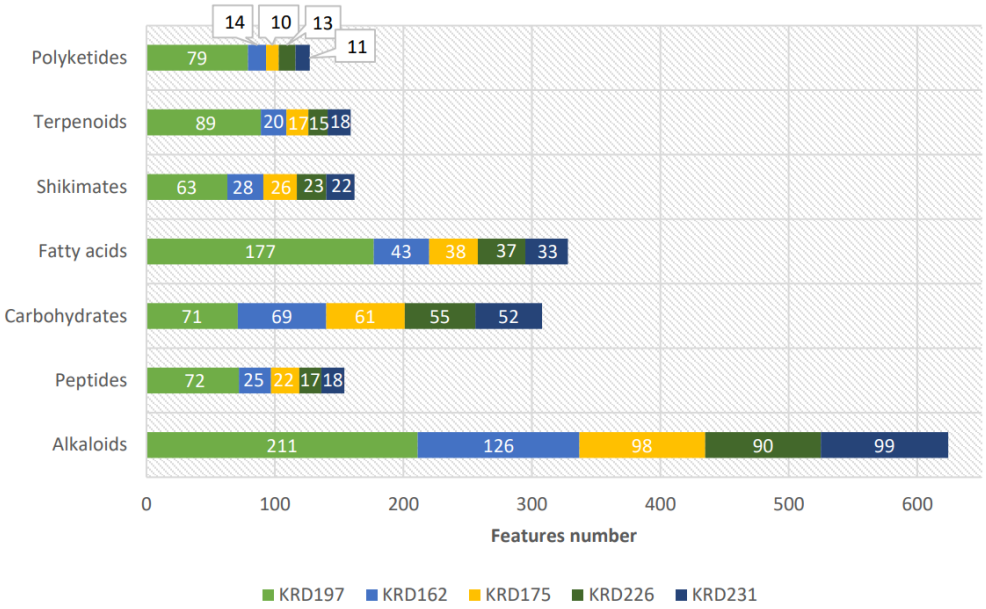

Figure S4.5. Number of metabolites per biosynthetic pathways for all *Rhodococcus* strains analysed at different temperatures (30 °C, 25 °C, and 20 °C). The biosynthetic pathways identified include alkaloids, amino acids and peptides, carbohydrates, fatty acids, polyketides, terpenoids, and shikimates/phenylpropanoids.

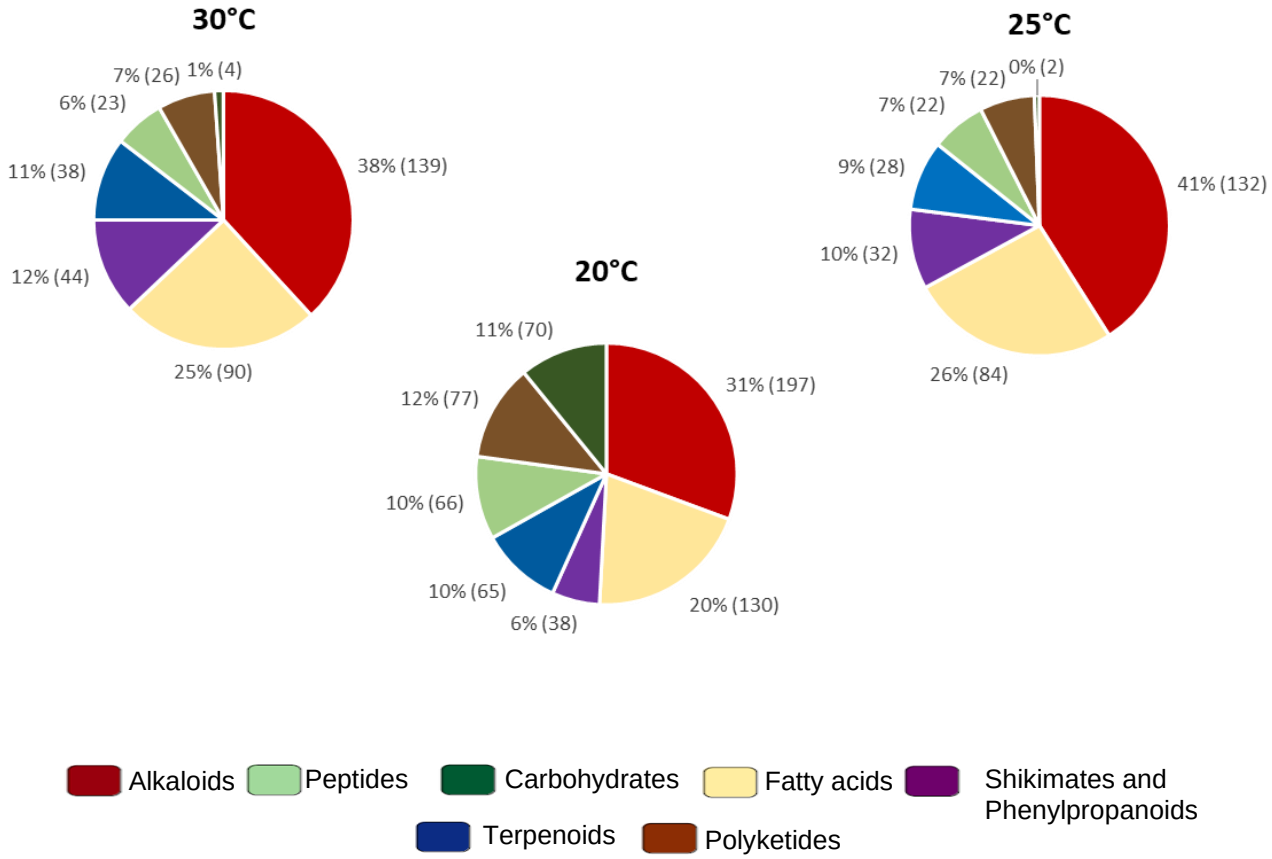

Figure S4.6. Pie chart illustrating the distribution of chemical classes produced by the *Rhodococcus* strain KRD197 across three incubation temperatures (20 °C, 25 °C, and 30 °C). Metabolites were categorised based on their biosynthetic pathways into alkaloids, amino acids and peptides, carbohydrates, fatty acids, polyketides, terpenoids, and shikimates/phenylpropanoids.

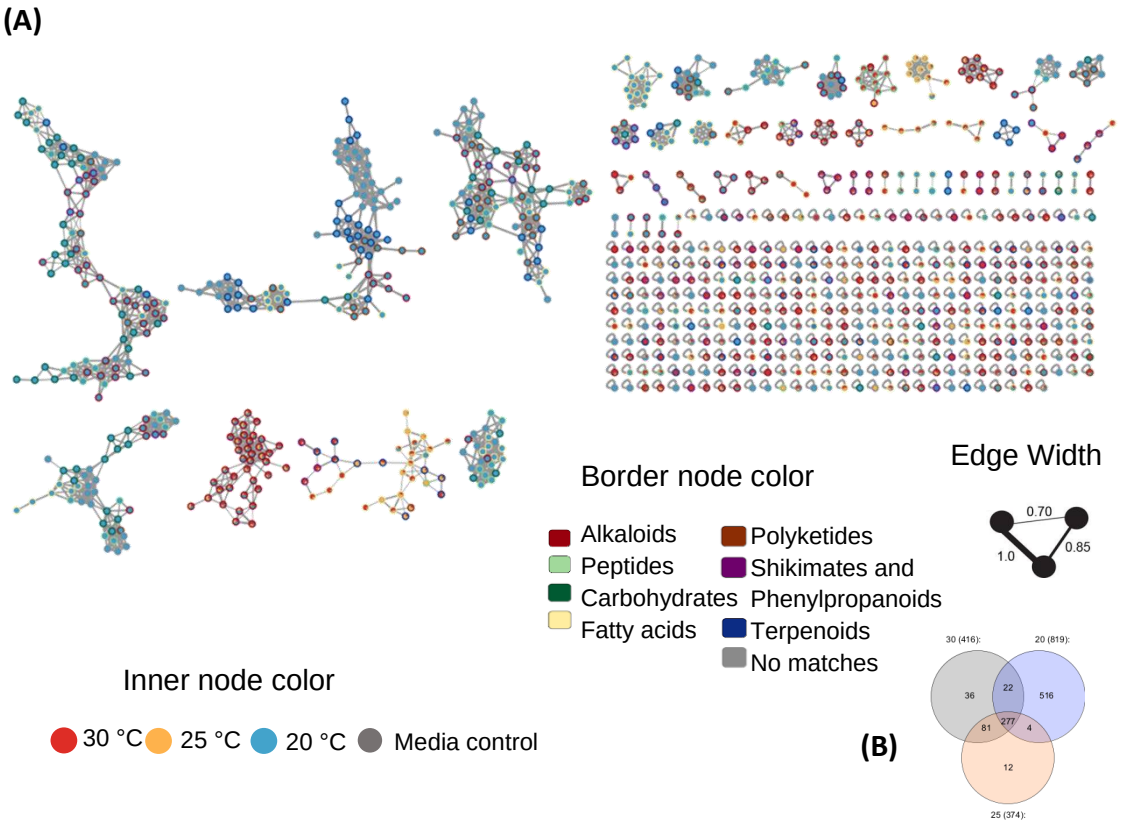

Figure S4.7. (A) Feature based molecular networking of *Rhodococcus* KRD197 at 20 °C, 25 °C and 30 °C. Inner pie chart node color represents the presence of each feature across the three temperatures; grey represents features found in solvent/media controls. Border node color represents the chemical class annotation by SIRIUS/CONAPUS, features without matches are colored grey. (B) Venn diagram of the number of strain specific and shared metabolites produced by KRD197 *Rhodococcus* strain across three temperatures.

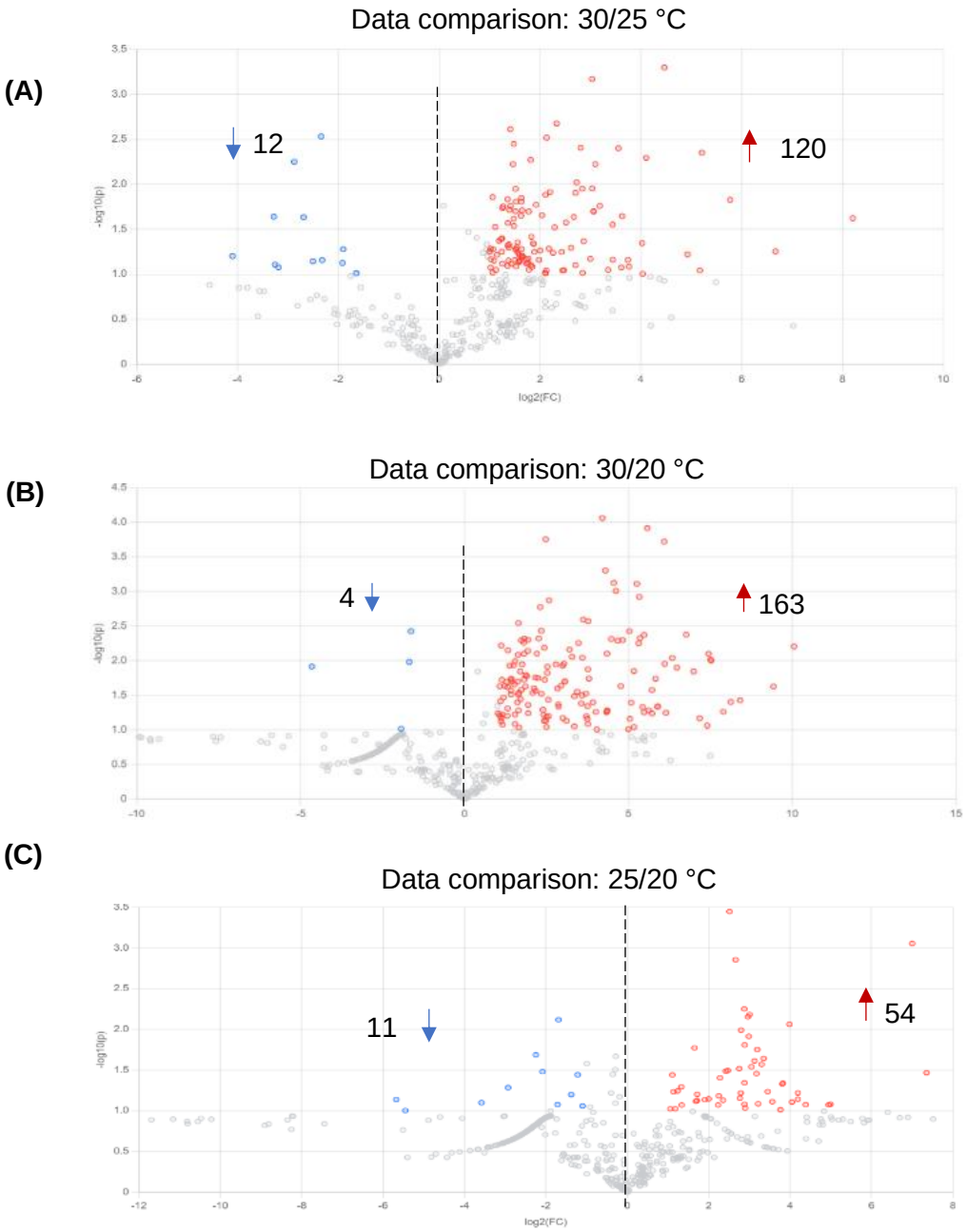

Figure S4.8. Volcano-plot of detected LC–MS/MS metabolite features in KRD197 cultured at 20 °C, 25 °C and 30 °C. The x-axis is the mean ratio fold-change (plotted on a log 2 scale) of the relative abundance of each metabolite between the two samples selected. The y-axis represents the statistical significance p-value (threshold: 0.1) of the ratio fold-change (threshold: 2.0) for each metabolite. Red dots/arrow indicate peaks increased by the higher temperature compared, blue indicates peaks decreased by higher temperature and the numbers represent the number of features with significant change. Grey dots represent metabolites detected, but that are not significantly different

by temperature. (A) Comparison between 30 °C and 25 °C, (B) comparison between 30 °C and 20 °C, and (C) comparison between 25 °C and 20 °C.

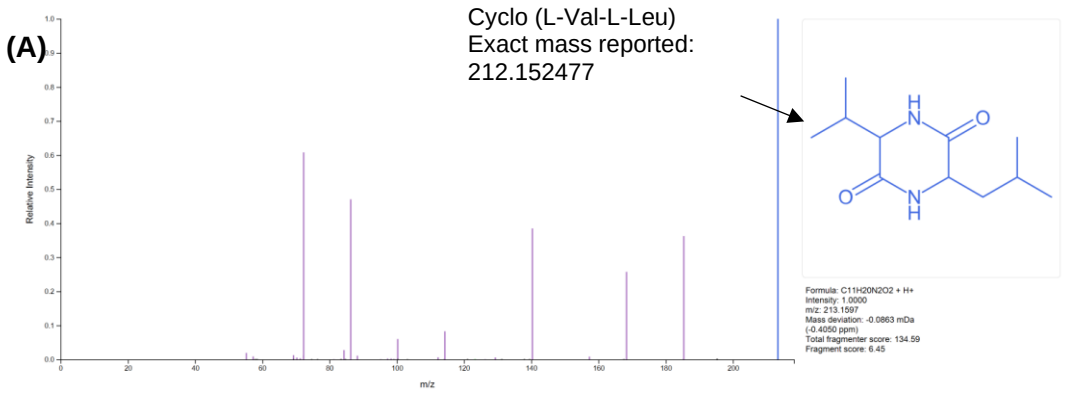

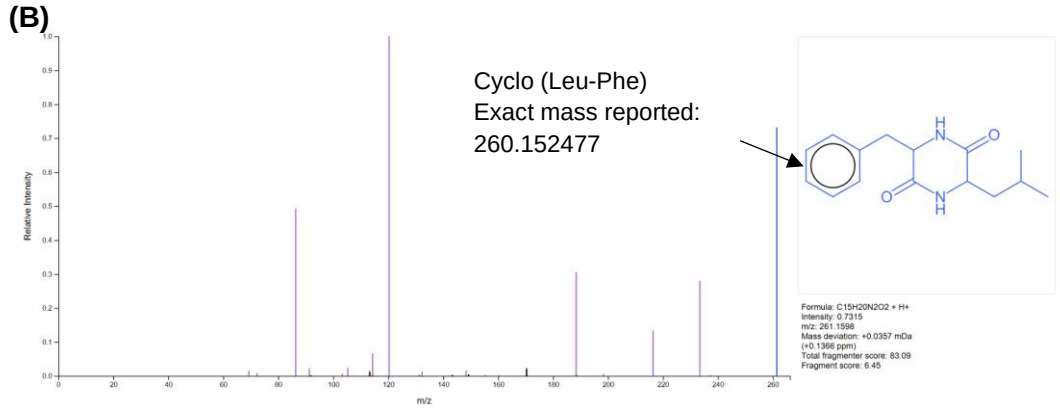

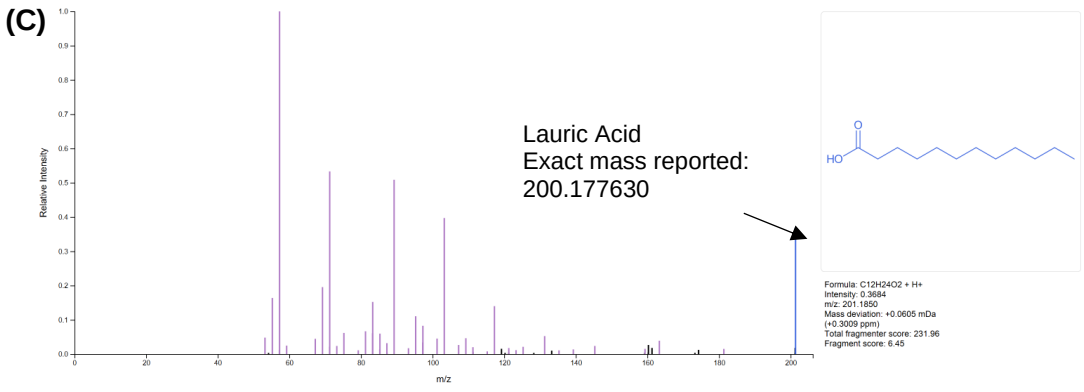

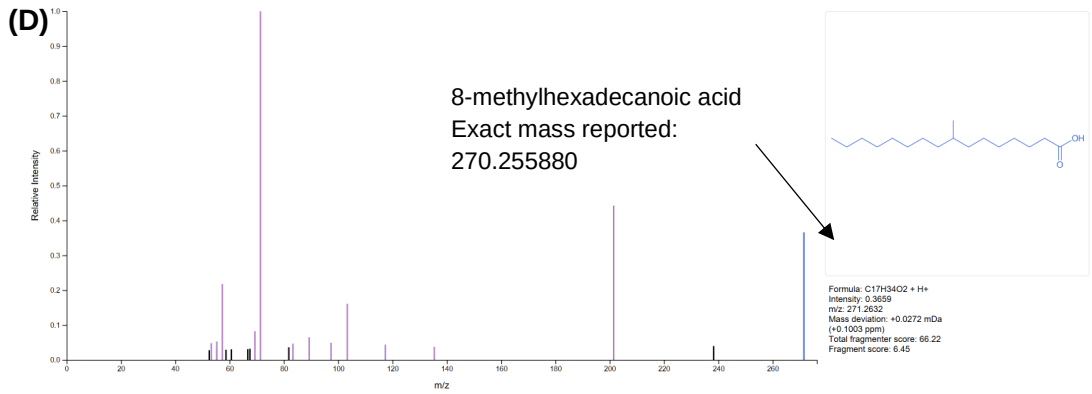

Figure S4.9. SIRIUS-annotated MS2 spectra acquired by UHPLC-Orbitrap MS/MS in positive mode: (a) Cyclo-(l-Val-l-Leu) (*m/z* $[M + H]^+$ 213.597), (b) Cyclo-(Leu-Phe) (*m/z* $[M + H]^+$ 261.1598), (c) Lauric Acid (*m/z* $[M + H]^+$ 201.1850) and (d) 8-methylhexadecanoic acid (*m/z* $[M + H]^+$ 271.2632). The exact mass reported of the compounds corresponds to the experimental data obtained in this work. The compound structure and the metadata below each structure (molecular formula, intensity, *m/z*, mass deviation in mDa, total fragmenter score, and fragment score) were predicted and annotated by SIRIUS (v5.8.6).

Note: The median mass error reported in the main text is expressed in ppm and represents the median difference between experimental and theoretical fragment masses. The mass deviation reported by SIRIUS in this figure refers to the spread (dispersion) of these errors and is expressed in mDa.

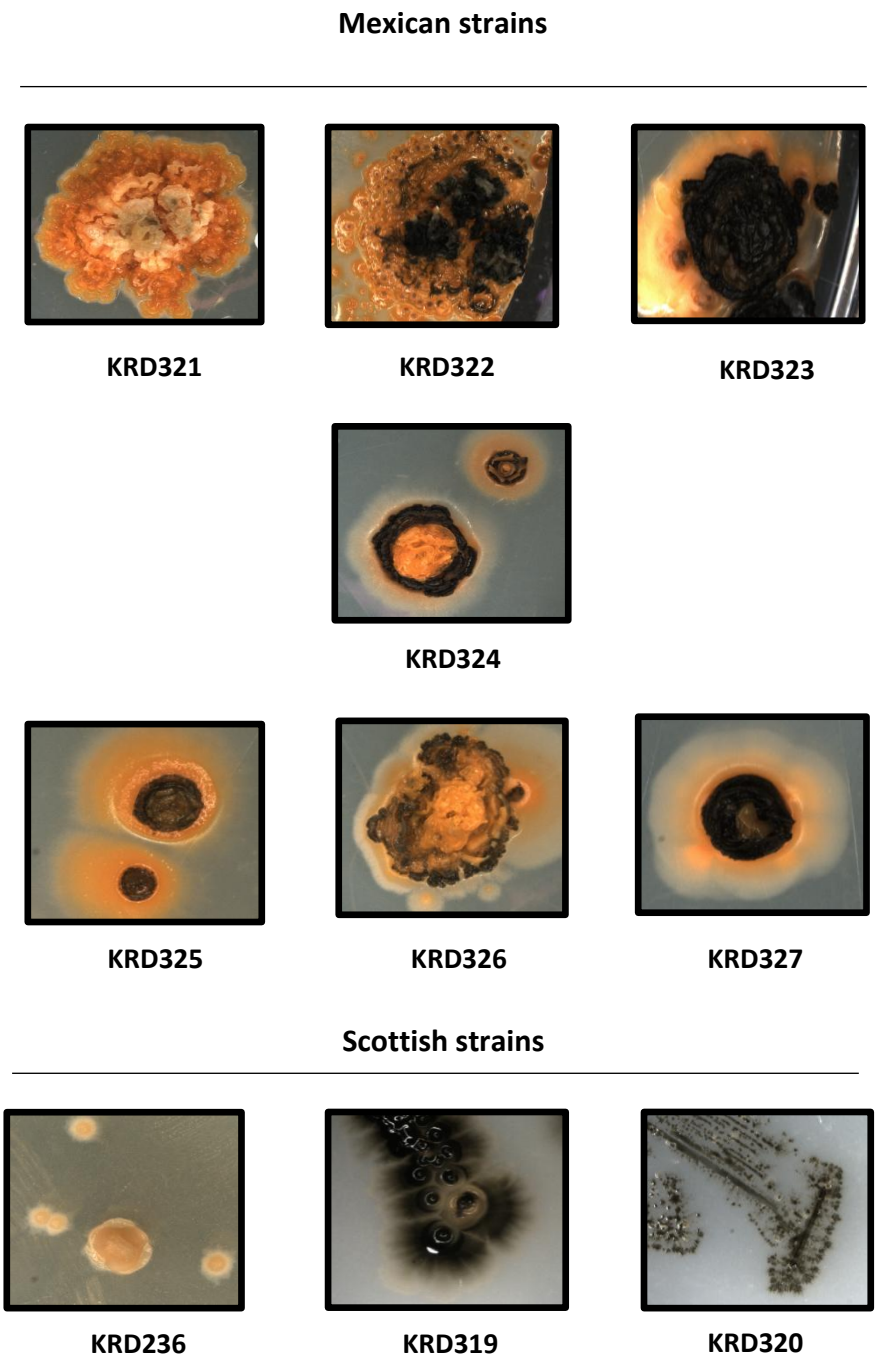

Figure S5.1. Colony morphology of *Micromonospora* strains, seven from Mexico (KRD321, KRD322, KRD323, KRD324, KRD325, KRD326, KRD327) and three from Scotland (KRD236, KRD319 and 320) from the Duncan lab bacterial culture collection, cultured on A1 medium. Images taken with a Leica stereomicroscope.

Table S5.1. *Micromonospora* strains (KRD) for phylogenetic analysis with closest hits from the NCBI database showing accession numbers, percent identity (%ID), query coverage (%QC) and sequence length (base pair) for each KRD strain.

Strain	Sequence length (bp)	NCBI reference strains with accession number	Percent identity	Query coverage
KRD321	831			
		Micromonospora spongicola NR_169445.1	100	100
KRD322	799			
		Micromonospora spongicola NR_169445.1	100	100
KRD323	805			
		Micromonospora spongicola NR_169445.1	100	100
KRD324	816			
		Micromonospora spongicola NR_169445.1	100	97
KRD325	829			
		Micromonospora spongicola NR_169445.1	100	100
KRD326	817			
		Micromonospora spongicola NR_169445.1	100	100
KRD327	498			
		Micromonospora spongicola NR_169445.1	100	100
KRD236	817			
		Micromonospora maritima NR_109311.1	99.77	100
KRD319	1901			
		Micromonospora aurantiaca NR_074415.1	100	100
KRD320	2123			
		Micromonospora aurantiaca NR_074415.1	99.45	100

(a)

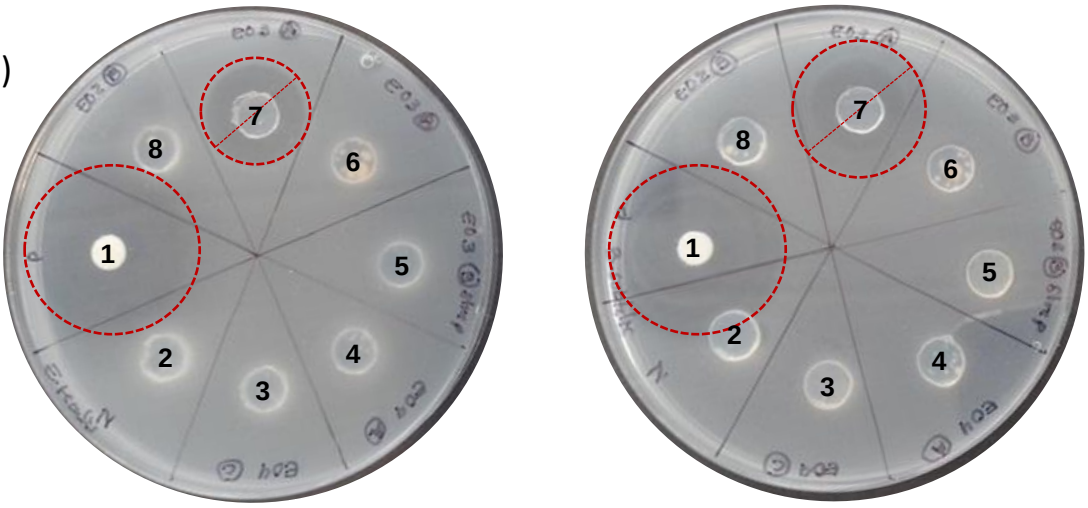

E. faecalis ***B. subtilis***

(b)

Code number on Petri dish	Strain	*B. subtilis* Diameter (mm)	*E. faecalis* Diameter (mm)
1	**Positive control**	30	32
2	**Negative control**	0	0
3	KRD326	0	0
4	KRD327	0	0
5	KRD321	0	0
6	KRD322	0	0
7	KRD324	26	18
8	KRD323	0	0
9	KRD325	0	0

Figure S5.2. Bioactivity assay using bacterial plug method. (a) Seven Mexican *Micromonospora* strains (KRD325 not show) grown on A1 medium were tested for antibacterial activity against *Enterococcus faecalis* ATCC 51299 (left) and *Bacillus subtilis* ATCC 23857 (right). Zones of inhibition (highlighted with red dashed circles) were measured to assess antibacterial activity. Gentamicin (10 µg/µL) was used as a positive control, and plain A1 medium plugs were used as a negative control. (b) Table summarising the diameter of inhibition zones (in mm) for the seven Mexican *Micromonospora* strains tested, along with their corresponding code numbers.

Table S5.2. **Sample recovery and molecular features of *Micromonospora* strains cultured under varying salinity conditions.** Strains were grown at salinities of 0‰, 15‰, 25‰, 35‰, and 40‰ (w/v). (a) Recovery status of biological triplicate cultures for metabolite extracts (green: samples recovered and red: samples lost due to fungal contamination). The number of nodes (molecular features) detected per extract based on LC-MS/MS data, with average values calculated for each strain and condition are show for (b) Mexican and (c) Scottish strains.

(a)

	Sample recovery for metabolite extraction																				
	Strains isolated from Mexico									Isolated from Scotland									Control		
Salinity (%)	KRD324			KRD327			KRD321			KRD236			KRD319			KRD320			Media A1		
0	A	B	C	A	B	C	A	B	C	A	B	C	A	B	C	A	B	C	A	B	C
15	A	B	C	A	B	C	A	B	C	A	B	C	A	B	C	A	B	C	A	B	C
25	A	B	C	A	B	C	A	B	C	A	B	C	A	B	C	A	B	C	A	B	C
35	A	B	C	A	B	C	A	B	C	A	B	C	A	B	C	A	B	C	A	B	C
40	A	B	C	A	B	C	A	B	C	A	B	C	A	B	C	A	B	C	A	B	C

(b)

	Molecular features of strains isolated from Mexico										
Salinity (‰)	KRD324			Average	KRD327			Average	KRD321			Average
0	645	252	-	448.5	237	237	287	253.6	301	258	243	267.3
15	298	762	341	467	320	475	327	374	306	-	-	306
25	355	356	-	355.5	344	309	275	309.3	281	301	293	291.6
35	359	250	294	301	245	291	322	286	280	330	332	314
40	286	253	-	269.5	280	316	342	346	404	298	278	326.6

(c)

	Molecular features of strains isolated from Scotland											
Salinity (‰)	KRD236			Average	KRD319			Average	KRD320			Average
0	239	262	236	245.6	735	692	661	696	327	320	-	323.5
15	232	309	337	292	392	420	391	401	373	689	-	531
25	553	687	366	535.3	701	620	676	665.6	706	706	425	612.3
35	289	362	614	421.6	510	484	744	579.3	701	697	-	699
40	662	391	603	552	736	447	702	628.3	692	670	-	681

Table S5.3. Curated list of putative metabolite identifications obtained via DEREPLICATOR+ for *Micromonospora* strains cultivated under all salinity conditions tested (0‰, 15‰, 25‰, 35‰ and 40‰ [w/v]). From a total of 115 matches, the 13 highest-confidence annotations are shown, filtered by ppm error and similarity score. Putative metabolite identifications were assigned based on spectral similarity scores against the DEREPLICATOR+ database. Shown values include compound name, PeptideMass (theoretical mass of the candidate metabolite), SpecMZ (experimental *m/z* value observed in the MS spectrum), score, retention time, mass difference, and adduct. All annotations remain tentative and were not confirmed by authentic standards.

Metabolite name	Similarity score	Peptide Mass (theoretical)	SpecMZ: (experimental m/z)	Retention time	MassDiff	Adduct
Salinilactam A	30	469.283	470.29	255.532	-2.00E-05	M+H
Dracolactam B	21	485.278	486.285	231.689	8.00E-05	M+H
Protylonolide	21	394.272	395.279	317.805	-0.00012	M+H
Rosamicin	20	581.356	582.364	264.63	-0.00092	M+H
Antibiotic_Sch_23831	19	560.346	281.18	258.887	-0.00044	M+2H
Rifamycin S	19	695.294	696.302	450.535	-0.00062	M+H
Cirramycin A/A1	18	597.351	598.359	247.043	-0.00092	M+H
Amycolactam	16	314.163	315.17	281.598	-0.00012	M+H
Leucomycin V	14	701.8	743.41	232.41	-0.00024	M+2H
Pyracrimycin A	13	138.08	139.09	42.95	-0.00032	M+H
Juvenimicin B	13	583.372	584.379	43.276	-2.00E-05	M+H
Sporeamicin-C	12	685.404	686.411	234.331	0.00018	M+H
Izenamicin B2	12	553.361	554.369	252.033	-0.00102	M+H

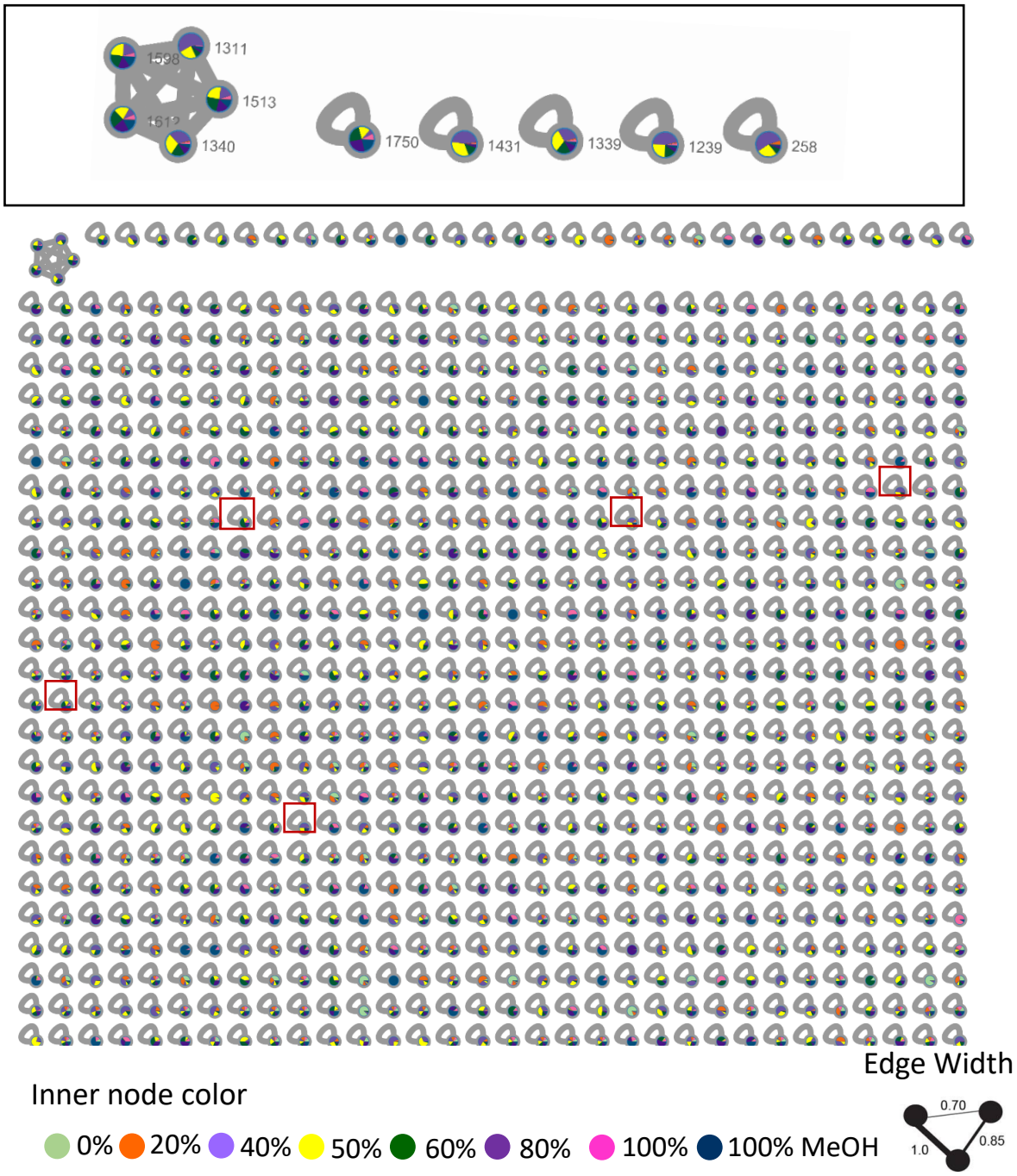

Figure S5.3. Feature-based molecular network (FBMN) of *Micromonospora* sp. KRD324 cultivated in A1 broth at 15‰ salinity. Node colours indicate the fraction in which each compound was detected, according to the percentage of acetonitrile used during C18 column fractionation (0-100%). Nodes outlined with a black box correspond to a molecular family related to juvenimicin-like compounds. Red square shows metabolites identified as putative juvenimicines.

(A)

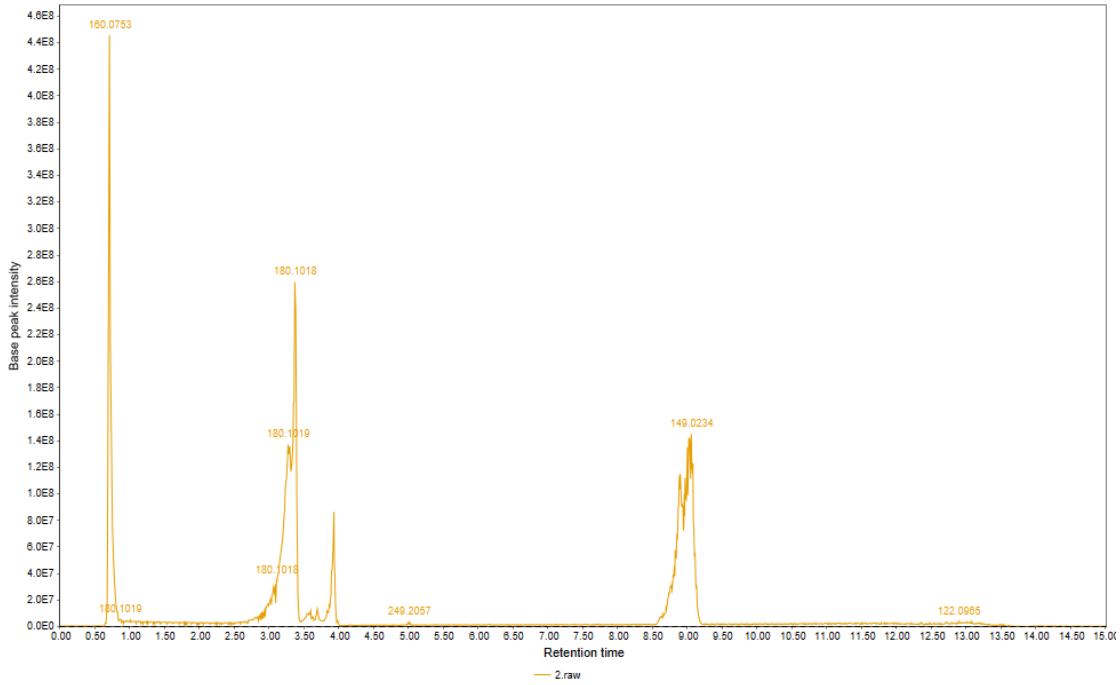
180.0753
180.1018
180.1019
180.1018
180.1019
249.2057
149.0234
122.0965
Base peak intensity
Retention time
2.raw

(B)

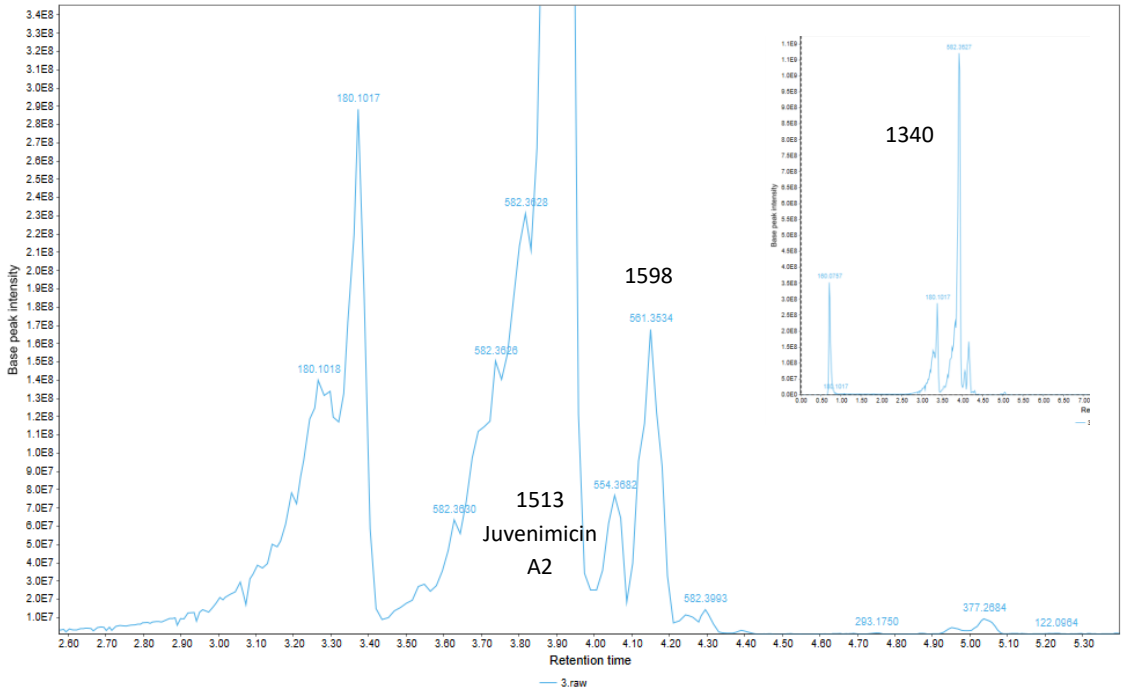
180.1017
180.1018
582.3628
582.3628
582.3600
1598
561.3534
1513
Juvenimicin
A2
554.3682
582.3993
293.1750
377.2684
122.0964
1340
Base peak intensity
Retention time
3.raw

(C)

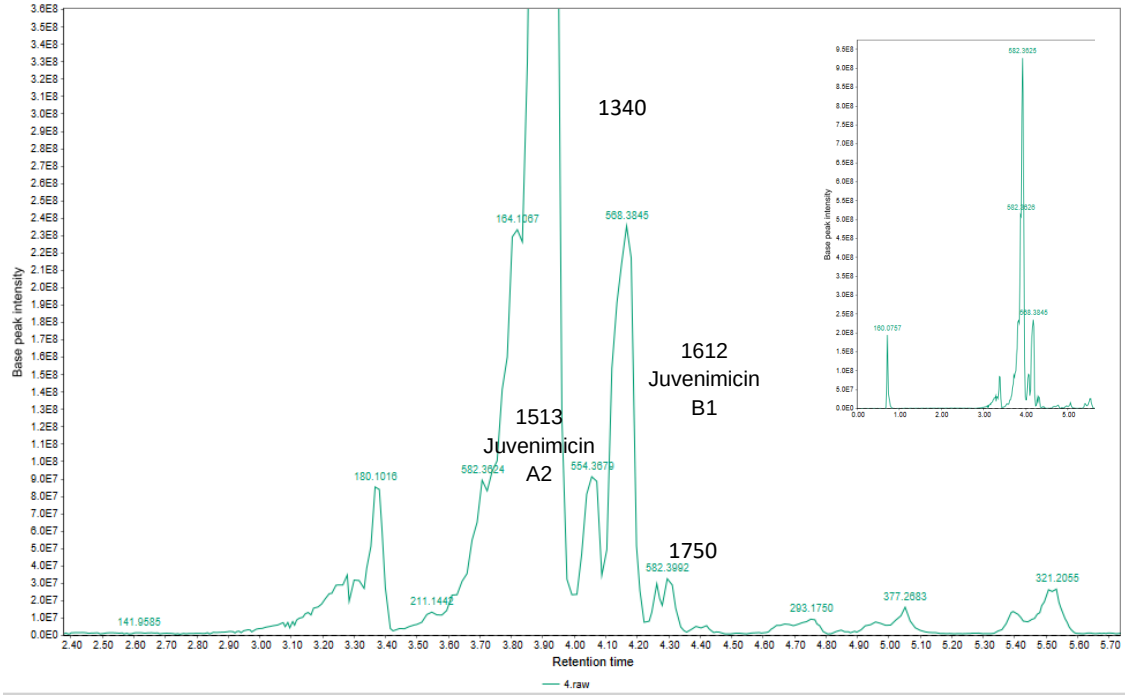
1340
1612
Juvenimicin
B1
1513
Juvenimicin
A2
1750
Base peak intensity
Retention time
4.raw

(D)

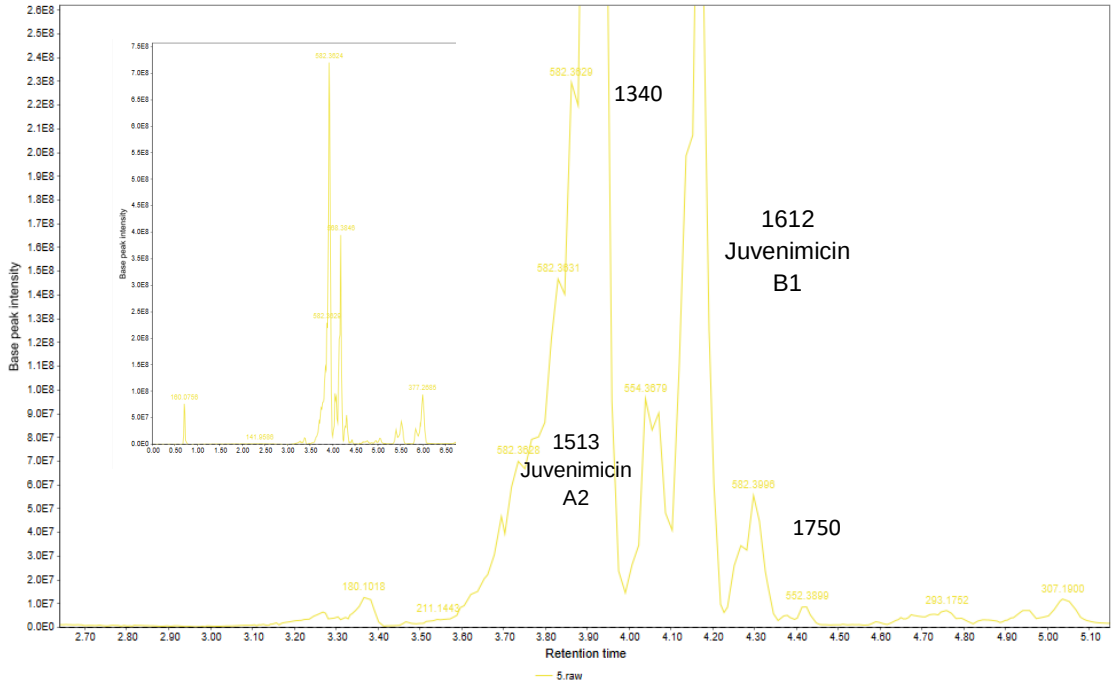
1340
1612
Juvenimicin
B1
1513
Juvenimicin
A2
1750
Base peak intensity
Retention time
5.raw

(E)

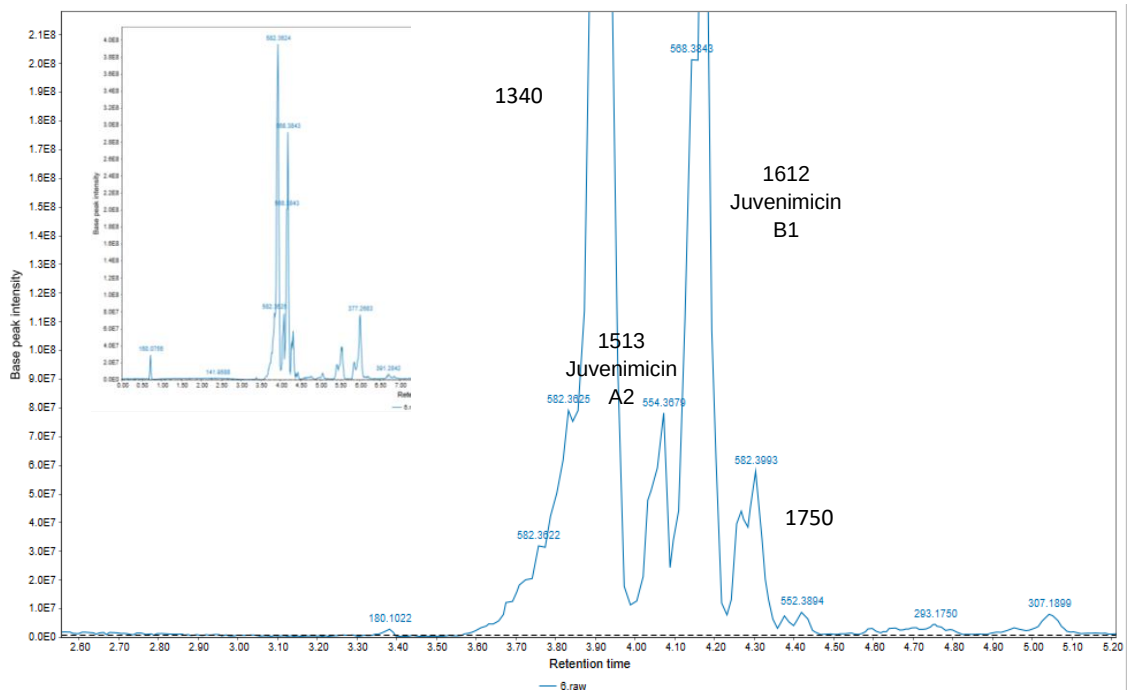
1340
1612
Juvenimicin
B1
1513
Juvenimicin
A2
1750
568.3843
582.3825
554.3679
582.3993
582.3822
562.3894
180.1022
293.1750
307.1899
Base peak intensity
Retention time
6.raw

(F)

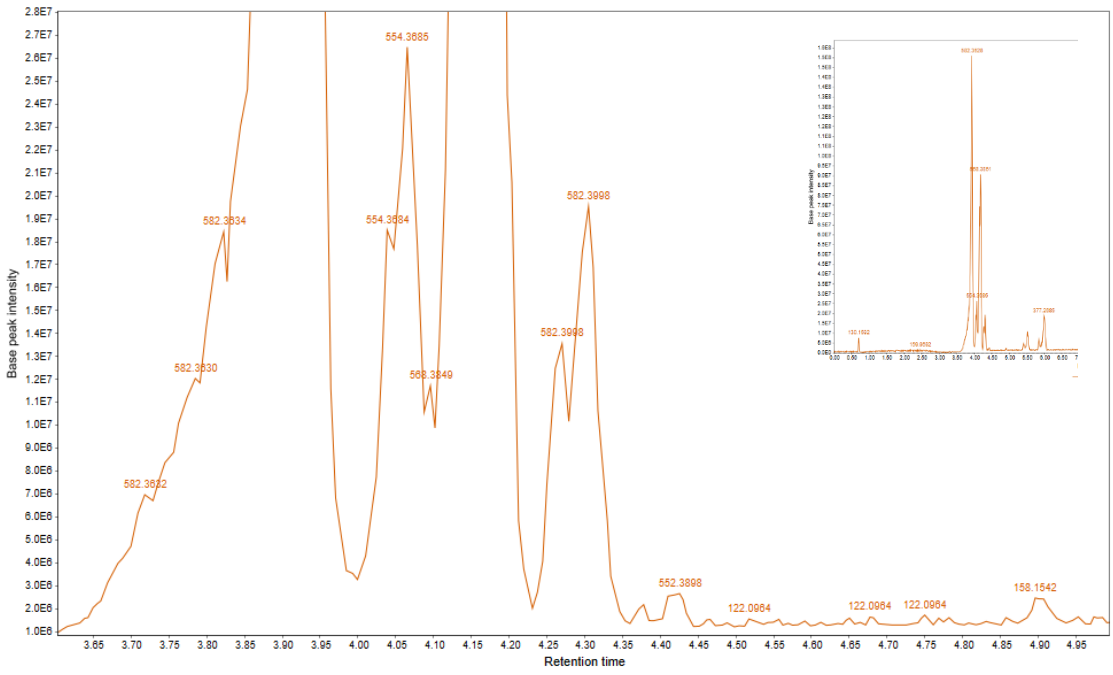
554.3685
582.3834
554.3684
582.3998
582.3830
582.3998
568.3849
582.3822
552.3898
122.0964
122.0964
122.0964
158.1542
Base peak intensity
Retention time

(G)

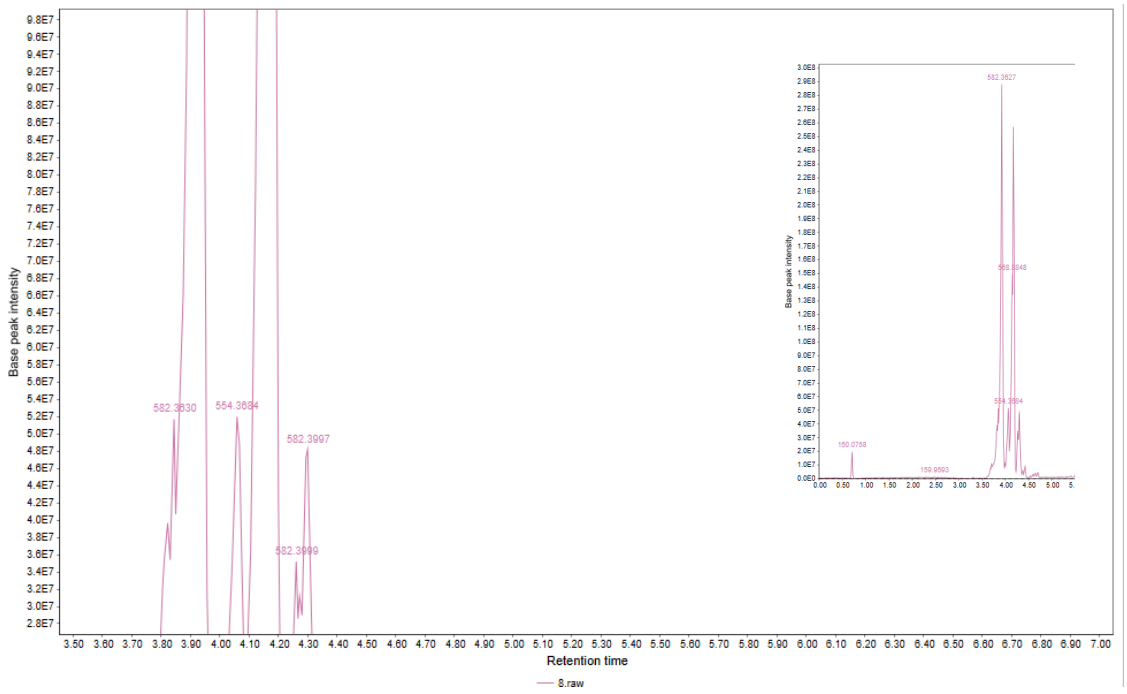

Figure S5.4. HR-LC chromatograms of seven fractions resulted from the semi-preparative C18 fractionation of *Micromonospora* sp. KRD324 crude extract grown at 15‰ salinity. (A) Fraction 2 (eluted with H_2O–MeCN 80:20); (B) Fraction 3 (eluted with H_2O–MeCN 60:40); (C) Fraction 4 (eluted with H_2O–MeCN 50:50); (D) Fraction 5 (eluted with H_2O–MeCN 40:60); (E) Fraction 6 (eluted with H_2O–MeCN 20:80); (F) Fraction 7 (eluted with H_2O–MeCN 0:100); (G) Fraction 8 (eluted with Methanol). The chromatograms were acquired in positive ionisation mode using UHPLC-HRMS. Retention times and intensity profiles are shown for macrolide-type features identified as juvenimicin analogues based on SIRIUS predictions (see Table 5.3). Peaks marked correspond to the features with parent *m/z* values of 582.3627 (1340), Sch 2831 (561.3534), 582.3992 (1750), Juvenimicin A2 (554.3682) and juvenamicin B1 (568.3845).

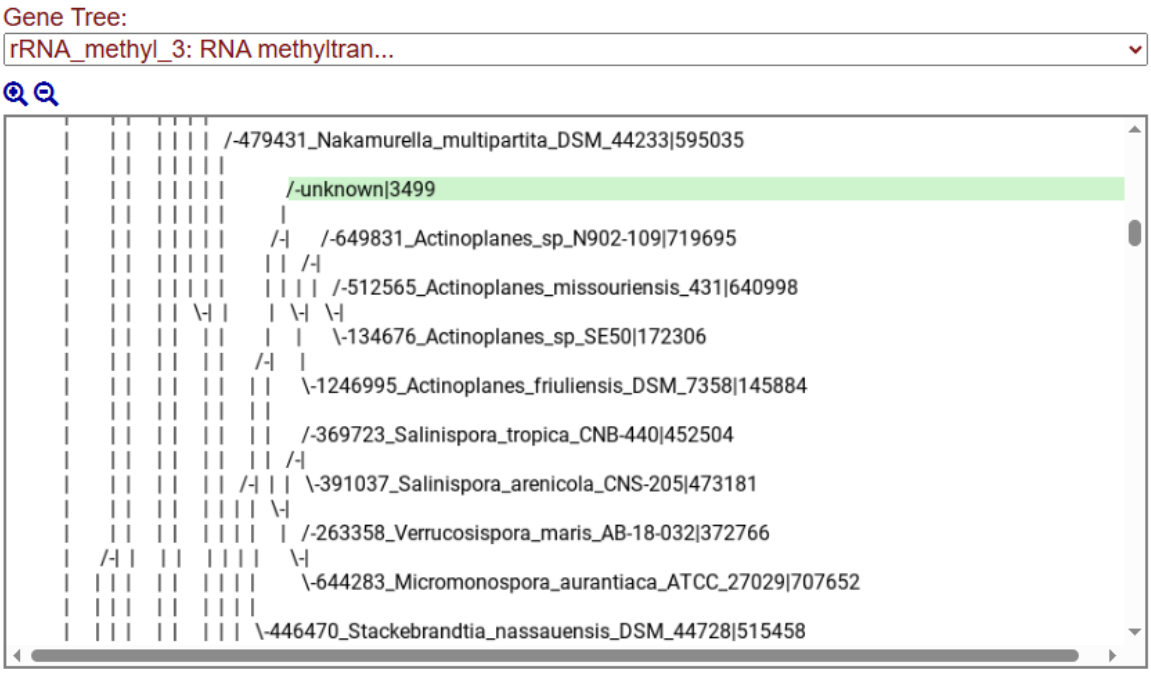

Figure S5.5. Phylogenetic reconstruction of the ARTS-predicted rRNA methyltransferase gene in the genome of *Micromonospora* KRD324 and related actinomycetes. The tree was generated using the ARTS (Antibiotic Resistant Target Seeker) (Mehmet *et al.,* 2020) platform based on homologous rRNA methyltransferase sequences. Strain KRD324 (highlighted in green) clusters with representatives of the genera *Actinoplanes*, *Salinispora* (*S. tropica* and *S. arenicola*), *Verrucosispora maris*, and *Micromonospora aurantiaca*, suggesting evolutionary conservation of this resistance determinant among these marine actinomycetes.